10 River to Bay: The Dynamic Simulation Framework

10.1 Introduction

This section provides the structural and procedural details of the dynamic simulation framework of Phase 6 Watershed Model (Phase 6 Model) simulating the transport and fate of nutrients and sediment in the Chesapeake watershed rivers and impoundments.

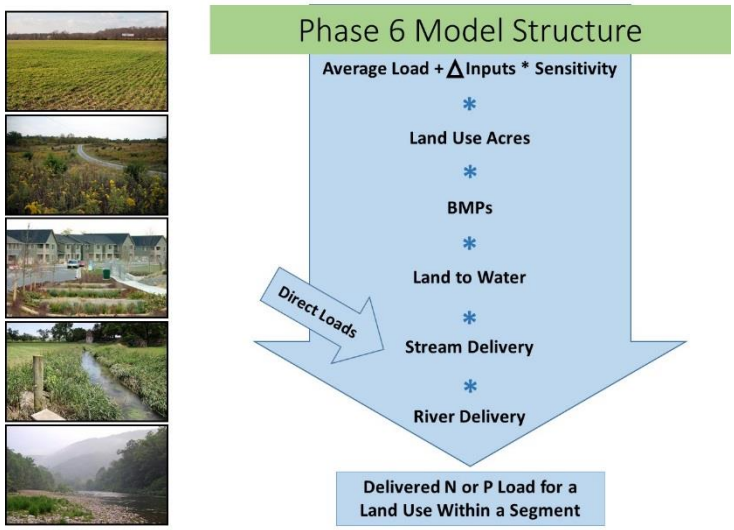

Figure 10-1: Phase 6 Model structure

The overall structure of the Phase 6 Model is shown in *Figure 10-1*. The figure shows the relatively simple time-averaged representation of the watershed processes of the Phase 6 Model that has been the primary focus of documentation in the previous sections. As described in Section 1, the time-averaged model, also called CAST, has several advantages as a management model compared to a numerically complex processed-based model. As previously described, the time-averaged framework is easily understood by the users' community and stakeholders. At the same time the simplified representation of watershed processes in the time-averaged framework allows the incorporation of emergent properties and responses from multiple models and lines of evidence. Furthermore, time-averaged operation of the model significantly reduces the runtime of a model simulation and improves portability of the model. The model can be reproduced as reduced-complexity versions, e.g., in the form of a spreadsheet that provides close approximations or exact copies of the model results for a management scenario.

In addition to estimating fate and transport of nutrients and sediment for a management scenario, the Phase 6 Watershed Model must be calibrated to observed data and provide daily inputs of flow, nutrients, and sediment to models of the tidal Chesapeake, among other purposes discussed in section 10.1. A dynamic simulation framework of the watershed is necessary to deliver that information. On an architectural level, both the time-averaged and dynamic simulation frameworks of the Phase 6 Model share the same model structure as shown in *Figure 10-1*, but they differ in terms of how time scales are represented in the model formulation, and the level of detail in which watershed processes are simulated. The dynamic simulation framework shares many of the same underlying descriptions of the watershed processes as in the time-averaged model. The closely defined linkage between the time-averaged model and dynamic simulation framework of the Phase 6 Watershed Model provides a foundation for the complementary use of the two interdependent systems.

The relationship between the time-averaged model and the dynamic simulation framework can be more easily understood by describing the processes that connect them. The dynamic simulation provides time-averaged hydrologic information to inform the prediction of edge-of-stream loads in the time-

averaged model. The time-averaged framework supplies the long-term edge-of-river loads of nitrogen, phosphorus, and sediment to the dynamic model. The dynamic model separates the long-term loads into hourly loads that are input to the simulated Phase 6 rivers. The process of temporal disaggregation of the loads is informed by hydrology, seasonality, and nutrient lag times. A biogeochemical river process model is then calibrated to observed concentration data in rivers. The resultant simulation is then used to estimate the river delivery factors in the time-averaged model (CAST).

10.1.1 Dynamic Simulation Framework

The Phase 6 dynamic simulation framework is an evolution of the Phase 5 Watershed Model (Shenk et al. 2012; Shenk and Linker 2013). It builds on the Phase 5 Model structure for the simulation of hydrology and sediment transport, but with several improvements in model inputs (Section 10.2), and refinements to the model calibration (Section 10.6). In addition, a strategic structural change was made to the land simulation scheme to explicitly include estimates of lag time in the nutrient transport rather than a directly simulating the nutrient biogeochemical transformation processes. Overall, the Phase 6 Model was developed through closely defined linkages between its time-averaged and dynamic simulation frameworks.

While the time-averaged simulation framework provides an improved accounting tool, which is preferred for a management model, the dynamic simulation framework is used for linkages to various Chesapeake estuarine models such as the Water Quality and Sediment Transport Simulation Model WQSTM), the SCHESM model of the tidal Chesapeake, the James River Chlorophyll Model of the tidal James, several versions of the Regional Ocean Modeling System (ROMS), and others. The dynamic simulation framework uses spatial differences of the time-averaged framework as a basis for the detailed temporal simulation of the watershed. The main purposes of the dynamic model are to:

1. Calibrate the watershed model to river and stream observations (Section 10.1.1.2)
2. Supply parameters to the simulation of nutrients in rivers and streams Section 10.1.1.3)
3. Estimate delivery factors for simulated rivers for use in the time -averaged simulation framework (CAST) (Section 10.1.1.4)
4. Create input loads for estuarine models of the Chesapeake (Section 10.1.1.5)
5. Investigate emergent riverine and impoundment watershed responses (Section 10.1.1.6)

10.1.1.1 Calibrate the Watershed Model to Observations

The Phase 6 Watershed Model was calibrated to the observations of daily flow across 254 monitoring stations for flow and more than a hundred stations for nutrients and sediment concentrations (see *Figure **10-9***, *Figure **10-11***, *Figure **10-12*** and Figure **10-13**).

Hydrologic parameters of the land segments, which are associated with the hydrologic response of land uses, were calibrated to daily flow observations. Land-based sediment processes were calibrated to long-term estimates of erosion rates of land uses as outlined in Section 2 and land-based nutrient simulations were constrained to match long-term estimates of nutrient loss from land-uses to the edge-of-stream as calculated by the time-averaged model.

Riverine water quality parameters were calibrated to observed concentrations of nutrients and sediments at monitoring stations, and then the calibrated model was validated against estimated loads from the Weighted Regressions on Time, Discharge, and Season (WRTDS) model (Hirsch et al. 2010;

Hirsch and Di Cicco 2014) across several monitoring sites capturing a range of spatial scales. Since the dynamic simulation framework is closely linked to the parameters used in the time-averaged model, the calibration process provides a cross-validation of protocols used in the drafting of those parameters while ensuring consistency between the two modeling frameworks.

Considering that the WRTDS loads are used to calculate the average edge-of-stream loads in Section 2, in the time-averaged simulation framework, calibrating to the WRTDS loads could seem circular at first consideration. However, the sum of the nine river input monitoring stations is used to calculate the spatially averaged edge-of-stream loads (Section 2) in the time-averaged framework, whereas the monitoring data of individual stations are used for calibration in the dynamic simulation framework. As the function of calibration is to generate spatial river-to-bay factors and validate other spatial factors, these two processes are independent.

10.1.1.2 Supply Parameters to the Simulation of Nutrients

As discussed in Section 2 and Section 4, the estimation of phosphorus loads from individual land uses is dependent in part on the long-term spatial variability in stormflow and sediment washoff. Average annual fluxes of stormflow and sediment were supplied to the time-averaged model from the calibrated dynamic model.

10.1.1.3 Estimate Delivery Factors for Simulated Rivers

The calibration of nutrients and sediment in the dynamic model to the monitoring data establishes the riverine parameters. These riverine parameters e.g. particulate settling rates, denitrification rates, etc., govern the fate and transport of nutrients and sediments in the simulated river reaches. The calibrated simulation of rivers in the dynamic model aggregated over a specified period of time supplies the river delivery factors or river-to-bay factors for the time-averaged CAST model. Specifically, simulated response quantified as the fraction of input to a river reach that is delivered to the Bay is the delivery factor.

10.1.1.4 Create Input Loads for The Estuarine Model

The Chesapeake Bay Program's estuarine Water Quality and Sediment Transport Model (WQSTM) is a linked hydrodynamic and water quality model. The WQSTM and other estuarine models of the Chesapeake require spatially explicit watershed outputs of flow and loads on a daily or sub-daily time step. Although the time-averaged model can provide an estimate of change in long-term (ten-year) average loads for a certain management scenario, it is unable to generate the daily temporal inputs required by the estuarine models of the Chesapeake Bay. Therefore, inputs for estuarine model calibration and scenarios must be generated with the dynamic model simulation.

10.1.1.5 Investigate Emergent Watershed Responses

The Phase 6 Model has the capability to investigate issues of importance to the Chesapeake Bay Partnership that were unaddressed in earlier versions. For the first time in a Chesapeake watershed model lag times are incorporated into the simulation to help investigate questions about the length of time between BMP implementation to reduce nutrients and sediment loads and anticipated changes in water quality. In addition, the CBP partnership is also faced with decisions to address climate change impacts on water quality which will be supported from the dynamic model which is capable of estimating changes in watershed responses due to the changes in rainfall and temperature.

10.1.2 Dynamic Model Structural Details

The overall software system that calculates nutrient and sediment loads from land uses, watershed inputs, and BMPs is described in Section 1. The time-averaged model represented in *Figure 10-1* is simulated by various components of that overall system. The dynamic simulation model described in Section 10 simulates those watershed processes at an hourly time step, while sharing some of the emergent properties of the catchments with the time-averaged model.

10.1.2.1 Phase 6 Dynamic Simulation Model Architecture Details

The Phase 6 dynamic simulation model is a hybrid of the Hydrologic Simulation Program – FORTRAN (HSPF) and other simulation modules developed by the Chesapeake Bay Program partnership. As shown in *Figure **10-2***, HSPF is used for the simulation of hydrologic and sediment responses of the land segments as well as for riverine transport of water quantity and quality variables. For the land nutrient simulation, the dynamic simulation uses the long-term export rates estimated by the time-averaged model, but similarly to flow and sediment responses, the nutrient transport from the land and rivers is simulated at hourly time steps. The Unit Nutrient Export Curve (UNEC, Section 10.5.3) and ranked Storage Selection module (rSAS, Section 10.5.4) are used for temporal disaggregation. The HSPF model is used for the simulation of hydraulics and water quality of large Chesapeake large rivers with average flow greater than 100 ft^3/s that are generally greater than 4th order.

The HSPF watershed model is widely used and supported by several federal agencies (Bicknell et al. 1997; Donigian et al. 1995a; Donigian et al. 1995b; Bicknell et al. 2001). HSPF is a semi-distributed, physically based, lumped-parameter model that simulates hydrology, sediment, and transport of pollutants in the soil and rivers. The model uses meteorological forcing, watershed and land-use characteristics, nutrient application data, and information on management practices to simulate watershed response. An HSPF model is normally calibrated to observed flow and instream water quality measurements.

In HSPF a watershed is represented as a number of discrete land segments, river reaches, and reservoirs. A land segment is generally defined as an area with similar hydrologic characteristics. For Phase 6, the watershed land segments are usually defined by county boundaries. This was done because it is the finest scale for many critical model inputs, such as fertilizer, manure, and crop types. As described in Section 11, some of the land segments were further divided to differentiate areas of high and low rainfall from the rest of the land segment. Thresholds for the further differentiation of a land segment was defined as areas of a land segment with either greater or less than 10 percent of the 30-year average rainfall for the county. The response for land uses are simulated on a per acre basis. Inputs of water, sediment, and water quality constituents for river segments are calculated by aggregating loads from the land segments with direct drainage to the river segments and simulated delivery from the upstream river segments. Direct loads from a number of sources, e.g., point sources, are transferred to the corresponding river reach or reservoir segment. The hydraulic and water quality processes of river channels or reservoirs are simulated by HSPF. River channels or reservoirs are treated as completely mixed reactors, i.e., the river reaches and reservoirs are completely mixed in width and depth.

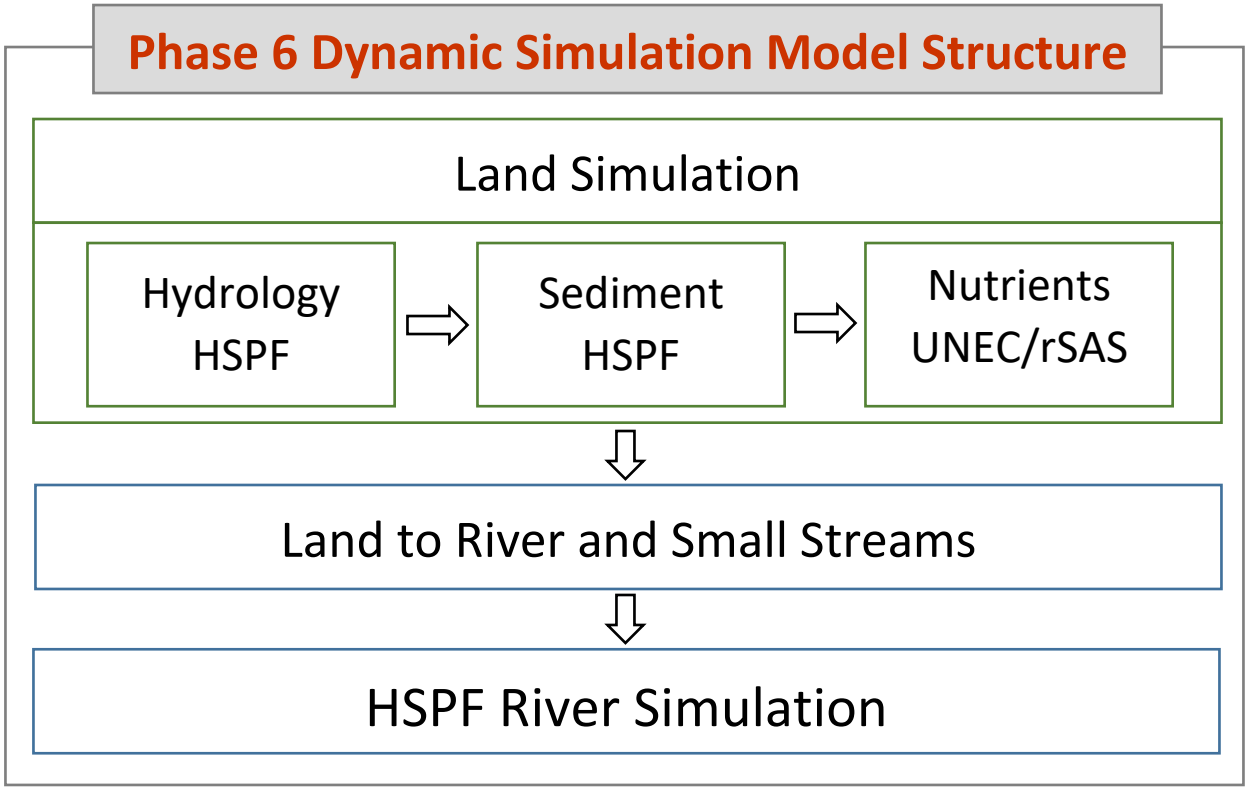

Figure 10-2: Phase 6 dynamic simulation model architecture

The dynamic model simulates several key state and flux data for flow, sediment, and water quality variables. Some of the key fluxes for the land and river simulations are listed in Table 10-1. Table 10-1 also shows the watershed linkage (in all caps) between the land and river processes.

Table 10-1: *Essential watershed variables simulated by the model*

Land Simulation	WATERSHED LINKAGE	River Simulation
Surface outflow Interflow outflow Active groundwater outflow	HYDROLOGY	River outflow
Heat energy in surface outflow Heat energy in interflow outflow Heat energy in groundwater outflow	ENERGY	Heat energy in river outflow
Sediment Washoff	SEDIMENT	Outflow of Sand Outflow of Silt Outflow of Clay
Nitrate in surface outflow Nitrate in interflow outflow Nitrate in groundwater outflow	NITRATE	Dissolved nitrate
Ammonia in surface outflow	AMMONIA	Dissolved ammonia

Ammonia in interflow outflow Ammonia in groundwater outflow Ammonia in sediment flux		Sand bound ammonia Silt bound ammonia Clay bound ammonia
Refractory nitrogen in surface outflow Refractory nitrogen in interflow outflow Refractory nitrogen in groundwater outflow Refractory nitrogen in sediment flux Labile nitrogen in surface outflow Labile nitrogen in interflow outflow Labile nitrogen in groundwater outflow Labile nitrogen in sediment flux	ORGANIC NITROGEN	Refractory nitrogen Biochemical oxygen demand
Phosphate in surface outflow Phosphate in interflow outflow Phosphate in groundwater outflow Phosphate in sediment flux	ORTHOPHOSPHATE	Dissolved phosphate Sand bound phosphate Silt bound phosphate Clay bound phosphate
Phosphate in surface outflow Phosphate in interflow outflow Phosphate in groundwater outflow Phosphate in sediment flux Phosphate in surface outflow Phosphate in interflow outflow Phosphate in groundwater outflow Phosphate in sediment flux	ORGANIC PHOSPHORUS	Refractory phosphorus Biochemical oxygen demand
		Phytoplankton
		Organic carbon
		Dissolved Oxygen

10.1.2.2 Phase 6 Dynamic Model Procedural Details

The Phase 6 dynamic model builds off an enhanced HSPF model structure that was developed for the Phase 5.3.2 Model (Shenk et al. 2012; Shenk and Linker 2013). Several preprocessors were developed to format input data and automatically generate HSPF input files for land and river simulations. The external transfer module (ETM) links the land simulation to the river simulation. Postprocessing programs are used for generating and displaying model outputs.

10.1.2.2.1 Preprocessors for Input File Generation

HSPF uses a User-Controlled Input (UCI) file to specify all information relevant to a simulation. In most HSPF applications, all land and river simulation modules are parameterized within a single UCI file. The water, nutrient, and sediment exports of each land use are multiplied by a single factor for land use acreage and another factor for translation between land variable types and units to river variable types and units. In a standard Version 11 HSPF application neither the land use nor the translation factors can be changed during the simulation; thus, an off-the-shelf HSPF model generally lacks the flexibility necessary for the Chesapeake large-scale watershed simulation.

To incorporate changes in land uses and management over time and provide overall flexibility in model simulation, structural changes were made to simulate land and river segments in separate UCIs.

Accordingly, the preprocessors to generate UCI files consist of two parts, a Land UCI Generator (LUG), and a River UCI Generator (RUG).

The LUG is a group of programs that were designed to automatically generate UCI files for land simulations. To create a UCI file, the LUG (1) obtains operation instructions from a user-defined control file; (2) reads input data and parameter information from predeveloped databases; and (3) writes all information into a standard UCI format. The operation instructions specify HSPF modules and data sets relevant to a particular land segment simulation and can be easily modified to accommodate a specific user need. Three databases—a nutrient application database, a module specification database, and a process parameter database—are preprocessed to store information on nutrient input to land surfaces, specific input and format of each HSPF module, and parameter information required for each HSPF module, respectively. These databases are a group of ASCII files whose formats are devised in accordance with the read/write functionality of the LUG. Separate UCI files are generated for every land use within a land-segment.

Similarly, the RUG is a group of programs that provide the functionality for automatically generating UCI file for river simulations. Like the LUG, the RUG reads operation instructions from a user-defined control file, obtains module and parameter information from a module specification database and a process parameter database, and then creates a standard river UCI file. A separate river UCI file is generated for each river segment. Before a river simulation is run, local land- segments/land use types and upstream rivers that drain to it must be identified. A separate program was developed to track the land-river connections and river network, which are preprocessed through GIS tools and stored in an ASCII file for the entire watershed. This program is outside the RUG structure but functions as an integrated part of it.

Separating land and river simulation into different UCIs not only provides great flexibility in model simulation but also offers computational scalability. With this structure, a simulation for a single land use within a land-segment is completely independent of any other land or river simulation. River simulation of a river segment is dependent on the land simulation of the segments that directly discharge to the segment and the upstream river simulations. This provides an efficient and meaningful way to deal with the complicated land-to-river and river-to-river logistics of a large-scale watershed simulation on a high-performance computing environment without compromising on parallelization efficiency.

10.1.2.2.2 Land Simulation

Water, energy, and sediment budgets for land uses are simulated using HSPF. HSPF executes modules for simulating these processes using the parameterization and input dataset descriptions specified in a land UCI file. The HSPF modules for Air Temperature Elevation Difference (ATEMP), Accumulation and Melting of Snow and Ice (SNOW), Water Budget for Pervious or Impervious land use (PWATER/IWATER), Production and Removal of Sediment (SEDMNT), Soil Temperatures (PSTEMP), and Water Temperature and Dissolved Gas Concentrations (PWTGAS) are executed. Nutrient budgets are simulated using UNEC (Section 10.5.4) and rSAS (Section 10.5.5). UNEC and rSAS use the water and sediment fluxes along with the nutrient inputs to calculate nutrient budgets for the land uses. Parameters for transit time distributions of nutrients are provided as inputs for both UNEC and rSAS based on estimates of lag times that are based on multiple models and other lines of evidence (Section 10.5.3). Simulated hourly

nutrient budgets are stored in the Water Data Management (WDM) files for land uses along with the HSPF simulated water, energy, and sediment state and flux variables.

10.1.2.2.3 External Transfer Module

The External Transfer Module (ETM), links the land simulation to the river simulation. The ETM consists of a group of data processing routines that aggregate water, sediment, and nutrient loads from the land segments draining to a river segment. During that process, the ETM also translates land variables to river variables (Table 10-1), using a predefined mapping. The mapping between the land and river variables are stored in an easily accessible database. While aggregating the loads, the ETM also applies transfer factors for (a) land-to-water factors accounting for the geographical differences not accounted for by the application rates (see Section 7.3), (b) reduction efficiencies for the best management practices (see Section 6.5), and (c) stream to river factors for attenuations in small streams (Section 9.1). The routines were developed within the ETM to read and write data directly to binary Water Data Management (WDM) files, which are the most efficient method of input, output, and storage for HSPF.

In the real world, change in land use is continual; however, land use and related input data are generally available for specific points in time. Therefore, the ETM was programmed to accept data at several points in time and interpolate and extrapolate through the simulation period as necessary. The user can specify as many of these as are needed to incorporate the changes over the simulation period. Overall, interposing this non-HSPF software between the land and river simulation allows for opportunities to address issues of flexibility that are difficult to manage in traditional HSPF applications. The land use data provided to Phase 6 for calibration was annual.

10.1.2.2.4 River simulation

The hydraulics and biochemistry of rivers are simulated using HSPF. A simulated river or reservoir reach has three broad categories of inputs – (a) loads from adjacent land segments, (b) direct inputs, (c) loads from the upstream river segments. As described above, loads from the adjacent land segments are combined by the ETM data processor. Direct inputs of flow, sediment, and nutrient loads from wastewater treatment plants, industrial point sources, riparian pasture deposition, rapid infiltration basins, septic systems, and atmospheric deposition to water bodies are added to the river segment inputs after small stream attenuation is applied. The HSPF model executes modules for these simulations using the activity and input dataset descriptions in a river UCI file. In the Phase 6 dynamic model simulation the following HSPF modules are activated: reach and reservoir modules for hydraulic behavior (HYDR), advection of fully entrained constituents (ADCALC), heat exchange and water temperature (HTRCH), behavior of inorganic sediment (SEDMNT), constituents involved in biochemical transformations (RQUAL), primary dissolved oxygen (DO) and biochemical oxygen demand (BOD) balances (OXRX), primary inorganic nitrogen and phosphorus balances (NUTRX), and plankton populations and associated reactions (PLANK).

Impoundments and reservoirs significantly influence nutrient and sediment budgets. Effects of impoundments and reservoirs are captured in the model using three accounting mechanisms as described in Section 9. First, the effects of small impoundments and dams, located in low order streams, are combined into the factors incorporated into stream-to-river delivery factors. Second, most of the largest reservoirs that are located directly on simulated rivers are directly simulated using HSPF. For reservoirs that are on a simulated Phase 6 rivers but not simulated directly as a reservoir by HSPF,

the reservoir effects on the transport of sediment and nutrients described in Section 9 were applied as an attenuation factor after the HSPF river simulation.

A new module simulating the scour of organic materials was added. This module is a part of the river simulation which is executed after the HSPF reach or reservoir simulation.

10.1.2.2.5 Operational Description of The Modeling System

A brief summary of key model operation steps is provided in the *Table **10-2***. *Figure **10-3*** illustrates the model data workflow corresponding to these key model operation steps. Model operations were parallelized to take advantage of high-performance computing with multiple processors. Operation steps related to the land simulation were designed to support parallel execution for land segments. Some of the computationally intensive land simulation steps were further discretized to further support parallel execution. Similarly, operation steps related to the river simulation were discretized to support parallel execution for river segments. Most of the river simulation steps can be run completely in parallel, except for those that depend on the output from an upstream river segment. For those operation steps parallelization was done on a hierarchical level following the Strahler stream order (Strahler 1957), where rivers with no upstream river simulation are run first, and then river segments downstream, and so on. Model operation takes advantage of Linux shell scripts to further streamline the model operations.

The Phase 6 software system has several advantages over a traditional HSPF application: (1) it has provisions for adjusting parameters during calibration of a large-scale watershed; (2) parallel computing operations become convenient, and thus simulation can be arranged more efficiently; (3) new land use types can be incorporated, which enables easy expansion of the model simulation; and (4) it can be easily integrated into outside databases for scenarios. The software system is compatible for execution on personal computers with the Linux operating system. However, shell scripts for the parallel operation of the model require Simple Linux Utility for Resource Management (SLURM), which is a workload manager for computer clusters. All supporting scripts, as well as HSPF, are open source, public domain software written primarily in Fortran 77.

Table 10-2: Key operation steps of the Phase 6 dynamic simulation model

Step	Operation	Description
1	Preprocess Input WDMs	Model input forcing – precipitation, atmospheric deposition, meteorology, wastewater, industrial discharge, combined sewage overflow, septic, riparian pasture deposition, and rapid infiltration basin loads are processed and stored in WDM files.
2	Generate LUG	Land UCIs are generated for land-uses through the LUG preprocessor.
3	Run Land Simulation	HSPF simulations are executed for land UCIs, and output is stored in individual Land WDM files for the land uses in land segments.
4	Nutrient Simulation	UNEC simulations are executed for land uses to calculate nutrient budgets. Model outputs are stored in land WDM files.

5	Run External Transfer Module (ETM)	The ETM is run, converting land outputs to river inputs, accounting for temporal changes in land use and BMPs, and also land-to-water delivery variances factors and small stream to river delivery factors. Output is stored in river-formatted WDMs.
6	Generate RUG	River UCIs are generated for river segments using the RUG.
7	Combine Loads	Direct loads from different source sectors are processed and combined for the river segments.
8	Run River Simulation	HSPF is run for the river UCIs, and output is stored in individual River WDM files.
9	Generate Output Summary	The postprocessor reads the river WDMs and writes ASCII output.
10	Generate WQSTM or Other Estuarine Model Inputs	Water Quality Sediment Transport Model (WQSTM) inputs are generated using the linkage information between the land-river segments and WQM cells.

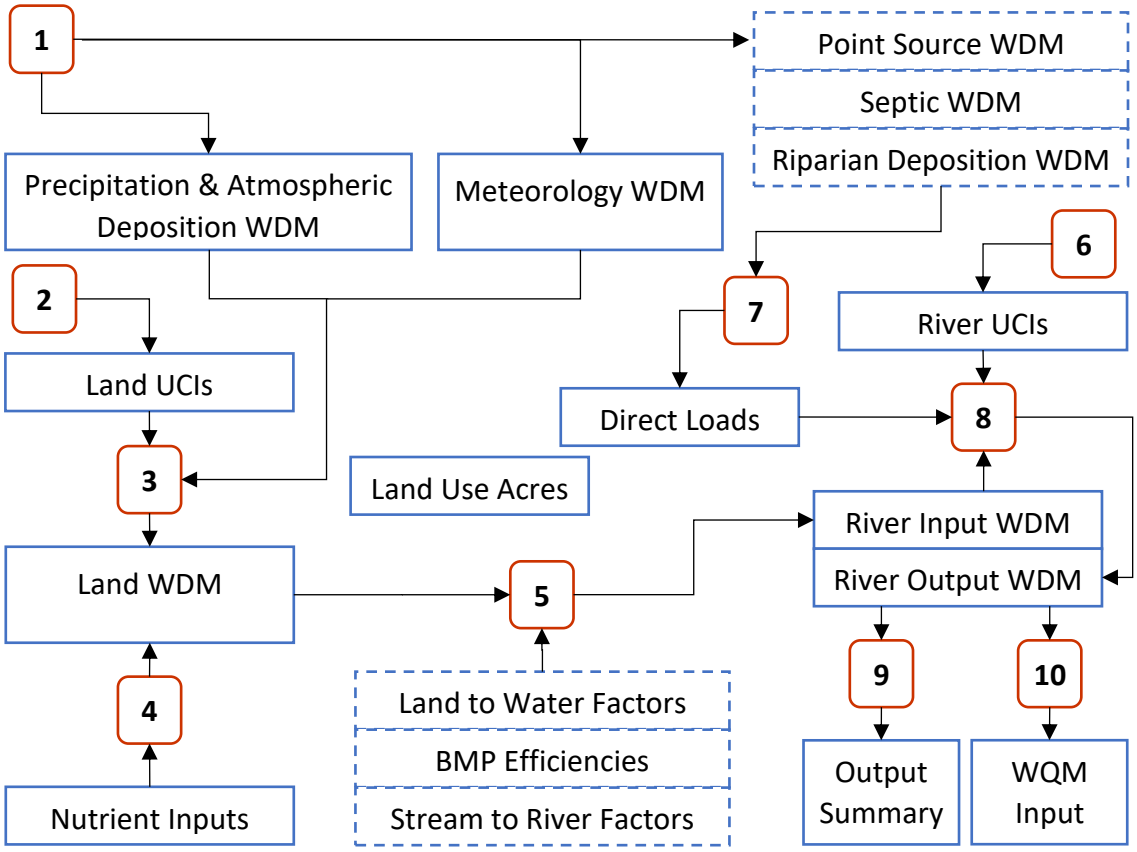

Figure 10-3: Model data workflow of the Phase 6 dynamic simulation modeling framework. Description of the major model operation steps are provided in **Table 10-1***Table 10-2.*

The LUG, RUG, and ETM model system along with compartmentalized HSPF simulation improves the application and calibration of HSPF at large scale watershed by incorporating time-varying anthropogenic forcing functions. With the proliferation of inexpensive Linux systems that can be clustered together, computing power that is normally reserved for large simulation projects is now affordable and generally accessible to more users.

10.1.3 Simulation Time Period

The Phase 6 Model has an expanded simulation period of 30 years (1985 to 2014) as compared to 21 years (1985 to 2005) used in Phase 5.3.2. The expanded simulation period allows for the incorporation of recent watershed inputs and monitoring data in the model. Moreover, the long-term model simulation provides an opportunity for the examination of water quality response over a varied degree of meteorological forcing, land-use change, and implementation of management practices over the last three decades.

10.2 Dynamic Model Forcing and Calibration Dataset

Input dataset for the Phase 6 dynamic simulation model can be grouped into three broad categories based on fundamental watershed processes for hydrology, sediment, and nutrient transport. Hydrology simulation requires inputs for rainfall, meteorological forcing (10.2.1), geospatial watershed properties (e.g. topography), diversions, and land use (Section 5) and associated model parameters. The sediment transport simulation requires inputs for crop cover (Section 3.6), detached sediment fractions (Section 3.7), and sediment targets (Section 2.3). Nutrient simulation requires several terrestrial inputs described in Section 3.2 through Section 3.5, such as land use nutrient targets, and effectiveness efficiencies for the implementation of best management practices (Section 6.5).

In addition to input dataset for model forcing and associated model parameters, monitoring information is needed for the calibration of the model. Daily observations of flow are used for the calibration of land-based hydrologic parameters. Riverine biogeochemical parameters are calibrated based on water quality monitoring samples for the concentration of nitrogen and phosphorus species, and suspended sediment.

Monthly and annual estimates of riverine nutrient and sediment loads from USGS-WRTDS (Moyer et al., 2015) are used for the validation of the model. These loads are not used in the model calibration.

10.2.1 Meteorological Forcing

The HSPF hydrology simulation requires hourly inputs of precipitation and meteorological forcing. These forcing variables include – (1) precipitation, (2) air temperature, (3) potential evaporation, (4) dew point temperature, (5) wind speed, (6) solar radiation, and (7) cloud cover. For Phase 6 Model, these datasets were derived from the North American Land Data Assimilation System (NLDAS). The NLDAS is a collaboration project among of several federal agencies and research institutions, including the Environmental Modeling Center, the Office of Hydrological Development, and Climate Prediction Center of the National Oceanic and Atmospheric Administration (NOAA); the National Aeronautics and Space Administration's (NASA's) Goddard Space Flight Center; Princeton University; the University of

Maryland; Rutgers University; and the University of Washington. The goal of NLDAS is to provide more accurate simulations of water and energy fluxes from land surfaces to help improve weather prediction.

The NLDAS Phase 2 (NLDAS2) data set contains hourly datasets for traditional land surface forcing fields. The precipitation field is based on the CPC analysis of daily rainfall CONUS gauge data (Higgins et al. 2000; Chen et al. 2008). The orographic adjustments are based on the PRISM climatology (Daly et al. 1994). Hourly precipitation is derived by disaggregating daily gauge products using preferential use of Doppler radar, CMORPH products, or HPD data.

The NLDAS2 primary forcing (NLDAS2 File A) are available at 1/8th degree spatial resolution. Over the Chesapeake Bay region, the grid is approximately 14 km by 14 km or 76 square miles. *Figure **10-4*** shows the NLDAS2 grid in relation to the Phase 6 land segments. Precipitation and meteorological dataset for Phase 6 land segments were calculated were aggregating hourly dataset for collocated NLDAS2 grids. *Table **10-3*** lists the meteorological variables in NLDAS Forcing Function File A used to calculate meteorological inputs.

Overall, there are two main benefits to using the NLDAS meteorological inputs: First, they are subject to extensive quality control procedures and validation (Cosgrove et al. 2003). Second, NLDAS meteorological inputs are made available publicly on a near real time basis. The second feature facilitates expanding and or updating of the Phase 6 calibration and/or simulation period.

Table 10-3: NLDAS2 primary forcing fields used in the Phase 6 Watershed Model

Time Series	**Symbol**	**Units**
Precipitation	P	kg/m^2/hour ≈ mm/hour
Air Temperature	T	°C
Specific Humidity	SH	kg/kg
Wind Speed (longitudinal)	U_x	m/s
Wind Speed (latitudinal)	U_y	m/s
Short Wave Radiation	R	W/m^2
Atmospheric Pressure	P_{atm}	Pa

Precipitation, air temperature, and shortwave solar radiation require only unit conversions to be useable in the watershed model simulation. The remaining meteorological inputs have to be calculated from the NLDAS2 primary forcing dataset. Dew point temperature and cloud cover were calculated at daily time steps. The calculations are presented below.

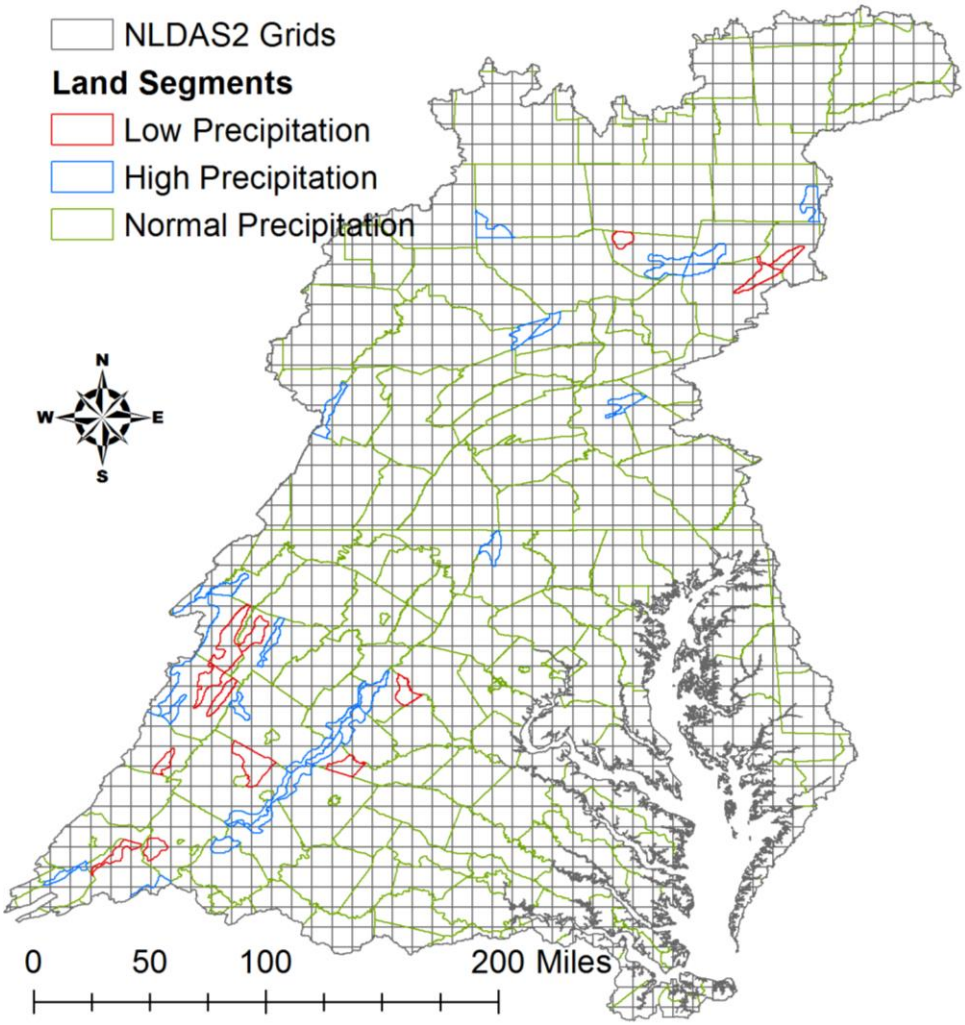

Figure 10-4: NLDAS2 grids in relation to Phase 6 land segments

10.2.1.1 Hourly Precipitation

Over the continental United States, the NLDAS precipitation data is based on the Climate Prediction Center's (CPC's) daily gauge-based precipitation analysis. The CPC gauge analysis provides daily precipitation totals on the 1/8th degree scale, interpolated from 6,500 daily gauge reports (Cosgrove *et al*. 2003). Prior to 2012, the Inverse Distance method was used to interpolate the gauge reports, but since 2012, the Optimal Interpolation method is being used. Chen et al. (2008) describe the two methods and highlights the advantages of the Optimal Interpolation method. The CPC gauge analysis also incorporates elevation and orographic corrections to the data set through the Precipitation-elevation Regressions on Independent Slopes Model (PRISIM) (Daily et al. 1994). Daily precipitation on the 1/8th degree grid is disaggregated to hourly values using weights derived from the National Weather Service's Stage 2 hourly precipitation data. The Stage 2 data is based on precipitation estimates from corrected WSR-88D Doppler radar data; however, the disaggregated hourly precipitation time series maintains agreement with the CPC gauge analysis on a daily basis. If no Stage 2 data is available to

perform the disaggregation, the NOAA CPC Morphing Technique (CMORPH) is the second choice, the CPC Hourly Precipitation Dataset (HPC) is the third choice, and the North American Region Reanalysis's (NARR's) precipitation data set is the fourth choice for disaggregation. *Figure **10-5*** shows the NLDAS2 average annual rainfall and average rainfall intensity over the 30-year simulation period.

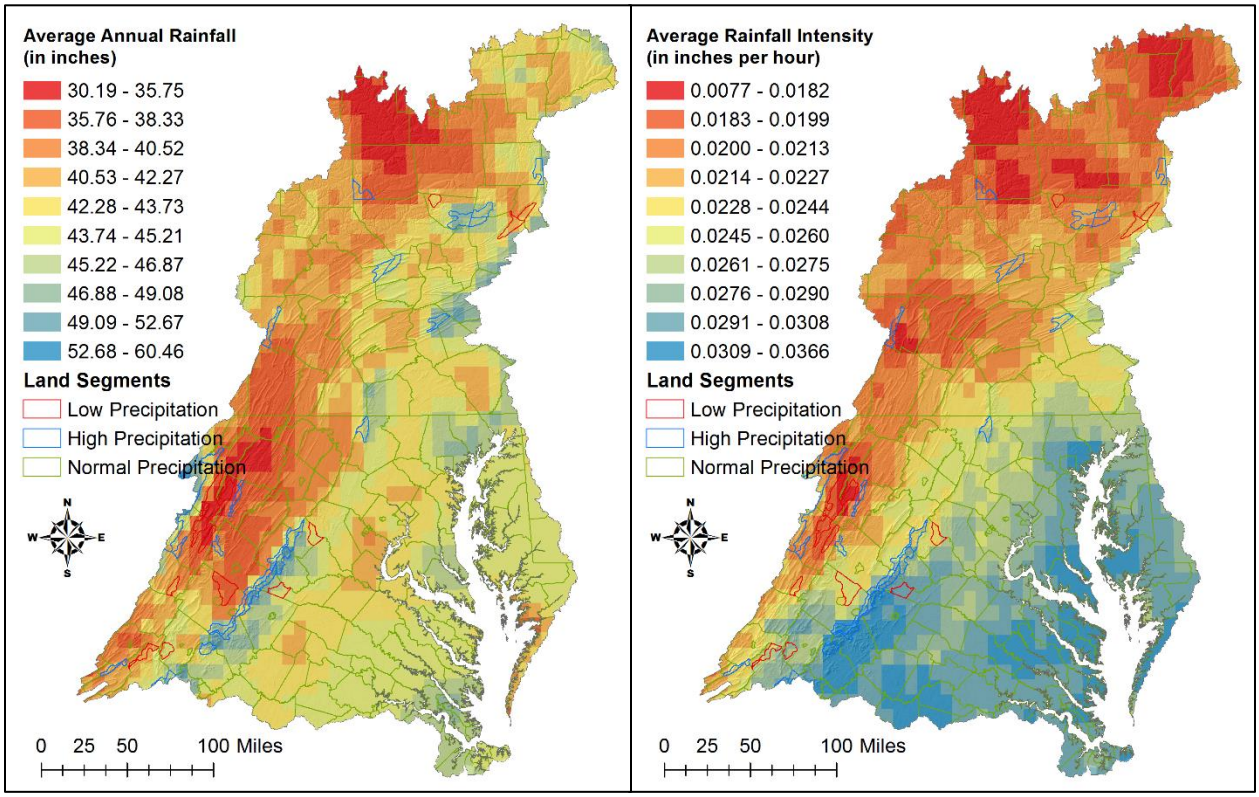

Figure 10-5: Average annual rainfall and average rainfall intensity across the Chesapeake Bay watershed.

10.2.1.2 Solar Radiation

Downward shortwave solar radiation is based on information collected by the Geostationary Operational Environmental Satellite (GOES) system. Estimated shortwave radiation is bias-corrected using the University of Maryland Surface Radiation Budget dataset (Pinker et al. 2003).

The remaining NLDAS inputs are based on the Eta Data Assimilation System (EDAS) or the Eta mesoscale model forecast field, if EDAS is not available (Cosgrove et al. 2003). The EDAS model-assimilated data are available on a 32-km grid at 3-hour intervals. When they are interpolated to the NLDAS grid, air temperature, pressure, and specific humidity are adjusted for differences in elevation.

10.2.1.3 Wind Speed (U)

The wind speed (U) was calculated from its latitudinal and longitudinal components:

$$U = \sqrt{(U_x + U_y)}$$

Equation 10-1

where,

U_x = latitudinal velocity (m/s) at 10 m

U_y = longitudinal velocity (m/s) at 10 m

10.2.1.4 Relative Humidity (RH)

Relative Humidity (RH) was calculated from the primary forcing data for specific humidity using a method documented by the World Meteorological Organization (2010):

$$VP = P_{atm}*(SH/(SH + 0.62198))$$

Equation 10-2

$$VPSat = 611.2* \text{Exp}(17.62*T/(243.12 + T))$$

Equation 10-3

$$RH = VP/VPSat$$

Equation 10-4

where RH is dimensionless and

VP = vapor pressure (millibars)
VPSat = saturated vapor pressure (millibars)

10.2.1.5 Potential Evapotranspiration (PET)

Potential evapotranspiration was calculated from average daily temperature (T_{avg}) and the number of daylight hours (DH), according to the Hamon method (Hamon, 1961). Daylight hour was calculated by the number of hours with short-wave radiation. The Hamon method:

$$VPsat = 6.108 * \exp(17.26939 * T_{avg} / (T_{avg} + 237.3))$$

Equation 10-5

$$VDsat = 216.7 * VPsat / (T_{avg} + 273.3)$$

Equation 10-6

$$PET = 0.0055 * (DH / 12)^2 * VDsat$$

Equation 10-7

where,

T_{avg} is average daily temperature (°C)
T_{avg} is average daily temperature (°C)
VPsat is saturated vapor pressure (millibars)
VDsat is saturated water vapor density (g/m^3)
PET is potential evapotranspiration in inches/day

The potential evapotranspiration calculated for a day was disaggregated to hourly values by using the fraction of daily solar radiation that occurs in that hour. *Figure **10-6*** shows spatial variability in average annual temperature and potential evapotranspiration across the watershed. For Phase 6 simulations of climate change the Hamon estimates of evapotranspiration were adjusted by estimates of evapotranspiration by Hargreaves and Samani (1982) which is a robust and practical method using readily available climatic data for computing potential evapotranspiration.

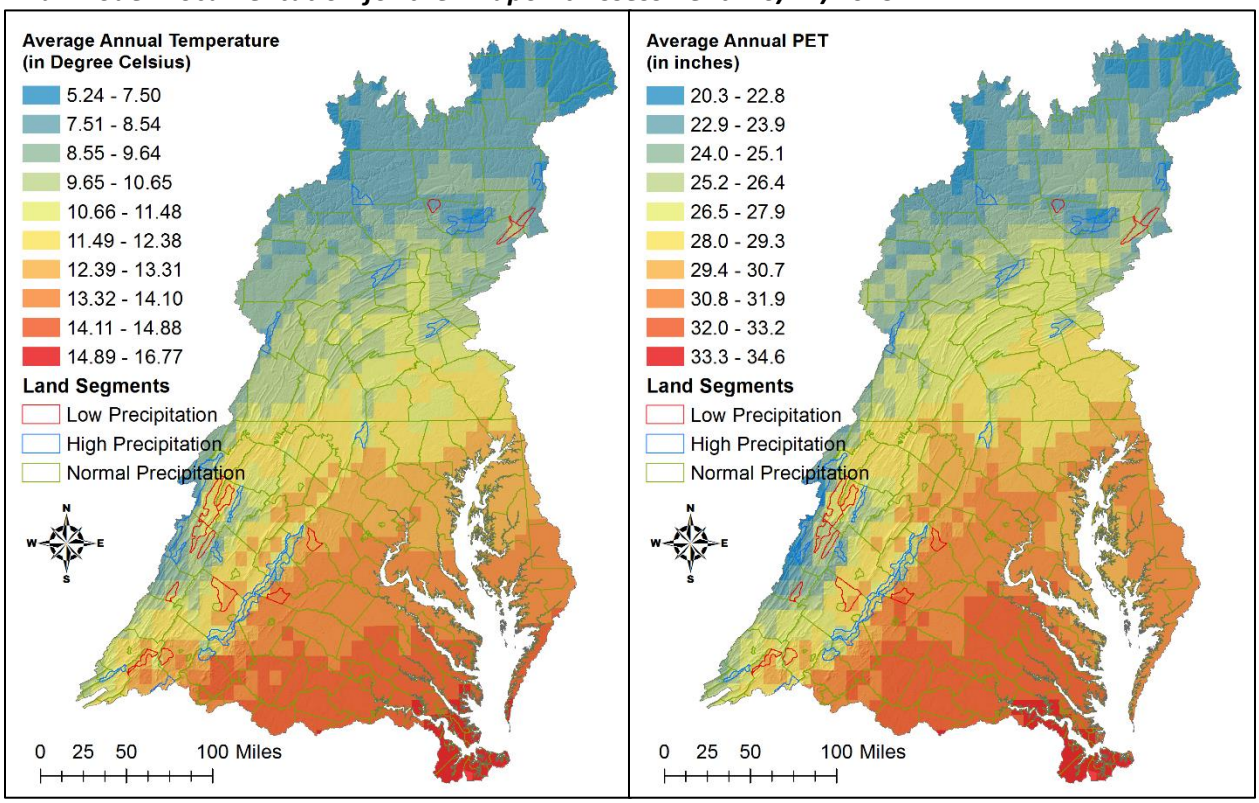

Figure 10-6: Average annual temperature and potential evapotranspiration estimated using Hamon method for the Chesapeake Bay watershed.

10.2.1.6 Dew Point Temperature

Dew point temperature was estimated from the hourly primary temperature forcing dataset and derived data for relative humidity that was calculated from specific humidity dataset. Daily dew point temperature for a land segment was estimated from the average of hourly values. The Magnus formula was used for the calculation of hourly dew point temperature:

$$DT = b * \gamma / (a - \gamma)$$

Equation 10-8

$$\gamma = a * T /(b + T) + \ln (RH)$$

Equation 10-9

where,

DT is dew-point temperature in °C
a = 17.271
b = 237.7
T is temperature in °C

10.2.1.7 Cloud Cover

Daily cloud cover for land segments was estimated from the radiation dataset. For a land-segment, hourly maximum solar radiation for an hour in a calendar year was calculated from the hourly dataset for the 30 years. Cloud cover for an hour was estimated as a function of hourly precipitation, solar radiation, and maximum long-term solar radiation for that hour. Cloud cover (CC) for an hour was calculated as:

$$CC = 10; \quad \text{if } P > 0$$
$$CC = 0; \quad \text{if } RN_{max} = 0$$
$$CC = 10 * (1 - RN) / RN_{max}$$

Equation 10-10

where,

CC is cloud cover (10 represents full cloud cover and 0 represents no cover)
RN is solar radiation
RN_{max} is the maximum observed solar radiation for a calendar hour.

Daily cloud cover was calculated from the average of the positive hourly cloud cover dataset.

10.2.2 Streamflow Observations

Daily streamflow observations were downloaded using the USGS EGRET/dataRetrieval tool. This tool is designed to retrieve USGS hydrologic data into the R environment. An R program was developed that uses USGS dataRetrieval functions to download streamflow observations for monitoring stations and create corresponding data files for the Phase 6 simulated rivers based on the file format specifications of the model calibration.

Observed streamflow data were downloaded for the expanded Phase 6 calibration period of 1985 to 2014. *Figure **10-7*** shows daily average annual flow for the monitoring stations across the watershed that were used in the model calibration. A comparison between the average streamflow observations used in the Phase 5.3.2 and Phase 6 Model is shown in *Figure **10-8***. The figure validates the assignment of the monitoring stations to the simulated river segments and the data processing. The minor deviations from the one-to-one line between the average annual observed flows for the monitoring stations in the two models can be attributed to the differences in data set period.

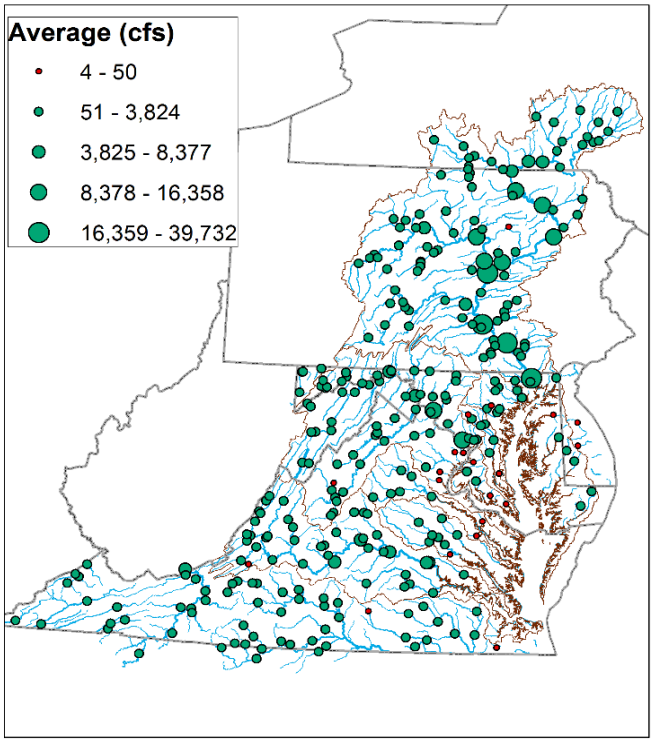

Figure 10-7: Phase 6 streamflow calibration stations. Map displays average streamflow for the period 1980 to 2014

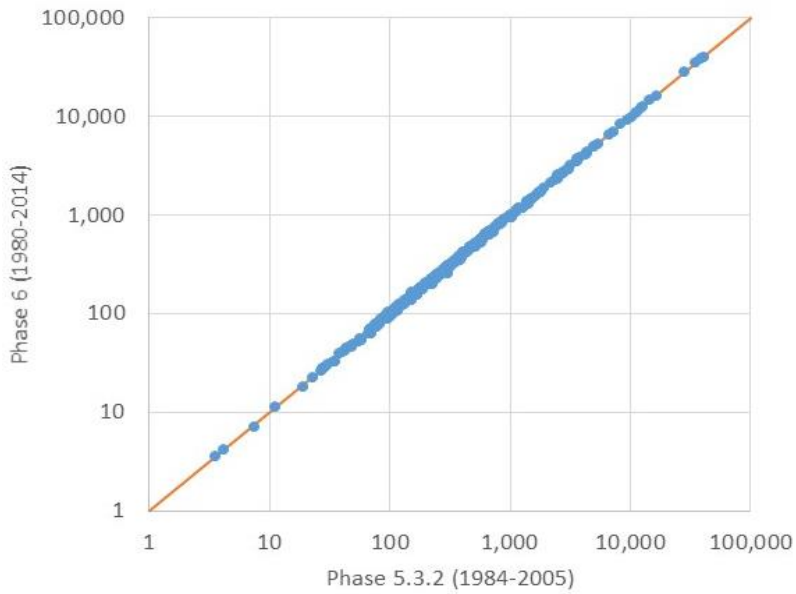

Figure 10-8: A comparison between average streamflow (in cfs) between Phase 5.3.2 and Phase 6

A total of 82 USGS streamflow monitoring stations were identified that were not used in Phase 5.3.2 model calibration but met the criteria for observations spanning a minimum of 3 years and have average

flow greater than 50 cfs. Two additional conditional criteria were applied – (a) that the drainage area of the monitoring station did not differ from the sum of upstream river segment areas by more than 5 percent and (b) that average point source flow was not more than 5 percent of the average annual streamflow. Based on this information a total of 26 new streamflow monitoring stations were identified that were suitable for use in the Phase 6 streamflow calibration (*Figure **10-9***).

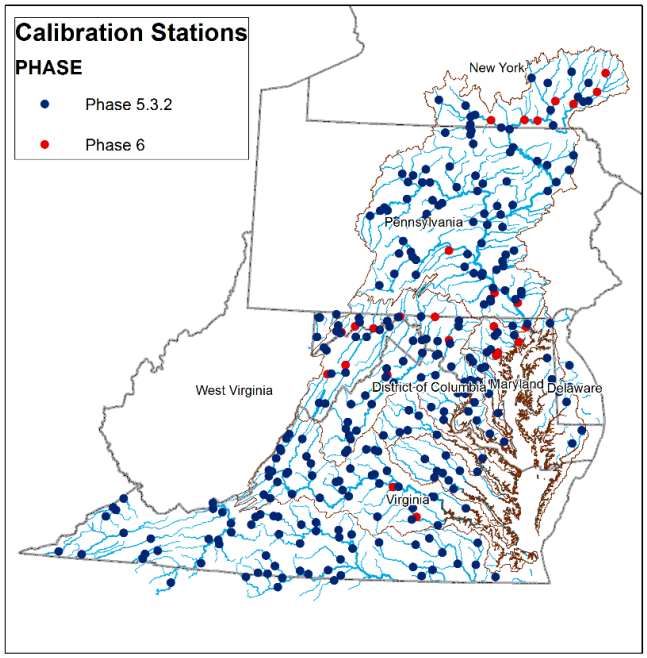

Figure 10-9: Streamflow monitoring stations used in model calibration. Observation records for monitoring stations used in Phase 5.3.2 (shown in blue) were updated to include recent observations. The 28 new streamflow monitoring stations (shown in red) were included in Phase 6 calibration.

10.2.3 Water Quality Observations

The water quality observations are used for the riverine calibration of the watershed model. Quality controlled water quality observations were collected (Langland, 2015). A set of aggregation rules were applied to the water quality observations in order to create calibration dataset for Phase 6 Model (*Table **10-4***).

Table 10-4: The aggregation rules used for creating the calibration dataset from water quality observations

Phase 6 observed data	USGS parameter name and code
Total Nitrogen	1. Total nitrogen [P600] 2. Total ammonia [P610] + total nitrate [P620] + total nitrite [P615] + total organic nitrogen [P605] 3. Total nitrite + nitrate [P630] + total kjeldahl [P625] 4. Total nitrate [P620] + total kjeldahl [P625] 5. Dissolved nitrogen [P602] + particulate nitrogen [P601] 6. Total nitrite + nitrate [P630]
Nitrate	1. Dissolved nitrite [P613] + total nitrate [P620]

	2. Total nitrite + nitrate [P630] 3. Dissolved nitrite + nitrate [P631] 4. Total nitrate [P620] 5. Dissolved nitrate [P618]
Ammonia	1. Dissolved ammonia [P608] 2. Total ammonia [P610]
Total Phosphorus	Total phosphorus [P665]
Dissolved Phosphate	Dissolved phosphate [P671]
Total Suspended Sediment	1. Total suspended sediment [P80154] 2. Total suspended solids [P530]
Dissolved Oxygen	Dissolved Oxygen [P300]
Water Temperature	Temperature [P10]
Chlorophyll a	Chlorophyll a [P32211]

The linkage between the monitoring station ID and river segment ID developed for Phase 5.3.2 were used for assigning observed data. The designation of monitoring stations to river segments were verified in GIS and corrections were made to update the designation of the stations that were incorrectly assigned (*Table **10-5***). Observations flagged as limit of detection (LOD) were left at the reported values. The values and flags were passed to the calibration routine to be handled as LOD values.

Table 10-5: Inconsistency in the designation of monitoring stations to model river segments, and recommended corrections.

STATIONID	AGENCY	LATITUDE	LONGITUDE	PHASE 5 RIVER SEGMENT	RECOMMENDED Phase 6 RIVER SEGMENT / COMMENTS
2-POT000.12	VADEQ	37.751667	-79.996950	JU4_7000_7300	JU2_7360_7000
WQN0211	PADER	40.191111	-76.731111	SL4_2140_2240	SL4_2240_2310
WQN0423	PADER	41.074722	-77.592222	SW0_1520_1600	SW3_1600_1580
WQN0418	PADER	41.261389	-77.902778	SW4_1430_1490	SW4_1490_1400
WQN0419	PADER	41.320000	-78.080833	SW3_1091_1380	SW3_1380_1490
WQN0332	PADER	41.948889	-76.517500	SU5_0610_0600	SU5_0600_0750
1AAUA007.92	VADEQ	38.463400	-77.385400	PL0_5010_5130	PL1_5690_0001
2-JKS030.65	VADEQ	37.841944	-79.989167	JU3_6950_7330	Located above point source facility

10.2.3.1 Averaging Multiple Observations Taken on the Same Day

High flow events are frequently monitored by taking multiple samples throughout the storm. The existence of days with multiple samples negatively influences quality of the calibration achieved with the Phase 6 Model's automated calibration procedure. The automated calibration procedure adjusts river simulation parameters based on a comparison of the cumulative frequency distributions (CFDs) of paired observed and simulated concentrations. Section 10.6.3.1 has a detailed description of the

calibration metrics. A sample CFD is shown in *Figure **10-50***. The observations are grab samples while the corresponding simulated concentrations are the daily average concentrations from the days on which the observations were made. Both the observed and simulated CFDs are distorted by the existence of multiple samples on the same day. The observed CFD is distorted because samples from the same day are spread throughout the distribution, and only the highest concentrations observed on the same day are in the highest percentiles of the CFD, which are used to adjust high flow parameters like the scour rate. On the other hand, for each sample taken on a particular day, an identical copy of the simulated daily average simulation is included in the CFD for comparison of the model estimate to the daily observation- an apples to oranges comparison which is essentially weighing the daily average simulation value by the sampling frequency of observations collected on the same day, not the frequency of occurrence of the observed sediment or nutrient concentration.

*Table **10-6***, shows the concentrations in the top bin (top 5 percent) of the paired observed and simulated concentrations from the NE Branch of the Anacostia River, which illustrates the problem. The observed data are instantaneous grab samples. *Table **10-6*** shows the date the sample was taken, the percentile of the daily flow on the date the sample was taken, and the total number of samples taken each day. Generally, concentrations in the top bin of the observed data are taken under high flow conditions. No other sample was taken on the day when the highest observed concentration occurred, but multiple samples were taken on most of the other days in which concentrations in the top 5 percent were observed. Four dates have two samples in the top 5 percent of the observed data, and no date has more than two samples in the top bin of data. On the other hand, for each observed sample, the simulated daily average concentration from the date is included in the empirical CDF of the simulated data. If more than one sample was taken on a date, multiple copies of the simulated daily average concentration were included in the CDF. The top bin of the simulated CDF contains multiple copies of the daily average concentration from just four sampling dates.

It is clear that the CDFs of the observed and simulated concentrations do not measure the same thing. However, they could be made more similar by substituting the flow-weighted average of the concentrations observed on the same day for the individual observations and keeping only one copy of the daily average simulated concentration for that day.

Table 10-6: Top bin of paired observed and simulated sediment concentrations, Northeast Branch of the Anacostia River

Observed					Simulated		
Date	Flow (cfs)	Flow Percentile	TSS (mg/l)	Samples Collected	Date	Flow Percentile	TSS (mg/l)
4/2/2005	1,500	0.996167	1,980	1	10/8/2005	0.999382	2,418.1
5/26/2009	2,100	0.998162	1,730	4	10/8/2005	0.999382	2,418.1
8/14/2011	572	0.977513	1,730	2	10/8/2005	0.999382	2,418.1
8/14/2011	572	0.977513	1,710	2	10/8/2005	0.999382	2,418.1
1/14/2005	2,110	0.998279	1,670	4	7/8/2005	0.992935	2,417.9
8/28/2009	498	0.971568	1,600	4	7/8/2005	0.992935	2,417.9
7/8/2005	975	0.991083	1,580	5	7/8/2005	0.992935	2,417.9
8/12/2010	575	0.977786	1,430	1	7/8/2005	0.992935	2,417.9
6/3/2009	420	0.964685	1,400	2	7/8/2005	0.992935	2,417.9
9/30/2010	1,420	0.995581	1,310	4	3/23/2005	0.997704	2,242.9
1/14/2005	2,110	0.998279	1,300	4	3/23/2005	0.997704	2,242.9
8/18/2010	2,020	0.998045	1,290	3	3/23/2005	0.997704	2,242.9
8/15/2011	517	0.973837	1,230	1	3/23/2005	0.997704	2,242.9
8/28/2009	498	0.971568	1,180	4	3/23/2005	0.997704	2,242.9
5/9/2008	1620	0.996832	1170	3	3/23/2005	0.997704	2242.9
5/26/2009	2100	0.998162	1170	4	5/12/2008	0.998852	2162.3

To address the issue, the data set of observations used in the calibration was revised by averaging the observations taken in the same day. The following rules for averaging observations taken on the same day were applied:

1. If the corresponding hourly flow is available for all samples taken on the same day, then these samples are to be replaced by the flow-weighted average of the samples; if this condition is not met, then the samples are replaced by their arithmetic average.
2. For flow-weighted averages, the hourly average flow is matched with the recorded hour of the observation (in other words, the time of the observation is truncated at the hour, not rounded to the hour).
3. If any sample collected in a single day has a qualifier that signals it is less than reported value (usually "<"), then the average sample is given the ",<" qualifier; otherwise, the qualifier for the average sample is the null qualifier, "-".
4. Flow-weighted averages and arithmetical averages are represented by "FWA" and "AA", respectively, in the station field of the observation data file.

*Table **10-7*** summarizes across stations the number of dates on which multiple samples were collected for total nitrogen, total phosphorus, and total suspended sediment. About 10 percent of the sample dates had multiple observations. On most of these dates only two samples were taken. Table 10-8 shows the percent of sampling dates with multiple observations at the RIM stations. Generally, sample dates with multiple observations are more common than average at RIM stations. For some of the

Virginia RIM stations, about a third or more of the sample dates have multiple observations of phosphorus and sediment.

Table 10-7: Number of sampling dates with multiple observations by constituent

Constituent	Total Number of Sampling Dates	Sampling Dates with a Single Observation	Sampling Dates with Given Number of Observations				
			More than 1	2	3	4	5 or More
Total Nitrogen	50,402	45,967	4,435	3,672	374	147	242
Total Phosphorus	56,632	51,319	5,313	4,151	702	200	260
Total Suspended Sediment	66,058	53,096	6,481	4,633	852	367	629

Table 10-8: Percent of sample dates with multiple observations, River Input Monitoring (RIM) Stations

Name	TN	TP	TSS
Appomattox	10%	32%	33%
Choptank	10%	9%	13%
James	14%	38%	38%
Mattaponi	8%	30%	36%
Pamunkey	14%	32%	36%
Patuxent	14%	16%	18%
Potomac	15%	18%	15%
Rappahannock	11%	12%	12%
Susquehanna	13%	13%	16%

Phase 6 model calibration was made using the water quality observations before and after the implementation of averaging of samples reported on the same day. Measuring the quality of the simulation by the Nash-Sutcliffe efficiency (NSE) between Phase 6 and WRTDS yields, averaged observations on the same day improved the simulation of nitrogen, phosphorus, and sediment. The NSE for nitrogen increased from 0.9169 to 0.9191, the NSE for phosphorus increased from 0.7626 to 0.8056, and the NSE for sediment from 0.6397 to 0.7960. The bias between Phase 6 simulated average annual sediment loads and WRTDS also decreased significantly at the Potomac and James RIM stations, although overall results were more ambiguous. Although its contribution to improving the nitrogen and phosphorus calibrations may be more modest, averaging observations made on the same day does seem to have made a significant contribution to improving the sediment calibration.

10.2.3.2 Data Quality Checks and Comparison with Phase 5.3.2

A rigorous quality check was performed on the processed calibration dataset by comparing them to Phase 5.3.2 dataset. A series of tables and figures are shows incremental analysis of the datasets. An overall data integrity check was performed by comparing the total number of observation samples between the two datasets (*Table **10-9***). A net increase in the number of observations is attributed to an expanded period of dataset in Phase 6 Model. *Figure **10-11*** shows the annual comparison of number of records.

Table 10-9: Total number of water quality observations in calibration dataset

Observations	Phase 5.3.2	Phase 6	Percent increase
Total Nitrogen	28,622	54,462	90%
Total Phosphorus	47,370	62,334	32%
Total Suspended Solids	67,324	70,526	5%

Figure ***10-11***, *Figure* ***10-12***, and Figure **10-13** show a geospatial assessment of increase in the number of observations and addition of new water quality monitoring stations in Phase 6 water quality calibration dataset. Spatial variability in observed concentration over the model calibration period of 1985-2014 is shown in *Figure* ***10-14***. *Figure* ***10-15***, *Figure* ***10-16***, and *Figure* ***10-17*** show monitoring segment level comparison of all observation samples in the calibration dataset.

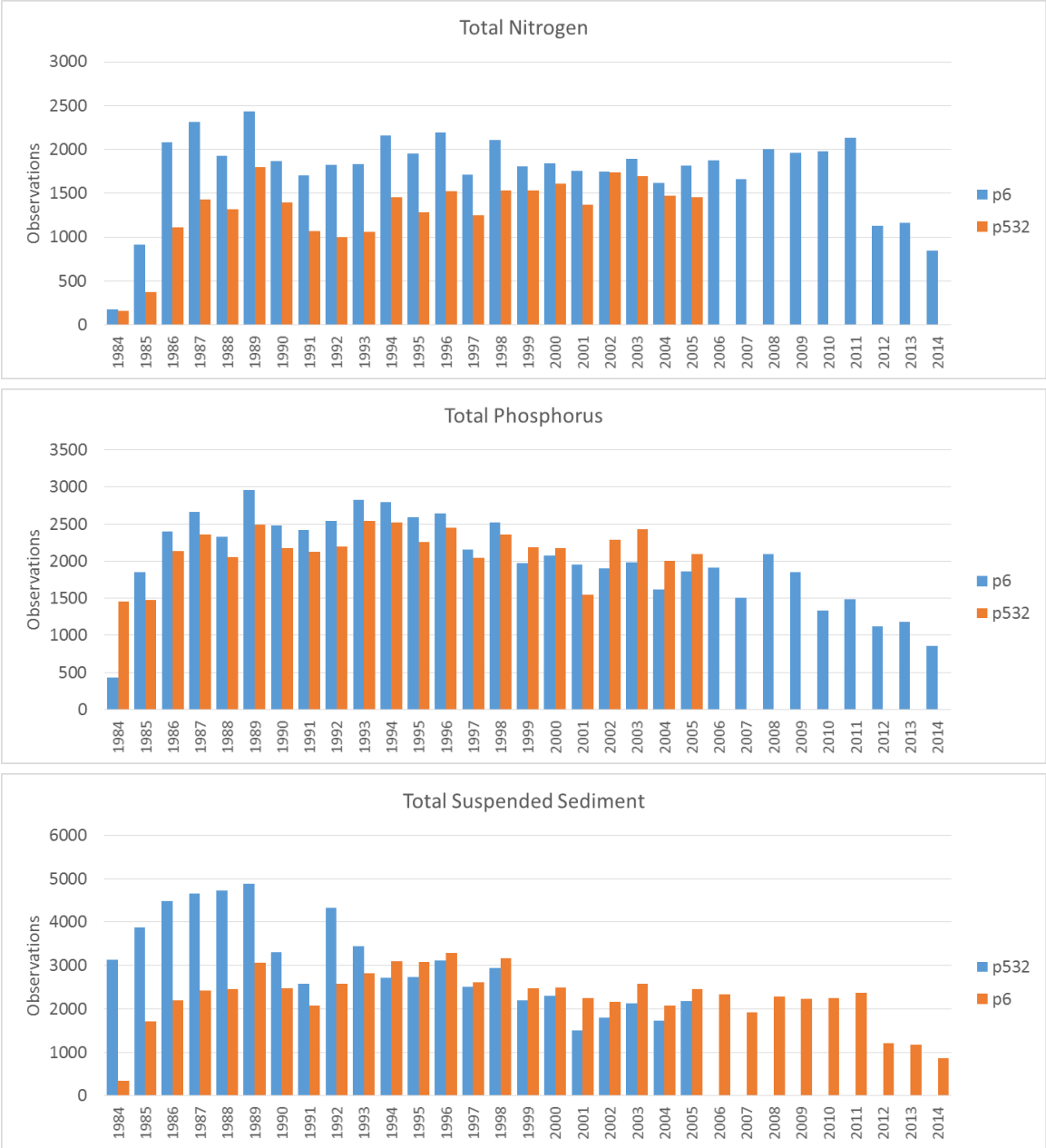

Figure 10-10: Comparison of number of observations in Phase 5.3.2 and Phase 6 calibration datasets for (a) total nitrogen, (b) total phosphorus, and (c) total suspended sediment.

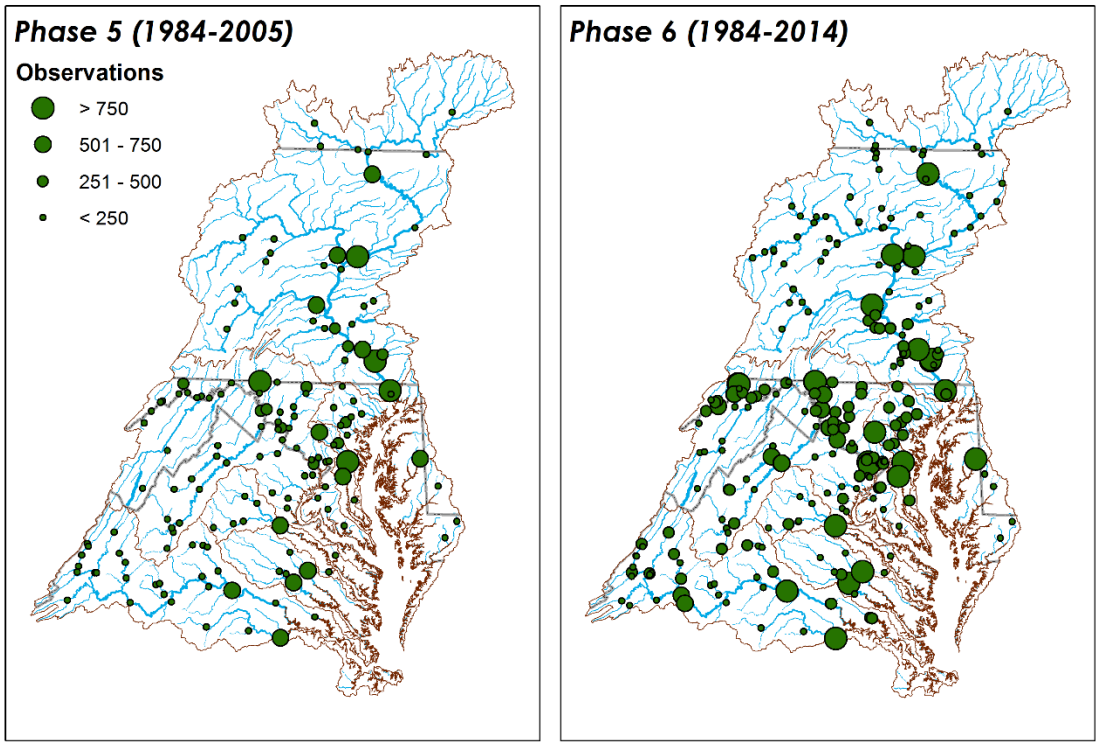

Figure 10-11: Number of total nitrogen observations for the monitoring sites in Phase 5.3.2 and Phase 6 calibration data set showing additional new monitoring sites for model calibration

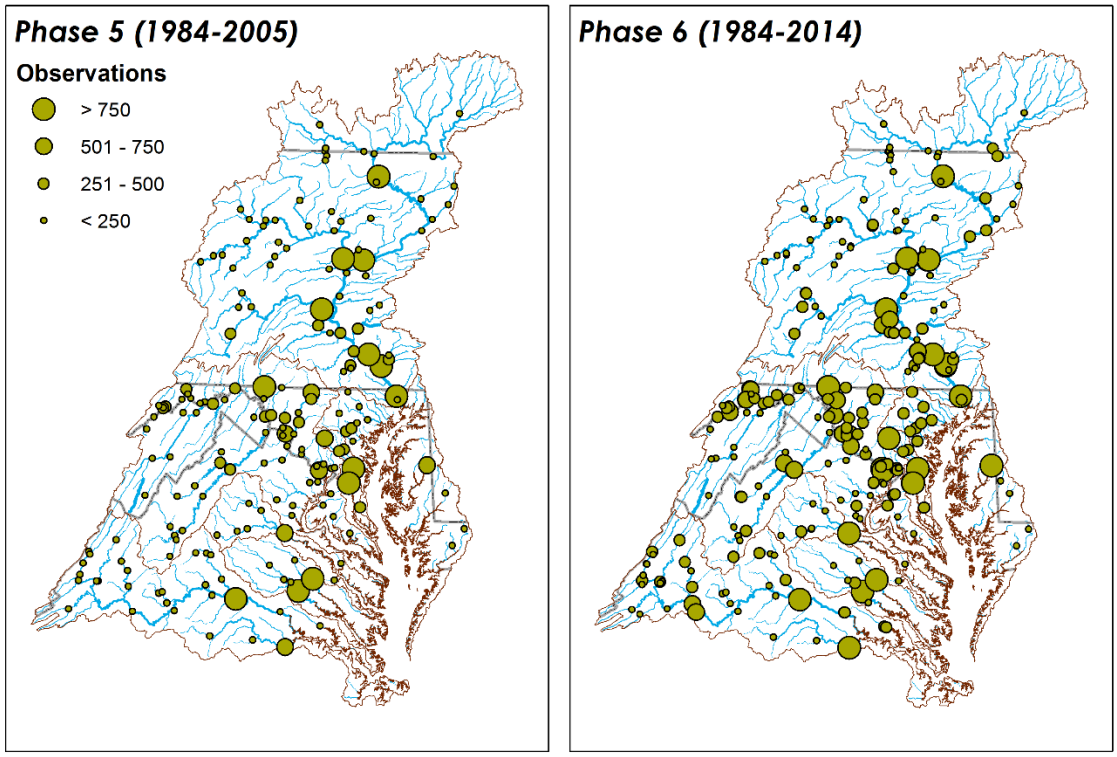

Figure 10-12: Number of total phosphorus observations for the monitoring sites in Phase 5.3.2 and Phase 6 calibration dataset showing additional new monitoring sites for model calibration

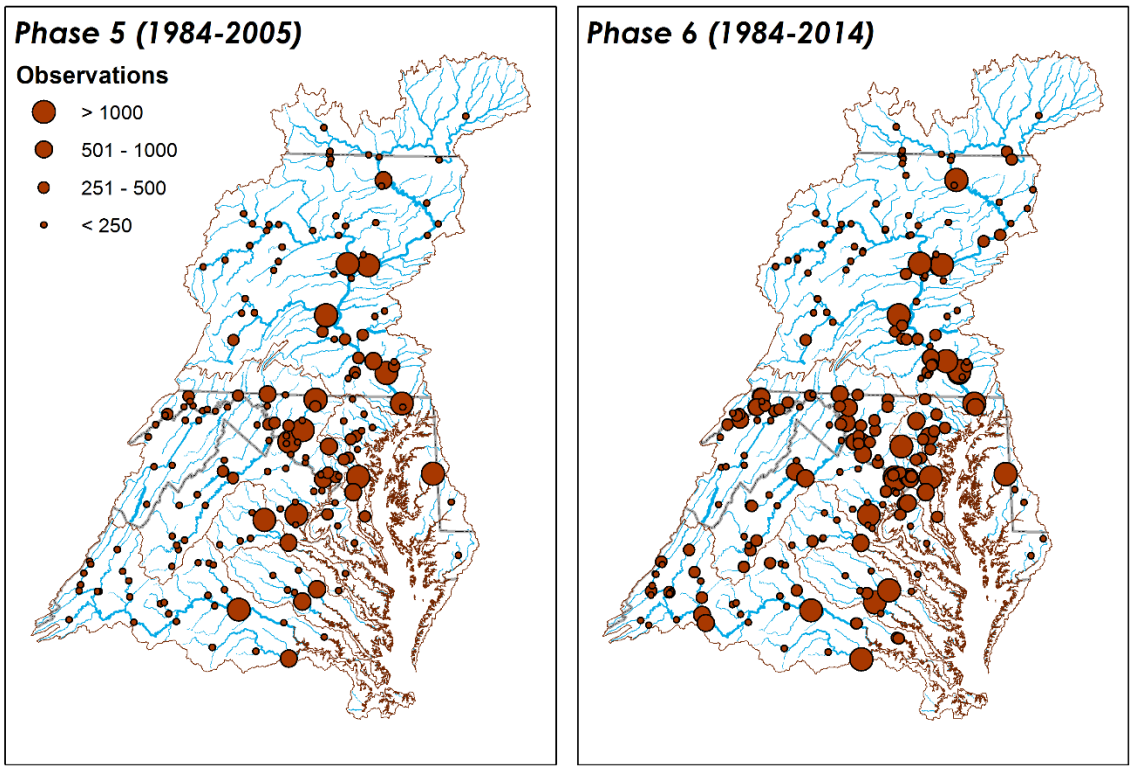

Figure 10-13: Number of total suspended sediment observations for the monitoring sites in Phase 5.3.2 and Phase 6 calibration dataset showing additional new monitoring sites for model calibration

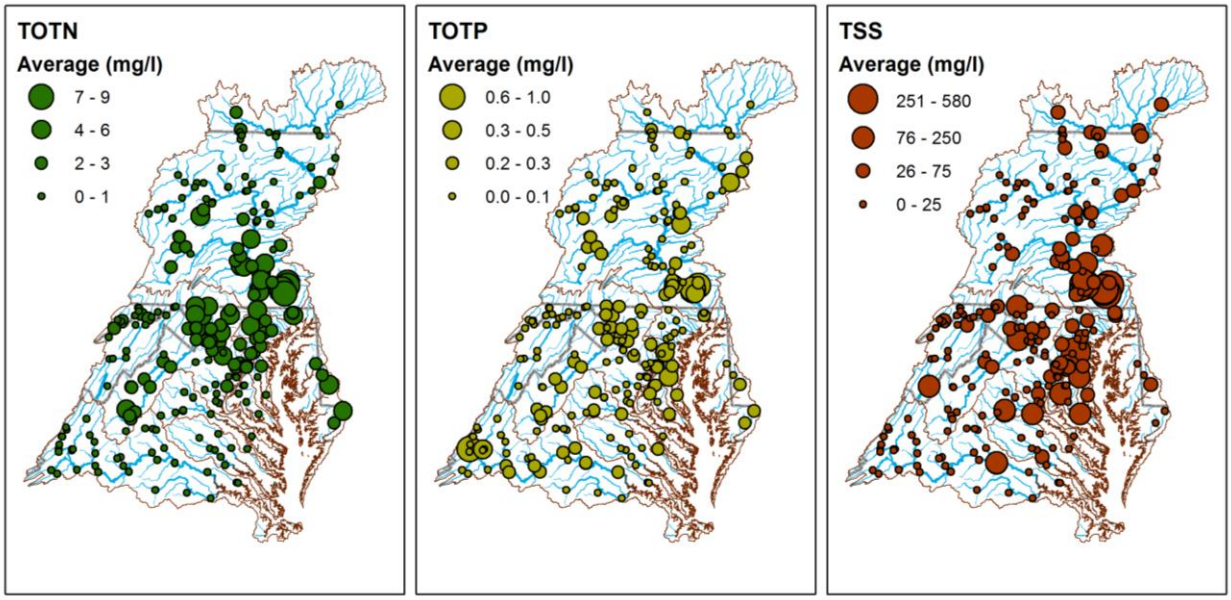

Figure 10-14: Spatial variability in observed concentration for (a) total nitrogen, (b) total phosphorus, (c) suspended sediment.

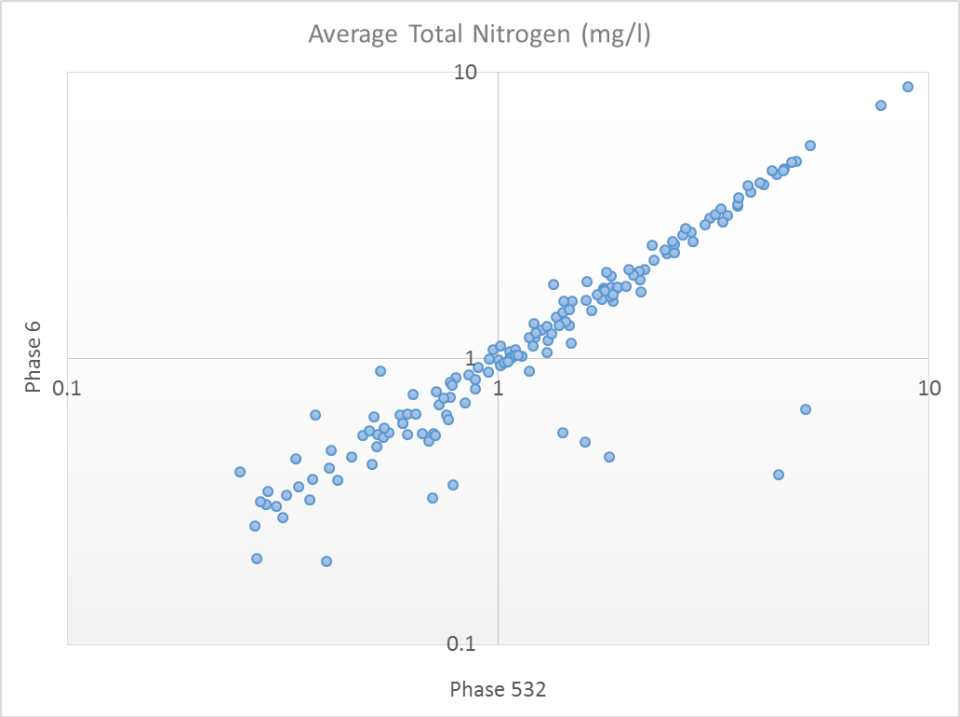

Figure 10-15: Average nitrogen concentration of observation samples in Phase 5.3.2 and Phase 6 calibration dataset. The dots on the chart correspond to individual monitoring stations.

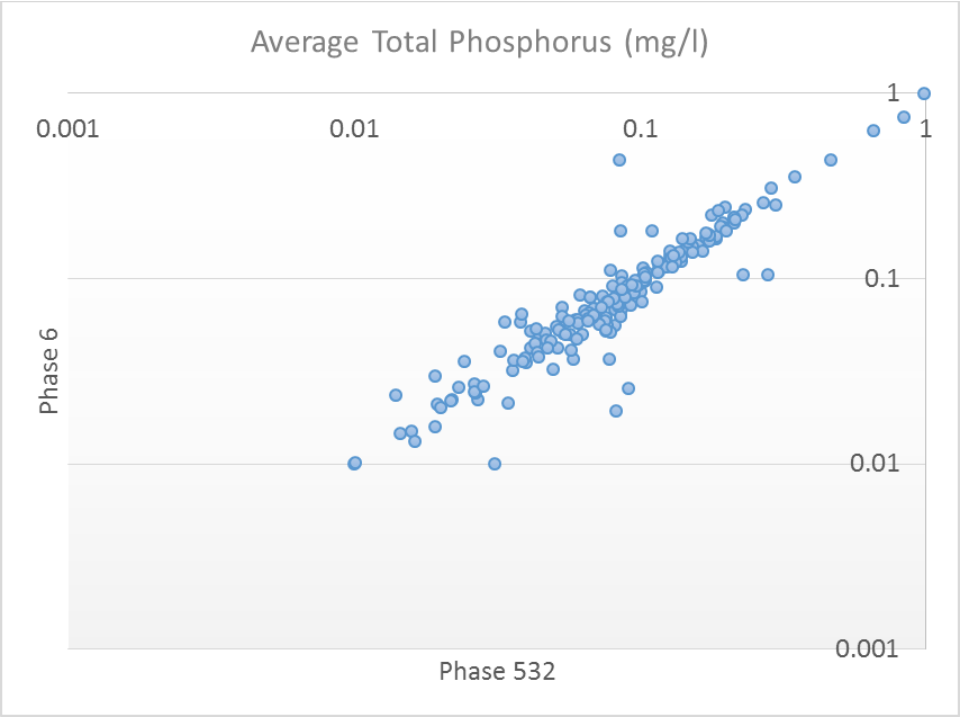

Figure 10-16: Average phosphorus concentration of observation samples in Phase 5.3.2 and Phase 6 calibration dataset. The dots on the chart correspond to individual monitoring stations.

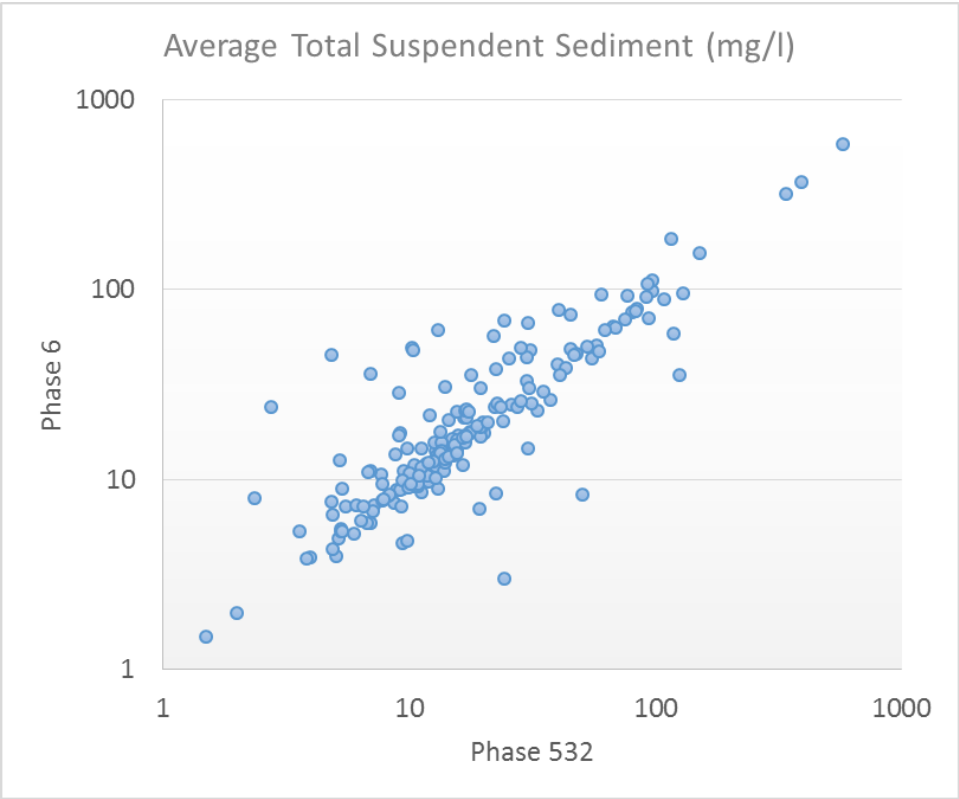

Figure 10-17: Average suspended solid concentration of observation samples in Phase 5.3.2 and Phase 6 calibration dataset. The dots on the chart correspond to individual monitoring stations.

During the fatal flaw review period. Delaware provided additional concentration data for the Nanticoke River for total nitrogen, nitrate, ammonia, total phosphorus, dissolved phosphate, total suspended sediment, water temperature, and chlorophyll-*a*.

10.2.4 USGS-WRTDS Estimated Loads

The USGS-WRTDS model (Hirsch et al. 2010; Hirsch and Di Cicco 2014) is a statistical model especially designed to estimate long-term trends in loads and concentrations. The starting point is the acknowledgment that over time, the relation between independent variables like flow and seasonality to concentration may change in a way that would fail to be accounted for by adding variables representing time to a single static regression model. This is particularly true of watersheds that have been subject, over time, to management actions to control nutrient or sediment exports. The WRTDS is a dynamic model akin to Locally Weighted Scatterplot Smoothing (LOWESS) methods. Specifically, WRTDS estimates of a concentration at a point in time are determined by the following steps:

1. On the two-dimensional range of interest in time T and flow Q, divide the domain into a grid of points (Q, T);
2. At each point, estimate the log of the concentration ln c according to the following weighted linear regression:

$$\ln c = \beta_0 + \beta_1 * t + \beta_2 * \ln q + \beta_3 * \sin 2\pi t + \beta_4 * \cos 2\pi t + \epsilon$$

Equation 10-11

where:

c = estimated concentration
t = time (yrs)
q = daily average flow (cfs)
ε = error
In each regression, observations are weighted by their difference in time, flow and season from the estimation point (Q, T).

3. A concentration estimate at a particular point (q_1, t_1) is then obtained from the set of regressions on Q's and T's by interpolation.

In this formulation, the WRTDS estimated concentrations can change over time, in response to changes in observed data. The WRTDS is especially powerful at estimating flow-normalized trends, but this topic lies outside the scope of this work.

Table 10-10: Mapping between the USGS WRTDS and Phase 6 simulated loads.

Phase 6 Water Quality Variable	USGS Parameter name and Code
Total Nitrogen	Total nitrogen [P600]
Nitrate	1. Total nitrite + nitrate [P630] 2. Dissolved nitrite + nitrate [P631]
Total Phosphorus	Total phosphorus [P665]
Dissolved Phosphate	Dissolved phosphate [P671]
Total Suspended Sediment	1. Total suspended sediment [P80154] 2. Total suspended solids [P530]

A list of stations for which nitrogen and phosphorus load estimates are available from the USGS in the Chesapeake Bay watershed is shown in *Table **10-11***. The table shows the USGS gage number, and where applicable, the Phase 6 river reach associated with the gage. The USGS estimates loads at 65 locations, 62 of which are associated with a Phase 6 reach and can be used for model verification. *Table **10-11*** also shows the number of years for which WRTDS loads are available for these sites.

In Phase 5.3.2, estimates of loads were obtained from USGS-ESTIMATOR. *Table **10-12*** compares the difference in average annual load estimates at the River Input Monitoring (RIM) stations between ESTIMATOR and WRTDS. The loads from ESTIMATOR are 20-year averages (1985-2004), but the loads from WRTDS are 28-year averages (1985-2012), reflecting the difference in the Phase 5.3.2 (1985-2005) and Phase 6 (1985-2014) calibration periods. Thus, the load differences reflect a difference in both statistical model and in averaging period. In all but one case, when the load difference is greater than

10 percent, the average annual WRTDS load is smaller than ESTIMATOR load. The exception is the Susquehanna River where the WRTDS phosphorus load is 33 percent larger than the ESTIMATOR load, probably because of Conowingo Reservoir infill by sediment and sediment associated nutrients (Hirsch 2012). The WRTDS estimated phosphorus loads are smaller in comparison to Estimator estimated loads in the Rappahannock River (-24 percent), the Potomac River (-17 percent), Pamunkey River (-12 percent), and the Appomattox River (-11 percent). Average annual nitrogen loads estimated by WRTDS are also smaller than ESTIMATOR loads in the Rappahannock (-12 percent), Appomattox (-11 percent), and Pamunkey (-10 percent) Rivers.

Table 10-11: Location of monitoring sites in the Chesapeake Bay watershed where WRTDS loads are available.

Gage ID	Station Name	Short Name	P6 River segment	Years
01487000	Nanticoke River near Bridgeville, DE	Nanticoke River	EL0_4562_0003	8
01488500	Marshyhope Creek near Adamsville, DE	Marshyhope Creek	EL2_4400_4590	8
01491000	Choptank River near Greensboro, MD	Choptank River	EM2_3980_0001	28
01491500	Tuckahoe Creek near Ruthsburg, MD	Tuckahoe Creek	No Segment	
01495000	Big Elk Creek at Elk Mills, MD	Big Elk Creek	No Segment	
01502500	Unadilla River at Rockdale NY	Unadilla River	SU4_0300_0310	8
01503000	Susquehanna River at Conklin NY	Susquehanna River (Conklin)	SU6_0480_0520	8
01515000	Susquehanna River near Waverly NY	Susquehanna River (Waverly)	SU7_0720_0003	9
01529500	Cohocton River near Campbell NY	Cohocton River	SU3_0370_0490	8
01531000	Chemung River at Chemung NY	Chemung River	SU5_0610_0600	9
01531500	Susquehanna River at Towanda, PA	Susquehanna River (Towanda)	SU7_0850_0730	28
01536500	Susquehanna River at Wilkes-Barre, PA	Susquehanna River (Wilkes-Barre)	SU7_1120_1140	28
01540500	Susquehanna River at Danville, PA	Susquehanna River (Danville)	SU8_1610_1530	28
01542500	WB Susquehanna River at Karthaus, PA	WB Susquehanna River (Karthaus)	SW5_1540_0003	9
01549760	WB Susquehanna River at Jersey Shore, PA	WB Susquehanna River (Jersey Shore)	SW7_1470_1340	8
01553500	West Branch Susquehanna River at Lewisburg, PA	WB Susquehanna River (Lewisburg)	SW7_1640_0003	28
01555000	Penns Creek at Penns Creek, PA	Penns Creek	SL3_1710_1740	9
01562000	Raystown Branch Juniata River at Saxton, PA	Raystown Branch	SJ4_2660_2360	9
01567000	Juniata River at Newport, PA	Juniata River	SJ6_2130_0003	28
01568000	Sherman Creek at Shermans Dale, PA	Sherman Creek	SL3_2290_2260	9
01570000	Conodoguinet Creek near Hogestown, PA	Conodoguinet Creek	SL4_2370_2330	9
01571500	Yellow Breeches Creek near Camp Hill, PA	Yellow Breeches Creek	SL3_2400_2440	9
01573560	Swatara Creek near Hershey, PA	Swatara Creek	SL4_2140_2240	9
01574000	West Conewago Creek near Manchester, PA	West Conewago Creek	SL3_2460_2430	9
01576000	Susquehanna River at Marietta, PA	Susquehanna River (Marietta)	SL9_2490_2520	27
01576754	Conestoga River at Conestoga, PA	Conestoga River	SL3_2420_2700	28
01576787	Pequea Creek at Martic Forge, PA	Pequea Creek	SL2_2410_2700	9
01578310	Susquehanna River at Conowingo, MD	Susquehanna River (Conowingo)	SL9_2720_0001	28
01578475	Octoraro Creek near Richardsmere, MD	Octoraro Creek	SL2_2480_0001	7
01580520	Deer Creek near Darlington, MD	Deer Creek	SL2_3060_0001	8
01582500	Gunpowder Falls at Glencoe, MD	Gunpowder Falls	WU2_3020_3320	28
01586000	North Branch Patapsco River at Cedarhurst, MD	N B Patapsco River	No Segment	
01589300	Gwynns Falls at Villa Nova, MD	Gwynns Falls	WM1_3660_3910	11
01591000	Patuxent River near Unity, MD	Patuxent River (Unity)	XU0_4130_4070	28
01594440	Patuxent River near Bowie, MD	Patuxent River (Bowie)	XU3_4650_0001	28
01594526	Western Branch at Upper Marlboro, MD	Western Branch	XL1_4690_0001	8
01599000	Georges Creek at Franklin, MD	Georges Creek	PU1_3940_3970	28
01601500	Wills Creek near Cumberland, MD	Wills Creek	PU3_3680_3890	28
01604500	Patterson Creek near Headsville, WV	Patterson Creek	PU2_4360_4160	8
01608500	South Branch Potomac River near Springfield, WV	S B Potomac River	PU4_4310_4210	8
01609000	Town Creek near Oldtown, MD	Town Creek	PU2_3370_4020	7
01610155	Sideling Hill Creek near Bellegrove, MD	Sideling Hill Creek	PU1_3100_3690	7
01611500	Cacapon River near Great Cacapon, WV	Cacapon River	PU3_3860_3610	8
01613095	Tonoloway Creek near Hancock, MD	Tonoloway Creek	PU1_3030_3440	8

Gage ID	Station Name	Short Name	P6 River segment	Years
01613525	Licking Creek at Pectonville, MD	Licking Creek	PU2_3080_3640	8
01614500	Conococheague Creek at Fairview, MD	Conococheague Creek	PU3_3290_3390	28
01616500	Opequon Creek near Martinsburg, WV	Opequon Creek	PU2_4220_3900	8
01619000	Antietam Creek near Waynesboro, PA	E B Antietam Creek	PU0_3000_3090	8
01619500	Antietam Creek near Sharpsburg, MD	Antietam Creek	PU2_3090_4050	28
01631000	S F Shenandoah River at Front Royal, VA	S F Shenandoah River	PS5_5240_5200	18
01634000	N F Shenandoah River near Strasburg, VA	N F Shenandoah River	PS3_5100_5080	18
01637500	Catoctin Creek near Middletown, MD	Catoctin Creek	PM1_3510_4000	28
01639000	Monocacy River at Bridgeport, MD	Monocacy River	PM2_2860_3040	28
01646580	Potomac River at Chain Bridge, at Washington, DC	Potomac River	PM7_4820_0001	28
01651000	Northwest Br Anacostia River Nr Hyattsville, MD	N B Anacostia River	PL0_4510_0001	7
01667500	Rapidan River near Culpeper, VA	Rapidan River	RU3_6170_6040	8
01668000	Rappahannock River near Fredericksburg, VA	Rappahannock River	RU5_6030_0001	28
01671020	North Anna River at Hart Corner near Doswell, VA	North Anna River	YP3_6330_6700	28
01673000	Pamunkey River near Hanover, VA	Pamunkey River	YP4_6720_6750	28[1]
01674500	Mattaponi River near Beulahville, VA	Mattaponi River	YM4_6620_0003	28
02024752	James River at Blue Ridge Pkwy Nr Big Island, VA	James River (Big Island)	JL6_7160_7440	8
02035000	James River at Cartersville, VA	James River (Cartersville)	JL7_7100_7030	28
02037500	James River near Richmond, VA	James River (Richmond)	JL7_6800_7070	20
02041650	Appomattox River at Matoaca, VA	Appomattox River	JA5_7480_0001	28
02042500	Chickahominy River near Providence Forge, VA	Chickahominy River	JB3_6820_7053	28

[1] 20 years for phosphorus

Table 10-12: Comparison of ESTIMATOR (1985-2004) and WRTDS (1985-2012) average annual loads (lb/yr) for total nitrogen and total phosphorus at River Input Monitoring (RIM) stations.

RIM Stations	River segments	Nitrogen		Phosphorus	
		WRTDS	ESTIMATOR	WRTDS	ESTIMATOR
Choptank River	EM2_3980_0001	486,200	489,400	30,630	28,330
Appomattox River	JA5_7480_0001	1,405,000	1,582,000	132,100	149,200
James River (Cartersville)	JL7_7100_7030	11,240,000	11,930,000	2,539,000	2,799,000
Potomac River	PM7_4820_0001	50,690,000	54,560,000	3,957,000	4,784,000
Rappahannock River	RU5_6030_0001	4,222,000	4,813,000	657,000	862,400
Patuxent River (Bowie)	XU3_4650_0001	1,569,000	1,691,000	122,400	123,100
Mattaponi River	YM4_6620_0003	609,700	638,200	57,100	59,750
Pamunkey River	YP4_6720_6750	1,390,000	1,550,000	160,000	181,700
Susquehanna River (Conowingo)	SL9_2720_0001	139,700,000	136,700,000	6,163,000	4,649,000

10.3 Hydrology Simulation

The hydrologic responses of landscapes are simulated using HSPF (Bicknell et al., 1997; 2001; Donigian et al. 1984; Johanson et al. 1980). The HSPF-PWATER module is used for simulating the hydrologic response of pervious land uses with processes such as interception storage, evapotranspiration, infiltration, and surface water and groundwater runoff. The HSPF-IWATER module is used for simulating the response of impervious land uses with processes such as interception storage, evaporation, and

surface water runoff. Each major land use type is parameterized separately so that the hydrologic simulation is sensitive to changes in land use.

The HSPF-HYDR module is used for hydraulic simulation of the rivers and reservoirs. The HSPF-HYDR module uses a mass balance approach based on a stage-volume-discharge relationship specified for river reaches. For further details on the structure of the HSPF model, see Bicknell et al. (2001).

HSPF requires that each simulated river reach or reservoir have a defined stage-volume-area-discharge relationship. That relationship is represented as a table rather than an analytic function. The HSPF term for the table is an FTABLE. Phase 6 uses the FTABLEs that were generated for the Phase 5.3 Model in a watershed wide study (Moyer and Bennett 2007) that related watershed size to stream characteristics for a given physiographic region. It was found that those relationships did not hold for reservoirs. Therefore, additional work was done to determine the appropriate stage-volume-discharge relationship for 42 of the largest reservoirs in the Chesapeake watershed (Appendix 10A).

Observed flow data from USGS streamflow gauging stations were used for the calibration of Phase 6 Model at 254 stations (Appendix 10B) in the Chesapeake Bay watershed. Informed by previous HSPF automated hydrology calibrations (Flynn et al. 1995) an automated calibration method was used (USEPA 2010a-08). Automated hydrology calibration provides the ability to perform a repeatable calibration, while ensuring that sub-watersheds across the Chesapeake watershed are treated in a consistent manner. The automated calibration method was applied primarily to parameters governing the hydrology simulation on pervious land. Outside the FTABLEs, only a few model parameters are used to characterize the river reaches. Most of those, such as reach length and change in elevation, were determined by GIS analysis.

10.3.1 Stage-Volume-Area-Discharge Tables (FTABLEs)

The Phase 6 Model uses the same FTABLEs that were used in the Phase 5.3.2 (USEPA 2010a-08). Eight additional simulated reservoirs were added, and the FTABLEs for those were provided by the respective states.

10.3.2 Hydrology Calibration

The Phase 6 Model uses updated and expanded inputs for many data products, including but not limited to the dataset for land use, precipitation, meteorological forcing, and streamflow observations. For the calibration of hydrology simulation, the Phase 6 Model uses the same automated calibration system that was used for the calibration of the Phase 5.3.2 Model. However, the automated calibration system in Phase 6 was parallelized to take advantage of high-performance computing.

10.3.2.1 Overview of hydrology calibration

The automated calibration procedure iteratively adjusts hydrologic parameter values on the basis of the agreement of simulated and observed hydrograph statistics at downstream calibration stations. The parameters are adjusted based on model performance statistics that summarize agreement between certain aspects of the simulated and observed hydrographs. The process for adjusting the model parameters are the same as that of the Phase 5.3.2 Model. The process uses decision rules that relate model parameters to model performance statistics to determine changes in the model parameters that will improve agreement.

The overall calibration process is a significantly simple technique as compared to other gradient-based or evolutionary algorithm-based optimization methods. The optimization process uses fixed derivatives of the model parameters with respect to the calibration objective (in other words sensitivity of a parameter to the calibration objective) over the entire calibration process. The derivatives were determined *a priori* on the basis of initial sensitivity analyses. The application of fixed derivatives speeds up the optimization by orders of magnitude, however, it can be used only when the parameters that are being calibrated are reasonably uncorrelated. Low values of sensitivity were selected to reduce oscillation of parameters during the calibration process. The calibration process simultaneously optimizes multiple calibration objectives rather than a single objective. However, each model parameter was assigned to optimize a separate calibration objective. A full description is available in USEPA 2010a-08.

10.3.2.2 Calibrated Hydrologic Parameters

The HSPF-PWATER module simulates the hydrology of a unit of homogeneous land segment in HSPF using approximately 20 parameters, some of which vary monthly. The hydrology simulation is sensitive to the values of only a few parameters. Lumb et al. (1994) developed an expert system for calibrating HSPF and identified a set of sensitive parameters. Doherty and Johnston (2003) using automated calibration methods, found a similar set of sensitive HSPF hydrology parameters. *Table **10-13*** lists the key hydrologic parameters that were calibrated, and the range over which they were allowed to vary during the calibration. The rest of the parameters were either set to default values or derived using GIS analysis of geospatial datasets available for the watershed. The default values and permitted range were set based on BASINS Technical Note 6 on parameterization (USEPA 2000).

Table 10-13. Key hydrology calibration parameters

Parameter	Description	Permitted range
LAND_EVAP	PET adjustment (similar to pan evaporation coefficient)	0.70 – 1.30
INFILT	Infiltration rate	0.001 – 1.181
LZSN	Lower zone soil moisture storage index	6.0 – 14.0
AGWR	Baseflow recession coefficient	0.92 – 0.995
INTFW	Ratio of interflow to surface runoff	1.0 – 5.0
IRC	Interflow recession coefficient	0.3 – 0.85
AGWTP	Evapotranspiration from groundwater storage	0.0001 – 0.6
KVARY	Non-exponential groundwater recession	0.000001 – 2.0

The upper zone soil moisture storage index (UZSN) was set as a fixed fraction of the lower zone soil moisture storage index (LZSN) as recommended in USEPA (2000). The ratio between UZSN and LZSN for major land uses are shown in *Table **10-14***.

Table 10-14. Ratio of Soil Moisture Storage Index for Upper Zone (UZSN) to Lower Zone (LZSN) by land uses

Land use	Natural	Crop	Grass, pasture, hay	Developed
UZSN: LZSN	0.12	0.14	0.1	0.08

Also, as recommended in USEPA (2000), the UZSN was allowed to vary monthly for cropland, to better represent how storage is affected by the crop growth cycle. The ratio of the monthly UZSN to its maximum value are shown in *Table **10-15***.

Table 10-15. Fractions determining monthly parameter values for upper zone soil moisture index

Month	Jan	Feb	Mar	Apr	May	Jun	Jul	Aug	Sep	Oct	Nov	Dec
Fraction	0.6	0.6	0.6	0.6	0.6	0.7	0.95	1.0	1.0	0.8	0.7	0.65

As shown in *Table* ***10-13***, eight model parameters were calibrated for each land uses. The parameters were adjusted spatially for the 235 Phase 6 Model land segments depending on the agreement between a number of hydrograph characteristics of simulated and observed flows at downstream monitoring stations. Section 10.3.2.5 provides more detail on linkage between the land segment and monitoring stations. However, each land segment was composed of several pervious land uses, and therefore insufficient information was available in the calibration data set to individually calibrate each pervious land use in each land-segment. To overcome this, the parameter values for other land uses were first grouped based on four major land use classes: natural; crops; pervious developed; and a grass, pasture, and hay category. In addition, the parameters for the four major land use classes were specified as a fraction of the crop land use parameters. The ratio between the parameter values for the crop and other major land use classes are shown in *Table 10-16*.

Table 10-16. Key hydrology parameter values for the major land use classes expressed relative to crop parameters

Land use	INFILT	LZSN	AGWR	INTFW	IRC	AGWETP	KVARY	LAND_EVAP
Forest	1.6	1.0	1.0	1.25	1.0	6.0	1.0	1.0
Pasture/Grass	1.5	1.0	1.0	1.0	1.0	1.5	1.0	1.0
Pervious Urban	0.8	1.0	1.0	0.9	1.0	2.0	1.0	1.0

10.3.2.3 Calibration Statistics

Moriasi et al. (2006) and Moriasi et al. (2012) discuss various statistics to quantify model performance. For a satisfactory reproduction of observed hydrograph by a model simulation, a Nash Sutcliffe Efficiency greater than 0.5, Root Square Error less than 0.7, and Bias less 25 percent are recommended.

A number of model parameters and model performance statistics were evaluated to identify relationships among them. For the calibration of model parameters, linkage between a statistic and a parameter was established based on strong correlation between them, and a relatively narrow range of sensitivity. A number of statistics were included to ensure that critical aspects of the hydrograph were captured.

A brief description of statistics that were used in the model calibration is provided in *Table 10-17*. Together, these statistics assess how well a calibrated model is matching the observed dataset. The relationship between the key statistics and model parameters is described in Section 10.3.2.4.

Table 10-17 Summary of statistics used in hydrology calibration for the evaluation of model performance

Statistic	Description
$TBias = \frac{\sum S - \sum O}{\sum O}$	**Total Bias** quantifies an overall agreement between the water-balance. A value of zero indicates a perfect agreement.

$WBias = \frac{\sum S - \sum O}{\sum O}$	**Winter Bias** quantifies the agreement between the water-balance for the winter months (DJF). A value of zero indicates a perfect agreement.
$SBias = \frac{\sum S - \sum O}{\sum O}$	**Summer Bias** quantifies the agreement between the water-balance for the summer months (JJA). A value of zero indicates a perfect agreement.
$WStat = \frac{WBias + 1}{TBias + 1}$	**WStat** is an index of winter bias normalized to the total model bias. A value of one indicates a perfect agreement.
$SStat = \frac{SBias + 1}{TBias + 1}$	**SStat** is an index of summer bias normalized to the total model bias. A value of one indicates a perfect agreement.
$QStat = \frac{QBias + 1}{TBias + 1}$	**QStat** is an index of quickflow bias normalized to the total model bias. A value of one indicates a perfect agreement.
$BStat = \frac{BBias + 1}{TBias + 1}$	**BStat** is an index of baseflow bias normalized to the total model bias. A value of one indicates a perfect agreement.
$QaveRI = \frac{\overline{S_{t+1}/S_t}}{\overline{O_{t+1}/O_t}}$	**QaveRI** is the ratio of stormflow recession index for simulated and observed. Recession index is calculated as the average of ratio of data at day *t+1* and *t.* A value of one indicates a perfect agreement.
$BaveRI = \frac{\overline{S_{t+1}/S_t}}{\overline{O_{t+1}/O_t}}$	**BaveRI** is the ratio of baseflow recession index for simulated and observed. Recession index is calculated as the average of ratio of data at day *t+1* and *t.* A value of one indicates a perfect agreement.
$PBias = \frac{\sum S - \sum O}{\sum O}$	**PBias** quantifies the agreement between first top 50 peaks, where peaks were identified as the flow greater than day before and after. A value of zeri indicates a perfect agreement.
$VPBias = \frac{\sum S - \sum O}{\sum O}$	**VPBias** quantifies the agreement between volume of the first top 50 peaks, where volume was calculated by adding stormflow preceding and following the peak that does not include a return to baseflow or another peak. A value of zero indicates a perfect agreement.
$L05Bias = \frac{\sum S - \sum O}{\sum O}$	**L05Bias** quantifies agreement between lowest 5 percent of the flow. A value of one indicates a perfect agreement.

(a) S indicates simulated. (b) O indicates observed. (c) JJA = June, July, and August. (d) DJF = December, January, and February. (e) Stormflow and baseflow were calculated through hydrograph separation using USGS-PART. (f) All values for simulated and observed are paired.

10.3.2.4 Calibration Procedure and Parameter Sensitivities

Eight key model parameters were adjusted in the automated hydrology calibration framework. Those eight model parameters are listed in *Table **10-13*** and they were linked to a specific statistics as described in Section 10.3.2.3 and *Table 10-17*. The Watershed Model is first run with a default parameter set, and the key model performance statistics are calculated for the river segments with monitoring data. The computed statistics are used for appropriately adjusting the model parameters

based on the multipliers described in *Table **10-18***. The model simulation is repeated with the updated parameter set. The process is repeated for 11 times followed by the calculation of statistics and parameter adjustment after each model calibration iteration.

Sensitivity distributions between parameters and statistics were found by experimentation. Using those distributions and a trial-and-error method, updated multipliers were established *a priori* that converged after a few iterations, while at the same time did not induce parameter oscillation and achieved a high average model efficiency. The final parameter update multipliers are in *Table **10-18***.

Most of the linkages between parameters and statistics are straightforward. For example, the LAND_EVPA parameter affects the overall water balance and therefore has a strong relationship with the Bias statistic. Any changes in LAND_EVAP will either increase or decrease PET and as a result the simulated streamflow. The infiltration parameter (INFILT) has a direct and predictable impact on the baseflow statistic (BStat), which is an index of baseflow bias normalized to the total model bias. Similarly, IRC, AGWR, and INTFW are conceptualized within HSPF to control a specific hydrologic process which can be measured through a targeted hydrologic statistic. A less obvious example is the impact of lower zone soil moisture index parameter (LZSN) on the ratio of winter to summer flows. More water is stored in the lower zone during wetter periods of winter and spring with reduced storage in the drier summer periods. Therefore, LZSN only has a strong effect on winter flows and can be used to adjust winter flows relative to summer.

Table 10-18. Update rules for calibration of hydrology parameters

Parameter	Statistic	Update multiplier
LAND_EVAP	Bias	2 / (2 – Bias)
LZSN	Wstat, Sstat	(2.5 – Sstat / Wstat) / 1.5
INFILT	Bstat	1 / Bstat
IRC	QaveRI	2 / (1 + QaveR I)
AGWR	BaveRI	2 / (1 + BaveRI)
INTFW	Pbias, Vpbias	1 + max(Pbias, Vpbias) / 2; *if* Pbias × Vpbias > 0 1.0; *if* Pbias × Vpbias < 0
KVARY	L05Bias	1 / (1 + L05Bias)

10.3.2.5 Linkage Between Land Segments and Monitoring Stations

Linkage between the monitoring stations and land segments determine how model performance statistics of a monitoring stations will be used for updating model parameters for the land segments. The developed linkage considers and addresses four important issues: (1) due to the nature of land-river

segmentation, a land segment can be part of the drainage area of two or more separate rivers; (2) a land segment could drain to multiple nested downstream stations; (3) regulated flow in reservoirs impact the relationship between the flow statistics and model parameters differently than rivers without reservoirs; and (4) some land segments do not drain to any calibration stations.

The first two issues were addressed with the same technique. The *importance score* of a land segment to a flow monitoring station was defined as the percent of the total monitoring station drainage area covered by that land segment. The importance score of each land segment was calculated with respect to each flow station. For each land segment, the results were scaled so that they added up to 100 percent across all flow stations. If the importance score of a flow station was less than 10 percent, it was dropped, and the results were again rescaled to 100 percent. The process was repeated until all importance scores were greater than 10 percent. The parameter adjustments for a land segment would then be determined by weighing the *update multipliers of the downstream* calibration stations by their importance score.

An example helps to explain the procedure. Suppose land segment A drains to monitoring station X, Y, and Z. Segment A makes up 100 percent of X, 50 percent of Y, and 10 percent of Z. The relative importance score of land segment A to monitoring station X is 100 / (100 + 50 + 10) or 62.5 percent, the importance score of A to Y is 31.2 percent, the importance score of A to Z is 6.2 percent. However, Z is below the 10 percent threshold, so it is dropped, and the ratios are adjusted to 66.7 percent for X and 33.3 percent for Y. Land segment A takes 66.7 percent of the recommended update multiplier from river gage X and 33.3 percent of the recommended update multiplier from river gage Y.

To address the third issue (reservoir effects), flow monitoring stations with more than 50 percent of the upstream watershed passing through a reservoir were removed from the automated calibration and in those cases the calibration rested on other stations that were unaffected by reservoir influences.

The fourth issue of parameters for the land segments that were not associated with any monitoring stations was addressed by setting these equal to similar land segments that were identified qualitatively based on several criteria. The criteria included proximity, similarity, and the degree to which the similar segments were well-calibrated. The last criterion was based on the maximum raw importance score. A total of 34 segments out of 235 were unmonitored land segments. *Table **10-19*** shows calibrated land segments that were assigned to such unmonitored land segment segments.

Table 10-19. Assignment of ungaged land segments to similar land segments

Ungaged	Similar		Ungaged	Similar		Ungaged	Similar		Ungaged	Similar
N10003	N10001		N51093	N51036		N51149	N51036		N51685	N51059
N24019	N24045		N51095	N51036		N51181	N51036		N51700	N51036
N24029	N24035		N51099	N51057		N51199	N51036		N51710	N51036
N24039	N24047		N51103	N51193		N51550	N51036		N51730	N51036
N24041	N24011		N51115	N51057		N51570	N51036		N51735	N51036
N51001	N24047		N51119	N51057		N51650	N51036		N51740	N51036
N51013	N51059		N51131	N24047		N51670	N51036		N51800	N51036
N51053	N51036		N51133	N51193		N51683	N51059		N51810	N51036
N51073	N51057								N51830	N51036

10.3.2.6 Calibration of Snow Parameters

The snow simulation in HSPF is based on an energy balance. The snow algorithm uses meteorological data to (a) partition precipitation into rainfall and snow, (b) simulate an energy balance of the snowpack, and (c) evaluate the effect of heat fluxes. Precipitation falling at less than 33 degrees Fahrenheit adds to the snow pack. However, snow pack decreases because of sublimation and melt processes simulated based on energy inputs from rain, shortwave radiation, longwave radiation, and the transfer of heat from the ground and air. The sensitive parameters are those related to the heat transfer from the ground and air. It was found that the optimal model efficiencies were found for the Potomac and Susquehanna rivers when the atmospheric heat flux coefficient parameter, CCFAC, was minimized and the ground heat coefficient, MGMELT, was maximized.

10.3.2.7 Special Cases

10.3.2.7.1 Hurricane Isabel

In the Phase 5.3.2 Model, the simulation of flow due to tropical storm Isabel around September 20, 2003 was inaccurate in the Rappahannock, with the simulated peak flow much higher than the observed peak. The over-simulation caused mass balance problems with the estuarine hydrodynamic model of the Chesapeake. To address the problem, adjustments were made to the FTABLEs in the Rappahannock to increase the floodplain volume, which brought down the simulated peaks. The adjustments affected only storms with return frequencies over approximately 2 years. The modified Phase 5.4.3 FTABLEs are used in Phase 6.

10.3.2.7.2 Susquehanna 1996 Big Melt and Ice Jam Event

Around January 7–12, 1996, three successive snow storms created a snow pack of 2 to 3 feet in many parts of the Susquehanna and Potomac River basins. One week later, warm air climbed over a cold air mass creating a warming event and rain storm of approximately 2 to 3 inches which caused a high flows and flooding in the Susquehanna and Potomac River basins.

It was noted that the flows were greatly underestimated during the event but steadily overestimated in the spring melt; therefore, the melting caused by the rain was suspected. The temperature of the precipitation was increased by 10 degrees Fahrenheit for a group of counties in the path of the storm. The increase was found by trial and error to produce the greatest increase in efficiency for the simulation of 1996 hydrology overall. There was widespread improvement of the simulation.

In addition, in January 1996, around 50 ice jams were documented in Susquehanna River basin (USACE, 1999). Based on this information and an in-depth analysis of hydrographs, ice jams were added to the model simulation through HSPF Special Actions at 8 river segments across the Susquehanna Basin. The HSPF Special Actions modified the stage discharge relationship over the 14-day ice jam period between 9AM Jan 7, 1996 and 9AM Jan 20, 1996. During the ice jam period, for a given stage level, flow was limited to 15 percent of flow under normal condition.

10.3.2.7.3 Hurricane Juan, 1985

The remnants of Hurricane Juan settled over the upper Potomac watershed in November 1985, dropping large amounts of rain on the watershed and producing extremely high flows. During the development of the Phase 5.3.2 Model variable calibration alternatives were tried, but none resulted in improved simulation of extreme flows during this period. Realizing that above a certain precipitation during extreme events, increased uncertainty in rain gage performance results in reduced rain gage

reliability the Phase 5.3.2 Model rainfall was corrected based on the available evidence of streamflow. This was consistent with reports that several rain gage stations were knocked offline during the 100-year storm of Hurricane Juan. Rainfall was increased to provide the volume of water needed to support the observed flow at the monitoring stations. A correction factor of 2.5 was applied to the hourly precipitation data if total precipitation was greater than 1 inch on a given day and was applied over a period of 4 days from November 1, 1985 to November 4, 1985.

10.3.2.7.4 Tropical Storm Lee, 2011

The adequacy of the rainfall data was verified both by comparing it with a number of gaging data as well as a mass-balance analysis to ensure the rainfall volume was sufficient for explaining the amount of streamflow recorded over this period. A special action was implemented for entire watershed and simulation period where the default INFEXP parameter value of 2 was changed to 8 when rainfall over the previous 14 days exceeded 6 inches. This action was applicable only for the pervious land uses for the entire watershed and was applied throughout the entire simulation period. The rationale behind such special action was to express the effect saturation of upper soil layer on infiltration due to a significant amount of rainfall over an intermediate period of time.

10.3.2.8 Hydrology Calibration Results

As previously noted in this section, the hydrology calibration procedure is an automated parameter optimization method for adjusting HSPF hydrologic parameters for land uses using model performance statistics at downstream river flow gages (Appendix 10B). The calibration process was run for 11 iterations at which point the model results were analyzed.

*Figure **10-18***, *Figure **10-19***, and *Figure **10-20*** show the improvement in model performance statistics over the calibration iterations. *Figure **10-18*** shows several index-based statistics (an ideal value of 1.0) that were used in the model calibration. These indices assess model performance for simulating winter, summer, quickflow, baseflow, and the recession rates of quickflow and baseflow. As shown in the *Figure **10-18*** the median of the calibrated rivers segments for all of these indices have converged to within ±5 percent of the ideal value after the completion of calibration iterations. *Figure **10-19*** shows biases in the simulated total and storm flows. Median bias for the total, peak, and peak volume have converged to within ±5, ±15, and ±10 percent respectively. *Figure **10-20*** shows an independent overall measure of model calibration performance. After the model calibration, the Nash Sutcliffe Efficiency (NSE) of daily flows has a median value greater than 0.65, while the median NSE of the daily log-flow is greater than 0.7, and the NSE of monthly flows is greater than 0.8. It is important to note that these efficiencies were not part of the objective function in the model calibration, yet the overall model statistic improved over the iterations suggesting that the statistics used in the calibration performed well in supporting these independent efficiencies. The NSE reaches its maximum value after a few iterations, implying that while the individual calibration statistics are still improving after 10 iterations, the overall agreement with data is not changing.

Many high biases and low efficiencies are associated with reaches with reservoirs and impoundments. Reservoirs and impoundments are difficult to simulate at a daily time step. That is because rather than using observed outflows or estimating outflows from observed parameters like surface elevation, the model uses idealized operating rules to simulate outflows from reservoirs. This was done so that model could be used for simulating management scenarios and effects of land use change that alter flow rates.

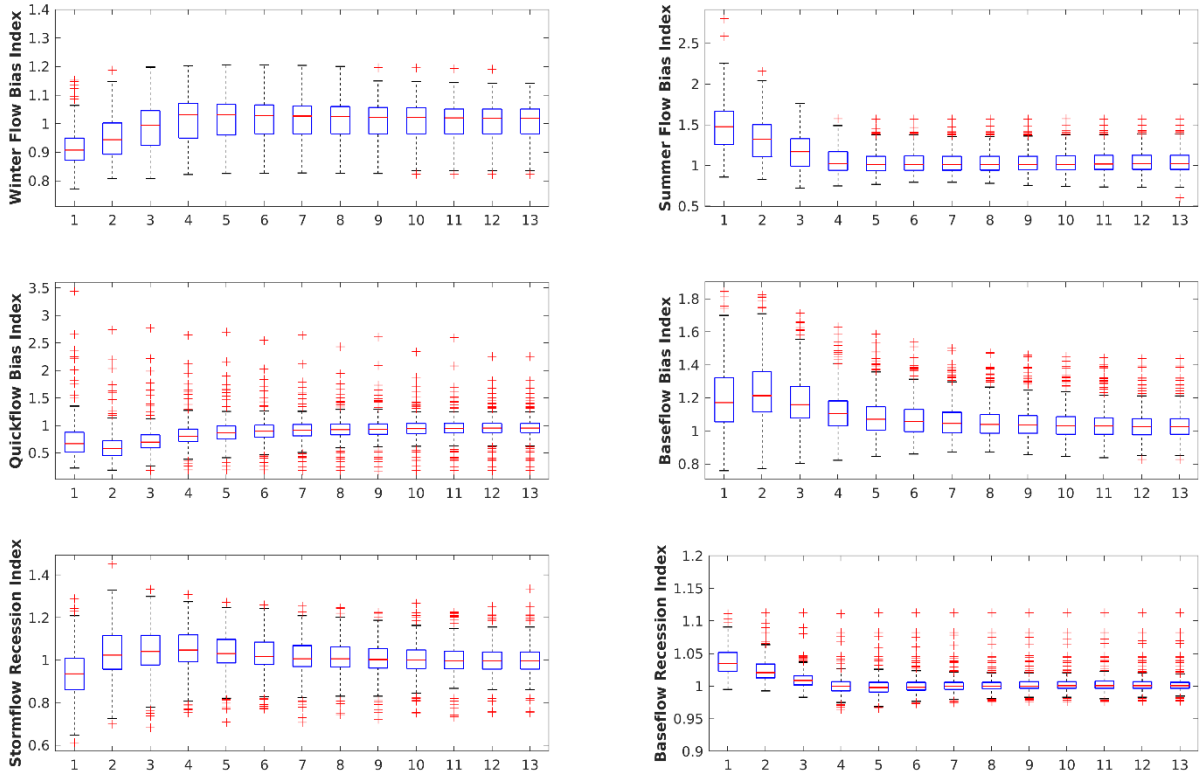

Figure 10-18. Improvement in calibration statistics over the calibration iterations. For index-based calibration statistics ideal value is 1.0. Box and whisker plot show the statistics for simulated river segments.

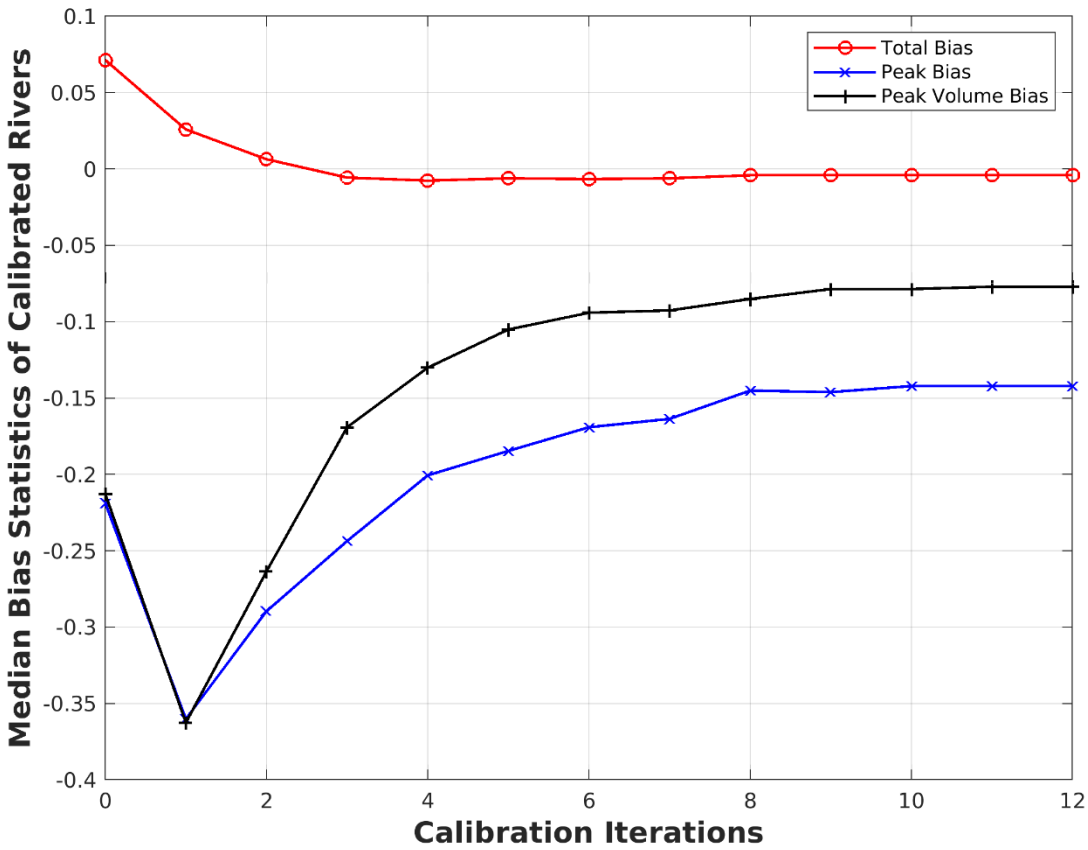

Figure 10-19. Improvement in overall bias statistics shown as the median for the calibrated river segments over the calibration iterations. Ideal value for bias statistics is 0.

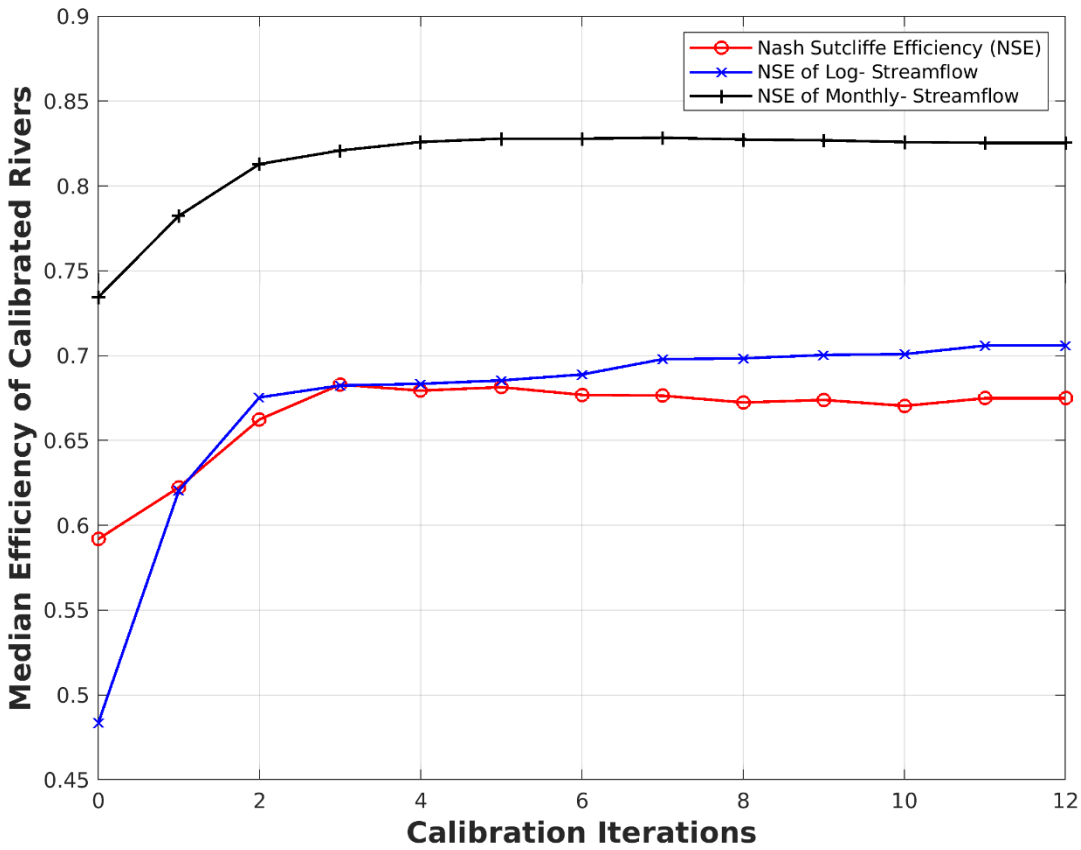

Figure 10-20. Improvement in overall Nash Sutcliffe model performance efficiency (NSE) for the calibrated river segments over the calibration iterations. Ideal value for NSE is 1.0.

10.4 Land Sediment Simulation

10.4.1 Introduction to the Sediment Simulation

In the Phase 6 dynamic model, the production and transport processes of sediment from land uses are simulated using HSPF. HSPF uses rainfall intensity to cause detachment of sediment and surface flow as the major driver of sediment transport. HSPF also provides the ability to simulate the effects of other sediment processes such as the (a) external addition or removal of sediment, e.g., cropland plowing and the washoff of the pool of unattached soil particles, (b) reattachment of detached soil particles over time to the soil matrix, and (c) effects of area covered by vegetation or mulch reducing detachment. The HSPF model can also simulate scour and gullying effects but this HSPF module was not used in Phase 6. Limiting conditions for storage and transport are used in the model for the hourly mass balance.

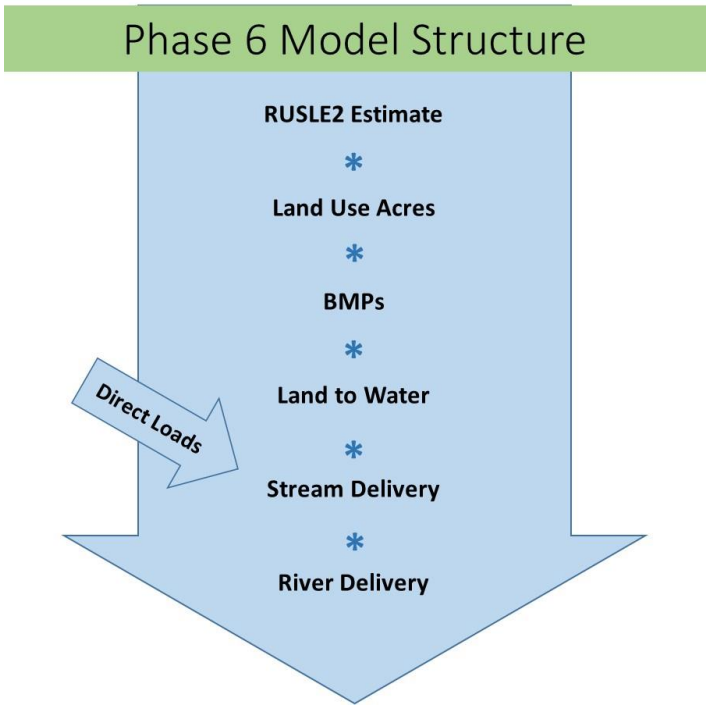

Figure 10-21: Time-averaged simulation of sediment

Edge-of-field sediment calibration targets as time-average loads for each land use and land-river segment are determined through a spatial evaluation of the RUSLE equation as detailed in Section 2 of the Phase 6 documentation. Accordingly, HSPF parameters for the land uses are calibrated such that the simulated time-averaged transport of sediment matches with the calibration target. Special practices, e.g., plowing and field operations that result in generation of sediment are estimated and included as inputs to the dynamic model. Inputs are also included for practices, e.g., cover, that limit the production of detached sediment due to rainfall. Effect of other best management practices are applied to the simulated loads where they are decremented temporally depending on the level of implementation. The calibration targets are time-average loads for 1985-2014. The dynamic model integrates all these time variable inputs within the simulation framework described above to simulate sediment erosion and transport at hourly time steps. The time-averaged model (*Figure 10-21*) uses the average of the sediment transport rate calculated by the dynamic simulation model over the 1991 to 2000 average hydrology period used for decision making.

Soil texture information is applied to the eroded sediment to estimate the hourly loads of sand, silt, and clay. A sediment delivery ratio (SDR) is applied to the calculated sediment loads to account for the effects of land and water interconnectivities of the landscape that are not captured in the sediment simulation. As discussed in detail in Section 7, a separate SDR is calculated for each major land use and land-river segment combination.

10.4.2 External Inputs for Sediment Simulation

Inputs for the rainfall-runoff response of land uses are the model's basic inputs for the simulation of sediment erosion and transport processes. In addition, the effects of field operations, such as plowing and harvesting, as well as crop management practices on sediment transport were incorporated. Section 3 provides a comprehensive account of how these inputs are prepared. Details are provided in the following subsections regarding how the model uses the inputs for sediment loads resulting from field operations, and the fraction of area covered by vegetation or plant/leaf litter.

10.4.2.1 Plow actions, field operations, and detached sediment

The dynamic model uses monthly input of sediment generated due to plowing, harvesting, and other agricultural operations. Sediment inputs for all crop land uses were estimated using RUSLE2 while considering information on various crops for the growing region (See Section 3.7). In HSPF, detached sediment is considered to be a pool of sediment mass that is available for export from land given sufficient availability of surface runoff. Estimates of monthly detached sediment mass for each land use are provided as a series of data files as snapshots for a number of years within the simulation period. Monthly values for detached sediment load are interpolated based on these snapshot input data files. Box and whiskers in *Figure **10-22*** show variability in average annual detached sediment loads for Phase 6 crop land uses and the among the land segments. In the model simulation, the detached sediment load for a given month is divided into 10 increments which are added to the detached sediment storage every three days over the month. The detachment is spread over the month to simulate a temporal distribution of farmer behavior. The pattern of ten increments is due to HSPF input requirements. To guard against plowing simulated on wet days these input loads are added to the storage only on days with rainfall less than 0.1 inches. The detached sediment storage is available for washoff by surface runoff or reattachment to the soil matrix over extended periods without surface runoff. A comparison of median detached sediment input and median of sediment eroded over the model calibration period is shown in *Figure **10-23***. Effects of land to water landscape interconnectivity and management practices on reducing the sediment transport are applied later in the model simulation.

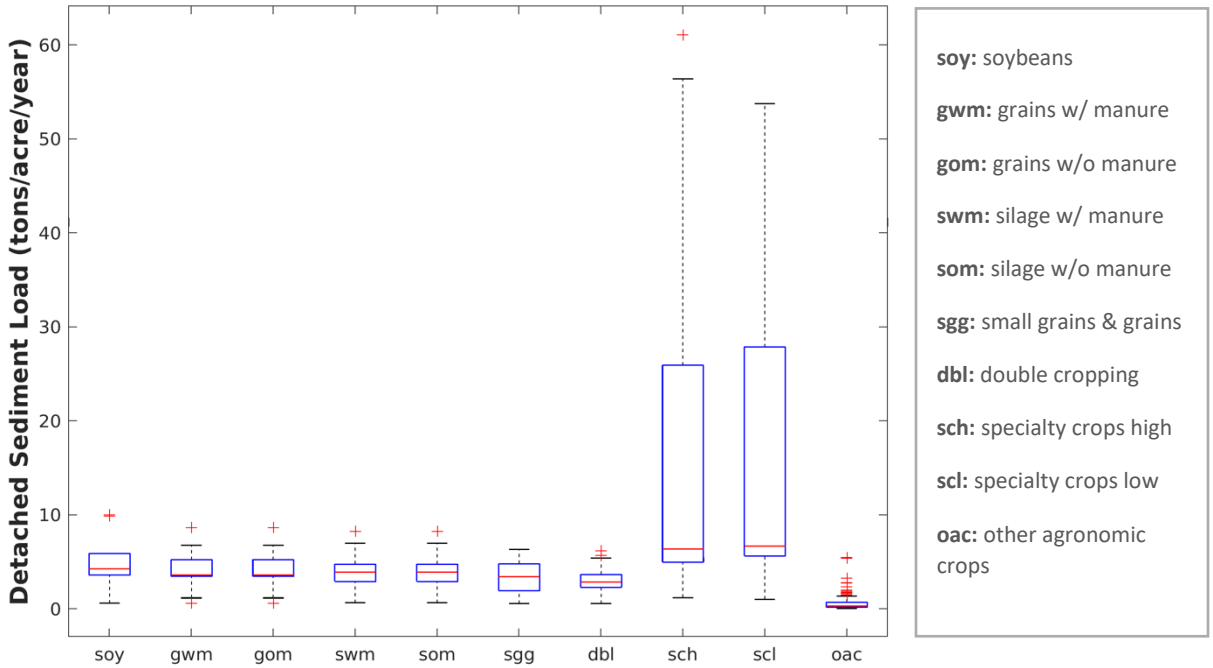

Figure 10-22: Average annual detached sediment loads for the crop land-uses. Distribution of loads for a land-use shows the variability across the model land segments.

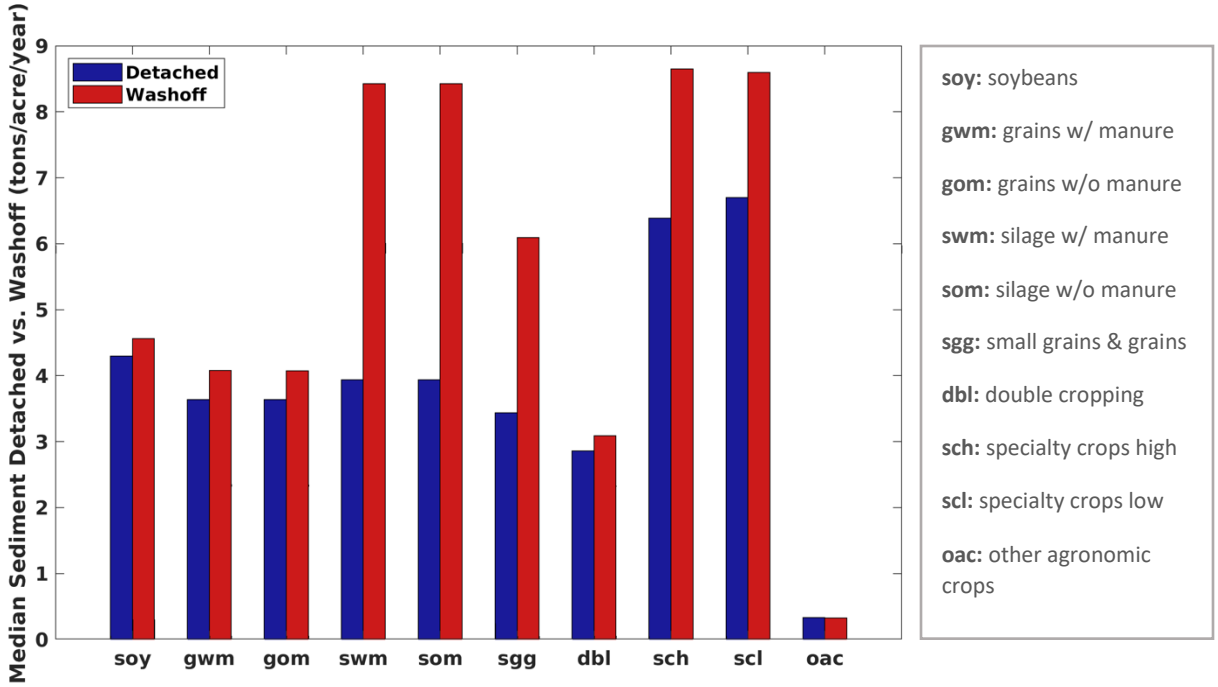

Figure 10-23: Median of detached sediment inputs from field operations (blue bars) and net sediment export (red bars) over the model calibration period (1985 – 2014) for Phase 6 crop land uses

10.4.2.2 Cover

Cover data represent both the vegetative canopy and all other ground covers such as leaf litter on a pervious land use. Cover prevents the detachment of soil particles from the soil matrix due to rainfall proportionate to the fraction of ground covered. Monthly cover data are provided as a percent of ground covered for all pervious land uses. Monthly values are provided for the entire year, not just the growing season. The monthly cover dataset is provided as a series of data files for the snapshot years within the simulation period. Monthly values for cover for the snapshot years are interpolated by HSPF which uses the interpolated monthly values for the simulation. A simulated HSPF land use with 100 percent cover would not have any sediment erosion generated due to rainfall and in that case sediment loss would be non-zero due detached sediment inputs from agricultural field operations. Furthermore, since detached sediment storage is decremented after each time step to account for the reattachment of soil particles into the soil matrix, the net erosion will be significantly less than the inputs for the detached sediment. The cover dataset is provided for crop, pasture, grass, and tree-canopy land uses. Box and whisker plots in *Figure **10-24*** show the cover fractions for some of Phase 6 land uses.

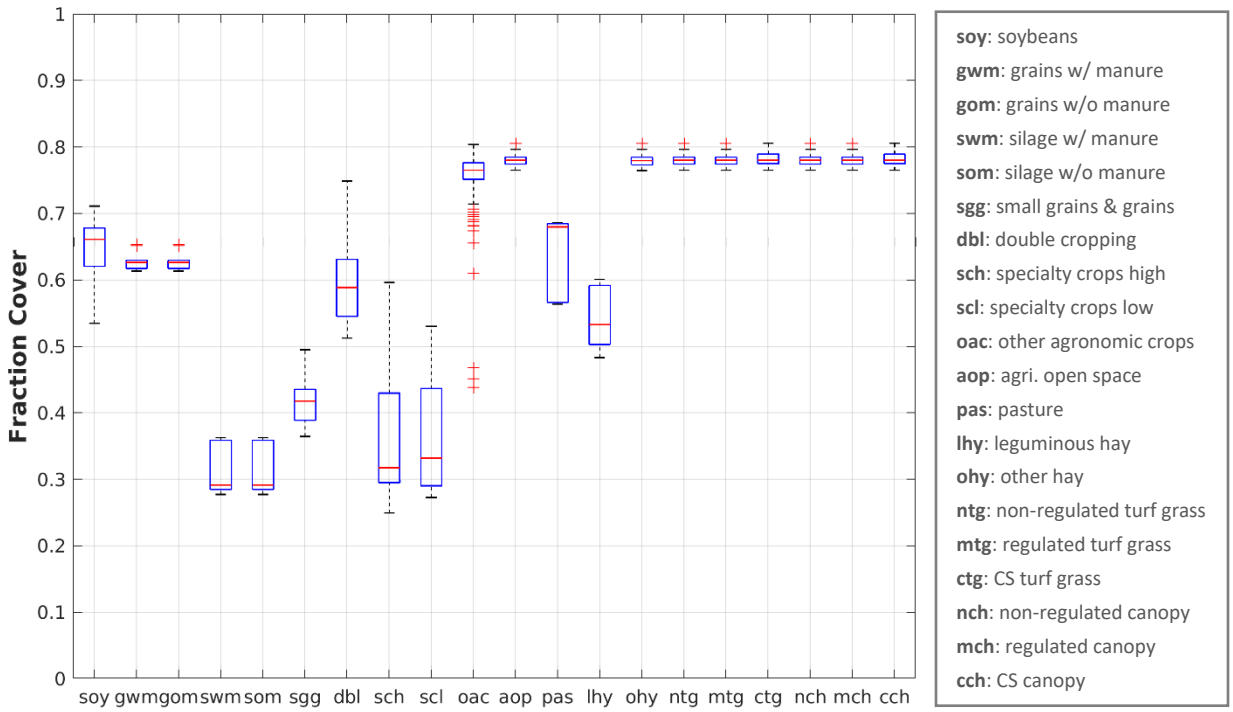

*Figure 10-24: Average annual cover fraction for the crop, pasture, grass, and tree-canopy land uses. Distribution of loads for a land use shows the variability across the model land segments***.**

10.4.3 Edge-of-Field Sediment Calibration Rules

HSPF simulates erosion from the land surface by three processes governing: (1) detachment of soil by rainfall, wind, or human activities; (2) removal of detached soil by runoff; and (3) production and reattachment of detached soil into the soil matrix due to physical processes and compaction. *Table **10-20*** provides a list of HSPF sediment parameters that govern the simulation of these processes.

Table 10-20. Key parameters in sediment calibration on land segments

Parameter	Description
KRER	Coefficient that determines how much sediment is detaches from the soil matrix as a function of rainfall.
JRER	Exponent that determines how much sediment is detaches from the soil matrix as a function of rainfall.
KSER	Coefficient that determines the sediment transport capacity as a function of surface outflow.
JSER	Exponent that determines the sediment transport capacity as a function of surface outflow.
NVSI	Rate at which sediment is added to detached soil from atmosphere; Negative values can simulate removal of sediment by wind or human activities.
COVER	Fraction of soil surface in vegetative cover and unavailable for erosion by rainfall; COVER varies monthly by land use.
AFFIX	Rate at which detached sediment is re-attached to soil matrix due to compaction.

An iterative program calibrates each land use type to a target average annual sediment erosion rate. Sediment erosion targets, as noted earlier, are *a priori* estimates of long-term sediment loss for land uses for the entire simulation period of 1985 to 2016 of the Phase 6 simulation. Of the 7 model parameters listed in *Table **10-20***, the COVER parameter is a direct model input based on average estimated cover for a land use as described in Section 10.4.2.2. The remaining 6 model parameters have to be calibrated to a single target calibration sediment erosion rate for a land use in a land segment. To address this ill-posed optimization problem, three calibration rules were established to reduce the number of parameters to be calibrated. As a result, an iterative automated calibration procedure is operationally feasible.

The automated calibration starts from a land use specific set of default model parameter and they are adjusted on the basis of how the target erosion rate compared with net simulated sediment loss over the calibration period. Following three rules were applied in the calibration process:

Rule 1. <u>Ninety percent of detached sediment is reattached to the soil matrix in 30 days.</u>
On days without rainfall detached sediment storage decreases each day as a result of the reattachment of detached soil particles to the soil matrix. In general, in the Phase 6 simulation detached sediment storage tends to gradually reach an equilibrium value as a balance between reattachment rate (AFFIX) and production rate (NVSI) and stay at a dynamic equilibrium state over time with episodic washoff removing some of all of the detached soil materials from time to time (*Figure **10-25***). The two rules (Rules 1 and 2) are used in an attempt to reflect this natural dynamic of sediment by regulating the behavior of AFFIX. This constraint is met by setting the first-order reattachment rate, AFFIX, to 0.07675 per day for all land uses and land segments.

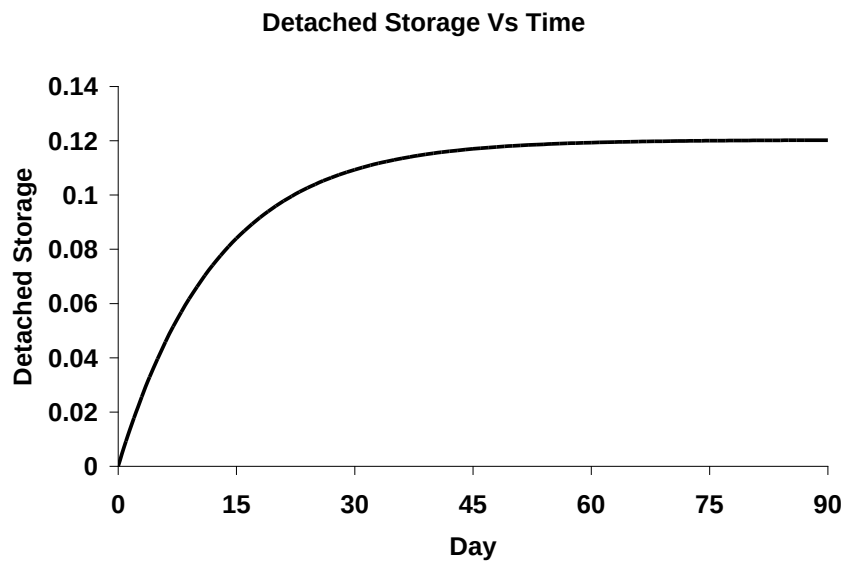

Figure 10-25. The dynamic of detached storage over time

Rule 2. <u>The NSVI parameter should be set high enough so that sediment concentrations during storms are larger on the rising limb of the hydrograph than on the falling limb.</u>
It has been observed that sediment concentrations during storms are higher on the rising limb of the hydrograph than on the receding limb. This behavior is attributed to the fact that often previously detached sediment is removed until storage is depleted during the onset of a stormflow event (Dinehart 1997). To simulate this behavior, sediment production rate (NVSI) was used to build up the detached sediment storage, so there is a sufficient supply of sediment available before each storm event. Within that context, NVSI also represents any net additions or removal of detached sediment by human activities or wind. Mathematically, the rule can be expressed as follows:

$$NVSI \times 365 = a \times \text{Sediment Erosion Calibration Target}$$

Equation 10-12

where, a is the fraction that relates *NVSI* to sediment export target. A value of 1.5 was used, which was determined together with the specification of *KSER*/*KRER* ratio, as discussed below.

Rule 3. <u>There should be no detached sediment in storage after large storms.</u>
Sediment storage is typically depleted during storm events and on a seasonal time scale (Van Sickle and Beschta, 1983). The qualitative effects of changing detached sediment mass for a specific discharge level during are reflected as decreasing sediment concentrations in a single storm event (i.e. rising vs. falling limbs) as well as over the seasonal time scale (i.e. consecutive stormflow events). In both cases the decrease in sediment concentration is due to decrease in sediment storage or supply with the flushing of sediment from the watershed with preceding events. However, from a long-term perspective, the accumulated sediment on the land surface should not be either continually increasing or decreasing (Gellis, 2004). The phenomena of decline in sediment concertation, over an event as well as seasonal scales, resulting in hysteresis

loops are always apparent in most watersheds and streams (VanSickle and Beschta, 1983). In that regard, based on a broad characterization of catchments sediment response in the Chesapeake region, it is anticipated that storms with a return frequency of 3 to 4 months should be sufficient to flush out all of the detached sediment mass from a pervious land use.

The rule is developed to reproduce the seasonal decline in sediment storage, and to capture the well-established differences in sediment concentration between the rising and falling limbs of the hydrograph as described above. The rule has important management implications, particularly for agriculture. Depending on the crops being grown and cropping practices a field may not be plowed at all, such as in no-till systems, or may be plowed during the spring planting season, the harvesting season in fall to make way for winter crops, or both. During plowing periods, the soil is loosened from land and added to detached storage which is available for wash off. As a result, the potential for sediment runoff from agriculture land typically increase during periods of planting and harvest because of increased sediment supply and low vegetation cover (Figure 10-26). To capture the impact of plowing and field operations on sediment loading and the effects of stormwater management strategies for erosion control, the simulated sediment storage needs to decrease to zero so that sediment supply would become storage limited over a longer time scale. However, there could be periods where sediment transport will be limited by the transport capacity.

Numerically, this is achieved by adjusting the remaining four model parameter (*KRER*, JRER, *KSER, and JSER)* within the permissible range. To further reduce the parameter set, a proportional relationship between these parameters were assumed in Equation 10-13:

Equation 10-13: relationships between HSPF sediment parameters

$$KRER = b \times KSER$$

$$JRER = JSER = c \times EXP(-KSER^{d})$$

Values for the parameters a, b, c, and d were established as 1.5, 0.075, 6.0, and 0.25 based on the empirical evidence that qualitatively aligned with the broader understanding of sediment response, and quantitatively satisfied criteria for: (a) the ability to calibrate the model for sediment erosion calibration targets, (b) the successful convergence of the automated calibration for all land uses and land segments.

*Figure **10-27*** shows the average annual sediment export rates for some Phase 6 land uses. These rates were calculated based on the application of RUSLE to high resolution (10-meter) land cover dataset as described in Section 2.3.

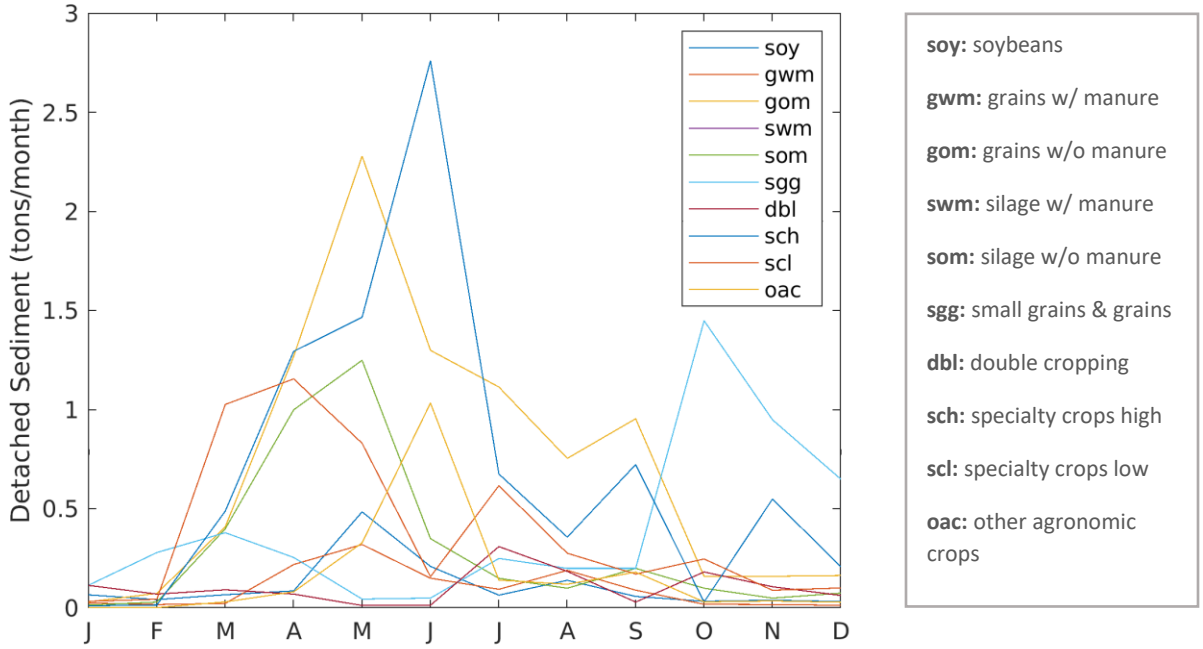

Figure 10-26: *Monthly detached sediment for the crop lands. Data from land segments with maximum crop area are shown.*

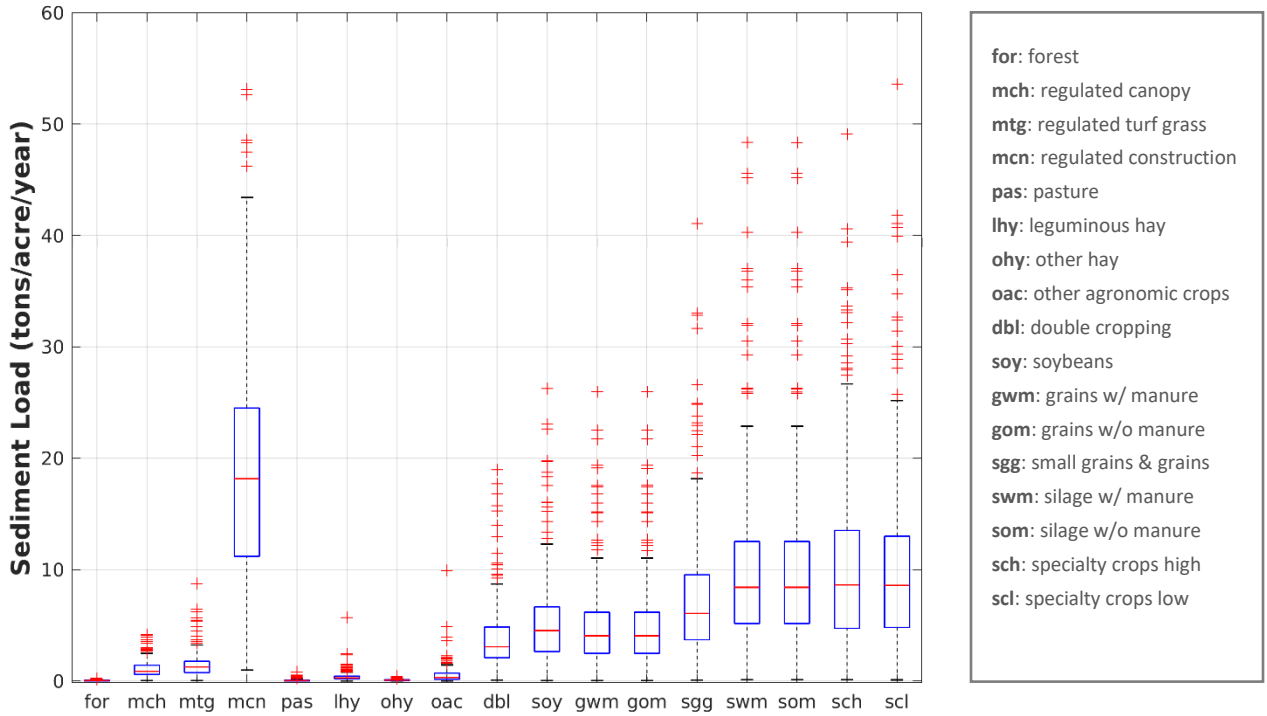

Figure 10-27: Average annual sediment export rate for select Phase-6 land uses. Box plot for a land use show spatial variability in the sediment export rates across Phase-6 land segments.

Figure ***10-28*** shows a comparison of sediment erosion calibration target and simulated sediment export rate after the model calibration. The figure shows data points for all calibrated land uses and land segments. Differences in colors for the data points represent land uses and highlights variability in sediment response. The Phase 6 sediment calibration had a total of 9,400 sediment response units reflecting 235 land segments and 40 land uses. There are a land segment and land use units where the calibration did not yield a good agreement between simulated sediment export rate and the erosion calibration target. In about 11 such units the simulated rates were higher than the calibration target because rainfall and surface runoff was considerably high to match very small (approx. 0.01 tons/acre) erosion rates. Whereas in other 11 such units, all belonging on one land segment (Harrisonburg, VA) and agricultural land use with higher calibration targets, the simulated rates were lower than the calibration target because surface runoff was extremely low.

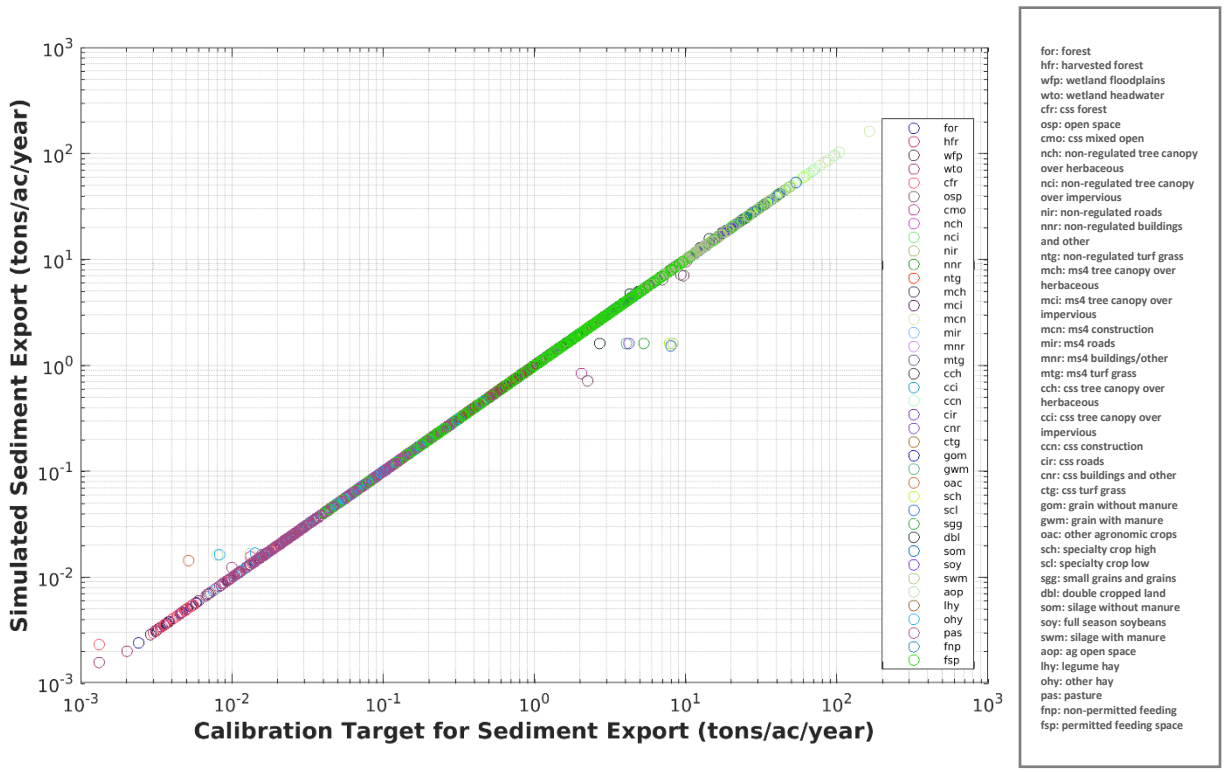

Figure 10-28: Agreement between calibration target for sediment erosion and simulated erosion rates are shown as data points match along 1 to 1 line. Data points on the chart correspond to 38 calibrated land uses and 235 land segments. Color coding qualitatively reflect land uses and sediment erosion range.

10.5 Land Nutrient Simulation Including Lag Time

The time-averaged model uses the long-term loading rates of nutrients as the baseline condition for the watershed. Section 2 of the Phase 6 documentation provides a detailed description of steps and processing involved in the calculation of time-averaged nutrient export rates. The dynamic model performs temporal disaggregation of time-averaged nutrient response at hourly time steps over the specified simulation period. The temporal disaggregation is based on the integration of time variable

nutrient inputs, hydrology, and sediment simulated responses with nutrient source sensitivities, watershed retention characteristics, and lag time. The average annual load of the resulting hourly temporal disaggregation is same as that of the time-average model.

10.5.1 Adjusting Low Values of Time-Average Load

Time-averaged nutrient (also referred as Calibration Target) loads are defined for each land use and land segment after accounting for local nutrient inputs. Readers are referred to Section 2 for the detailed description of steps and processing involved. In rare cases, the method resulted in time-averaged loads that were less than time-averaged loads for forest in the same land segment. The Chesapeake Bay Program Modeling Workgroup on February 14, 2017 determined that sediment and nutrient loads on all non-forest land uses after sensitivities were applied should be greater than or equal to that of the forest load. To comply with this decision, the calculated load after sensitivities are applied for each land use in a land segment were compared to the forest loads in that land segment separately for total nitrogen and total phosphorus. If the predicted load was lower, it was set to the forest load in the same land segment. Nutrient species ratios from the original land uses are not altered to match forest ratios.

The Modeling Workgroup agreed that differences in land-to-water factors could reasonably result in non-forest load sources being less than forest load sources. Non-forest loads could be less than forest loads based on distance to the water for the acres in each sector and catchment. For example, there could be a catchment with crop lands on the higher elevation and forest in the bottom lands.

The Urban Stormwater Workgroup and Agricultural Workgroups determined that BMPs could drive developed or agricultural land loads below that of forest or wetlands. Therefore, the adjustment to make forest the lowest loading load source is made only in generating the model calibration targets.

Nutrient Calibration Targets are calculated for each land segment and land use where there are acres. Targets also are calculated where there are no acres by using a regional average of the inputs. That means that for land segments in locations where there are zero acres in that land use, such as any agricultural land use in the District of Columbia, there will be a target. Of course, the Phase 6 Watershed Model will not attribute a load in the calibration since there are no acres. However, it is necessary to have a target calculated for scenarios that could include land use acres in land segments that were not in the calibration.

10.5.2 Nutrient Speciation

Time average nitrogen calibration targets are determined by nutrient species. Nutrient species include nitrate, ammonia, labile organic nitrogen, refractory organic nitrogen, phosphate, labile organic phosphorus, and refractory organic phosphorus. Except as noted below in Section 10.5.2.1 for nitrate, the amount of each nitrogen or phosphorus species is determined by the ratio from the Phase 5.3.2 Watershed Model calibration edge-of-stream loads. Since there are no loads for the land uses representing the watersheds of combined sewer areas, the nutrient split is established as the same as the nonregulated or regulated versions of those last uses. For example, pervious developed in combined sewer areas is split into nutrient species following nonregulated pervious developed.

The nitrogen targets were calculated by nutrient species for all land uses and land segments while the phosphorus targets were calculated by total phosphorus. The phosphorus targets are divided into phosphate and organic phosphorus using the fraction of each nutrient species from the Phase 5.3.2 calibration scenario.

The targets are divided into baseflow and stormflow. Organic nitrogen and phosphorus targets are also divided into labile and refractory portions. These divisions come from the Phase 5.3.2 targets. The impervious land uses have no baseflow, so all of the load is in the surface for these land uses. The Phase 5.3.2 targets had zero nitrate on the impervious land uses, consistent with a comparison of percent impervious and observed percent nitrate (USEPA 2010a-10, section 10.2.15). This remains true for Phase 6.

10.5.2.1 Nitrate Analysis

Nitrate targets are specified for stormflow and baseflow. It was recognized that the partition of nitrate loads between stormflow and baseflow had implications on the resulting nitrate concentration-discharge relationship. Three observation-based approaches were tested to investigate the fraction of total nitrogen loads that are nitrate, and the fraction of nitrate loads that are groundwater. An observation-based method was found to estimate the fraction of total nitrogen loads that are nitrate. A second method, used only in the coastal plain, estimated the fraction of total nitrate that is delivered though the groundwater. The third method was not used.

In the unused method, groundwater nitrate loads were estimated for agriculture, developed, and non-developed land cover types using a regression model that was based on monitoring data of 156 small streams with watershed size of less than 500 square miles (Terziotti et al., 2017). However, that did not improve model performance. These regression-based estimates appear to suggest considerably lower groundwater contributions for nitrogen than previous analysis or other methods with approximately 34% at the watershed scale, and 39%, 28% and 7% for agriculture, developed, and un-developed land cover types respectively.

10.5.2.1.1 Nitrate Fraction of Total Nitrogen

To estimate the fraction of total nitrogen that is nitrate throughout the watershed, USGS WRTDS annual and average annual data available between 1985 and 2014 were analyzed for 77 monitoring stations in the Chesapeake watershed. The analysis showed a good predictive relationship between nitrogen load per acre and nitrate load per acre across these watersheds of different spatial scales ranging between 8 to 27,000 square miles (Figure **10**-**29**). This relationship, shown as Edge of River Phase 6 Regression in Figure **10**-**29**, was derived by combining the linear and polynomial equations for the average annual data. A 5% buffer was applied as a factor of 1.05 to both linear and polynomial equations to account for losses in nitrate due to denitrification and other riverine processing. Since the polynomial equation performed better at the lower range, it was used for nitrogen rates less than 1 lb/acre/year. The linear equation was used for nitrogen rates greater than 2.4 lbs/acre/year and linear interpolation was used for point between 1 and 2.4 lbs/acre/year. The resulting relationship was applied at each river segment between the land and river simulations to the edge of river nitrogen loads from the adjacent drainage area to estimate annual fractions of nitrate delivery. The data were interpolated linearly between two points. Ammonia and organic nitrogen loads were appropriately adjusted also at an annual time step to conserve edge of river nitrogen load. The linear and polynomial equations were developed using the average annual data. The annual data showed similar behavior, suggesting the relationship could also be applied at an annual time step. Although applying the regression for the average annual time period performed slightly better, it was applied at an annual time step to achieve better consistency in simulations between scenarios when loads differed for a limited period of the simulation. But overall,

use of the edge of river regression between nitrogen load per acre and nitrate load per acre improved the model calibration performance.

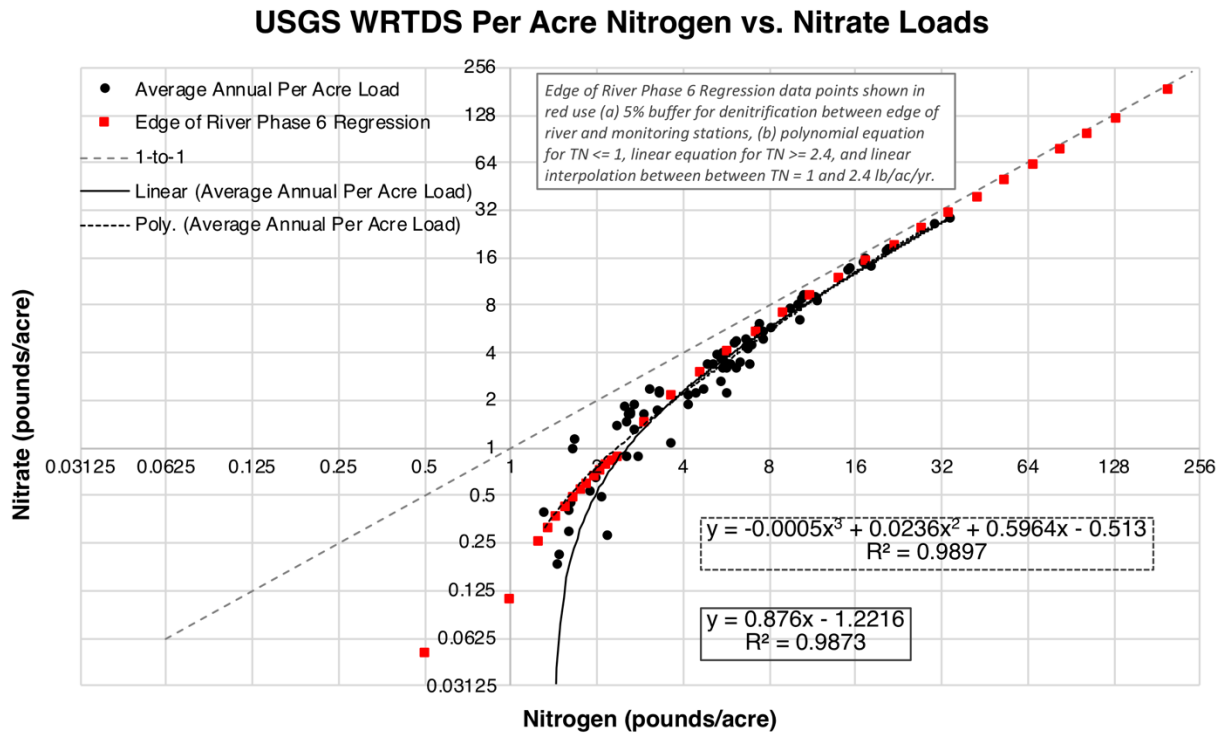

Figure 10-29: Regression between per acre nitrogen and nitrate loads show good predictive relationship across 77 watersheds in the Chesapeake Bay watersheds of different scales between 8 to 27,000 square miles. The Edge of River Phase 6 Regression was applied to every river segment's edge of river nitrogen load at annual time step.

10.5.2.1.2 Nitrate Stormflow and Baseflow Partitioning in the Coastal Plain

The fraction of total nitrate partitioned to stormflow or baseflow was carried forward from phase 5.3.2 except in the coastal plain land segments where an observation-based approach was used. Paired observed nitrate concentrations and flow data for the coastal plain monitoring stations were analyzed, where the average concentration of the top 1% streamflow samples were considered to represent entirely stormflow nitrate concentration and bottom 20% streamflow to represent entire baseflow nitrate concentration. The ratio of baseflow to stormflow concentrations along with simulated hydrology were used for estimating the proportion of baseflow nitrate loads using Equation 10-14.

$$Percent\ Baseflow\ Nitrate = \frac{Baseflow \times C_{baseflow}}{Baseflow \times C_{baseflow} + Stormflow \times C_{stormflow}}$$

$$Percent\ Baseflow\ Nitrate = \frac{Baseflow \times \left({C_{baseflow}}/{C_{stormflow}} \right)}{Baseflow \times \left({C_{baseflow}}/{C_{stormflow}} \right) + Stormflow}$$

Equation 10-14

A strong linear relationship was found between percent baseflow and percent baseflow nitrate load for about 28 monitoring stations. Accordingly, the proportion of groundwater nitrate was estimated based on the proportion of simulated baseflow in total flow in 71 land segments in the coastal plain.

Final land use loads for the calibration are given in Appendix 10C: Nutrients and Sediment Calibration Targets.csv

10.5.3 Estimates of Lag Time

Jasechko et al. (2016) found that globally most water is younger than three months old, and that steeper areas are more likely to have older water than flat areas. Sanford (2015) found similar behavior in that the groundwater ages for watersheds in the simulation of Upper Potomac river basin are explained primarily by steepness and groundwater recharge. *Figure **10-30*** (a) and (b) together show that the catchments with steeper slope had deeper mean depth to groundwater table and longer groundwater lag time, as did areas with lower groundwater recharge. This emergent behavior of the catchments was based on the analysis of simulated time-averaged responses of catchments using the USGS-MODFLOW model with 500 feet spatial resolution. The model used a dual-porosity formulation that provides a better calibration against an observed tritium tracer.

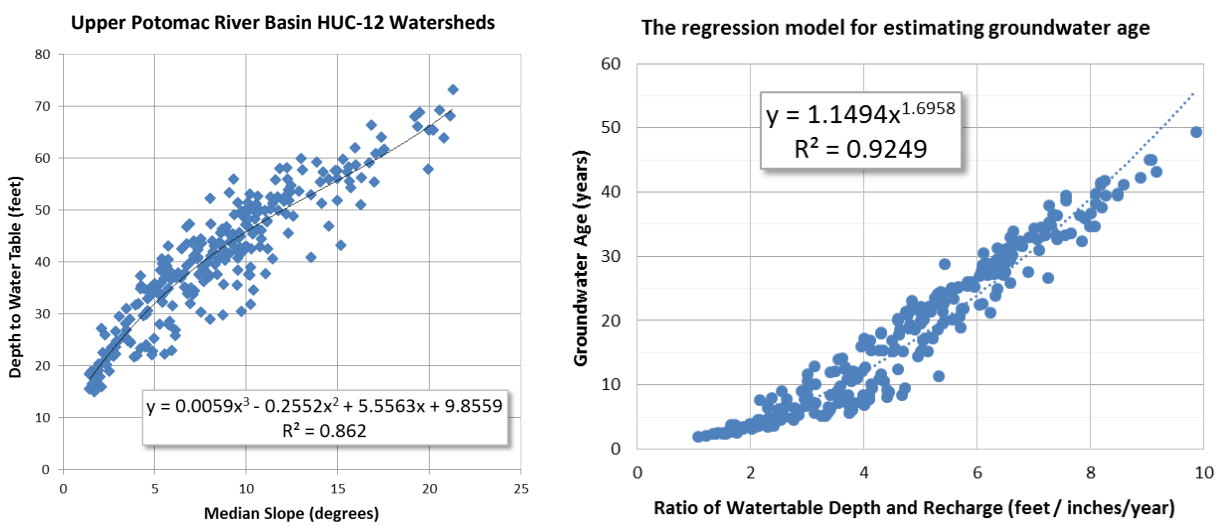

Figure 10-30: (a) Relationship between depth to water table and time constant. The time constant is indicative of lag time associated with groundwater table for a catchment. Smaller values for time constant indicate higher lag time. (b) An emergent characterization of simulated catchments show mean depth to groundwater is inversely related to mean topographic slope. [Adapted from Sanford (2015)]

The emergent behavior of the catchment response was captured as pair of highly significant regression equations (***Figure 10-30***) which relate groundwater age to steepness and recharge rates. The regression model was applied to the Chesapeake Bay watershed at the HUC-12 catchment scale. Depth to groundwater table was estimated using the median topographic slope of catchments computed using 30-meter topographic geospatial data. The USGS national data publication was used for the mean annual groundwater recharge (Wolock, 2003). The data publication provides average groundwater

recharge as 1-km raster grids, which was calculated using base-flow index and mean annual runoff for the 30-year period of 1951-1980. The 1-km raster dataset were spatially aggregated for estimating mean annual groundwater recharge rates for the HUC-12 catchments. The groundwater recharge estimates for the HUC-12 catchments were adjusted to remove biases as compared to the recharge estimated from chemical hydrograph separation.

The regression model performed quite well for the catchments across the watershed with the exception of Coastal Plain catchments. To overcome this challenge a separate statistical model was developed for the coastal plain region. It was found that among several statistical methods that were tested for the analysis that gradient boosted regression trees performed the best for the Coastal Plain in explaining spatial variability in groundwater age. The developed statistical model uses several catchment attributes as explanatory variables to establish a relationship with the groundwater age. The estimates for groundwater age from a USGS study on the Eastern Shore were used (Ward and Pope, 2013) in the analysis. An extensive list of watershed characteristics was tested for their potential as explanatory variables. Along with physical characteristics of the catchments, such as slope and depth to groundwater, the USGS data publications on surficial hydrogeologic framework for the Mid-Atlantic Coastal Plains (Ator et al., 2005) were used to obtain additional geospatial catchment attributes. The attributes used in the statistical model development included 6 physiographic providences, 7 physiographic frameworks, 4 lithology classes, 12 surficial geology, and 16 sub-cropping geologies. These watershed attributes were first normalized, and a principle component analysis was performed.

The statistical model performed quite well on the Eastern Shore, where the model was trained (Figure 10-31). The statistical model did not produce a numerical equation due to the nature of the gradient boosted regression trees, but as shown in Figure 10-32, it provided insights into what watershed attributes were important for explaining the variability in groundwater age. Figure 10-32(a) shows the principle components that were identified as the most important in explaining the variability in groundwater age. The composition of weights for the top four important principle components are shown in Figure 10-32(b). The figure shows some of the hydrogeologic watershed attributes, e.g. lithology, physiographic framework, sub-cropping geology, were most important for estimating groundwater age of the Coastal Plain region, in contrast with the rest of the watershed, where topography and groundwater recharge were important.

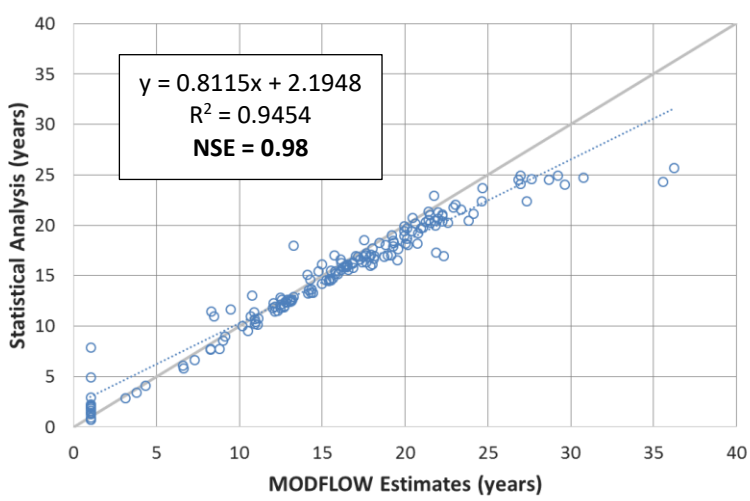

Figure 10-31: The performance of the statistical model in reproducing the groundwater age in the Delmarva region of the Chesapeake Bay Coastal plain HUC12 catchments. The statistical model was developed with gradient boosted

regression trees using MODFLOW-MODPATH estimated ages and lithological, physiographic, geological and physical attributes of the catchments.

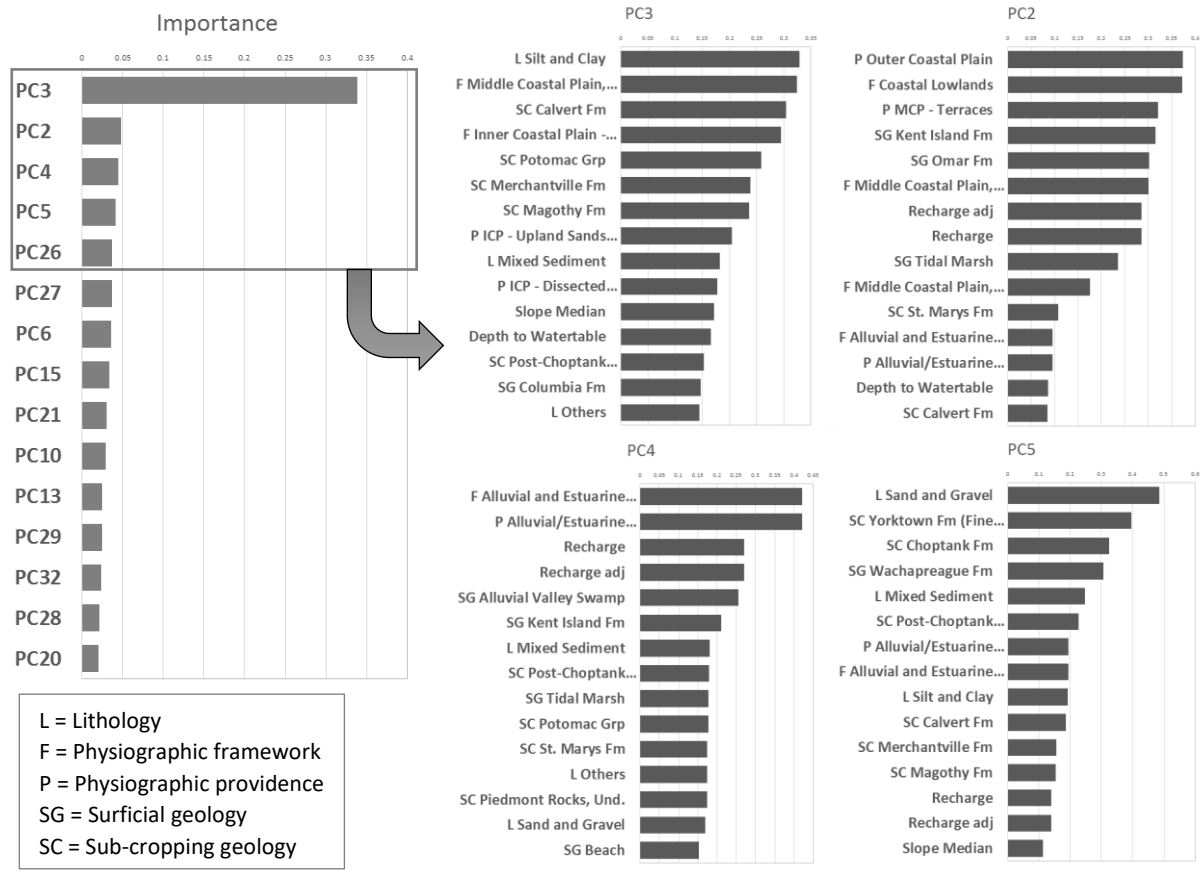

Figure 10-32: (a) Importance of the Principle components (PCs) in the statistical model for explaining the groundwater age. As shown, PC3 was the most important component in the model. (b) The weights of the lithological physiographic, geological and physical watershed attributes in the principle components. The weights for the 4 most important PCs are shown that reveals importance of lithological, physiographic, and geological attributes on groundwater age in the Chesapeake Coastal Plains.

Figure 10-33(a) shows the estimated groundwater age for the HUC-12 catchments of the Chesapeake Bay watershed. The groundwater age for the HUC-12 catchments were spatially aggregated to the Phase-6 land segments using recharge volume weighed averaging so that it can be used in the Phase 6 model for the simulation of groundwater lag in the transport processes. The Figure 10-33(b) shows the groundwater age for the Phase-6 land segments.

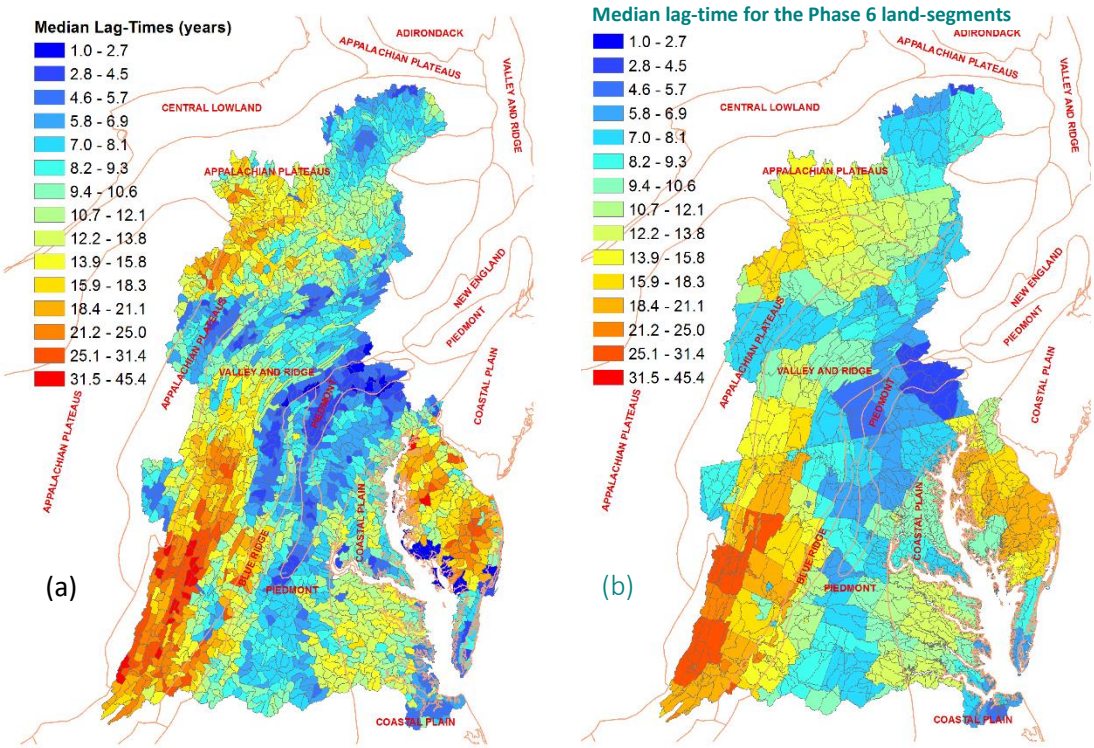

Figure 10-33: (a) The estimates for the median groundwater age for the HUC-12 catchments in the Chesapeake Bay watershed estimated using a regression model and a statistical model. (b) The median groundwater age for the Phase-6 land-segments that was calculated using the recharge volume weighted spatial aggregation of HUC-12 groundwater age.

The median lag-times for surface and sediment flow paths were estimated as linear relationships to simulated surface flow and sediment washoff respectively. Both relationships had negative slopes, meaning the greater the flow or washoff, the shorter the lag time. Distributions of estimated median lag-times in nutrient transport though groundwater, surface water, and sediment flow paths for the 235 Phase 6 land segments are shown in Figure 10-34.

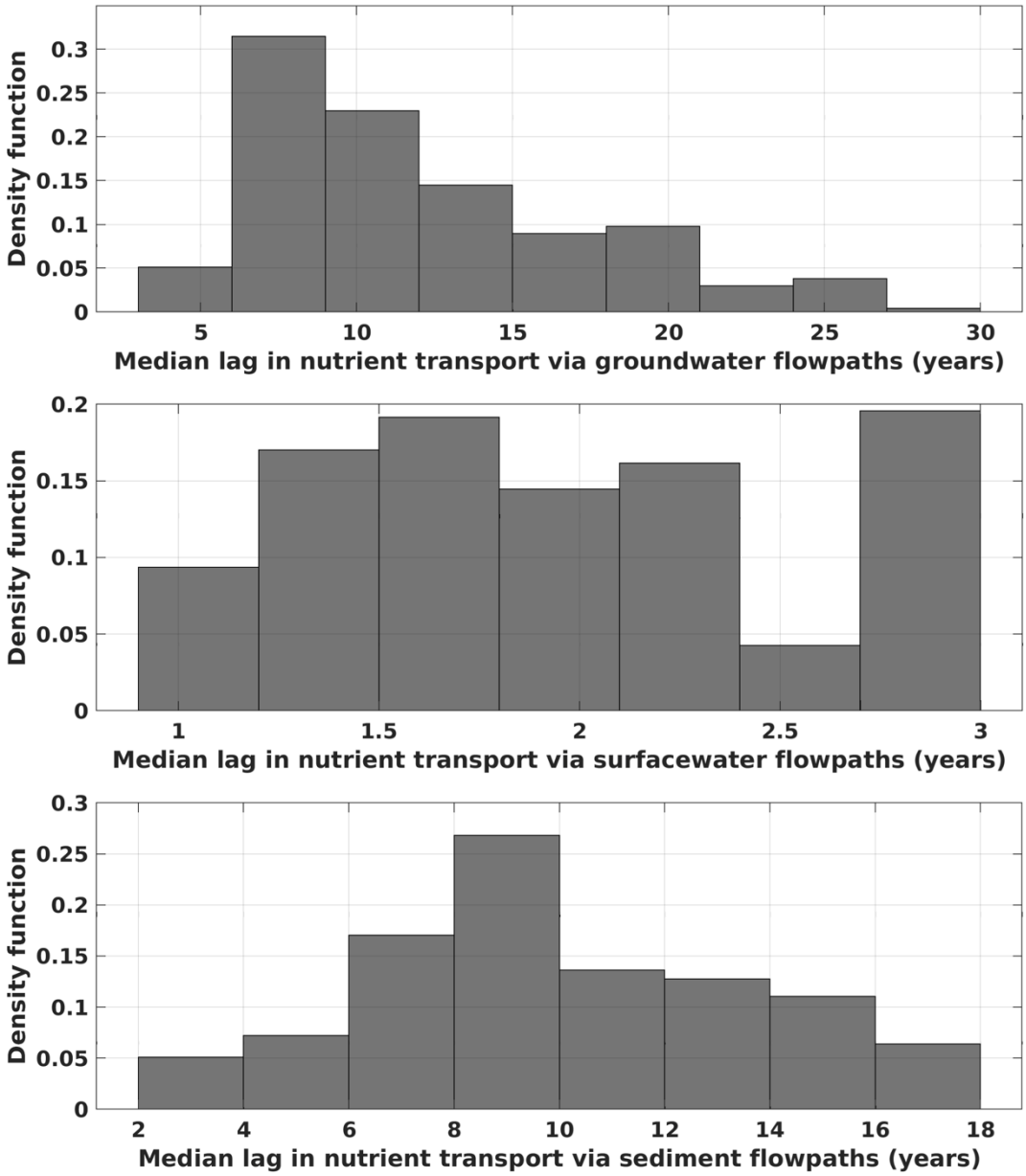

Figure 10-34: Estimated median lag-times in nutrient transport through groundwater, surface water and sediment flow paths.

10.5.4 Unit Nutrient Export Curves (UNEC)

As discussed previously, one of the primary functions of the dynamic watershed model is to provide daily loads for flow, sediment, and nutrient constituents to the linked simulation of various estuarine models. The HSPF model was used for the dynamic simulation of flow and sediment transport. For nutrients, a new simulation framework called Unit Nutrient Export Curves (UNEC) was developed that uses data for nutrient inputs, simulated hourly flow, and sediment responses to calculate the nutrient export from a catchment while explicitly incorporating the externally supplied lag time information in

the model. This dynamic simulation framework was specifically designed to ensure consistency between the simulated dynamic responses for nutrients and the time-averaged model.

The key steps in the application of UNEC are as follows:

For each land use, land segment, nutrient species, and transport path:

1. The time series of nutrient input loads (total nitrogen or total phosphorus) for each source (fertilizer, manure, legume fixation, atmospheric deposition etc.) are calculated on a monthly time step;

2. Sensitivities (described in Section 4) are applied to the respective time series so that inputs from different sources can be combined into a net input time series;

3. Each month's sensitivity adjusted inputs are converted to an output monthly time-series for the current month and all future months based on UNEC calculated using the lag-time parameters;

4. For each month, the output time-series for prior month inputs are summed to arrive at a "proto-concentration", creating a monthly output time series for the simulation period;

5. The monthly time series of proto-concentrations is multiplied by the hourly time series of flow (or eroded sediment) to produce an intermediate hourly time series of loads;

6. The intermediate load time series is renormalized over a specified period such that it is equal to the time-averaged load for the same period.

The new nutrient framework builds upon the principles of HSPF-PQUAL simulation scheme but adds a dynamic linkage between the nutrient inputs with a simplified representation of lag-time to determine the temporal variability in concentration for a given flow path. Numerically, the simulation system works as a transfer function that links nutrient applications (fertilizer, manure, legume fixation, atmospheric deposition, etc.) to the nutrient export without explicitly simulating the processes between nutrient inputs and export. The transfer function uses a simplified, externally derived understanding of lags in the nutrient response of critical watershed processes that are estimated *a priori* from a synthesis of available data points from model studies, empirical evidences, and regional observations.

The Phase 5.3.2 Model used the HSPF-AGCHEM module to simulate the fate and transport of nutrients for a majority of agricultural land uses. The AGCHEM module represents the transport of nutrients in runoff, interflow, erosion, infiltration, percolation, and groundwater discharge. It also simulates the transformation of nutrient species through processes such as fixation, nitrification, and mineralization. Although AGCHEM provided a process driven approach for simulating nutrient transport, it was time-consuming to calibrate, and produced some counterintuitive model results when used to simulate the effects of management scenarios. As an alternative to AGCHEM, HSPF provides PQUAL, which a simpler module for simulating the fate and transport of water quality constituents. The PQUAL module uses a fixed monthly concentration for nutrient constituents for interflow and groundwater, and a slightly more complex coefficient-based simulation of surface washoff for simulating watershed nutrient response. In the Phase 5.3.2 Model, PQUAL concentration parameters were changed annually to capture the interannual variability in inputs. However, that limited the ability of the simulation to

capture the effects of variability in nutrient inputs at monthly to seasonal time scales as well as relinquished any influence of inputs from prior years on the response. Neither AGCHEM nor PQUAL effectively simulated groundwater lags or provided any mechanism for the quantification of lag in the simulated response.

Different types of tracers have been widely used in studies as an age-dating tool and for developing the understanding of watershed mixing processes (Thompson et al., 1974; Randell and Schultz, 1976; Schultz et al., 1976; Plummer et al., 1993). Some of the conservative environmental isotopic tracers have also been used along with a number of models and analytical approaches for the characterization of watershed response and lag times (Maloszewski et al., 1983; Pearce et al., 1986; Steward and Maloszewski, 1991; Lindström and Rodhe, 1992;). Analysis of breakthrough curves provide a technique for quantifying integrated lag time response of a watershed based on tracer experiments. The concept of a breakthrough curve was taken from tracer studies used to estimate aquifer properties in karst regions (Field, 1999), but have been applied in many other fields. The unit hydrograph, for example, is a type of a breakthrough curve. The EPA-QTRACER Program (Field, 1999) is an analysis tool that provides detailed information regarding the sub-surface flow dynamics of a watershed. *Figure **10-35*** shows a generalized description of a breakthrough curve formed along a select flow path in response to an instantaneous injection of a tracer at an upstream location (Kilpatrick and Wilson, 1989; Field, 1999).

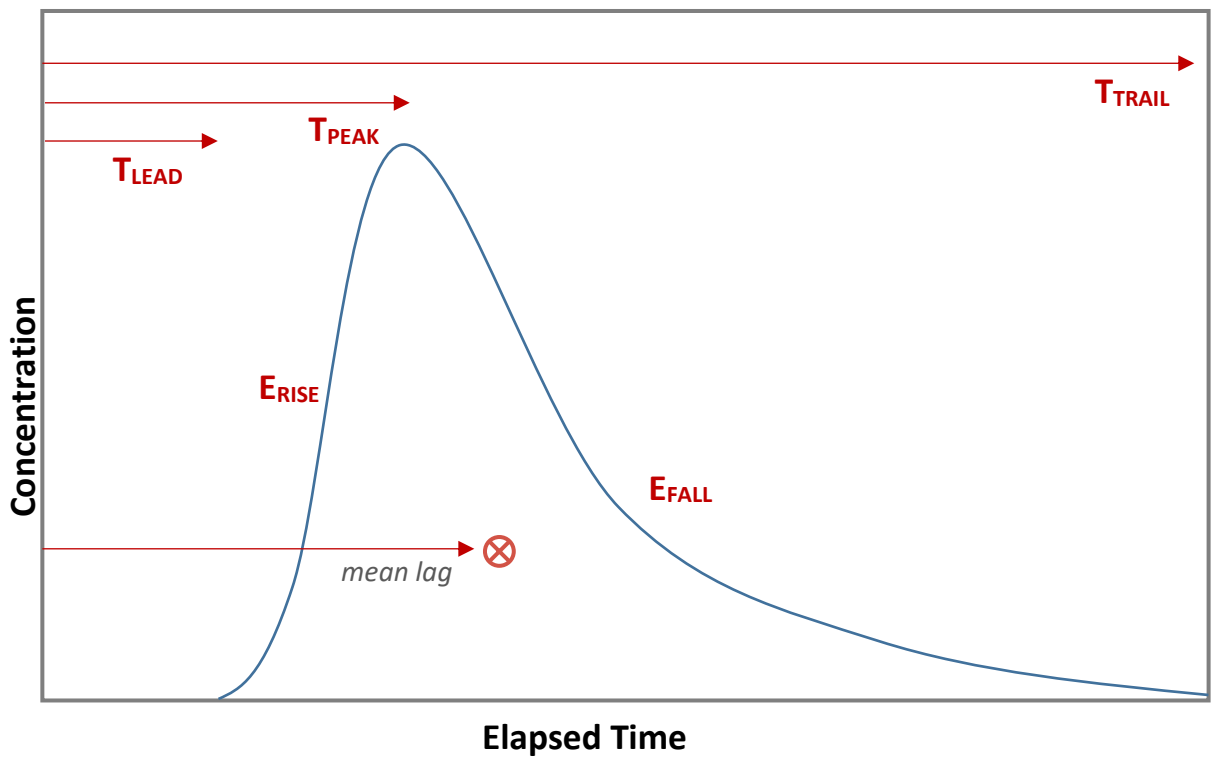

Figure 10-35: A generalized description of breakthrough curve. Adapted from EPA-QTRACER (Field 1999). Adaptation of breakthrough curve in the nutrient simulation is called Unit Nutrient Export Curve (UNEC).

Unit Nutrient Export Curve (UNEC) uses these key descriptors of a breakthrough curve as model parameters. As referenced in *Figure **10-35*** parameters T_{LEAD}, T_{PEAK}, and T_{TRAIL} are the time it takes for the leading edge, peak, and trail, respectively, to occur from the time of an instantaneous input of a tracer.

Two additional parameters, E_{RISE} and E_{FALL}, are used to capture a simplified representation of the rising and falling limbs of the concentration.

UNEC creates a forward temporal disaggregation of nutrient response for every input event. The aggregate response is then calculated by the superposition of UNECs for these input events. *Figure **10-36***(a) shows a simplified functional description of this process for a single input event. For a single event the watershed response is a single curve as shown in *Figure **10-36***(b). The resultant load from the watershed is shown in *Figure **10-36***(c) where the concentration curve is combined with the simulated flow, which for this example was assumed to be a sine function that repeated every year. Although the flow is same year after year the delivery of load decreases over time due to UNEC. The response is observed over several years after the input event, which is determined by the UNEC parameter. For two input events, UNECs for each input event are superposed as shown in *Figure **10-37***(b). Although the magnitudes of both events are same, the net response after the second event is larger because the second event is superposed on the antecedent condition of the first event. The estimated load is showing in *Figure **10-37***(c) where flow is combined with the UNEC response. Building on the last two examples, *Figure **10-38*** shows the details for a complex loading example that consists of several input events of different magnitudes. As before, the same underlying UNEC response is used for the catchment, but the response for every input event is separately calculated by weighting the UNEC response corresponding to the magnitude of the input event and then combined for estimating the net response. In other words, all input events are assigned the same amount of lag time, but the net simulated concentration response are higher for the larger application events.

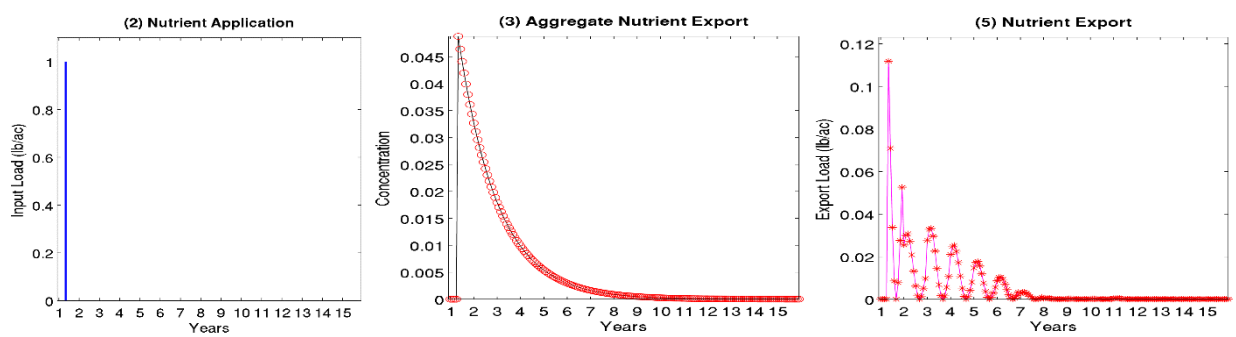

Figure 10-36: An illustration of watershed response for a unit input. (a) Unit input. (b) UNEC - estimated relative concentration response. (c) Time variable load estimated from relative concentration and simulated flow. A long-term mass-balance is imposed so that long-term output is same as input.

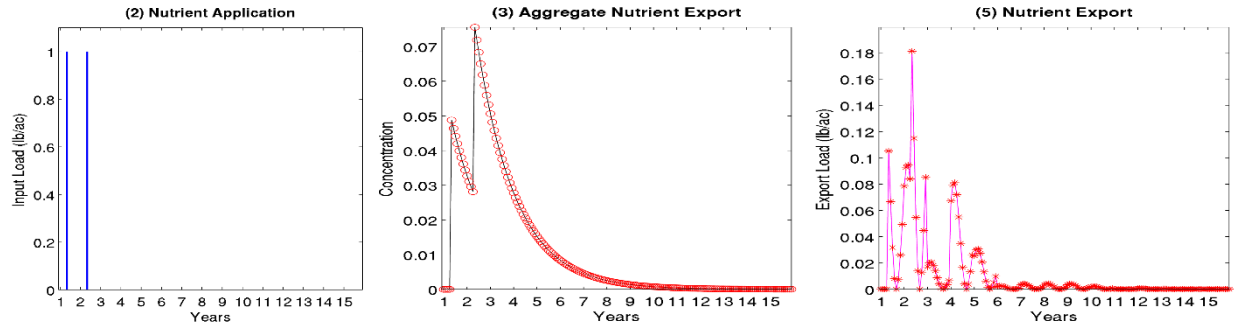

Figure 10-37: An illustration of watershed response for two instantaneous inputs. (a) Two step inputs. (b) Estimated relative concentration response resulting from the superimposition of two UNECs. (c) Time variable load estimated from relative concentration and simulated flow. A long-term mass-balance is imposed so that long-term output is same as input.

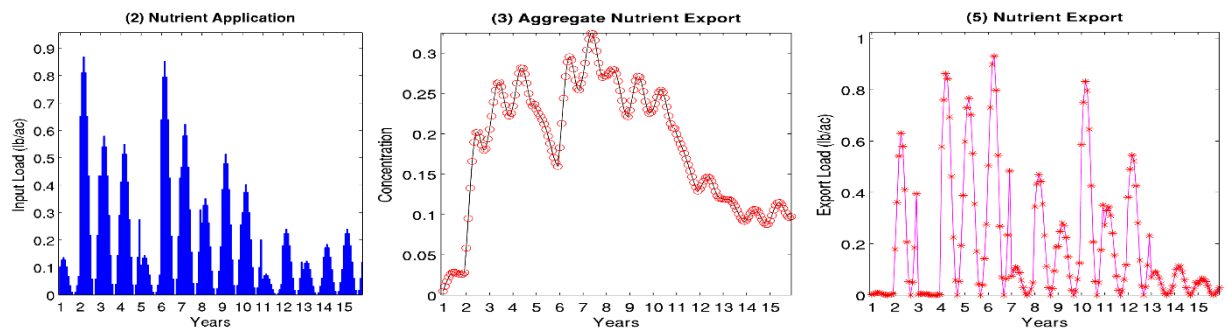

Figure 10-38: An illustration of watershed response for a time varying input. (a) Time varying input. (b) Estimated relative concentration response resulting from the superimposition of UNECs. (c) Time variable load estimated from relative concentration and simulated flow. A long-term mass-balance is imposed so that long-term output is same as input.

Separate UNECs are used for four transport flow paths of sediment-associated, groundwater (base flow), interflow, and surface flow. That provides the ability to integrate different amounts of lag times for these transport flow paths. For example, nutrient transport with baseflow is likely have significantly longer lag time as compared to that through surface flow path. In addition to the use of different UNECs for account for the differences in lag of the flow paths, separate UNECs are used for the nutrient species. It provides a mechanism for representing differences in the response for nutrient species (e.g. nitrate vs. ammonia) for a same flow path. *Table **10-21*** shows the combinations of nutrient species and flow paths that were used in the dynamic simulation model.

Table 10-21 Nutrient species and transport paths used to specify UNECs

Nutrient Species	Transport Paths			
	Surface	Sediment	Interflow	Baseflow
Nitrate	X		X	X
Ammonia	X	X	X	X
Labile organic nitrogen	X	X	X	X
Refractory organic nitrogen	X	X	X	X
Orthophosphate	X	X	X	X
Labile organic phosphorus	X	X	X	X
Refractory organic phosphorus	X	X	X	X

UNEC uses inputs from various sources e.g., atmospheric deposition, manure, fertilizer, crop uptake, legume fixation in the simulation. The composition of nutrient species varies for these sources as described in Section 3, however inputs for total nitrogen and total phosphorus are used for the simulation of export species for nitrogen and phosphorus respectively. Section 4 describes the export nutrient species expected from each input type. The relationship between input type and export species is summarized in Table 10-22. From a process point of view, nutrient species can transform as they undergo various biogeochemical processes, e.g., fertilizer applied as ammonia can transform by nitrification into nitrate. That transformation can take place either at the surface or after the ammonia infiltrates into the soil. Section 4 describes the proportions of different export species that are expected from each input source type. These proportions are retained in the UNEC algorithm.

For example, inputs of atmospheric deposition are available as nitrate and ammonia, but these are summed to total nitrogen inputs. Exports due to atmospheric deposition are split into nitrate, ammonia, labile organic nitrogen, and refractory organic nitrogen as shown in Table 10-22. Each of the nitrogen species will have a separate UNEC for surface, interflow, and baseflow, with all but nitrate also having a sediment UNEC as shown in *Table **10-21***.

Table 10-22 Nutrient sources and species used for the construction of UNECs for the species

	Output Species						
Input	Nitrate	Ammonia	Labile organic nitrogen	Refractory organic nitrogen	Ortho-phosphate	Labile organic phosphorus	Refractory organic phosphorus
Atmospheric Dep.	X	X	X	X			
Fertilizer	X	X	X	X	X	X	X
Manure	X	X	X	X	X	X	X
Legume	X	X	X	X	X	X	X
Uptake	X	X	X	X	X	X	X
Water Extractable P					X	X	X

UNEC has four parameters that can be used for targeting a relatively complex response of a catchment. However, in real word applications, it is difficult to find information needed to estimate those parameters. To overcome this, the exponent for the falling limb (E_{FALL}) was the only parameter that was considered to vary spatially with the sub-watersheds, and it was linked to the estimate of the mean lag-time for the watershed processes, e.g. groundwater lag, sediment transport lag, etc. A fixed value of 70 years for the time to the trailing edge (T_{TRAIL}) was used. The time for the leading edge (T_{LEAD}) and the peak (T_{PEAK}) were estimated using lines of empirical evidence. One of the most critical lines of empirical evidence was based on a comprehensive analysis of the monthly concentrations for the 9 river input monitoring (RIM) stations estimated from the data provided by the USGS's WRTDS analysis. Other lines of evidence included a review of emergent seasonality in the observed concentration data at several

monitoring sites as well as model's functional input-output response. The monthly concentration response of nitrate, dissolved orthophosphate, and difference of total nitrogen and nitrate were analyzed to draw generalizable inferences on the seasonality of the nutrient species responses. Subsequently, the model parameter selections were made for the nutrient species to match the timing of the lows and the highs of the seasonal cycles in the WRTDS concentration data at the RIM stations and were held constant for each land segment.

Following the simplifying assumptions outlined for the UNEC in the previous paragraph, the exponent parameter E_{FALL} was estimated as follows:

$$as\ per\ the\ definition\ of\ mean\ time:$$

$$Half\ of\ the\ load\ exported\ between\ time\ 0\ and\ T_{TRAIL} = Load\ exported\ between\ time\ 0\ and\ T_{MEAN}$$

$$0.5\int_0^{T_{TRAIL}} e^{-E_{FALL}t}dt = \int_0^{T_{MEAN}} e^{-E_{FALL}t}dt$$

$$0.5\left.\frac{e^{-E_{FALL}t}}{-E_{FALL}}\right|_0^{T_{TRAIL}} = \left.\frac{e^{-E_{FALL}t}}{-E_{FALL}}\right|_0^{T_{MEAN}}$$

$$0.5\left(\frac{e^{-E_{FALL}T_{TRAIL}}}{-E_{FALL}} - \frac{e^{-E_{FALL}0}}{-E_{FALL}}\right) = \frac{e^{-E_{FALL}T_{MEAN}}}{-E_{FALL}} - \frac{e^{-E_{FALL}0}}{-E_{FALL}}$$

$$0.5(e^{-E_{FALL}T_{TRAIL}} - 1) = (e^{-E_{FALL}T_{MEAN}} - 1)$$

$$Solve\ \{0.5(e^{-E_{FALL}T_{TRAIL}} - 1) - (e^{-E_{FALL}T_{MEAN}} - 1)\} = 0, for\ given\ T_{TRAIL}\ and\ T_{MEAN}\ to\ obtain\ E_{FALL}$$

Equation 10-15

A MATLAB subroutine was developed to iteratively solve Equation 10-15 for each land segment and flow path (i.e. stormflow, baseflow, and sediment). The subroutine accepted T_{TRAIL} and T_{MEAN} as inputs for the land segment and flow paths to estimate the corresponding E_{FALL} UNEC parameter. Estimated lag times for the stormflow, baseflow and sediment transport processes and corresponding UNEC parameters are shown in *Table **10-23***. Lag times for groundwater are based on Section 10.5.3. The mean lag times for stormflow and sediment transport were estimated as 2 and 10 years respectively and varied spatially between the land segments based on the relative edge of stream flow and sediment deliveries.

Table 10-23: Estimated lags in transport processes and corresponding Unit Nutrient Export Curve (UNEC) parameters.

Transport	**Stormflow**		**Baseflow**		**Sediment**	
Land segment	Lag (Years)	UNEC Parameter	Lag (Years)	UNEC Parameter	Lag (Years)	UNEC Parameter
N10001	2.4	0.02379	16.0	0.00330	16.1	0.00327
N10003	2.2	0.02572	11.6	0.00487	8.8	0.00652
N10005	1.8	0.03213	18.6	0.00264	17.2	0.00297
N11001	1.1	0.05382	9.6	0.00596	10.2	0.00558
N24001	2.4	0.02385	17.7	0.00285	8.2	0.00703
N24003	2.0	0.02946	10.1	0.00566	12.3	0.00456
N24005	1.5	0.03977	7.4	0.00775	8.2	0.00699
N24009	2.2	0.02641	9.4	0.00609	9.5	0.00604
N24011	1.4	0.04011	18.9	0.00258	15.2	0.00352
N24013	2.0	0.02844	6.5	0.00883	3.1	0.01864
N24015	2.0	0.02954	14.3	0.00380	7.2	0.00804
N24017	2.3	0.02514	8.8	0.00650	14.0	0.00390
N24019	2.1	0.02812	9.6	0.00594	15.7	0.00338
H24021	2.0	0.02882	8.5	0.00676	9.0	0.00633
N24021	1.9	0.02971	7.3	0.00794	3.4	0.01691
H24023	1.1	0.05382	7.5	0.00769	4.4	0.01299
N24023	1.3	0.04346	8.5	0.00675	3.6	0.01611
N24025	1.7	0.03322	7.9	0.00728	8.8	0.00650
N24027	1.9	0.03108	6.7	0.00860	7.9	0.00724
N24029	1.9	0.03107	18.9	0.00257	8.3	0.00693
N24031	1.7	0.03396	6.6	0.00870	9.1	0.00626
N24033	1.7	0.03414	10.1	0.00563	11.1	0.00511
N24035	1.8	0.03212	16.7	0.00309	11.3	0.00500
N24037	2.3	0.02492	7.0	0.00828	13.0	0.00428
N24039	2.4	0.02400	13.9	0.00393	17.2	0.00297
N24041	1.4	0.04178	17.5	0.00291	11.2	0.00504
N24043	2.4	0.02401	8.3	0.00696	10.9	0.00521
N24045	1.9	0.02963	21.0	0.00214	14.4	0.00375
N24047	2.2	0.02618	16.7	0.00311	15.7	0.00336
N24510	1.1	0.05382	8.0	0.00718	9.6	0.00598
N36003	2.2	0.02592	13.2	0.00420	7.5	0.00763
N36007	1.5	0.03809	8.6	0.00669	8.1	0.00711
N36015	2.8	0.02093	14.4	0.00375	9.4	0.00608
N36017	1.4	0.04278	7.3	0.00793	8.2	0.00705
N36023	1.3	0.04342	7.6	0.00753	5.7	0.01006
N36025	1.4	0.04104	8.7	0.00659	6.3	0.00910
N36043	1.2	0.05014	4.4	0.01314	6.5	0.00882
N36051	1.9	0.03076	14.2	0.00382	2.5	0.02285
N36053	1.5	0.03732	6.9	0.00838	7.5	0.00773
N36065	1.6	0.03558	5.9	0.00973	5.8	0.00988

N36067	1.5	0.03745	5.5	0.01050	7.6	0.00755
N36069	1.8	0.03151	14.3	0.00380	3.9	0.01477
N36077	1.4	0.04023	8.2	0.00705	6.6	0.00870
N36095	1.4	0.04099	9.0	0.00639	7.8	0.00740
N36097	2.1	0.02762	12.8	0.00435	10.3	0.00554
N36101	2.7	0.02133	15.2	0.00351	7.1	0.00817
N36107	1.7	0.03328	9.9	0.00578	7.5	0.00770
N36109	1.8	0.03221	11.6	0.00486	10.0	0.00571
N36123	1.8	0.03205	9.4	0.00607	7.9	0.00732
N42001	1.9	0.03075	5.7	0.01015	8.7	0.00656
N42009	2.1	0.02795	15.3	0.00348	8.5	0.00675
N42011	1.2	0.04891	3.7	0.01582	7.3	0.00792
H42013	1.8	0.03208	10.7	0.00530	9.6	0.00595
N42013	1.6	0.03691	10.3	0.00552	8.5	0.00679
N42015	1.8	0.03151	12.2	0.00457	7.7	0.00750
N42021	1.7	0.03302	7.4	0.00781	5.9	0.00976
N42023	1.6	0.03510	16.0	0.00330	11.3	0.00498
N42025	1.2	0.04849	5.9	0.00981	5.4	0.01061
H42027	1.3	0.04590	8.6	0.00665	14.7	0.00367
N42027	2.1	0.02710	7.0	0.00823	10.4	0.00545
N42029	1.7	0.03383	6.6	0.00877	6.1	0.00940
N42033	1.4	0.04265	7.2	0.00796	7.8	0.00739
N42035	1.4	0.04184	10.5	0.00543	10.9	0.00522
N42037	1.5	0.03944	8.2	0.00700	5.8	0.00997
N42041	1.6	0.03604	4.8	0.01191	9.2	0.00625
H42043	1.8	0.03166	9.2	0.00625	16.7	0.00311
N42043	1.9	0.03055	6.4	0.00900	8.3	0.00694
N42047	1.5	0.03900	11.5	0.00490	11.9	0.00470
N42055	2.2	0.02604	7.6	0.00757	13.6	0.00403
N42057	2.5	0.02333	16.1	0.00325	9.9	0.00576
N42061	1.7	0.03348	12.3	0.00455	9.0	0.00638
N42063	1.3	0.04363	8.5	0.00679	6.2	0.00924
N42065	1.4	0.04212	7.9	0.00725	9.9	0.00578
N42067	2.0	0.02899	10.2	0.00560	8.4	0.00685
L42069	3.0	0.01895	7.5	0.00766	15.8	0.00333
N42069	1.6	0.03521	7.8	0.00742	9.5	0.00605
N42071	1.8	0.03216	4.3	0.01343	9.0	0.00633
N42075	1.8	0.03300	4.4	0.01324	8.0	0.00722
H42079	1.3	0.04540	10.0	0.00569	17.1	0.00300
L42079	3.0	0.01948	7.2	0.00801	14.5	0.00373
N42079	1.3	0.04450	7.2	0.00799	9.9	0.00576
N42081	1.4	0.04192	12.1	0.00463	8.5	0.00678

N42083	1.6	0.03637	20.0	0.00233	11.5	0.00490
N42087	1.5	0.03864	9.8	0.00580	8.6	0.00671
N42093	2.0	0.02944	6.7	0.00864	5.5	0.01052
N42097	1.5	0.03959	7.9	0.00731	4.9	0.01175
N42099	1.7	0.03475	9.6	0.00593	8.3	0.00690
N42105	1.7	0.03459	18.2	0.00274	8.8	0.00653
N42107	1.3	0.04330	6.7	0.00855	7.4	0.00777
N42109	1.6	0.03569	8.3	0.00689	6.4	0.00908
N42111	1.4	0.04150	15.2	0.00351	6.4	0.00900
H42113	1.1	0.05054	9.5	0.00600	16.5	0.00316
L42113	1.6	0.03606	11.3	0.00502	9.9	0.00579
N42113	1.3	0.04430	11.0	0.00517	10.9	0.00522
H42115	1.2	0.05014	7.1	0.00816	9.9	0.00578
N42115	1.6	0.03535	10.9	0.00521	6.9	0.00834
H42117	1.5	0.03922	15.0	0.00358	13.7	0.00402
N42117	2.0	0.02948	14.8	0.00364	7.8	0.00740
H42119	1.3	0.04335	9.8	0.00585	14.7	0.00368
N42119	1.3	0.04444	7.3	0.00786	8.4	0.00683
N42127	1.1	0.05079	7.9	0.00732	8.7	0.00657
H42131	1.5	0.03779	10.7	0.00531	14.8	0.00363
N42131	1.7	0.03436	11.4	0.00494	8.8	0.00653
N42133	2.1	0.02778	6.3	0.00921	4.3	0.01333
N51001	2.4	0.02404	8.2	0.00702	16.8	0.00306
H51003	2.7	0.02125	20.0	0.00234	9.7	0.00592
N51003	2.2	0.02570	11.5	0.00489	8.5	0.00676
N51005	2.4	0.02445	26.8	0.00116	10.6	0.00535
N51007	3.0	0.01895	7.5	0.00769	12.3	0.00452
H51009	1.3	0.04342	21.1	0.00213	9.4	0.00606
N51009	2.1	0.02740	14.3	0.00380	9.1	0.00627
N51011	2.7	0.02100	8.9	0.00647	8.4	0.00688
N51013	1.1	0.05382	12.3	0.00454	6.0	0.00962
H51015	1.8	0.03291	15.4	0.00345	9.3	0.00618
L51015	3.0	0.01895	9.6	0.00592	6.3	0.00915
N51015	2.3	0.02496	16.5	0.00316	6.8	0.00846
N51017	2.6	0.02241	25.2	0.00140	11.5	0.00491
N51019	2.8	0.02080	16.7	0.00311	9.0	0.00637
H51023	2.6	0.02205	27.7	0.00102	12.4	0.00451
L51023	2.3	0.02535	20.4	0.00225	11.9	0.00473
N51023	2.2	0.02644	19.1	0.00253	7.8	0.00735
N51029	2.8	0.02080	8.2	0.00704	11.4	0.00495
N51031	3.0	0.01895	10.4	0.00545	7.7	0.00752
N51033	2.9	0.01978	11.3	0.00501	15.4	0.00345

N51036	3.0	0.01895	12.6	0.00442	14.9	0.00360
N51041	2.3	0.02485	12.7	0.00436	16.0	0.00330
N51043	3.0	0.01945	8.5	0.00677	8.7	0.00662
H51045	1.9	0.03034	19.5	0.00245	9.3	0.00619
N51045	2.0	0.02841	19.6	0.00243	10.7	0.00533
N51047	2.6	0.02263	6.4	0.00902	8.7	0.00661
N51049	3.0	0.01949	7.8	0.00739	13.6	0.00403
N51053	2.8	0.02034	9.8	0.00585	13.8	0.00397
N51057	2.4	0.02438	13.3	0.00413	13.3	0.00416
N51059	1.7	0.03443	9.4	0.00606	12.1	0.00462
N51061	2.6	0.02209	9.1	0.00629	8.4	0.00686
N51065	3.0	0.01895	8.3	0.00695	11.2	0.00506
N51069	3.0	0.01895	12.5	0.00446	9.0	0.00640
N51071	2.2	0.02670	18.2	0.00273	11.2	0.00503
N51073	2.1	0.02702	9.5	0.00602	16.8	0.00308
N51075	2.9	0.02007	9.2	0.00623	13.0	0.00425
H51079	1.7	0.03399	14.7	0.00369	8.7	0.00660
L51079	2.4	0.02387	10.4	0.00548	7.2	0.00804
N51079	1.8	0.03234	13.7	0.00401	6.4	0.00904
N51085	2.7	0.02104	10.5	0.00540	13.6	0.00402
N51087	1.9	0.03056	11.1	0.00511	15.2	0.00352
L51091	1.8	0.03226	21.2	0.00210	9.3	0.00617
N51091	1.7	0.03467	23.1	0.00176	4.4	0.01310
N51093	2.7	0.02154	7.8	0.00736	12.9	0.00430
N51095	2.2	0.02592	10.6	0.00536	14.5	0.00374
N51097	2.8	0.02068	12.2	0.00458	14.9	0.00361
N51099	2.4	0.02417	11.5	0.00492	14.1	0.00388
N51101	2.5	0.02278	13.3	0.00415	14.1	0.00385
N51103	2.3	0.02560	11.0	0.00513	15.6	0.00340
N51107	2.2	0.02675	6.9	0.00838	7.7	0.00752
N51109	2.8	0.02095	7.1	0.00813	13.5	0.00406
H51113	1.4	0.04020	20.7	0.00220	9.6	0.00597
N51113	2.0	0.02876	11.1	0.00509	6.6	0.00876
N51115	2.2	0.02625	6.3	0.00922	17.2	0.00297
N51119	2.3	0.02528	12.1	0.00461	14.3	0.00379
N51121	2.8	0.02045	21.8	0.00200	13.5	0.00408
H51125	2.0	0.02851	19.5	0.00245	7.8	0.00741
N51125	1.4	0.04232	14.8	0.00366	9.7	0.00588
N51127	3.0	0.01895	11.4	0.00494	16.5	0.00316
N51131	2.5	0.02337	6.3	0.00910	14.6	0.00371
N51133	2.2	0.02588	10.5	0.00539	12.3	0.00456
N51135	2.9	0.01971	8.0	0.00715	12.8	0.00434

N51137	3.0	0.01895	7.3	0.00785	7.9	0.00728
H51139	2.9	0.01977	20.3	0.00228	10.4	0.00546
N51139	3.0	0.01954	17.6	0.00287	9.2	0.00625
N51145	2.7	0.02125	7.6	0.00759	14.4	0.00378
N51147	2.8	0.02052	9.8	0.00582	11.8	0.00476
N51149	2.9	0.01991	12.8	0.00434	14.7	0.00366
N51153	2.2	0.02672	7.5	0.00763	10.8	0.00527
H51157	1.8	0.03142	18.4	0.00268	10.3	0.00552
L51157	2.2	0.02646	12.1	0.00461	8.7	0.00661
N51157	1.8	0.03142	15.2	0.00351	7.1	0.00814
N51159	2.3	0.02476	12.5	0.00447	13.2	0.00420
N51161	2.5	0.02268	20.0	0.00233	5.4	0.01067
L51163	2.7	0.02107	22.7	0.00183	4.9	0.01185
N51163	2.0	0.02825	19.7	0.00240	5.6	0.01033
H51165	1.7	0.03309	24.6	0.00150	9.8	0.00580
N51165	2.7	0.02149	18.9	0.00257	6.8	0.00844
N51171	2.6	0.02256	16.5	0.00314	8.8	0.00653
N51177	2.7	0.02151	9.7	0.00588	13.7	0.00401
N51179	2.4	0.02408	7.9	0.00729	13.9	0.00393
N51181	3.0	0.01957	12.9	0.00430	13.2	0.00418
N51187	3.0	0.01895	15.6	0.00340	9.4	0.00612
N51193	2.3	0.02529	12.4	0.00450	12.0	0.00466
N51199	1.2	0.04662	9.1	0.00630	13.2	0.00417
N51510	1.1	0.05382	12.0	0.00469	7.2	0.00799
N51530	1.5	0.03891	21.9	0.00196	7.5	0.00763
N51540	1.6	0.03684	12.5	0.00448	10.0	0.00570
N51550	2.2	0.02667	5.7	0.01019	17.2	0.00297
N51570	1.7	0.03350	12.6	0.00442	15.7	0.00338
N51580	1.1	0.05358	24.6	0.00150	8.4	0.00682
N51600	1.7	0.03403	10.8	0.00524	11.4	0.00496
N51610	1.6	0.03685	11.8	0.00475	13.7	0.00399
N51630	2.1	0.02790	11.0	0.00516	11.5	0.00488
N51650	1.7	0.03437	6.9	0.00841	15.7	0.00337
N51660	1.8	0.03272	7.5	0.00763	7.2	0.00798
N51670	1.1	0.05382	12.5	0.00444	3.0	0.01936
N51678	1.3	0.04343	15.8	0.00334	7.9	0.00726
N51680	2.2	0.02628	9.9	0.00576	8.8	0.00652
N51683	1.9	0.03093	6.8	0.00853	10.5	0.00540
N51685	2.0	0.02876	9.0	0.00637	8.4	0.00680
N51700	1.1	0.05033	6.9	0.00834	15.3	0.00348
N51710	1.1	0.05382	7.0	0.00819	14.5	0.00374
N51730	1.1	0.05382	12.4	0.00450	12.6	0.00441

N51735	2.0	0.02880	5.8	0.01003	17.2	0.00297
N51740	1.4	0.04026	5.2	0.01108	16.0	0.00328
N51760	1.1	0.05382	13.1	0.00422	10.3	0.00554
N51790	1.9	0.03114	10.5	0.00544	5.1	0.01137
N51800	2.3	0.02536	6.4	0.00906	13.8	0.00396
N51810	1.4	0.04041	6.6	0.00875	17.2	0.00297
N51820	1.1	0.05382	7.9	0.00725	10.2	0.00556
N51830	2.0	0.02885	8.6	0.00667	12.5	0.00444
N51840	1.7	0.03345	6.1	0.00942	10.6	0.00535
N54003	2.9	0.02012	8.8	0.00655	12.9	0.00430
H54023	1.1	0.05189	7.7	0.00750	3.1	0.01857
L54023	3.0	0.01895	19.9	0.00237	5.2	0.01110
N54023	2.1	0.02740	17.6	0.00288	2.9	0.01969
N54027	2.8	0.02082	20.3	0.00228	10.5	0.00543
H54031	2.8	0.02055	24.6	0.00151	7.6	0.00754
L54031	3.0	0.01895	18.9	0.00258	8.0	0.00721
N54031	2.9	0.02016	25.6	0.00134	8.1	0.00709
N54037	2.7	0.02109	6.2	0.00935	12.5	0.00448
H54057	1.4	0.04095	9.5	0.00604	2.4	0.02431
N54057	3.0	0.01895	15.3	0.00350	8.6	0.00670
N54063	2.3	0.02543	20.0	0.00235	8.2	0.00703
N54065	2.3	0.02482	19.2	0.00250	12.1	0.00463
H54071	1.3	0.04402	26.4	0.00122	2.4	0.02431
L54071	2.6	0.02197	26.3	0.00122	5.0	0.01150
N54071	2.8	0.02035	26.2	0.00124	2.4	0.02431
N54077	1.1	0.05266	7.2	0.00796	2.4	0.02431
N54093	1.1	0.05382	8.1	0.00712	5.3	0.01099

Since the simulated nutrient response in UNEC is a function of history of inputs, it is necessary that input for several years prior from the start of the simulation is available for an appropriate spin-up of the model simulation. Alternatively, some appropriate simplifying assumptions will be needed. The latter approach was used in the Phase 6 simulation, where the issue of spin-up was addressed by repeating the inputs for the first year of simulation, i.e., 1984, for 30 prior years prior to the simulation period. Figure 10-39 compares the nitrate response for a segment with a spin up to the one where spin-up was not used to illustrate significance of a long spin-up time. Figure 10-39(a), which lacks an appropriate spin-up, has a significantly lower concentration for approximately first 10 years before the system reaches a dynamic equilibrium. Irrespective of differences in the spin-up, since both simulations were calibrated to same time-averaged nutrient export, the absence of an appropriate spin-up also affects the response for the years in the later part of the response. This is shown in the Figure 10-39(a)-(b), where the response for the later years is higher for the scenario without spin-up as compared to that with spin-up.

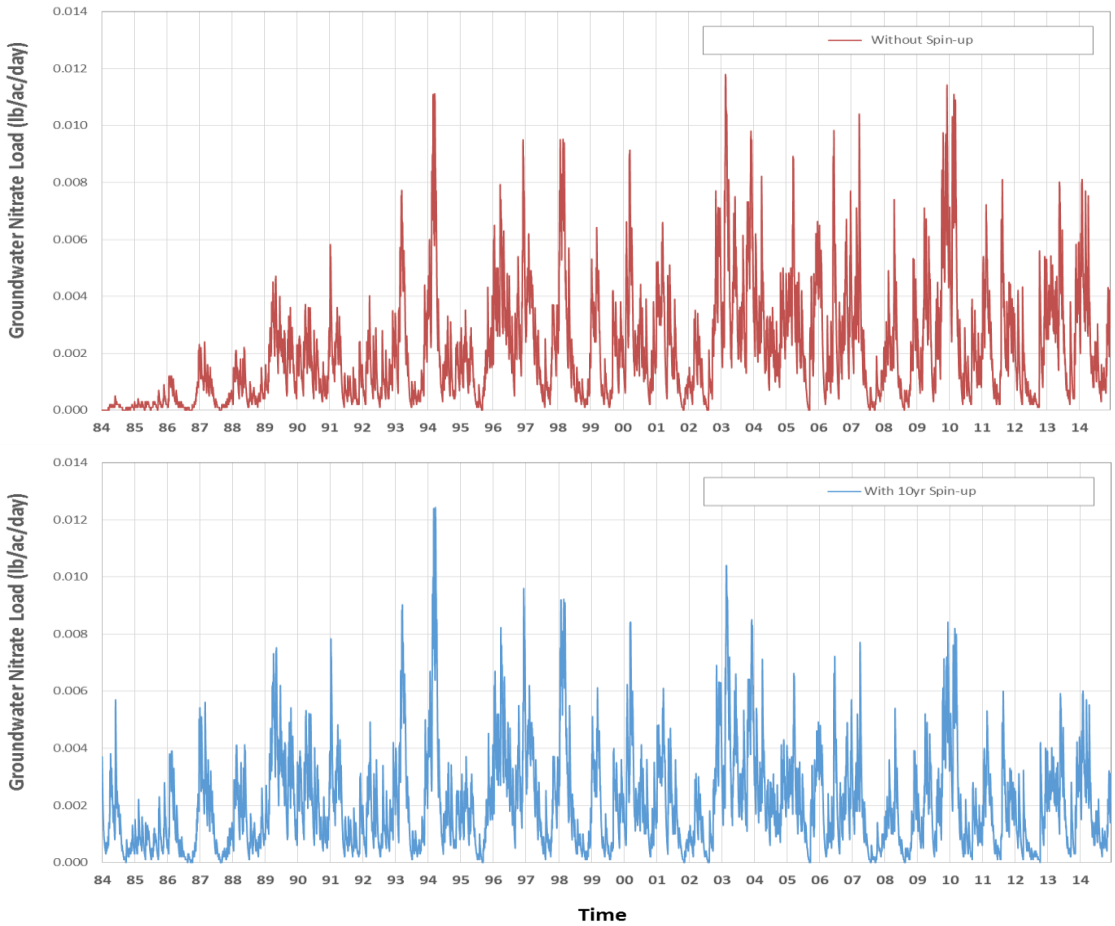

Figure 10-39: (a) Simulated groundwater nitrate load without a spin up of catchment's concentration response. In absence of a spin-up simulated loads for the early years are lower and higher for the later years. (b) Simulated groundwater loads with a 10-year spin up. Spin up was based of the nutrient inputs for the first year.

10.5.5 Ranked Storage Selection rSAS

Ranked Storage Selection (rSAS) is an approach to simulate transient age responses of the system. rSAS performs a formal accounting of the age based on the quantification of the fluxes across the boundaries (Harman et al. 2016). The model was applied in Rappahannock, a moderate size river basin with drainage area 1,595 of sq. miles, to simulate its groundwater nitrate response. The rSAS model results were compared with the UNEC to evaluate the difference in simulated loads and the seasonal agreement of the simulated loads with WRTDS. For this purpose, the riverine transport processes were calibrated using the same automated process, with the only difference being how daily groundwater nitrate loads were simulated using the two models. *Figure **10-40*** shows minor differences in the simulated monthly groundwater nitrate loads for a land segment and land use. The differences in the results are entirely due to model formulations, where rSAS performs a formal accounting of age in the groundwater storage but requires a considerable amount of computation time as compared to UNEC.

Figure ***10-41*** and *Figure* ***10-42*** show the comparison of model performances evaluated with a beta version of the watershed model in terms of (a) the agreement between the simulated and USGS-WRTDS estimates for average annual nitrate and nitrogen loads for four sub-basins, and (b) the agreement of the simulated seasonality by the two models with USGS-WRTDS, expressed as correlation of monthly loads for the nitrate and total nitrogen loads.

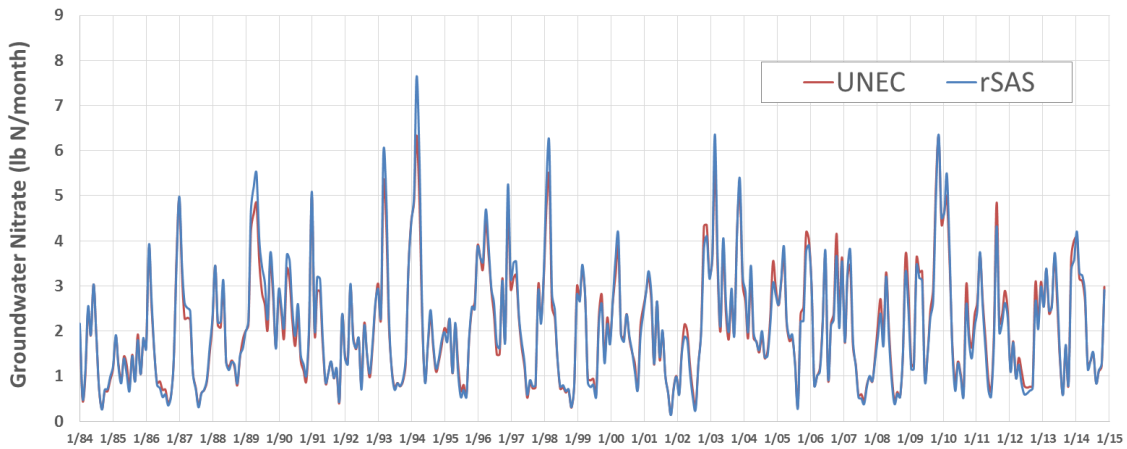

Figure 10-40: The differences in simulated monthly nitrate load using rSAS and UNEC for a land segment land use. Both models were forced using same inputs, including the estimates for groundwater lag-time, but they included differences in assumptions for model formulation. Therefore, the differences in loads are entirely due to differences in the model formulation. rSAS uses a gamma function for the representation of the transit time distribution.

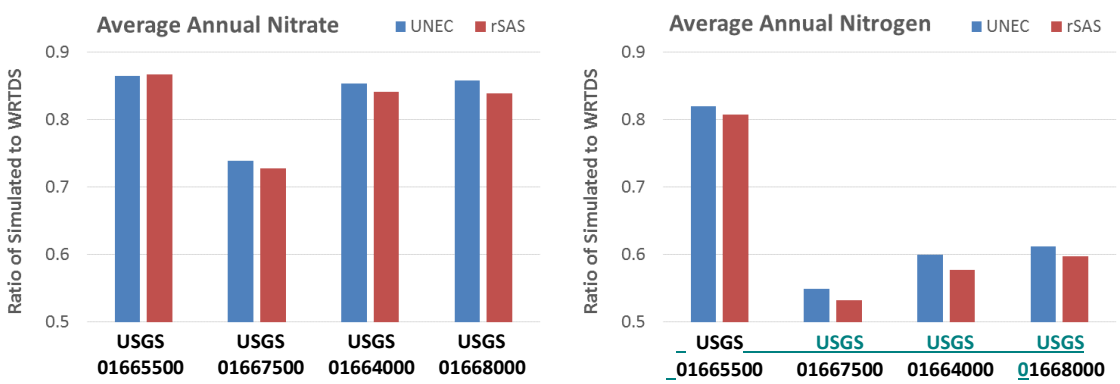

Figure 10-41: Comparison of simulated average annual nitrate and nitrogen loads with WRTDS for the four Rappahannock sub-basins. The same automated riverine calibration process was applied for both applications. The differences in model performances are due to the differences in the model formulation of rSAS and UNEC.

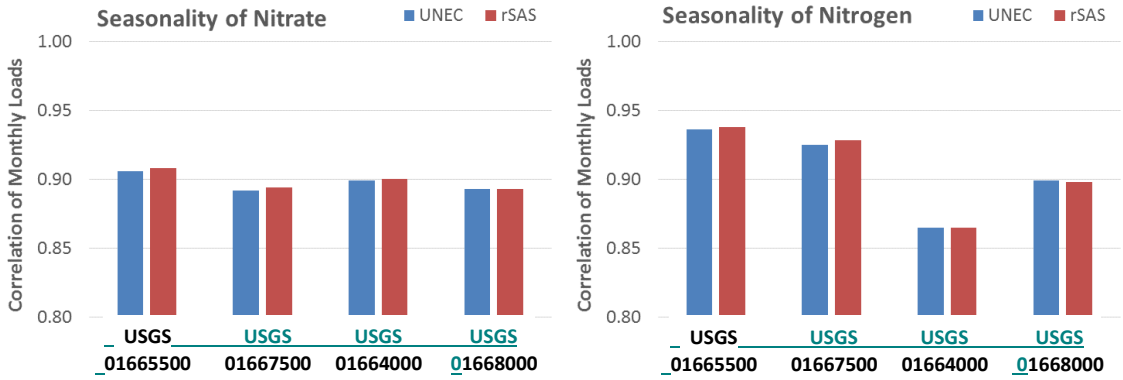

Figure 10-42: Comparison of seasonality of the simulated loads for the four Rappahannock sub-basins. Correlation coefficients were calculated between the simulated and WRTDS monthly loads. The same automated riverine calibration process was applied for both applications.

The comparative analysis discussed above show that despite underlying structural differences in rSAS and UNEC, both models resulted similar groundwater nitrate delivery as well as riverine model calibration performance for the sub-basins of different scales (165 to 1595 sq. miles) in Rappahannock river basins. It suggests, UNEC can be used as a computationally efficient temporal disaggregation model.

10.5.6 Performance of UNEC Simulation

A direct validation of the UNEC simulation is difficult because observations of lag times are not available. However, an important performance assessment of the UNEC simulation can be made by evaluating the seasonality in the riverine simulation. Correlation coefficients were used to statistically quantify the degree of agreement of the simulated monthly loads with USGS-WRTDS estimated loads, where higher values for the correlation coefficient indicates better agreement. Correlation coefficients were calculated for each location where USGS estimates for monthly nutrient loads were available. The distribution of correlation coefficients over numerous sites across the watershed was compared with the Phase 532 Watershed Model so that the performance of UNEC could be compared to the process-based model that was previously judged as appropriately calibrated for management purposes.

For the performance assessment, a riverine water quality calibration was made with the nutrient response for the land uses and land segments simulated using UNEC. The riverine water quality simulation uses loads simulated by UNEC at hourly time steps which are spatially aggregated over land uses and land segments of the drainage area. The integrated effect of key watershed properties, emergent geographic properties, small streams, and best management practices on the nutrient processing are applied to these non-point source loads as shown in *Figure 10-1*. The non-point source loads are combined with the point source loads and provided as an input for the river simulation. *Figure **10-43*** and *Figure **10-44*** show comparison between Phase 532 and Phase 6 model performances in terms of correlation coefficient statistics to show agreement between the simulated and USGS-WRTDS

monthly loads for the nitrate and nitrogen respectively. Higher correlation coefficients show improvement in model performance. *Figure **10-45*** and *Figure **10-46*** show the similar comparisons for the dissolved inorganic phosphorus and total phosphorus respectively. The box and whisker plots show a comparison of the distribution of correlation coefficients for the monthly loads at several monitoring stations across the Chesapeake watershed where WRTDS loads are available. It is noted that USGS-WRTDS monthly loads are an estimate as Pellertin et al. (2014) discuss the uncertainty of monthly WRTDS nitrate load estimates, finding that they can vary by approximately 20 percent. A significant improvement in the model's performance in capturing the seasonality is realized for all four constituents as shown in *Figure **10-43*** through *Figure **10-46***. This can be in part due to several factors, including improvements in the seasonality of inputs, hydrology simulation, nutrient simulation with lag-times using UNEC, and scientific understanding that is reflected as a revised mass-balance for the nutrient processing in landscape, small-streams and large rivers. During the Phase 6 model development, it was identified that for the most part the improvements were due to the simpler representation of transport processes in UNEC relative to the AGCHEM and PQUAL simulations of Phase 5.

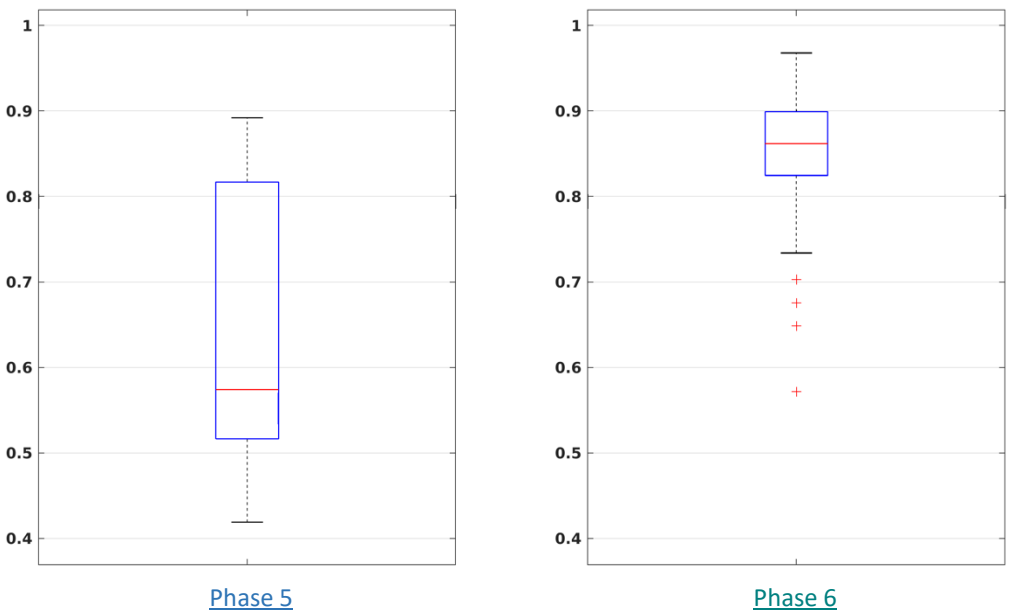

Figure 10-43: Box and whisker plots for the distribution of correlation coefficient statistics showing the degree of agreement of Phase 5 and Phase 6 models with USGS-WRTDS monthly nitrate loads for monitoring sites in the watershed.

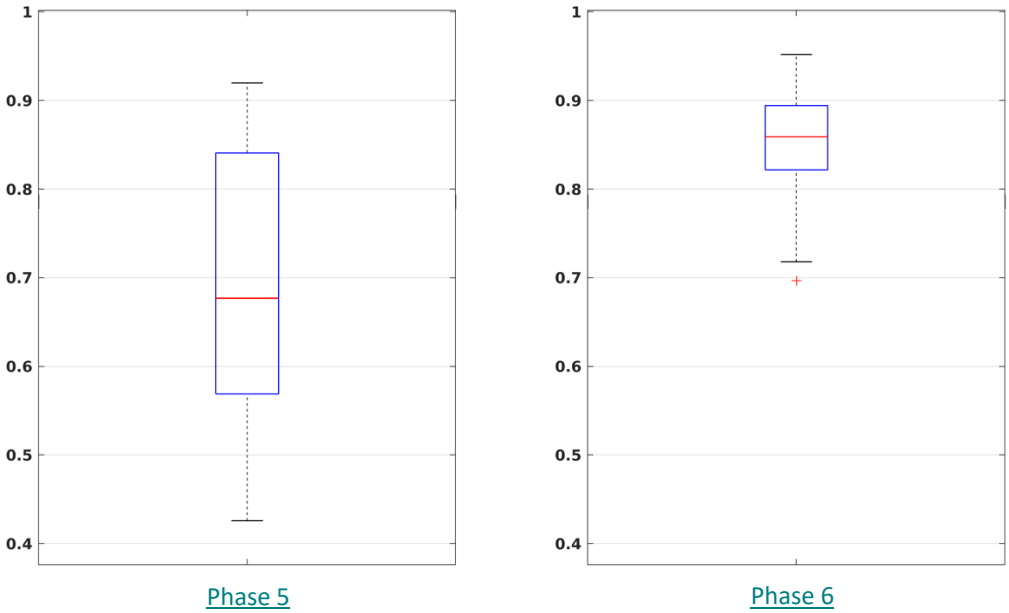

Figure 10-44: Box and whisker plots for the distribution of correlation coefficient statistics showing the degree of agreement of Phase 5 and Phase 6 models with USGS-WRTDS monthly total nitrogen loads for monitoring sites in the watershed.

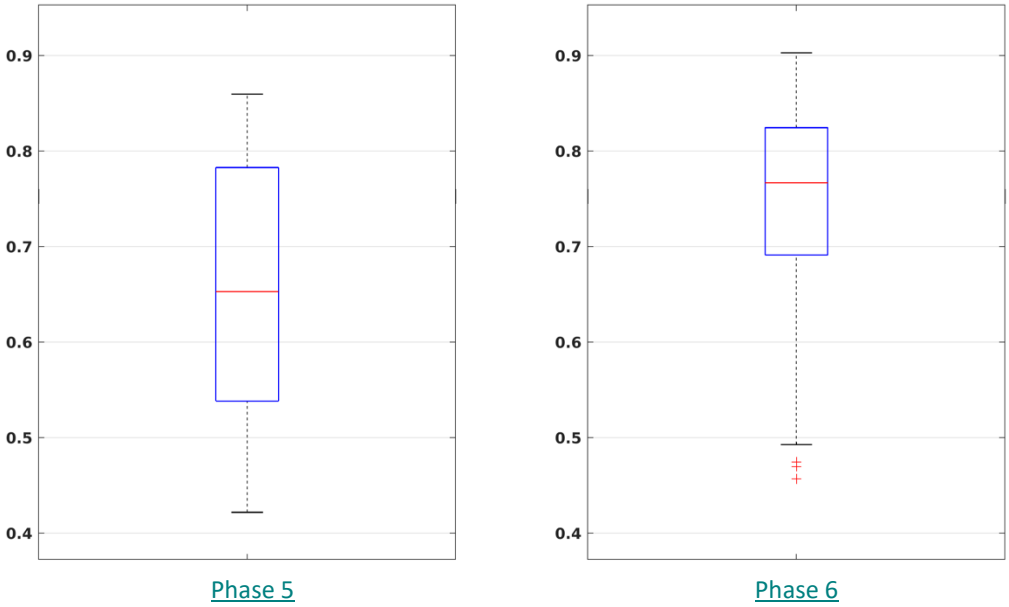

Figure 10-45: Box and whisker plots for the distribution of correlation coefficient statistics showing the degree of agreement of Phase 5 and Phase 6 models with USGS-WRTDS monthly dissolved inorganic phosphorus loads for monitoring sites in the watershed.

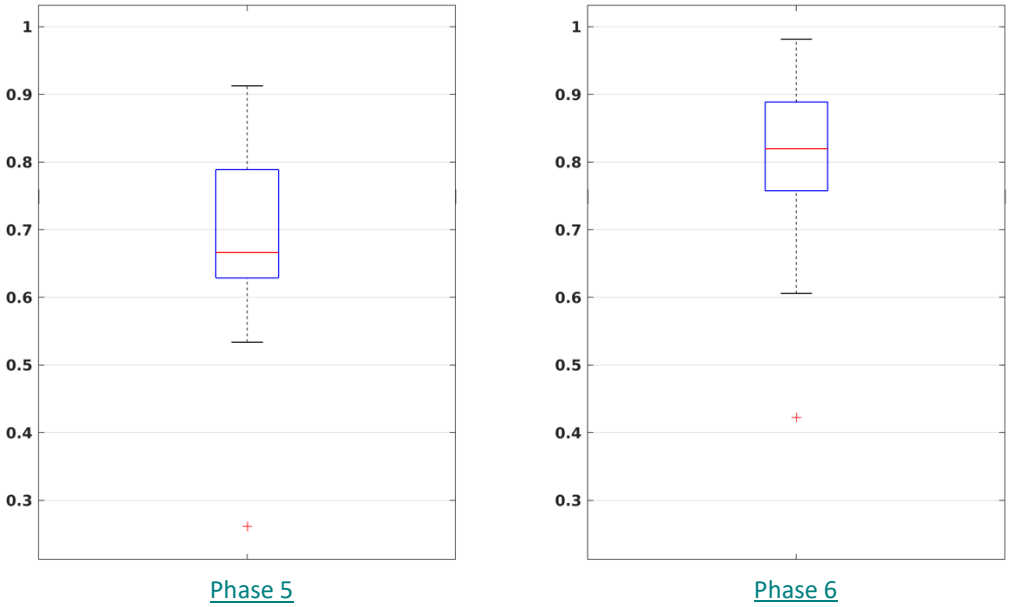

Figure 10-46: Box and whisker plots for the distribution of correlation coefficient statistics showing the degree of agreement of Phase 5 and Phase 6 models with USGS-WRTDS monthly total phosphorus loads for monitoring sites in the watershed.

10.6 River Water Quality Simulation

10.6.1 Introduction

Riverine physical, chemical, and biological processes, including the fate and transport of nutrients and sediment that directly impact the water quality, are simulated using HSPF modules (Bicknell et al. 1997; 2001; Donigian et al. 1984; Johanson et al. 1980). The HTRCH module simulates the energy budget; OXRX simulates oxygen and biochemical oxygen demand (BOD) dynamics; NUTRX simulates inorganic nitrogen and phosphorus; PLANK simulates phytoplankton and benthic algae; and SEDTRN simulates the entrainment, scour, and deposition of sediment.

Similar to the hydrology and land sediment calibrations discussed earlier in this chapter, the riverine water quality calibration is a rule-based multi-parameter optimization where the sensitivities of the model parameters are linked to a specific set of riverine calibration metrics. The riverine calibration metrics are a measurement of the degree of agreement between statistical representations of the simulation and monitoring data. The sensitivities assigned to model parameters relative to calibration metrics were established heuristically through calibration experience, numerous sensitivity tests, and trial and error. Temperature is handled differently than other water quality calibrations. The calibration of temperature is a simple optimization, maximizing model efficiency with a single river parameter.

The representation of river reaches as completely mixed trapezoidal prisms has implications for parameter selection. A parameter controlling a process that occurs with dissolved constituents as a function of volume or area, such as the algal growth rate, may be reasonably constrained by physical measurements. However, a parameter controlling a process that is a function of depth or velocity may be reasonably set outside of physical measurements to account for the total effect of the process over a geomorphologically variable river reach. For example, a typical physical river reach with shallower and deeper sections will experience shear stresses in the shallow sections that are much higher than average shear stress calculated for a trapezoidal prism.

10.6.2 Water Quality Parameters

A brief overview for the constituents of riverine water quality calibrations is provided in the subsections below. However, Bicknell et al. (2001) is recommended for more detailed information on HSPF model formulation of riverine water quality processes and parameters.

10.6.2.1 Soil Water Temperature Simulation

Water temperature is simulated in two components, first for the surface and subsurface water discharge from land, and then subsequent heat exchanges that occur as water is transported in the rivers. For the land, the hourly temperatures of four soil layers are simulated in HSPF, where the soil layers and the water stored in them are assumed to be in equilibrium at the same temperature. The temperatures for the surface and upper soil layers are linear functions of the air temperature as shown in Equation 10-16. The intercepts of these linear functions can vary monthly introducing a seasonal difference between air and water temperatures. The temperatures for the lower soil layer and groundwater are specified as monthly values as described below using the parameters in *Table **10-24***, Equation 10-17, and air temperature data. The heat balance is simulated for the riverine processes that include inflow, outflow,

sensible heat transfer from the bed and the meteorological inputs of precipitation, evaporation, shortwave radiation, and longwave radiation.

WATER TEMPERATURE = INTERCEPT + SLOPE x AIR TEMPERATURE

Equation 10-16

The temperature parameters for the soil layers were calculated using a set of empirical equations. Equation 10-17 was used for estimating slope and intercept parameters for the surface and upper soil layers using the parameter values shown in Table 10-24. Kurylyk et al. (2013) used this equation for estimating future groundwater temperature based on changes in air temperature from global climate model projection.

$$GWT_i = MAGST + D \times (GST_{i-L} - MAGST) + B$$

Equation 10-17

where,

GWT is groundwater temperature for month *i* in degree Celsius
GST is the monthly ground surface temperature
MAGST is the average of monthly GST
D is a parameter for damping effect of subsurface thermal diffusivity
L is a lag parameter (in months)
B is parameter to account for shallow heat transfer

D and L parameters were estimated as a function of depth (in meters) using following empirical Equation 10-18 and Equation 10-19 (Kurylyk et al., 2013).

$$D = e^{-0.3724 \times Depth}$$

Equation 10-18

$$L = 0.6504 \times Depth$$

Equation 10-19

Table 10-24 shows the parameter set that were used for estimating soil temperature from the air temperature. Figure 10-47 shows an example of estimated soil temperature for a land segment. The slope parameter for a land segment was calculated using the ratio between the variability in soil temperature and air temperature as shown in the Equation 10-17.

Variability in soil temperature for a given month was estimated as twice the difference in monthly soil temperature with respect to temperatures of the preceding and the following months (Figure 10-47). With the known slope parameter for a land segment, the intercept parameter was calculated using the mean monthly temperatures for the air and soil in the Equation 10-17. Estimated monthly temperatures for the lower soil layer, as shown in Figure 10-47, were used directly as model

parameters. Since the temperature for the lower soil layers were estimated as a function of the observed air temperature, it is anticipated that that estimated temperature for the soil layers would capture anticipated geospatial variability.

Table 10-24: Parameters used in the estimation of monthly temperature for various soil layers from the air temperature

	Surface Layer	Upper Layer	Lower Layer
Depth	0.1 m	0.5 m	2.5 m
D	0.963	0.830	0.394
L	0 months	0 months	2 months
B	2.0 °F	1.5 °F	1.0 °F

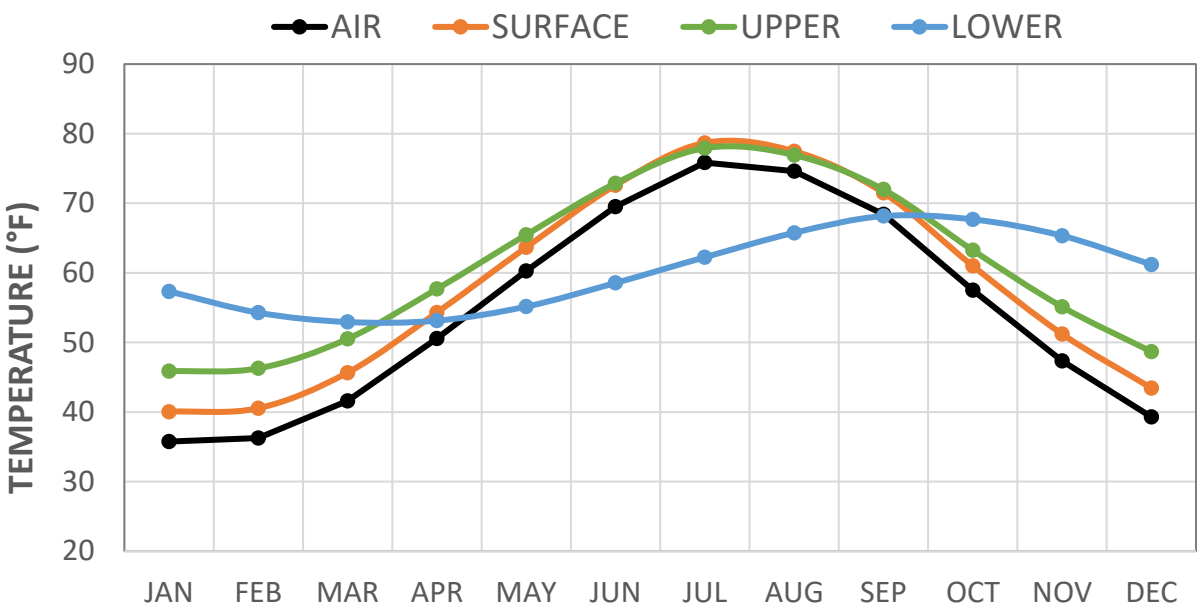

Figure 10-47: Mean monthly air temperature for a land segment from 30-year NLDAS2 dataset, and estimated mean monthly temperature for the soil layers

Water temperature simulation for the land segments were performed with the soil temperature parameters estimated using the process described above, and the riverine temperature parameter was calibrated to achieve better agreement with the riverine temperature observations as described in Section 10.6.3.2.1.

10.6.2.2 Sediment Transport Processes

HSPF has a relatively simple process-based simulation of riverine sediment transport. HSPF performs an hourly simulation of a reach as a completely mixed reactor. The flow for each hour is estimated by a stage-discharge relationship that is called an FTABLE in HSPF. Shear stress is calculated from hourly flow, which is used in the determination of deposition or scour condition (Figure 10-48). If the shear is below a user-specified critical shear stress, deposition will occur. Scour occurs when shear stress is

above a separate user-specified critical shear stress. Typically scour critical shear stress is higher than deposition critical shear stress but the scour critical shear stress may be set either higher or lower than the deposition critical shear stress, allowing conditions where both the scour and deposition processes are occurring simultaneously, only one at a time, or neither.

Levels of critical flow (critical shear stress) for scour and deposition are set independently for silt and clay. Sand scour is handled slightly differently and occurs only at high flows. Settling rates for sand, silt, and clay are also set separately. Each of the user-defined parameters is set to be as consistent as possible with the monitoring data, but some data are very sparse, such as observed sand, silt, and clay partitions.

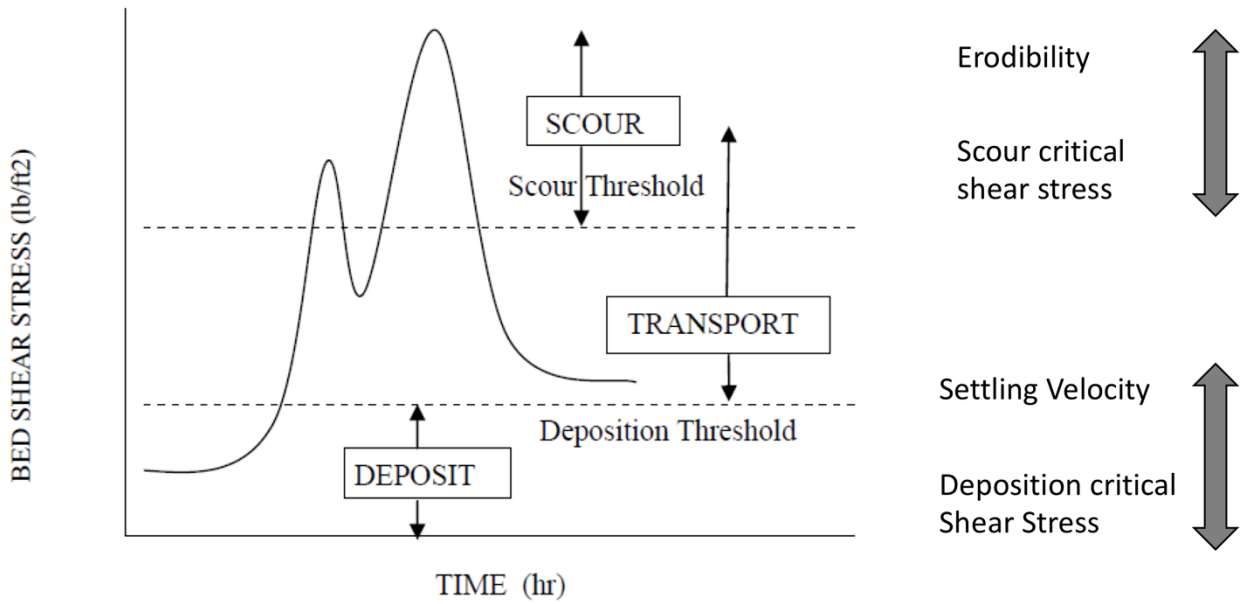

Figure 10-48: Shear stress for a river reach is estimated from hourly flow. A set of critical shear stress parameters define thresholds for scour and deposition condition. Adapted from HSPF v10 Users Documentation.

The deposition or scour of cohesive sediments are controlled by bed shear stress, τ, which is calculated by the following formula:

$$\tau = \gamma \times R \times S$$

Equation 10-20

where γ is the weight of water, *S* is the reach slope, and *R* is the hydraulic radius, which is calculated internally as a function of the simulation of the hydraulic routing in the reach. As discussed earlier, scour occurs when the bed shear stress is above a specified scour critical shear stress, and the amount of scour is proportional to the user-defined erodibility parameter for the segment. Deposition occurs when bed shear stress is below a specified critical shear stress. The amount of deposition is a function of the particle's fall velocity and the average water depth in the reach.

Sand is simulated differently from cohesive sediments. The amount of sand transported through a reach is determined by the transport capacity of the flow, which is calculated as a power function of the average velocity in the reach. Deposition of sand occurs when the concentration of sand in the reach exceeds its transport capacity of the flow, and sand is scoured from the bed if the concentration of sand is below the transport capacity.

Although there are several model parameters that control the sediment transport only a limited number of those parameters are calibrated to improve agreement with the monitoring data. *Table **10-25*** summarizes the HSPF SEDTRN parameters used in the sediment calibration in the reaches.

Table 10-25. Key sediment transport parameters that are used in model calibration

Parameter	Description
TAUCD	Critical bed shear stress for deposition of silt and clay
TAUCS	Critical bed shear stress for scour of silt and clay
W	Fall velocity in still water for silt and clay
M	Erodibility coefficient of silt and clay
KSAND	Coefficient of sand load power function
EXPSND	Exponent of sand load power function

10.6.2.3 Other Water Quality Constituents

Constituents other than flow, heat, and fixed solids are simulated variously in the HSPF modules OXRX, NUTRX, and PLANK. Each water quality constituent has a primary module, but it can have dependence in other modules. For example, biochemical oxygen demand (BOD) is primarily simulated in the oxygen subroutine group OXRX, but it is also modified by phytoplankton dynamics in the PLANK module. Therefore, these water quality constituents will all be discussed together. Generally, all constituents are subject to advection, which is modeled as a function of flow with no user-controlled parameters. Particulate constituents are also subject to deposition and loss to the system. Generally, deposition is a function of water depth and deposition velocities, which are parameterized separately for each particulate water quality constituent including refractory organic material, algae, and nutrients attached to inorganic particulates.

The dissolved oxygen simulation includes reaeration, saturation, BOD decay, benthic demand, benthal release of BOD material, algal production, and nitrification. The BOD simulation includes deposition, decay, benthic release, and phytoplankton death. BOD is considered to be ultimate BOD (BOD_u).

Simulated nitrogen consists of ammonia/ammonium, nitrate/nitrite, and organic forms. Organic forms of nitrogen include BOD, refractory organics, and phytoplankton. Transformations between the forms include nitrification, sorption and desorption of ammonia, BOD decay, and phytoplankton growth and death. Changes in total mass include denitrification, volatilization of ammonia, settling of particulate forms, benthic release, and benthic scour. The phosphorus simulation is similar to the nitrogen simulation and shares BOD and phytoplankton-related masses, as well as settling and scour of particulate forms but there is no counterpart to the non-conservative simulations of denitrification or ammonia volatilization. An external subroutine simulates the scour of organic nitrogen and phosphorus.

10.6.2.4 BOD and Organics

In the HSPF river simulation, BOD and phytoplankton are simulated as constituents. There is no other tracking of labile organics, so these are considered to be the complete representation of labile organics in the stream. Labile organics are entered into the river simulation from the land as BOD. Since the N:P stoichiometric ratio for BOD is set in the river simulation at 16:1, the N:P ratio for labile organics from the land to river are set at 16:1 as well. The remaining organics from land are tracked as separate refractory N and P constituents in the HSPF river simulation .

The molar ratio of labile N:P is set at 16:1 as the HSPF default. This makes for a fixed ratio of 7.23:1 by weight for labile organics based on following calculation.

(16 mols N / 1 mol P) * (14 g N / mol N) * (31 g P / mol P) = 7.23

In Phase 5, the AGCHEM simulation of phosphorus considered all organic P as subject to mineralization and did not have a desorption routine or dissolved organic pathway. Therefore, organic P was not tracked and was always calculated as a 1/7.23 of the labile organic N and 1/72.3 of the refractory organic N. In order to maintain mass-balance, calibration targets for land phosphate simulation were generated accordingly by subtracting the organic P values based on organic N targets from the total P targets. This method caused difficulty in BMP tracking since each P BMP also effected N and N BMPs effected P.

In Phase 6, all phosphorus and nitrogen constituents are simulated independently for the lands, including separate simulations of labile N and P and refractory N and P. However, when they are aggregated for transferring into the river simulation, the labile N and P must be in the exact ratio of 7.23:1 to maintain 16:1 molar ratio of N and P. Therefore, the limiting value of labile N or P is identified and the labile nutrient in excess is converted to refractory to maintain organic N and P mass balance.

10.6.3 Water Quality Calibration

An automated method of water quality calibration was used. The water quality automated calibration method is conceptually similar to the hydrology calibration and the land nutrient and sediment calibration in terms of how model parameters are paired with model performance metrics such that each parameter can be optimized to a unique set of metrics. However, there are several differences.

The river calibration has a procedural advantage over the other calibrations because the river simulation does not require a rerun of the corresponding land segments simulation and the software that aggregates the land loads and applies BMPs. That is because during the riverine calibration only river segment model parameters are optimized. As a result, the function evaluation time, or model run time, is significantly shorter. In addition, river model parameters specific to river segments, so there is no issue with parameters applying across multiple river systems as with the hydrology calibration, where land model parameters were calibrated. The ability to independently run river segments that are of the same stream order allows for greater parallelization of runs.

Nested stations were considered for the calibration of a river segment parameters by assigning a relative weight to every downstream station for a given segment. The weight function was equal to the number of observations above the limit of detection and discounted by 90 percent when downstream of

another water quality station. The approach of discounting puts decreasing priority on the downstream monitoring stations while retaining the significance of monitoring stations with more observed water quality samples. The weights were then scaled to add up to 1 for each river segment. For example, suppose a river segment has two downstream water quality stations. The first downstream station has 50 observations, of which 20 are below the detection limit. The second downstream station has 400 observations, of which 200 are below the detection limit. The first downstream station is assigned a weight of 30, i.e. number of observations above detection limit. The second downstream station is assigned an initial weight of 200, but it is then discounted by 90 percent to a weight of 20. The stations are then scaled so the first downstream station has a weight of 60 percent while the second downstream station has a weight of 40 percent. As a result, the model parameters for the river segment will be adjusted with 60% weight for the degree of disagreement between simulated and monitoring data at first downstream station, and 40 % weight for that at the second downstream station. Weights are calculated separately for each water quality constituent.

The river calibration has significant challenges compared to other calibrations as well. There are fewer stations with water quality monitoring data than for streamflow, and for the most part, the stations that do exist have far fewer water quality observations than streamflow. Typically, streamflow is measured daily, but water quality at most sites have monthly samples plus some storm samples. A well-monitored station may have 20 to 30 samples per year, while others have fewer samples per year or are only monitored for a few years. This data paucity relative to flow means that the same types of descriptive statistics cannot be calculated, which increases the difficulty of separating the effect of various water quality model parameters. In addition, nitrogen and phosphorus processes are coupled, where many processes affect the dynamics of both nutrients. Therefore, for a successful calibration of the riverine simulation it is important to calibrate these processes together. This creates constraints for independently defining the calibration objectives and limits its flexibility.

Nitrogen, phosphorus, and sediment responses were all calibrated simultaneously. Relationships between model parameters and calibration performance metrics were defined and coded into automated calibration software. The software automatically updates the parameters between the calibration iterations similarly to the hydrology and land-based sediment calibrations except that the sensitivities are updated after each iteration. The sensitivities are based on the change in the calibration performance metrics relative to the change in the parameter between the current and previous iterations. The likelihood of interaction between the parameters and subsequently the possibility of introducing oscillation in the calibration iterations also needed to be considered. These were minimized by carefully selecting specific calibration performance metrics that had minimal parameter interaction, by reducing the absolute value of the calculated sensitivity, and by constraining the calculated sensitivity to keep it within a specified narrow range. Reasonable ranges of sensitivity were found through sensitivity tests over all river segments. Through trial and error, it was found that the approach of calculating, reducing, and constraining the sensitivities resulted in better calibrations than specifying a universal sensitivity as was done in the hydrology and land sediment calibrations.

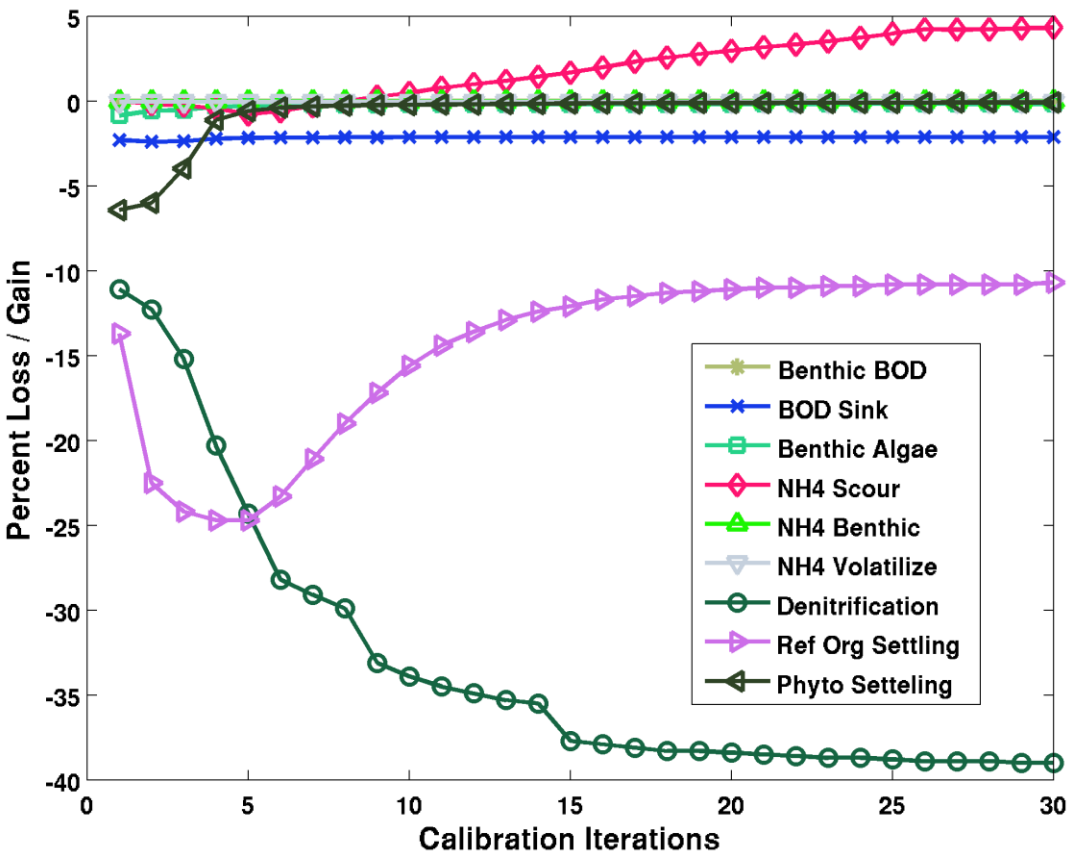

Figure 10-49: Automated calibration iterations and progress of nitrogen simulation in the Rappahannock river basin is shown. Key nitrogen processes are adjusted through changes in model parameters prior to each calibration iteration to improve agreement of the simulated concentrations with the observations.

The automated calibration routine was run for a total of 32 iterations or until convergence criteria were met for each calibrated model parameter and water quality constituent. *Figure **10-49*** shows the calibration iterations and progress of the Rappahannock river for the Phase 6 water quality calibration. Simulated responses of several nitrogen processes are separately plotted as lines showing their effect in terms of the magnitude of loss or gain over the calibration iterations. The vertical axis shows the percent of total nitrogen input that is lost or gained. The figure shows that refractory organic settling and denitrification processes are the dominant nitrogen processes simulated in the Rappahannock river. It also shows that this particular calibration becomes stable within 10-15 iterations and has reached an acceptable calibration performance where the effects of nitrogen processes are not changing significantly. Depending on the selection of initial parameters, there may be considerable shifts

between initial iterations, which tend to decrease as the model parameters are with adjusted with the progression of the calibration process.

10.6.3.1 Calibration Performance Metrics

Moriasi et al. (2006) and Moriasi et al. (2012) discuss calibration statistics for evaluating model performance. Moriasi et al. (2006) found that a satisfactory model simulation has a bias of under 55 percent for sediment and under 70 percent for nitrogen and phosphorus.

Calibration performance metrics are used for quantifying the agreement between simulated and observed concentrations and for inferring changes needed for improving simulated response. One of the most common calibration performance metrics used in the Phase 6 calibration system is the agreement of observed and simulated cumulative frequency distributions measured in terms of differences in the average values of quintiles (five partitions). This is illustrated in *Figure **10-50*** that shows cumulative frequency distributions (CFDs) of paired observation and simulated daily total nitrogen concentrations for the Rappahannock river. First, simulated and observed data are paired, meaning that only days in which both existed are selected, and a cumulative frequency distribution is created for both. The nitrogen CFDs are divided with anchor points of 20, 40, 60, and 80 percentiles into five partitions, each representing 20 percent of the values. The differences in the simulated and observed averages of the CFD partitions are used as the statistic for quantifying the agreement between the observed and simulated concentrations, the quality of model performance, and the goodness of fit for model parameters. *Figure **10-50*** shows the CFDs of observed and simulated total nitrogen concentration for the Rappahannock river near Fredericksburg, VA. The red and green points represent the average concentration for each quintile that is used for quantifying the differences between simulated and observed. Specifically the simulated average concentrations are higher than observed average concentrations for the quintiles 1 and 5, whereas simulated average concentrations are lower than observed average concentrations for the quantiles 2, 3 and 4. Within the automated calibration subroutines, adjustments to sensitive model parameters are used to reduce the differences in quintile averages.

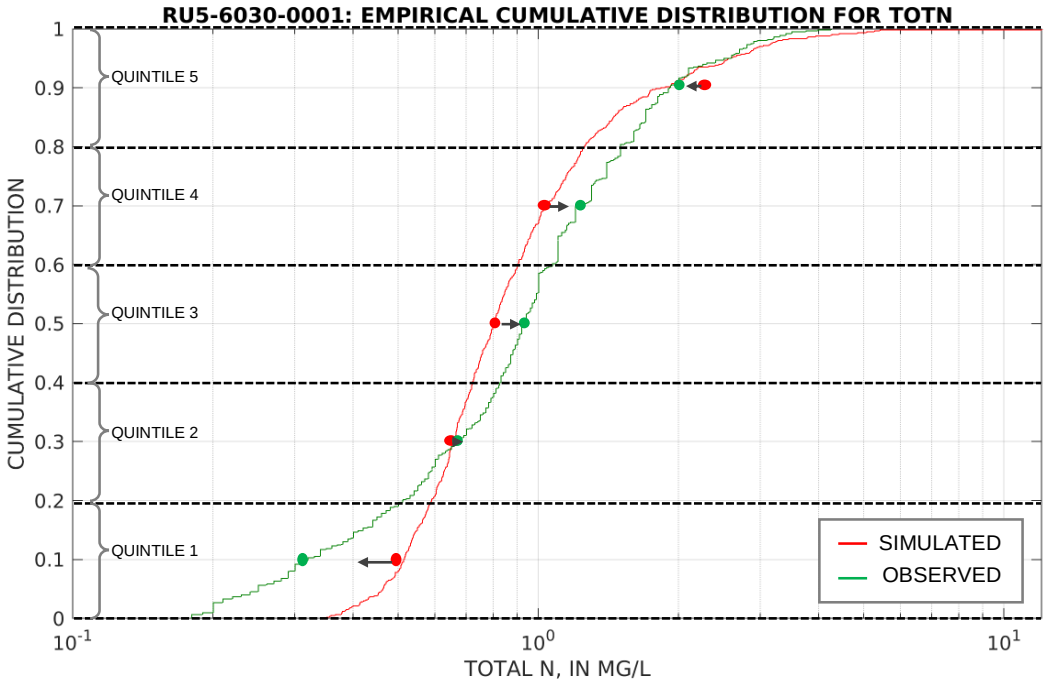

Figure 10-50. Cumulative frequency distributions (CFDs) of simulated and observed total nitrogen concentrations for Rappahannock river near Fredericksburg, VA is shown. CFDs are divided into 5 partitions with equal number of samples or quintiles, and differences in simulated and observed concentration averages for the quintiles are used in automated calibration subroutines for adjusting model parameters.

The differences in the simulated and observed average for any quintile is referred to here as the quintile bias, where a positive quintile bias indicates that the simulated response has a higher concentration than the observed. The lowest quintile is referred to as quintile 1 and the highest quintile is quintile 5. In *Figure* ***10-50***, quintiles 1–3 have a positive bias and quintile 5 has a negative bias. The average of all five biases is referred to as the average bias, and is an indicator of overall bias in simulated response.

Sediment and total phosphorus CFDs were divided into 5 partitions with anchor points of 20, 40, 80 and 95 percentiles (Figure 10-51). This determination was made based on the analysis of USGS-WRTDS daily loads for a few monitoring locations. For example, USGS-WRTDS data for the Potomac river near Washington DC show that on average about 50% of the phosphorus load is transported during 2-3% days with high streamflow. The corresponding daily phosphorus concentration data show a point of inflection around the top 5-6%, where the concentration values are considerably higher than rest of the dataset. The top 4-5% of the daily observations show a similar point of inflection with characteristically higher concentration than rest of the monitoring samples. It was presumed that this characteristically different behavior in observed response was due to the dominance of scour processes during periods of high streamflow. The scour processes have considerable impact on sediment and phosphorus transport processes contributing to significant transport during periods of high streamflow. A narrow partition separating the high concentration response of cumulative frequency distribution as shown in Figure 10-51 improved its alignment with the conclusions drawn from the observed dataset as well as provided a mechanism for better targeting of model scour parameters. Figure 10-51 also shows that this change

resulted in better agreement of simulated high concentration total phosphorus responses with observations, specifically the top 5 percent of the concentrations. As indicated earlier this is significantly important as the top 5 percent of the concentration response is responsible for about 50% of the transported phosphorus load.

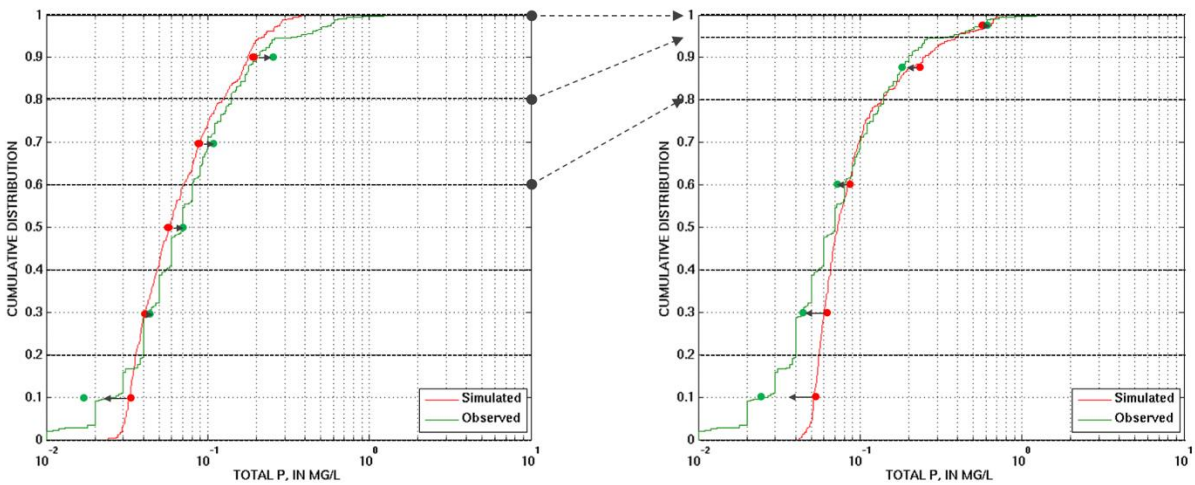

Figure 10-51: Comparison of calibrated total phosphorus response using two different approaches for partitions of cumulative frequency distribution. Differences in average of subsets are used for adjustment of model parameters. Partitions with 80 and 95 percentile partition anchor points yielded better agreement between observed and simulated high concentration response.

Some constituents, particularly dissolved phosphate, had significant numbers of observations that were labeled in the source data as less than the limit of detection (LOD). When both observed and simulated concentration are less than the LOD, there is no clear evidence that the simulation has to be adjusted one way or the other. However, when the observed value is less than the LOD, but the simulated concentration is greater than the LOD, it is implied that parameter should be adjusted to decrease the simulated concentration at least to the LOD. Therefore, the following rules are applied when constructing the cumulative frequency distributions: (1) observed values at the LOD are kept at the LOD, and (2) simulated values below the LOD are moved to the LOD value on days when the observed value is below the LOD.

While quintiles of the CFD are the most common metric used in the automated calibration, information on nutrient balances and delivery factors are used in some cases to improve calibration. In the calibration of temperature response and corresponding sensitive model parameter the NSE is used directly as the calibration performance metric.

10.6.3.2 Calibration Rules

Calibration rules establish formal relationships for using calibration performance metrics in estimating changes to the model parameters needed to improve simulated response. Through numerous trial and error and sensitivity model runs, separate calibration rules for each important model parameter were developed that use parameter values as well as quintile biases of prior calibration iterations in estimating parameter value for the next iteration. Most of the Phase 6 water quality calibration rules are adapted from Phase 5.3. However, some changes were made to parameter sensitivities and to the

positioning of concentration CFD quantiles. Also new calibration rules were added for the optimization of model parameters for the new subroutine that simulates scour of refractory organic material.

Riverine model parameters that control the simulated response of water quality constituents are listed in Appendix 10D. As with the hydrology calibration, only a subset of available HSPF model parameters were used in the calibration. The model parameters that are calibrated and their corresponding water quality constituents are detailed below.

Some simulated river segments cannot be calibrated because they do not have downstream water quality monitoring data. Similar to other river segments, most parameters for these rivers are default values as described in Appendix 10D or measured quantities, but water quality monitoring data is not available to support the calibration of remaining model parameters. In some cases, such as for the parameters controlling chlorophyll, the parameters are calibrated to keep a water quality constituent within a specified range. But, as described in Section 10.6.3.3, the remaining water quality parameters were strategically assigned parameter values from calibrated "surrogate" river segments based on carefully established similarity conditions.

10.6.3.2.1 Water Temperature

The land parameters governing temperature were set as described in Section 10.6.2.1, and the simulated temperature response of each river segment was calibrated against the temperature data at downstream monitoring stations. The simulated heat balance for riverine processes include inflow, outflow, precipitation, evaporation, shortwave radiation, longwave radiation, and sensible heat transfer from the river bed. The heat balance processes are mostly fully constrained by other physical processes and laws governing them, but HSPF has a river simulation parameter associated with longwave radiation, KATRAD, which regulates the transfer of heat from the atmosphere to the stream. The simulation of bed heat conduction is not temperature-related, so it is argued that this longwave radiation adjustment can be used to account for heat received by the stream from both longwave radiation and conduction.

Model efficiency quantifying the degree to agreement in simulated and observed temperature data was a concave function of KATRAD with a monotonic first derivative for all investigated river segments. Therefore, KATRAD was calibrated using a simple gradient-based optimization method.

10.6.3.2.2 Dissolved Oxygen

For overall mass balance, the average dissolved oxygen bias is related to the reaeration coefficient. For rivers, the model parameter for reaeration coefficient is REAK; and for reservoirs, it is CFOREA. To correct the shape of the distribution, the model parameter for supersaturation coefficient, SUPSAT, is related to the biases in fourth and fifth quintiles of the cumulative frequency distributions of observed and simulated data, while the benthic oxygen demand parameter, BENOD is related to the biases in first and second quintiles of the cumulative frequency distributions.

10.6.3.2.3 Chlorophyll-*a*

The phytoplankton settling rate, PHYSET, has the highest sensitivity to overall chlorophyll mass and affects the lower concentrations by a greater amount than the higher concentrations. PHYSET is adjusted according to the average bias for the second, third, and fourth quintiles of chlorophyll cumulative frequency distributions. The maximum algal growth rate, MALGR, is also important for

regulating overall chlorophyll mass and especially affects higher concentrations. Therefore, MALGR is adjusted according to the bias in the fifth quintile.

Monitoring data for chlorophyll-a concentrations are relatively rare, with only 39 monitoring stations having observations. Of those stations, only a few stations have observations spread over the entire 30-year calibration period. Most stations have about 200-300 samples. The river segments with no chlorophyll data for calibration are constrained to the interquartile range of the basin-wide observed data.

10.6.3.2.4 Total Suspended Sediment

The critical shear stresses for scour and deposition are the most important parameters for the calibration of total suspended sediment (TSS) response. The simulated shear stress can vary between river reaches within the same river system due to differences in the FTABLE development. Setting the same critical shear stress value for multiple river segments was found to cause large differences in sediment dynamics between the rivers. This issue is addressed by calculating percentiles of shear stress for each river reach after completing the hydrology calibration. River segments upstream of a TSS water quality monitoring station are calibrated together by assigning critical shear stress corresponding with a specific percentile level rather than equal shear stresses.

For example, a simulated shear stress of 0.1 pounds per square foot is reached in only 3 percent of the hours for the terminal segment of the Patuxent while it is reached in 40 percent of the hours in the next upstream segment (Figure 10-52). To deal with this issue, river segments upstream of a particular TSS water quality monitoring station are calibrated together by assigning equal shear percentiles rather than equal shear stresses. In the example above the river segments would be set so that they would both scour 3 percent of the time at 0.10 and 0.21 pounds per square foot for the terminal and upstream segments respectively (Figure 10-52).

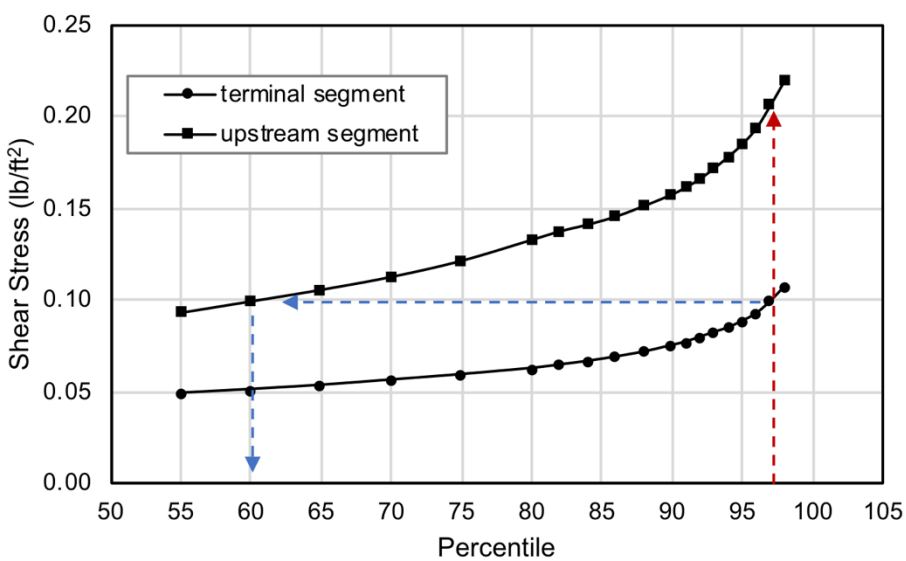

Figure 10-52: Distribution of simulated shear stress for two Patuxent river segments.

Critical shear stress for scour and critical shear stress for deposition are allowed to overlap. In a real river system of several dozen miles represented by a model reach segment, it is reasonable to assume

that under a range of conditions, net scour and deposition would occur simultaneously at different points in the reach.

In general, silt requires higher stress to scour and can deposit under higher shear stresses than clay. Silt critical shear stresses for both scour and deposition are kept at half the distance to the 100th percentile as clay. For example, if the clay critical shear stress for scour is at the 80th percentile in a given river, the silt critical shear stress for scour will be set at the 90th percentile.

Rivers are first checked to see if the previous iteration resulted in a complete loss of the bed sediment. In HSPF, the bed has a total mass of sediment that is available for scouring. In cases of high scour, this entire mass can be eroded, which causes a step change in the response to shear stress after the bed sediment is exhausted. If a complete loss of sediment is detected, the critical shear stresses for scour for silt and clay are raised by moving them half the distance to the 100th percentile of simulated shear stress.

The critical shear stress for scour, TAUCS, regulates the conditions when scour occurs that is represented in upper most fifth partition of the suspended sediment cumulative frequency distribution that is represented by 95 to 100 percentiles. Therefore, the TAUCS parameter was related in the calibration rule to the average bias of upper partition of the cumulative frequency distributions. The critical shear stress for deposition, TAUCD, is similarly related to the lower half of the distribution with the difference is biases of the third and first quintiles. Raising the critical deposition shear stress will lower the median relative to the first quintile.

The erodibility coefficient parameter, M, has the most dominant effect during scour events as compared to that of other model parameters and therefore is related to the upper most fifth partition of the suspended sediment cumulative frequency distribution. The erodibility parameter for both silt and clay are changed in proportion with the bias of the fifth partition. The settling velocity parameter, W, has the most effect on lower concentrations and thus is related to the bias of the second and third partitions. However, in situations where the fifth partition has a positive bias but a low erodibility coefficient indicating that the land-based loads are not being sufficiently attenuated at high flow. Therefore, under those circumstances deposition velocity is related to the average bias. The silt settling velocity is kept at 10 times of the clay settling velocity.

Sand is a small part of the overall TSS observed and simulated load. Over the long-term, only a small portion of the sand that enters a river reach is transported out. The transport capacity of sand is simulated using a power function, which is a different numerical formulation as compared to silt and clay particles. The exponent parameter for the power function, EXPSND, is held constant value of 4. The coefficient for the sand power function, KSAND, is calibrated such that only 1 percent to 10 percent of the influent sand is transported out of the river segment.

All critical shear stress parameters for reservoir segments are set at the 100th percentile of simulated shear stress so that they never scour and always deposit, except in the special case of the Conowingo Reservoir discussed later in this section. The TSS calibration of reservoirs is controlled by the settling velocity W. Accordingly, reservoir parameters for the clay settling velocity is negatively related to the average bias of the TSS CFD, while the silt settling velocity is negatively related to the average bias of the fourth and fifth partitions which represents top twenty percentile concentrations.

10.6.3.2.4.1 Calibration of Sand, Silt, and Clay Fractions

As discussed earlier, sand, silt, and clay transport processes are simulated separately in the river reaches and receive independent model parameters. These three sediment components are added together along with freshwater phytoplankton to get simulated TSS consistent with the samples collected at monitoring stations.

Monitoring data that separate these components of TSS are sparse. The Chesapeake Bay River Input Monitoring (RIM) stations, which are most downstream water quality monitoring stations before discharge to tidal waters, have some observed data on the splits of sand and fines (silt and clay). Using all available observations taken at these RIM stations, it was found that the TSS observed loads were mostly fines (*Table **10-26***). USGS data for parameter code 70331 was used that provides the percentage of suspended sediment data that have particles that are less than 0.0625 mm in diameter. The major river basins of the Susquehanna, Potomac, and James have a median percent fines of 97 percent, 91 percent, and 85 percent, respectively (*Figure **10-53***, *Figure **10-54***, and *Figure **10-55***). Usually, rivers with significant impoundments, like the Susquehanna, have a greater percentage of fines, and the sand fraction is more typically 5 percent. Surprisingly, no correlation was seen between flow and percent fines.

To reflect the understating gained from the analysis of observations for the proportions of sand and fines in TSS, the annual average target of percent sand was set at 15 percent for all river reaches except for those reaches that have impoundments. In the case of impoundments—as in the Susquehanna observations with the impoundments of Conowingo, Safe Harbor, and New Haven just above the monitoring station—an annual average target of 5 percent sand was set, which approximates the observed median and mean of 3 percent and 4.7 percent, respectively.

Only three samples are available for the silt/clay splits, and they indicate that the percent clay was 52 percent and 46 percent on two occasions in the Patuxent, and 79 percent on one occasion in the Potomac.

Table 10-26. Percent fines (silt and clay) in the Chesapeake rivers. The table was compiled using USGS dataset for Chesapeake Bay River Input Monitoring (RIM) monitoring stations. RIM stations are the most downstream monitoring before discharging into the tidal waters of the Bay.

USGS Station ID	USGS RIM Station Name	Drainage Area	%fine Median	%fine Mean	%fine Max	%fine Min
01578310	SUSQUEHANNA RIVER AT CONOWINGO, MD	27,100	97	95	100	41
01646580	POTOMAC RIVER AT CHAIN BRIDGE, AT WASHINGTON, DC	11,570	91	89	100	46
02035000	JAMES RIVER AT CARTERSVILLE, VA	6,252	83	80	100	13
01668000	RAPPAHANNOCK RIVER NEAR FREDERICKSBURG, VA	1,595	86	82	100	6
02041650	APPOMATTOX RIVER AT MATOACA, VA	1,342	87	84	100	40
01673000	PAMUNKEY RIVER NEAR HANOVER, VA	1,078	87	83	100	9
01674500	MATTAPONI RIVER NEAR BEULAHVILLE, VA	603	82	78	100	5
01594440	PATUXENT RIVER NEAR BOWIE, MD	348	92	90	100	16
01491000	CHOPTANK RIVER NEAR GREENSBORO, MD	113	90	86	100	24

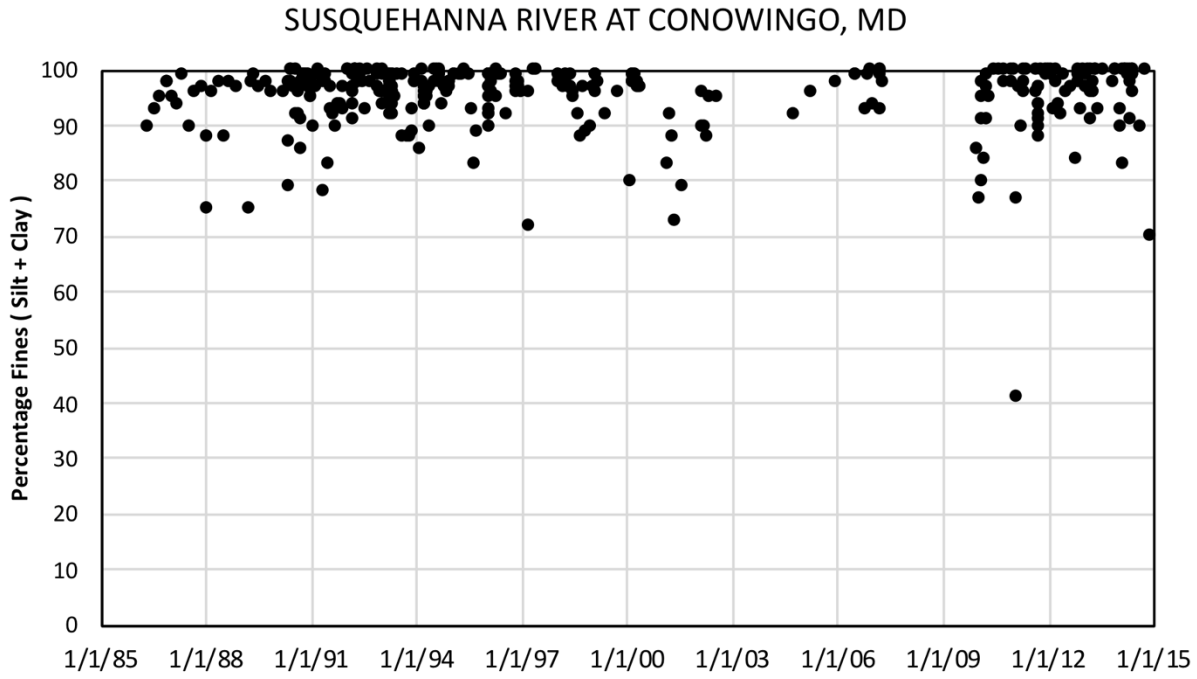

Figure 10-53. Percent fines (silt + clay) of observed data from 1985 to 2014 for the Susquehanna River at Conowingo, MD monitoring station. USGS parameter code 70331 that provides percentage of suspended sediment particles less that 0.0625 mm in diameter was used.

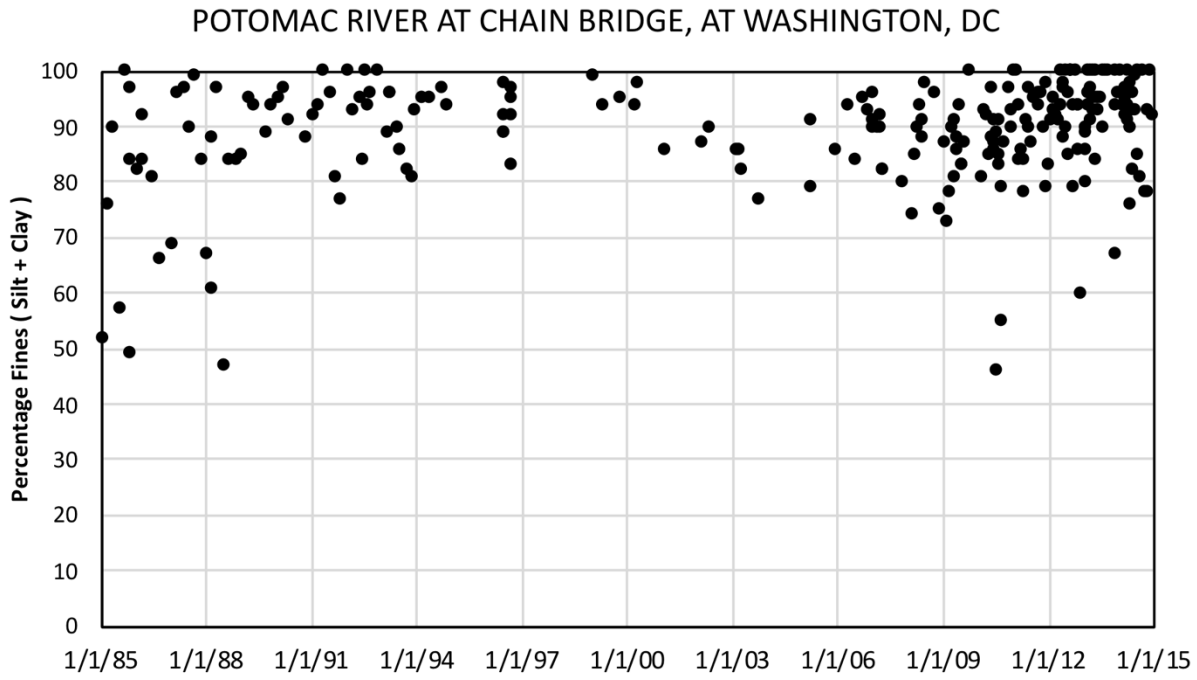

Figure 10-54. Percent fines (silt + clay) of all observed data from 1985 to 2014 for the Potomac River at Chain Bridge, Washington, D.C. monitoring station. USGS parameter code 70331 that provides percentage of suspended sediment particles less that 0.0625 mm in diameter was used.

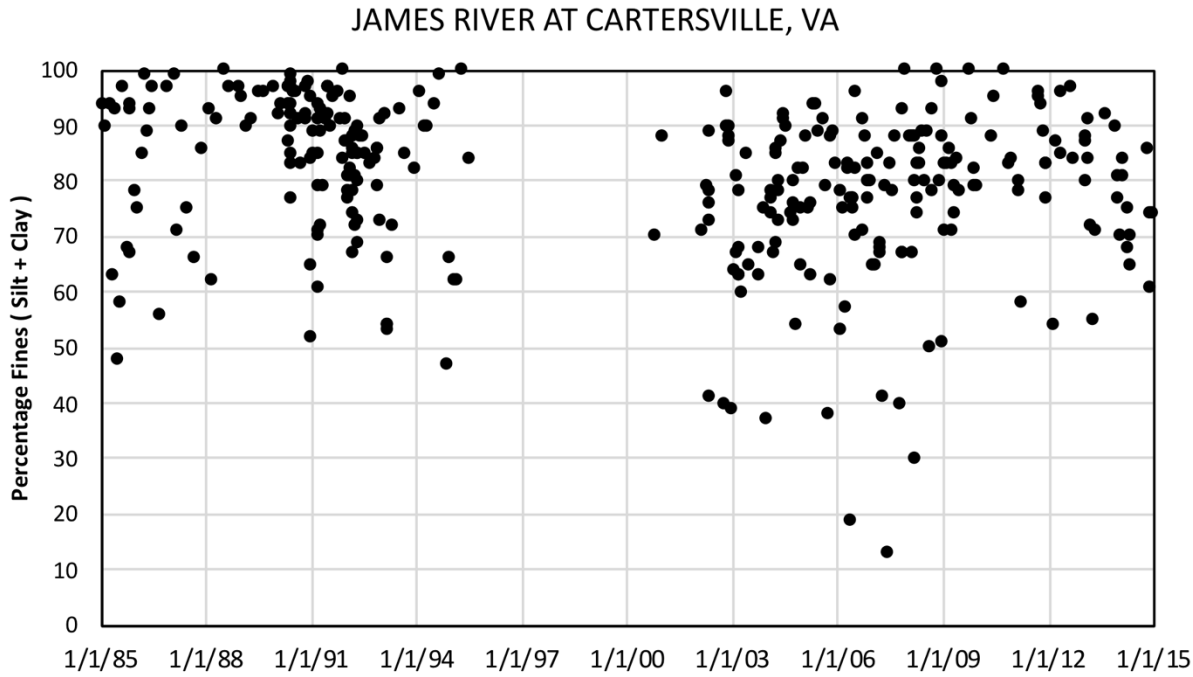

Figure 10-55. Percent fines (silt + clay) of all observed data from 1985 to 2014 for the James River Cartersville, VA monitoring station. USGS parameter code 70331 that provides percentage of suspended sediment particles less that 0.0625 mm in diameter was used.

10.6.3.2.5 Nutrients

Fate and transport of nitrogen and phosphorus are connected through processes that control both nutrients. Individual species of nutrients are also connected. For example, algal uptake converts inorganic nutrients into organic nutrients for both nitrogen and phosphorus.

10.6.3.2.5.1 Settling of Refractory Organics

The settling of refractory organics is one of the more important mechanisms for attenuating excess nitrogen and phosphorus in the river reach. Ideally, the rate of settling of dead refractory organics parameter, REFSET would be related to observations for organic nutrients. If there are sufficient organic nutrient data, then this is the case and the organic nutrient cumulative frequency distribution is used for the calibration. However, if there are more than twice as many total nitrogen observations as organic nitrogen observations for a station, then total nitrogen is used instead. The same applies for total phosphorus and organic phosphorus observations. REFSET parameter is related to average biases in both nitrogen and phosphorus the average for nitrogen and phosphorus of the average bias statistic.

10.6.3.2.5.2 Scour of Refractory Organics

The scour of refractory organics was added to the Phase 6 watershed model simulation recognizing its importance during high stormflow events. Similar to the calibration of refractory organics settling, it would be ideal to calibrate scour concentration parameters for nitrogen (SCRRORN) and phosphorus (SCRRORP) in relation to observations for organic nutrients. However, since organics observations are very limited, total nitrogen and total phosphorus were used for the calibration of SCRRORN and SCRRORP parameters respectively. SCRRORN parameter was related to the biases of fifth quantile of

total nitrogen, SCRRORP parameter was related to the biases of the upper quantile of the phosphorus cumulative frequency distribution. At the same time maximum transport factor constraints of 1.0 and 1.5 was applied to nitrogen and phosphorus respectively in the calibration of these parameters.

10.6.3.2.5.3 Inorganic Nitrogen

Denitrification is related to the average bias of the lower three quintiles of nitrate concentration. The denitrification parameter, KNO320, is increased if the bias is high, but only if the total nitrogen bias is positive. Conversely, KNO320 is decreased if the bias is low, but only if the total nitrogen bias is negative.

The benthic release rate parameter for ammonia has a low value for use under aerobic conditions, BRTAM1, and a high release rate for use under anaerobic conditions, BRTAM2. The sediments are assumed anaerobic when the water column reaches the dissolved oxygen level set by the parameter ANAER. ANAER is set to roughly the 20th percentile of dissolved oxygen (DO) by averaging the first and second quintiles of simulated DO. The calibration of ammonia released from reservoir sediments is regulated relative to the average total nitrogen bias in simulated response. These actions have the effect of releasing more ammonia from riverine sediments during warmer summer temperatures, but the amount of benthic ammonia release is guided by the calibration of the average total nitrogen bias.

Ammonium also enters the water column attached to sediment particles that are scoured. The concentrations (mass/mass) are set by the parameters BEDNH4CLAY, BEDNH4SILT, and BEDNH4SAND with the scour of clay, silt, and sand respectively. Since scoured ammonium represents a pulse of nutrients under high-flow conditions, it has a major effect on the higher concentrations of nitrogen. These parameters are adjusted according to the average bias in the fourth and fifth quintiles of total nitrogen, and the three parameters are kept in a constant ratio to each other as 100:10:1 for clay, silt and sand respectively.

The nitrification rate, that simulates the oxidation of ammonium and nitrite by chemoautorophic bacteria, is used to adjust the simulated ratio of nitrate and ammonia relative to the observed ratio. The nitrification rate is increased by increasing the ammonia oxidation parameter, KTAM20, to produce more nitrate and less ammonia, but the overall mass of inorganic nitrogen is unaffected. KTAM20 is adjusted according to the difference in average biases of ammonia and nitrate concentrations.

10.6.3.2.5.4 Phosphate

The calibration of model parameters regulating the response of benthic release and scour of phosphate processes are handled similarly to that for ammonia. A difference is that the contribution of scour of phosphate is a much larger portion of total phosphorus than scoured ammonium is of the nitrogen balance, especially during higher streamflow conditions. As with ammonium, the phosphate scour parameters, BEDPO4CLAY, BEDPO4SILT, and BEDPO4SAND are related to the average bias of the upper two quintiles of total phosphorus, and these three parameters are kept in a constant ratio to each other as 100:10:1 for clay, silt and sand respectively. The benthic release parameters BRPO41 and BRPO42 in case of reservoirs only are related to the lower four quintiles excluding the phosphorus response during high streamflow condition. BRPO42 parameter for the orthophosphate release rate during anaerobic condition is kept at 5 times the BRPO41 release rate during aerobic condition. An additional mechanism to adjust the balance between dissolved phosphate and total phosphorus is the TSS adsorption coefficient parameter for orthophosphate, ADPM, for clay, silt and sand, which are related to the

average bias in upper two quintiles of dissolved phosphate. A fixed ratio of 9:3:1 is used for clay, silt and sand orthophosphate adsorption parameters.

10.6.3.3 Calibration of Reaches Without Downstream Monitoring

There are river segments in the Phase 6 watershed model that do not have downstream water quality monitoring stations, and therefore do not have data for supporting the calibration of river model parameters. These mostly include smaller tributary segments or smaller river segments between a monitoring station and tidal open waters. *Table **10-27*** shows the list of these unmonitored river segments.

Table 10-27: Unmonitored Phase 6 river segments indicating if the segment is a reservoir and if the segment has no water quality data or is just missing Total Suspended Solids.

River Segment	Name	Reservoir	No Data	Missing TSS
DE0_3791_0001	Jones River		X	
DE0_4141_0001	Murderkill River		X	
DE0_4231_0001	Mispillion River		X	
EL0_4562_0001	Nanticoke River		X	
EL0_5400_0001	Wicomico River		X	
EL0_5767_0001	Tony Tank Lake	X	X	
EL1_5150_0001	Chicamwicomico River		X	
EL1_5430_0001	Nassawango Creek			X
EL1_5570_0001	Dividing Creek		X	
EL1_6000_0001	Marumsco Creek		X	
EL2_4590_0001	Marshyhope Creek		X	
EL2_5270_0001	Pocomoke River		X	
EL2_5272_5270	Adkins Pond	X	X	
EM2_4100_0001	Tuckahoe River		X	
EU0_3726_3724	Urieville Lake	X	X	
EU0_3830_0001	Chester River Unicorn Branch		X	
EU1_2810_0001	Little Northeast Creek		X	
EU2_3520_0001	Chester River Andover Branch		X	
GY0_3950_3952	Bear Creek		X	
JA0_7291_7290	Swift Creek	X	X	
JA2_7290_0001	Swift Creek		X	
JB0_7051_0001	Yarmouth Creek	X	X	
JB0_7052_0001	Diascund Creek	X	X	
JB1_8090_0001	Lake Mead Dam	X	X	
JB2_7800_0001	Western Branch Dam	X	X	
JB3_7053_0001	Chickahominy River	X	X	
JL7_7070_0001	James River		X	
PL0_5490_0001	Quantico Creek		X	
PL0_5510_0001	Gilbert Swamp Run		X	
PL0_5530_5710	Clark Run		X	
PL0_5710_0001	Clark Run		X	

River Segment	Name	Reservoir	No Data	Missing TSS
PL0_5720_0001	Nanjemoy Creek		X	
PL0_5730_5690	Aquia Creek			X
PL0_5750_0001	St Clement Creek			X
PL0_5830_0001	McIntosh Run		X	
PL1_4780_0001	Rock Creek		X	
PL1_5130_0001	Accotink Creek		X	
PL1_5690_0001	Aquia Creek		X	
PL1_5910_0001	St Marys River		X	
PL2_5300_5630	Zekiah Swamp Run			X
PL2_5630_0001	Zekiah Swamp Run		X	
PL3_5250_0001	Occoquan Main Dam	X		X
RL0_6540_0001	Piscataway Creek			X
RL1_6180_0001	Cat Point Creek			X
SL2_2480_0001	Octoraro Creek		X	
WM0_3740_0001	Herring Run		X	
WM1_3910_0001	Gwynns Falls		X	
WU0_3250_0001	Bynum Run		X	
WU0_3670_0001	Whitemarsh Run		X	
WU1_3240_3331	Winters Run		X	
WU1_3330_0001	Winters Run		X	
WU1_3331_3330	Winters Run		X	
WU1_3482_0001	Western Run		X	
YL2_6580_0001	Piankatank River		X	
YM4_6620_0001	Mattaponi River		X	
YP0_6840_0001	Totoponomoy Creek		X	
YP0_6860_6840	Totoponomoy Creek			X
YP4_6750_0001	Pamunkey River		X	

Some reaches generally had some water quality monitoring data to calibrate parameters but had little or no sediment monitoring data. In such cases, the available sediment data was either suspected for data quality issues or did not have sufficient number of samples for stormflows. The reaches accordingly are flagged in *Table **10-27***.

These unmonitored river segments were strategically assigned parameters from calibrated river segments based on careful consideration of a number of watershed characteristics. The unmonitored "strays" river segments are listed in *Table **10-28*** along with the calibrated "surrogate" river segments that provide the parameters are shown.

First, a distinct subset of stray reaches was identified, called "pseudo-strays," which were downstream of calibrated reaches. All of these reaches were simply matched to the reach immediately upstream as long as there were no dramatic differences in hydrogeomorphology. Such pseudo-stray river segments

are clearly marked in *Table **10-28*** along with their upstream surrogates. A total of 15 pseudo-stray river segments (approx. a quarter) were identified out of 58 stray river segments.

Table 10-28: Pseudo-stray river segments with upstream surrogate reaches.

Stray River Segment	Stray River Name	Surrogate River Segment	Surrogate River Name
EL0_4562_0001	Nanticoke River	EL0_4561_4562	Deep Creek
EL0_4562_0001	Nanticoke River	EL0_4560_4562	Nanticoke River Gravelly Fork
EL2_4590_0001	Marshyhope Creek	EL2_4400_4590	Marshyhope Creek
EL2_5270_0001	Pocomoke River	EL2_5110_5270	Pocomoke River
JA2_7290_0001	Swift Creek	JA0_7291_7290	Swift Creek
JB3_7053_0001	Chicahominy River	JB3_6820_7053	Chicahominy River
JL7_7070_0001	James River	JL7_6800_7070	James River
PL0_5490_0001	Quantico Creek	PL0_5540_5490	Quantico Creek
PL1_4780_0001	Rock Creek	PL1_4460_4780	Rock Creek
PL1_5130_0001	Accotink Creek	PL0_5010_5130	Accotink Creek
PL1_5690_0001	Aquia Creek	PL0_5730_5690	Aquia Creek
PL2_5630_0001	Zekiah Swamp Run	PL2_5300_5630	Zekiah Swamp Run
WM1_3910_0001	Gwynns Falls	WM1_3660_3910	Gwynns Falls
YM4_6620_0001	Mattaponi River	YM3_6430_6620	Mattaponi River
YM4_6620_0001	Mattaponi River	YM1_6370_6620	Marracossic Creek
YP0_6840_0001	Totoponomoy Creek	YP0_6860_6840	Totoponomoy Creek
YP4_6750_0001	Pamunkey River	YP4_6720_6750	Pamunkey River

Second, a new procedure was implemented matching surrogates to the remaining stray river segments based on a number of watershed characteristics such as size, location, hydrogeomorphology, and land use. Size is measured by size indicator of the river segment ID, i.e. the third digit, such as the "0" in EU0 or the "1" in PL1. The region classes that were used to define location, have been listed in *Table **10-29***. The region classes are generally larger than a minor basin and can cut across major basins.

Hydrogeomorphic region (HGMR) for each reach was defined according to the largest HGMR acreage obtained by adding the land-river segment acres for the HGMR classification, which is used for the accounting of BMPs suitability and effectiveness. Physiographic province was defined based on HGMRs. *Table **10-30*** shows the HGMRs and physiographic provinces in the Chesapeake Bay watershed. All stray segments were within either the Coastal Plain or Piedmont physiographic provinces.

Table 10-29: Region Class Definitions used in Stray-Surrogate Matching

Class	Description	Definitions
PL	Lower Potomac	All PL Minor Basin
E	Eastern Shore	All E Major Basin except EU's in Piedmont
W	Western Shore	All W Major Basin
SLEU	Lower Susquehanna	All small SL Minor Basin and EU's in Piedmont
YJLAB	Near Fall Line Virginia	YL, YM, YP, JB, JA, JL

Table 10-30: Hydrogeomorphic Regions and Physiographic Provinces

ID	Hydrogeomorphic Regions	Physiographic Province
APC	Appalachian Plateau Carbonate	Appalachian Plateau
APS	Appalachian Plateau Siliciclastic	Appalachian Plateau
BR	Blue Ridge	Blue Ridge
CPD	Coastal Plain Dissected Upland	Coastal Plain
CPL	Coastal Plain Lowlands	Coastal Plain
CPU	Coastal Plain Uplands	Coastal Plain
ML	Mesozoic Lowlands	Piedmont
PCA	Piedmont Carbonate	Piedmont
PCR	Piedmont Crystalline	Piedmont
VRC	Ridge and Valley Carbonate	Ridge and Valley
VRS	Ridge and Valley Siliciclastic	Ridge and Valley

Land use was defined as a three-letter class, representing high, medium, and low levels of the percent of cropland, developed land, and natural land in the watershed (1991-2000 average), according to *Table **10-31***.

Table 10-31: Land use classification used in stray-surrogate matching

Level	Crop	Developed	Natural
L, Low	<10%	<10%	<50%
M, Medium	10-30%	10-30%	50-75%
H, High	>30%	>30%	>75%

A LU classification is given by a three-letter identifier specifying the sequential levels of cropland, developed land and natural land in the river segment. For example, land use classification "HML" indicates a high level of crops, medium levels of developed land use, and low level of natural land use.

The pool of potential surrogates included calibrated reaches in the regions represented in ***Table 10-33***. Reservoirs were included among both the stray reaches, as indicated in ***Table 10-33***, and the initial pool of surrogates. As discussed previously, in contrast to river reaches reservoirs behave differently, where the settling process is enhanced by the larger residence time, and as a result there is greater exchange of nutrients and dissolved oxygen across the sediment-water column interface. These differences are reflected in differences in parameterization. None of the reservoirs in the initial pool of surrogates were in the same region or HGMR as the stray reaches, which are all in the Coastal Plain in the Eastern Shore, so reservoirs were removed from the pool of surrogates, and the stray reservoirs were matched to river reaches in the absence of a better alternative.

Stray-surrogate matching was implemented in R as a script. For each stray, the subset of surrogates matching the similarity condition was determined. If the subset was not empty, all the surrogates were considered identified as surrogates of that stray. The following similarly conditions are ranked and executed in order of descending similarity:

1. Match exactly size, region, HGMR, and three-letter LU class
2. Match exactly size, region, physiographic province, and LU class
3. Same as (2), but match any two letters (i.e. two levels) of LU class i.e. HMM matches HLM
4. Match region, HGMR, LU (exact) and size ± 1 of stray size
5. Same as (4), but physiographic province instream of HGMR
6. Same as (5), except two-level match of LU
7. Match size, region, and physiographic province. No restriction on land use
8. Match region and physiographic province, two-levels of LU, and ± 2 of stray size
9. Match region two-levels of LU, and ± 1 of stray size. No restrictions on HGMR or physiographic province
10. Match region and physiographic province, ± 1 of stray size, and one-level of LU

Whenever a non-empty subset of surrogates matches a similarity condition, the script stops looking for additional surrogates.

For a very few river segments (three river segments to be precise) none of the similarity conditions yielded a match. In such cases, the upstream reach was matched with a surrogate and the downstream reaches were treated as pseudo-strays for consistency, i.e., they were assigned the same parameters as the upstream reach, and the downstream reaches were designated as an "inherited" river segment. The inherited river segments are shown in Table 10-32.

Table 10-32: Stray river segments without a similarity match

Stray River Segment	Stray River Name	Surrogate River Segment	Surrogate River Name
WU1_3330_0001	Winters Run	WU1_3350_3490	Western Run
WU1_3331_3330	Winters Run	WU1_3350_3490	Western Run
PL0_5710_0001	Clark Run	PL0_5070_0001	Piscataway Creek

Table 10-33 shows the surrogates matched to stray river segments by the R script and used in the Phase 6 for all water quality constituents except sediment. *Table* ***10-34*** shows the surrogates matched to stray river segments for sediment.

Table 10-33; Stray-surrogates matches used for all water quality constituent parameters except sediment

Strays					Surrogates				Case
River Segment	Reservoir	Region	HGMR	LU	River Segment	Region	HGMR	LU	
DE0_3791_0001		E	CPUN	MML	EL0_4560_4562	E	CPUN	HML	3
DE0_4141_0001		E	CPUN	HML	EL0_4560_4562	E	CPUN	HML	1
DE0_4231_0001		E	CPUN	HLL	EL0_4561_4562	E	CPUN	HLL	1
EL0_5400_0001		E	CPUN	MML	EL0_4560_4562	E	CPUN	HML	3
EL0_5767_0001	X	E	CPDN	HML	EL0_4560_4562	E	CPUN	HML	2
EL1_5150_0001		E	CPLN	HLL	EL0_4561_4562	E	CPUN	HLL	5
					EL2_4400_4590	E	CPUN	HLL	5
					EL2_5110_5270	E	CPUN	HLL	5
EL1_5570_0001		E	CPDN	MLH	EL1_5430_0001	E	CPUN	MLH	2
EL1_6000_0001		E	CPLN	HMM	EM2_3980_0001	E	CPUN	HMM	5
EL2_5272_5270	X	E	CPUN	MLM	EM2_3980_0001	E	CPUN	HMM	3
EM2_4100_0001		E	CPDN	HLL	EL2_4400_4590	E	CPUN	HLL	2
					EL2_5110_5270	E	CPUN	HLL	2
EU0_3726_0001	X	E	CPDN	HLL	EL0_4561_4562	E	CPUN	HLL	2
EU0_3830_0001		E	CPDN	HLL	EL0_4561_4562	E	CPUN	HLL	2
EU1_2810_0001		SLEU	PCRN	MML	EU1_2650_0001	SLEU	PCRN	MML	1
					SL1_2830_2760	SLEU	PCRN	MML	1
EU2_3520_0001		E	CPDN	HLL	EL2_4400_4590	E	CPUN	HLL	2
					EL2_5110_5270	E	CPUN	HLL	2
GY0_3950_3952		G	APSN	LLM	GY0_4531_4532	G	APSN	LLM	1
JA0_7291_7290	X	YJLAB	ML_N	LMH	JA1_7600_7570	YJLAB	PCRN	LLH	6
					JA1_7640_7280	YJLAB	PCRN	LLH	6
					JL1_6770_6850	YJLAB	PCRN	LLH	6
					JL1_7170_6800	YJLAB	PCRN	LLH	6
					YP1_6570_6680	YJLAB	PCRN	LLH	6
					YP1_6680_6670	YJLAB	PCRN	LLH	6
JA2_7290_0001		YJLAB	CPUN	LMM	JB3_6820_7053	YJLAB	CPUN	LMM	4
					YP3_6700_6670	YJLAB	CPUN	LMM	4
JB0_7051_0001	X	YJLAB	CPDN	LLL	YP0_6860_6840	YJLAB	CPUN	MMM	7
JB0_7052_0001	X	YJLAB	CPDN	LLH	YM1_6370_6620	YJLAB	CPUN	MLH	6
JB1_8090_0001	X	YJLAB	CPLN	MMM	YP0_6860_6840	YJLAB	CPUN	MMM	5
JB2_7800_0001	X	YJLAB	CPUN	MLM	YP3_6670_6720	YJLAB	CPDN	MLM	5
PL0_5510_0001		PL	CPUN	MMM	PL0_5750_0001	PL	CPUN	MMM	1
PL0_5530_5710		PL	CPUN	LMM	PL0_5070_0001	PL	CPUN	LMM	1
PL0_5710_0001		PL	CPDN	MMM	PL0_5750_0001	PL	CPUN	MMM	2
PL0_5720_0001		PL	CPUN	LLH	PL0_5070_0001	PL	CPUN	LMM	7
					PL0_5750_0001	PL	CPUN	MMM	7
PL0_5830_0001		PL	CPUN	MMM	PL0_5750_0001	PL	CPUN	MMM	1

Strays					Surrogates				Case
River Segment	Reservoir	Region	HGMR	LU	River Segment	Region	HGMR	LU	
PL1_5910_0001		PL	CPUN	LMH	PL1_5230_0001	PL	CPUN	LMM	3
SL2_2480_0001		SLEU	PCRN	HML	SL2_2750_2720	SLEU	PCRN	HML	1
					SL2_2910_3060	SLEU	PCRN	HML	1
WM0_3740_0001		W	CPDN	LHL	WM1_3660_3910	W	PCRN	LHL	9
					WU1_3490_3480	W	PCRN	LHM	9
WU0_3250_0001		W	PCRN	MHL	WM1_3882_3880	W	PCRN	MML	6
					WU1_3350_3490	W	PCRN	MML	6
WU0_3670_0001		W	CPDN	LHL	WM1_3660_3910	W	PCRN	LHL	9
					WU1_3490_3480	W	PCRN	LHM	9
WU1_3240_3331		W	PCRN	MML	WM1_3882_3880	W	PCRN	MML	1
					WU1_3350_3490	W	PCRN	MML	1
WU1_3330_0001		W	CPDN	LHL	WM3_4060_0001	W	CPDN	LHM	8
WU1_3331_3330		W	PCRN	LHL	WM1_3660_3910	W	PCRN	LHL	1
WU1_3482_0001		W	PCRN	MML	WM1_3882_3880	W	PCRN	MML	1
					WU1_3350_3490	W	PCRN	MML	1
YL2_6580_0001		YJLAB	CPUN	MLH	YM1_6370_6620	YJLAB	CPUN	MLH	4

Table 10-34: Stray-surrogate matches used for sediment parameters

Strays					Surrogates				Case
River Segment	Reservoir	Region	HGMR	LU	River Segment	Region	HGMR	LU	
DE0_3791_0001		E	CPUN	MML	EL0_4560_4562	E	CPUN	HML	3
DE0_4141_0001		E	CPUN	HML	EL0_4560_4562	E	CPUN	HML	1
DE0_4231_0001		E	CPUN	HLL	EL0_4561_4562	E	CPUN	HLL	1
EL0_5400_0001		E	CPUN	MML	EL0_4560_4562	E	CPUN	HML	3
EL0_5767_0001	X	E	CPDN	HML	EL0_4560_4562	E	CPUN	HML	2
EL1_5150_0001		E	CPLN	HLL	EL0_4561_4562	E	CPUN	HLL	5
					EL2_4400_4590	E	CPUN	HLL	5
					EL2_5110_5270	E	CPUN	HLL	5
EL1_5430_0001		E	CPUN	MLH	EL0_4561_4562	E	CPUN	HLL	10
					EL2_4400_4590	E	CPUN	HLL	10
					EL2_5110_5270	E	CPUN	HLL	10
EL1_5570_0001		E	CPDN	MLH	EL0_4561_4562	E	CPUN	HLL	10
					EL2_4400_4590	E	CPUN	HLL	10
					EL2_5110_5270	E	CPUN	HLL	10
EL1_6000_0001		E	CPLN	HMM	EM2_3980_0001	E	CPUN	HMM	5
EL2_5272_5270	X	E	CPUN	MLM	EL2_4400_4590	E	CPUN	HLL	7
					EL2_5110_5270	E	CPUN	HLL	7
					EM2_3980_0001	E	CPUN	HMM	7
EM2_4100_0001		E	CPDN	HLL	EL2_4400_4590	E	CPUN	HLL	2

Strays					Surrogates				Case
River Segment	Reservoir	Region	HGMR	LU	River Segment	Region	HGMR	LU	
EM2_4100_0001		E	CPDN	HLL	EL2_5110_5270	E	CPUN	HLL	2
EU0_3726_0001	X	E	CPDN	HLL	EL0_4561_4562	E	CPUN	HLL	2
EU0_3830_0001		E	CPDN	HLL	EL0_4561_4562	E	CPUN	HLL	2
EU1_2810_0001		SLEU	PCRN	MML	EU1_2650_0001	SLEU	PCRN	MML	1
					SL1_2830_2760	SLEU	PCRN	MML	1
EU2_3520_0001		E	CPDN	HLL	EL2_4400_4590	E	CPUN	HLL	2
					EL2_5110_5270	E	CPUN	HLL	2
GY0_3950_3952		G	APSN	LLM	GY0_4531_4532	G	APSN	LLM	1
JA0_7291_7290	X	YJLAB	ML_N	LMH	JA1_7600_7570	YJLAB	PCRN	LLH	6
					JA1_7640_7280	YJLAB	PCRN	LLH	6
					JL1_7170_6800	YJLAB	PCRN	LLH	6
					YP1_6570_6680	YJLAB	PCRN	LLH	6
					YP1_6680_6670	YJLAB	PCRN	LLH	6
JA2_7290_0001		YJLAB	CPUN	LMM	JB3_6820_7053	YJLAB	CPUN	LMM	4
					YP3_6700_6670	YJLAB	CPUN	LMM	4
					YP3_6700_6670	YJLAB	CPUN	LMM	4
JB0_7051_0001	X	YJLAB	CPDN	LLL	JA1_7600_7570	YJLAB	PCRN	LLH	9
					JA1_7640_7280	YJLAB	PCRN	LLH	9
					JL1_6560_6440	YJLAB	BR_N	LLM	9
					JL1_6760_6910	YJLAB	PCRN	LLM	9
					JL1_6910_6960	YJLAB	PCRN	LLM	9
					JL1_7080_7190	YJLAB	BR_N	LLH	9
					JL1_7170_6800	YJLAB	PCRN	LLH	9
					JL1_7190_7250	YJLAB	PCRN	LLM	9
					JL1_7200_7250	YJLAB	PCRN	LLM	9
					JL1_7530_7430	YJLAB	PCRN	LLM	9
					YP1_6570_6680	YJLAB	PCRN	LLH	9
					YP1_6680_6670	YJLAB	PCRN	LLH	9
JB0_7052_0001	X	YJLAB	CPDN	LLH	YM1_6370_6620	YJLAB	CPUN	MLH	6
JB1_8090_0001	X	YJLAB	CPLN	MMM	YM1_6370_6620	YJLAB	CPUN	MLH	7
JB2_7800_0001	X	YJLAB	CPUN	MLM	YP3_6670_6720	YJLAB	CPDN	MLM	5
PL0_5510_0001		PL	CPUN	MMM	PL0_5070_0001	PL	CPUN	LMM	3
PL0_5530_5710		PL	CPUN	LMM	PL0_5070_0001	PL	CPUN	LMM	1
PL0_5710_0001		PL	CPDN	MMM	PL0_5070_0001	PL	CPUN	LMM	3
PL0_5720_0001		PL	CPUN	LLH	PL0_5070_0001	PL	CPUN	LMM	7
PL0_5730_5690		PL	PCRN	LMH	PL0_5540_5490	PL	PCRN	LLH	3
PL0_5750_0001		PL	CPUN	MMM	PL0_5070_0001	PL	CPUN	LMM	3
PL0_5830_0001		PL	CPUN	MMM	PL0_5070_0001	PL	CPUN	LMM	3
PL1_5910_0001		PL	CPUN	LMH	PL1_5230_0001	PL	CPUN	LMM	3
PL2_5300_5630		PL	CPUN	LMM	PL1_5230_0001	PL	CPUN	LMM	4
PL3_5250_0001	X	PL	PCRN	LMM	PL3_5360_5250	PL	PCRN	LMM	1

Strays					Surrogates				Case
River Segment	Reservoir	Region	HGMR	LU	River Segment	Region	HGMR	LU	
RL0_6540_0001		YJLAB	CPDN	MLH	YM1_6370_6620	YJLAB	CPUN	MLH	5
RL1_6180_0001		YJLAB	CPUN	MLM	YM1_6370_6620	YJLAB	CPUN	MLH	3
SL2_2480_0001		SLEU	PCRN	HML	SL2_2750_2720	SLEU	PCRN	HML	1
					SL2_2910_3060	SLEU	PCRN	HML	1
WM0_3740_0001		W	CPDN	LHL	WM1_3660_3910	W	PCRN	LHL	9
					WU1_3490_3480	W	PCRN	LHM	9
WU0_3250_0001		W	PCRN	MHL	WM0_3650_0001	W	PCRN	LHL	3
WU0_3670_0001		W	CPDN	LHL	WM1_3660_3910	W	PCRN	LHL	9
					WU1_3490_3480	W	PCRN	LHM	9
WU1_3240_3331		W	PCRN	MML	WM1_3882_3880	W	PCRN	MML	1
					WU1_3350_3490	W	PCRN	MML	1
WU1_3330_0001		W	CPDN	LHL	WM3_4060_0001	W	CPDN	LHM	8
WU1_3331_3330		W	PCRN	LHL	WM1_3660_3910	W	PCRN	LHL	1
WU1_3482_0001		W	PCRN	MML	WM1_3882_3880	W	PCRN	MML	1
					WU1_3350_3490	W	PCRN	MML	1
YL2_6580_0001		YJLAB	CPUN	MLH	YM1_6370_6620	YJLAB	CPUN	MLH	4
YP0_6860_6840		YJLAB	CPUN	MMM	YM1_6370_6620	YJLAB	CPUN	MLH	10

10.6.4 Water Quality Simulation Results

The assessment of model calibration was made based on the recommendations from the Scientific and Technical Advisory Committee (STAC) review of the Watershed Model (STAC 2008, STAC 2017). Calibration metrics presented in this document and recommended by the STAC review are meant to give an overview of model performance across monitoring stations rather than a detailed examination at a particular station.

Many different measures were used to assess the agreement between observed and simulated concentrations and loads for water quality constituents including nutrient and sediment. Those include

- Summary statistics such as minimum, mean, maximum, and median values
- Time series plots
- Scatter plots of concentration or log concentration
- Cumulative distribution of paired observed and simulated concentrations or log concentrations
- Statistical measures of degree of agreement such as model efficiency or correlation coefficients
- Comparison of simulated loads with USGS-WRTDS estimates at different spatial scales
- Comparison of per acre loads for the basins with USGS-WRTDS estimates

Plots of simulated and observed instantaneous concentrations and loads for all monitoring stations that were used in the model calibration are accessible on the FTP link:

ftp://ftp.chesapeakebay.net/Modeling/Phase6/Phase_6_201710/Watershed_Model/WSM_Outputs/Calibration_Figures/00_Calibration_Figures_All_Phase6.pdf [~300 MB]

The plots of flow (FLOW), water temperature (WTMP), dissolved oxygen (DOXX), total nitrogen (TOTN), total phosphorus (TOTP), total suspended sediment (TSSX), nitrate (NO3X), ammonia (NH3X), dissolved orthophosphate (PO4X), and chlorophyll (CHLA) for the individual river segments can be accessed at the following ftp site:

ftp://ftp.chesapeakebay.net//Modeling/Phase6/Phase_6_201710/Watershed_Model/WSM_Outputs/Calibration_Figures/

In addition, rating curves, representing the relation between flow and water quality concentration, were also compared. A special set of plots and statistical measures were developed to take into account the following three obstacles in comparing simulations to observed concentrations of water quality constituents, e.g., sediment and phosphorus:

1. Sediment concentrations vary widely over a storm, but most available sediment observations consist of grab samples taken at a moment in time.
2. Simulated storms can lead or lag the real events due to multiple factors including rainfall inputs, so simulated concentrations or loads can be in agreement with their observed counterparts but lead or lag them in time.
3. Over a wide range of low flows, suspended sediment concentrations are low, contribute little to sediment loads, and are made up mostly of organic solids.

To take those problems into account *windowed* plots and several statistics were used. In a windowed plot, observed data are compared to a one-day window of simulated values, before and after the observation. If the observation falls within the range of simulated values, the simulated value is set equal to the observed value. If the range of simulated values is above or below the observed value, the simulated value is set equal to the minimum or maximum simulated value, respectively. Such a procedure was used for both concentrations and loads. *Figure **10-56*** shows an example of windowed concentration plots for the Potomac River at Chain Bridge; *Figure **10-57*** shows the windowed load plots for the Potomac River at Chain Bridge.

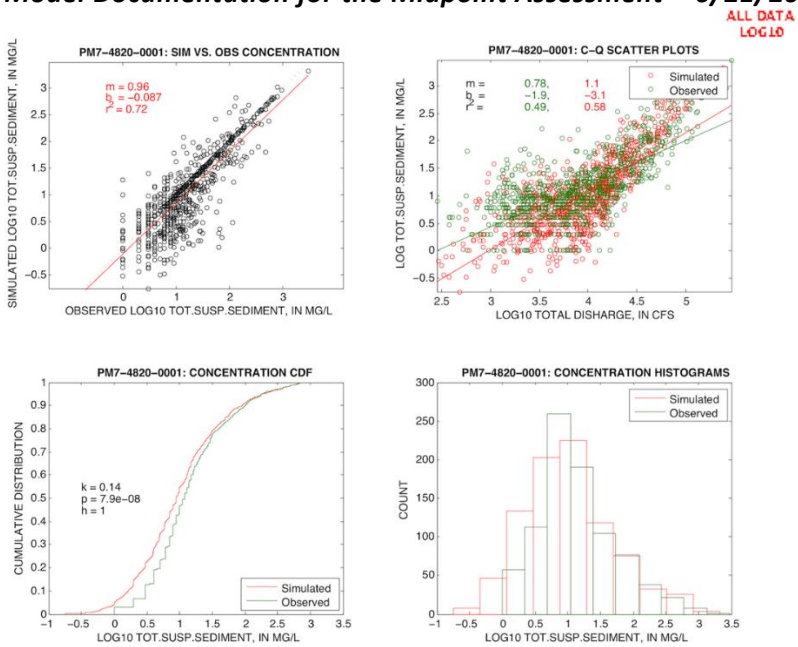

Figure 10-56. An example of 'windowed' concentration plots. Simulated and observed total suspended sediment windowed concentration data for Potomac River at Chain Bridge, Washington D.C. are shown.

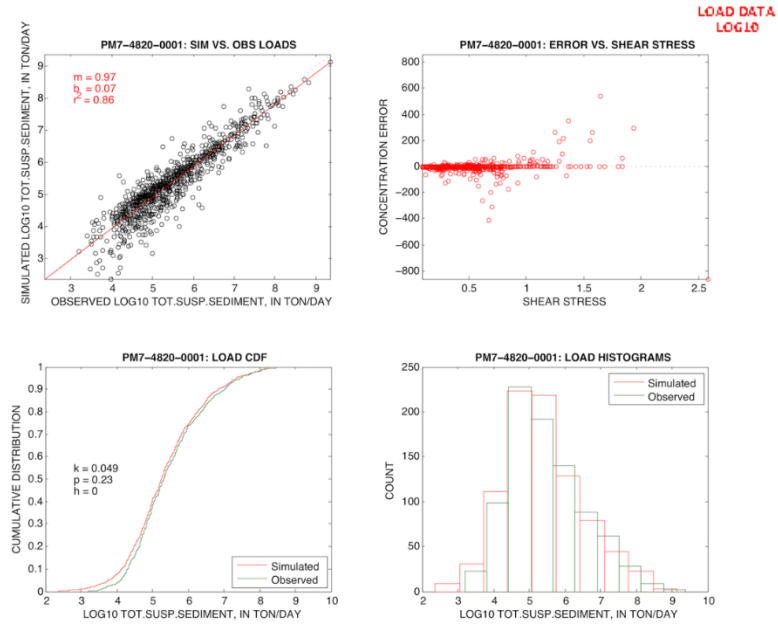

Figure 10-57. An example of 'windowed' load plots. Simulated and observed total suspended sediment windowed load data for Potomac River at Chain Bridge, Washington D.C. are shown.

Another assessment for the quality of the model calibration can be made by comparing simulated loads with USGS-WRTDS estimates of monthly and annual loads for nutrients and sediment. In addition, USGS's River Input Monitoring (RIM) program, which evaluates nutrient and sediment loads entering Chesapeake Bay and its tidal tributaries at the RIM stations can be used for an integrated assessment of the model calibration.

In the following subsections analyses have been made for nested spatial and temporal scales. For the nested spatial scale model performance was evaluated for the combined RIM stations, individual RIM stations, and all monitoring stations. For these spatial scales, level of agreement was analyzed for nested average annual, annual, and monthly temporal scales. Statistics such as bias, correlation coefficients, and Nash-Sutcliffe efficiencies were used for quantifying the degree of agreement in loads and the quality of model performance.

A summary of model performance for the streamflow and temperature simulation are shown in *Figure **10-59*** and *Figure **10-60*** respectively. The box and whisker plots show the distribution of model performance statistics for the river segments at monitoring stations. The distributions of biases and Nash Sutcliffe Efficiencies (NSE) are shown, where for any given monitoring station an exact match between the observation and simulation data would have a Bias of 0 and NSE of 1.

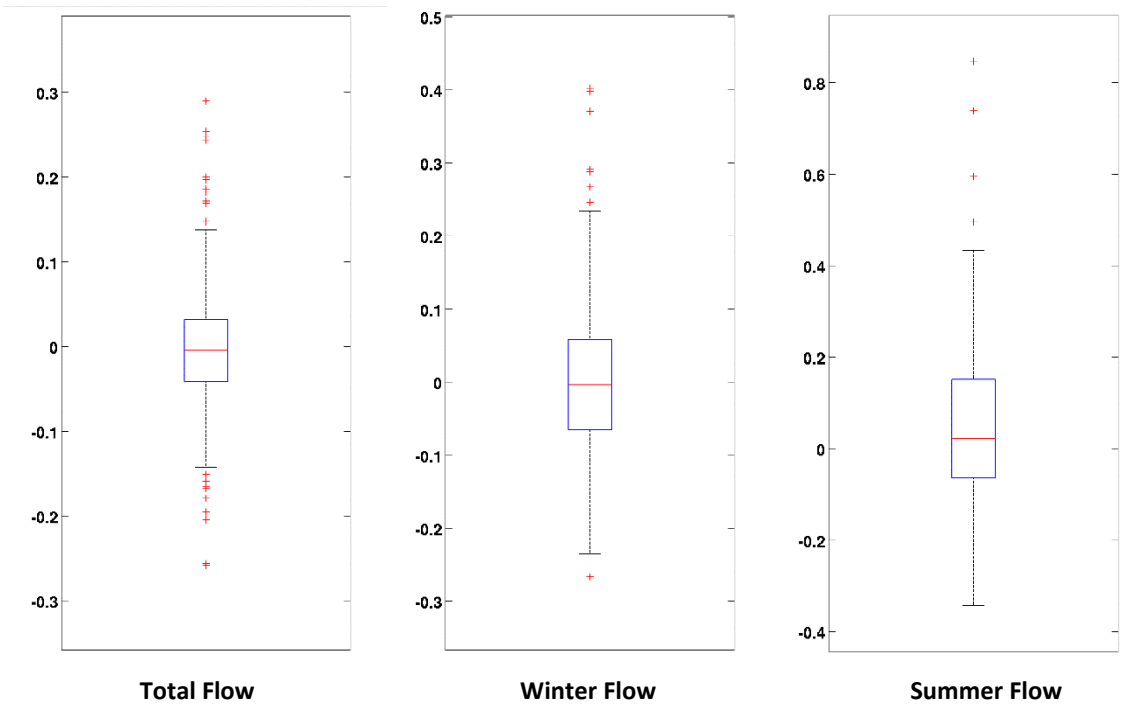

Figure 10-58: The overall model performance for the streamflow in terms of Biases in simulated daily flow. Biases for the 253 monitoring sites are shown using box and whisker plot. For a monitoring site, a bias of 0 suggests an exact match between the observation and simulation with 0 percent difference in volume.

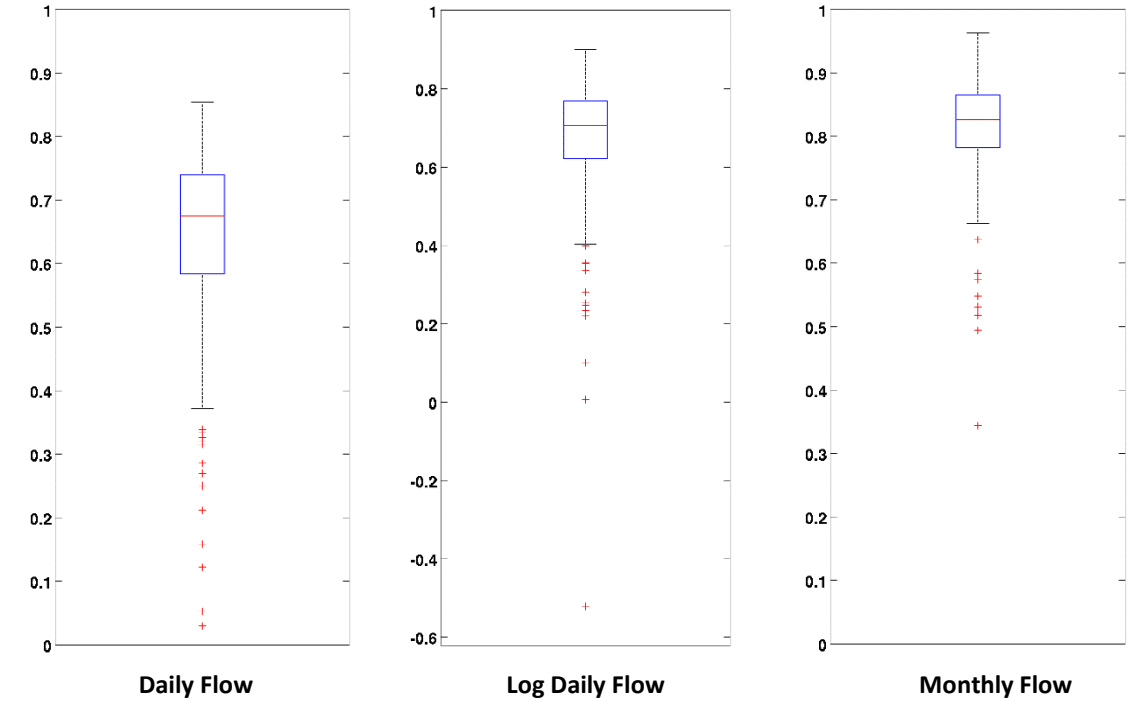

Figure 10-59: The overall model performance for streamflow simulation in term of Nash Sutcliffe Efficiency (NSE). NSE for daily, log-daily, and monthly streamflow were calculated. A NSE of 1 suggests an exact fit between the observation and simulation. Higher value for NSE indicates better model performance.

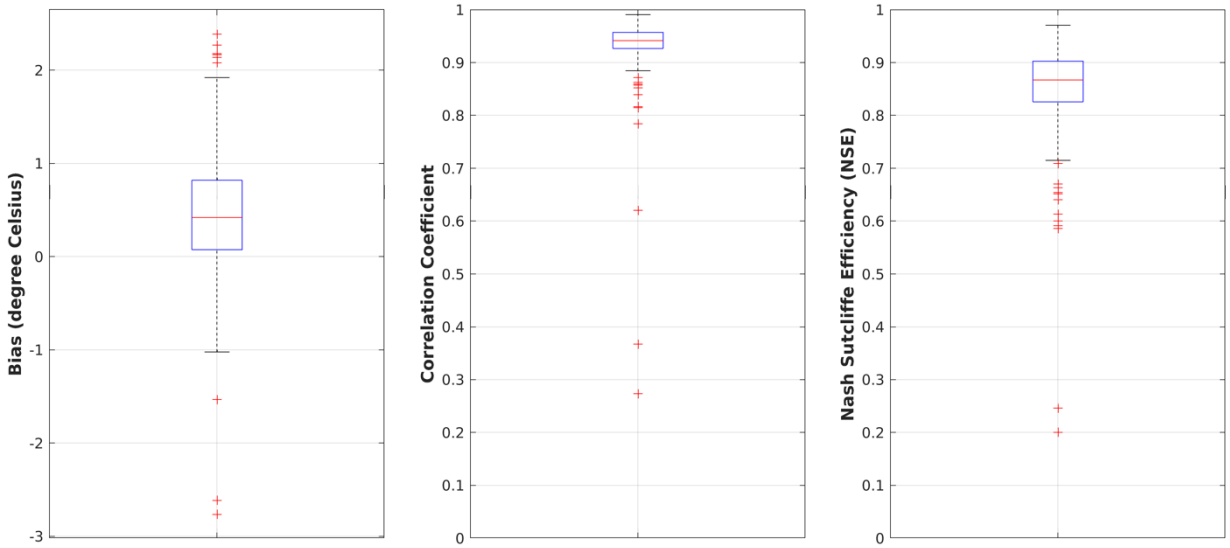

Figure 10-60: The overall model performance for temperature simulation in term of Bias, Correlation coefficient, and Nash Sutcliffe Efficiency (NSE) for the river segments at the monitoring sites. Bias closer to 0 indicates better model performance. Correlation coefficient or NSE of 1 suggests an exact fit between the observation and simulation. Higher value for NSE indicates better model performance.

10.6.4.1 Average Annual Loads for RIM and Non-RIM Watersheds

The Chesapeake Bay River Input Monitoring (RIM) stations are the most downstream water quality monitoring stations before discharge to tidal waters (https://cbrim.er.usgs.gov/). It includes 9 major rivers of the Chesapeake Bay Watershed that have long-term USGS monitoring data. The drainage area for the RIM stations covers about 79% of the watershed area. *Figure **10-61*** and *Figure **10-62*** show the simulated average annual total nitrogen and phosphorus delivery loads for the RIM and the Non-RIM portions of the watersheds, and the degree of agreement with the USGS-WRTDS. The RIM loads are the sum of the separately calculated average annual loads of the 9 RIM stations for the matching years between the USGS-WRTDS and simulation for 1985 to 2014 period. Non-RIM loads are the loads from the portions of the Chesapeake Bay watershed that do not drain to any of RIM stations. USGS-WRTDS loads are not available for the Non-RIM watershed as it uses flow and water quality monitoring data for the estimation of loads. Therefore, simulated Non-RIM loads are compared with that from Phase 5.3.2 Watershed Model.

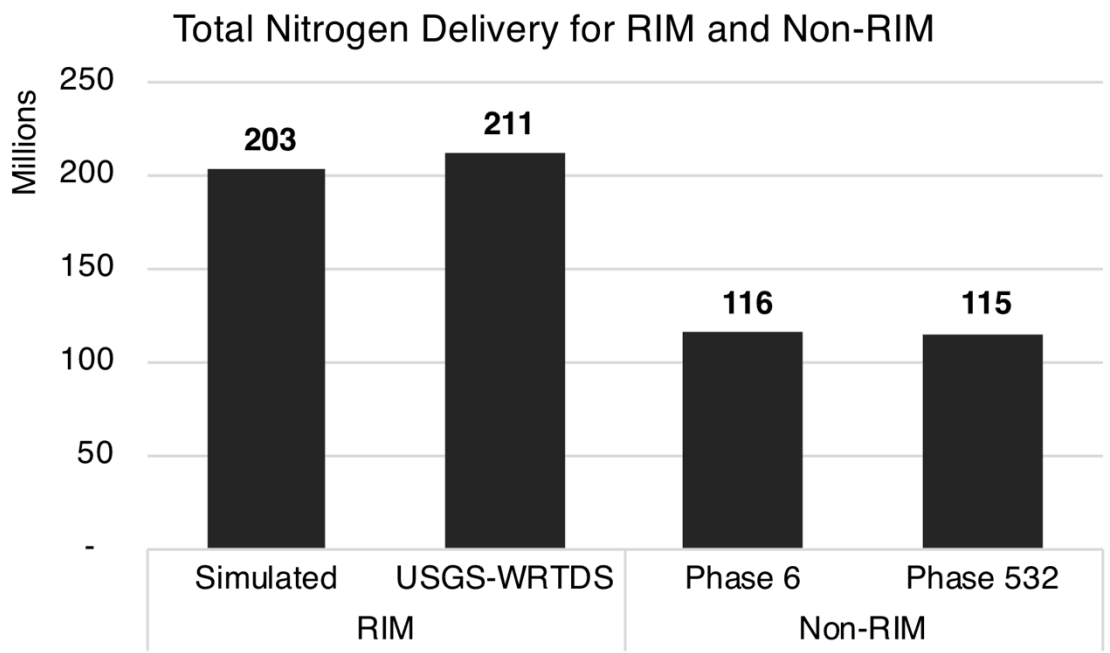

Figure 10-61: An inter model comparison of average annual nitrogen load delivery from the Bay watershed. (a) Nitrogen loads from 9 river input monitoring (RIM) stations. (b) Nitrogen loads from Non-RIM stations. Phase 6 and Phase 532 loads are for the entire calibration period i.e.1985 to 2014 and 1985 to 2005 respectively.

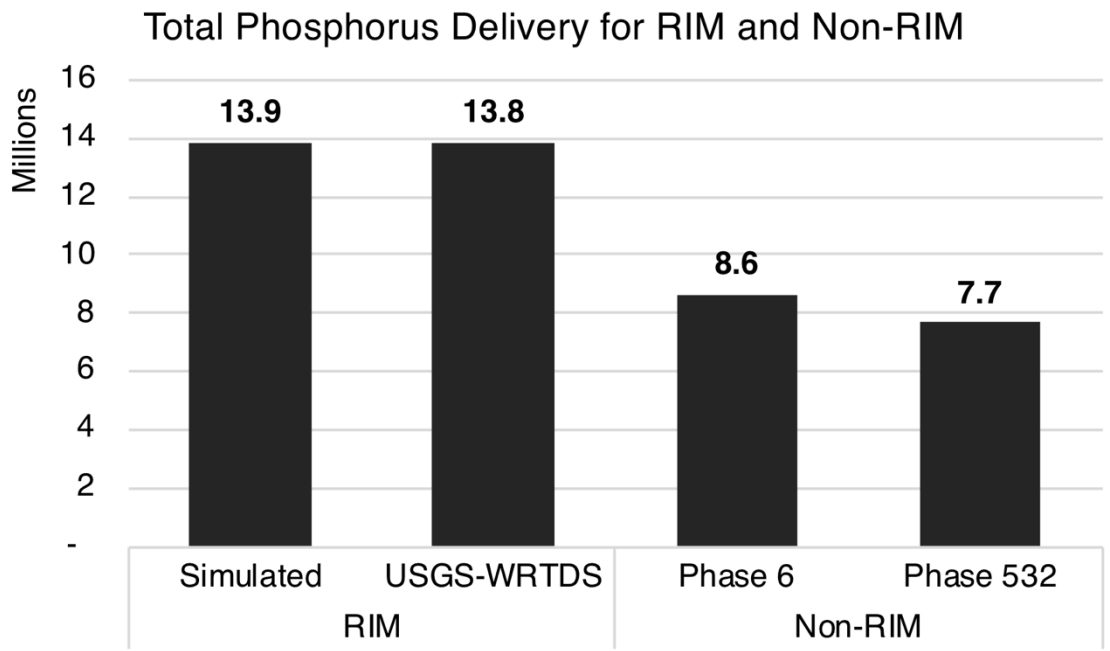

Figure 10-62: An inter model comparison of average annual phosphorus loads delivery from the Bay watershed. (a) Phosphorus loads from 9 river input monitoring (RIM) stations. (b) Phosphorus loads from Non-RIM stations. Phase 6 and Phase 532 loads are for the entire calibration period i.e.1985 to 2014 and 1985 to 2005 respectively.

Early versions of the Phase 6 model that contained the Coastal Plain land-to-water factor for phosphorus as discussed in Section 7 over-simulated phosphorus loads on the Eastern Shore. Once that factor was removed from the simulation as described in Section 7.3.2, the agreement with monitored data were substantial as shown in Figure 10-63. These annual Non-RIM phosphorus flux for small scale watersheds in coastal plain were estimated using a tool similar to WRTDS by UMCES and SERC (Lyubchich et al., 2015)

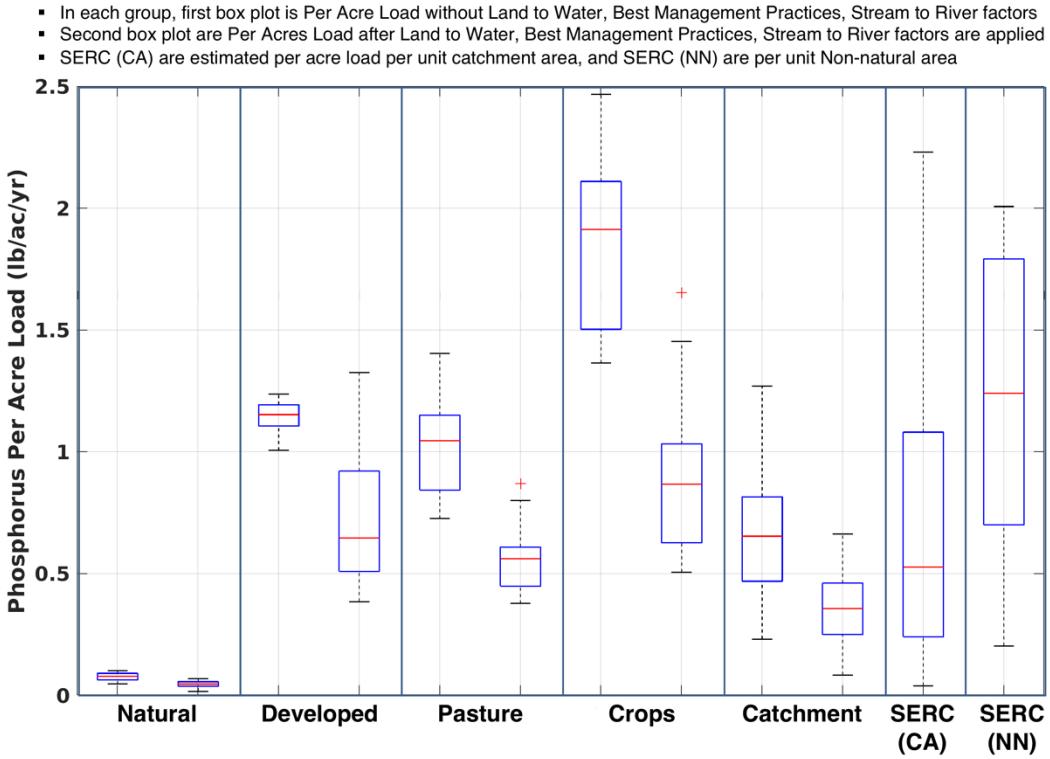

Figure 10-63: Simulated per acre phosphorus load for 16 Phase 6 land river segments that intersect with 36 small scale catchments where load estimates reported by Lyubchich et al. (2015) were calculated using a statistical model. A few boxplot outliers in the estimated loads are not shown to clearly display the range for major land use groups. A good agreement in simulated and estimated per acre loads are found.

10.6.4.2 Average Annual Loads for RIM Sites

The model performance was evaluated by comparing the degree of agreement in average annual loads for individual river input monitoring sites. *Figure **10-64*** and *Figure **10-65*** show a comparison of average annual WRTDS loads with the simulated loads for nitrogen and phosphorus respectively at the 9 RIM stations. The labels refer to the Susquehanna, Potomac, James, Rappahannock, Appomattox, Pamunkey, Mattaponi, Patuxent, and Choptank rivers, respectively.

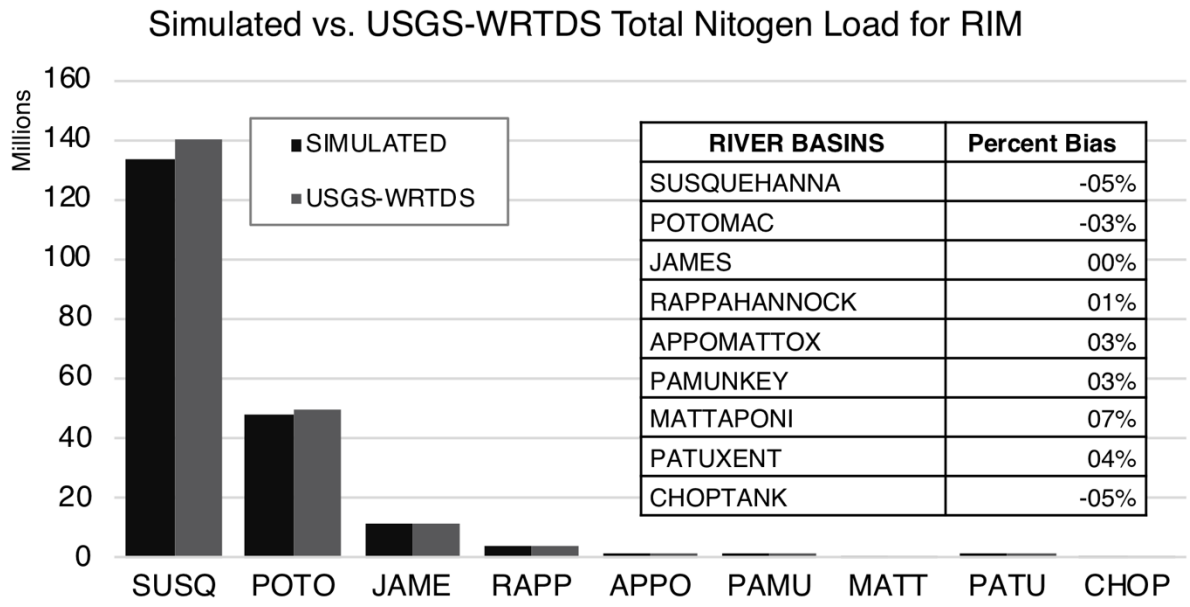

RIVER BASINS	Percent Bias
SUSQUEHANNA	-05%
POTOMAC	-03%
JAMES	00%
RAPPAHANNOCK	01%
APPOMATTOX	03%
PAMUNKEY	03%
MATTAPONI	07%
PATUXENT	04%
CHOPTANK	-05%

Figure 10-64: Comparison of simulated average annual nitrogen loads with USGS-WRTDS loads for the 9 river input monitoring (RIM) sites. The differences in nitrogen loads are tabulated as percent biases.

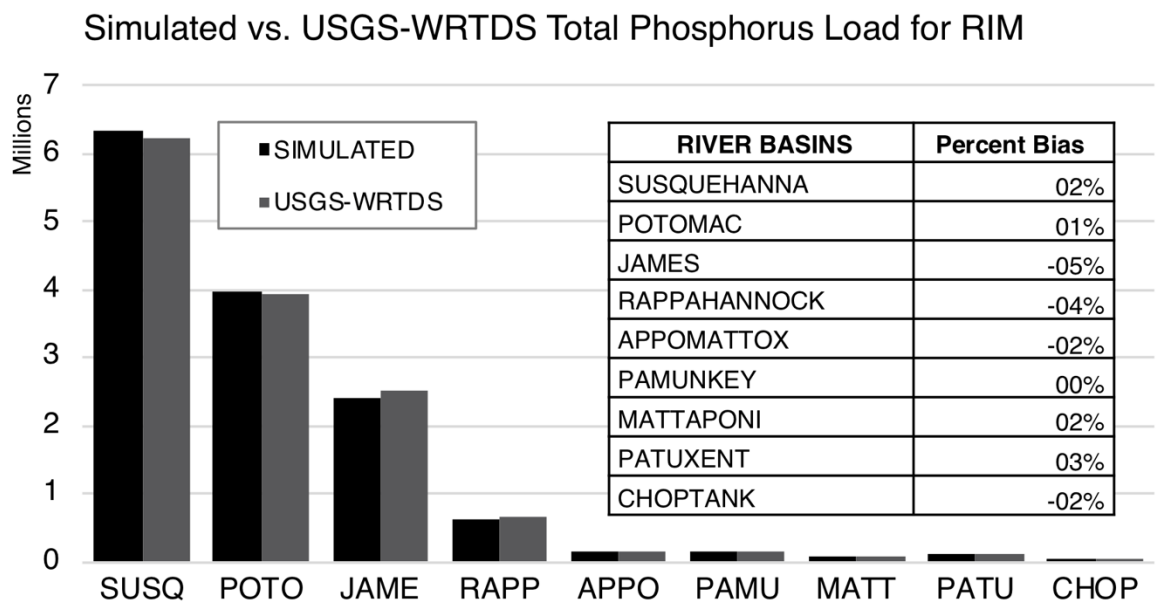

RIVER BASINS	Percent Bias
SUSQUEHANNA	02%
POTOMAC	01%
JAMES	-05%
RAPPAHANNOCK	-04%
APPOMATTOX	-02%
PAMUNKEY	00%
MATTAPONI	02%
PATUXENT	03%
CHOPTANK	-02%

Figure 10-65: Comparison of simulated average annual phosphorus loads with USGS-WRTDS loads for the 9 river input monitoring (RIM) sites. The differences in phosphorus loads are tabulated as percent biases.

10.6.4.3 Average Annual Loads at WRTDS Sites

The watershed model performance was evaluated for the watershed at several monitoring sites where load estimates from USGS-WRTDS were available. These sites include watershed responses for a wide range of spatial scales ranging between 7.4 to 27086 square miles. *Figure **10-66***, *Figure **10-67*** and *Figure*

10-68 show a comparison of average annual load at these sites for nitrogen and phosphorus and sediment respectively. High (close to 1) values for NSE and Log-NSE indicates good agreement between the simulated and WRTDS loads. Average annual loads for nitrogen and phosphorus at the monitoring sites are provided in *Table **10-35*** and *Table **10-36*** respectively. Differences in simulated and WRTDS loads are shown as percent biases but it is noted that both WRTDS and Phase 6 have an unknown degree of uncertainty associated with them.

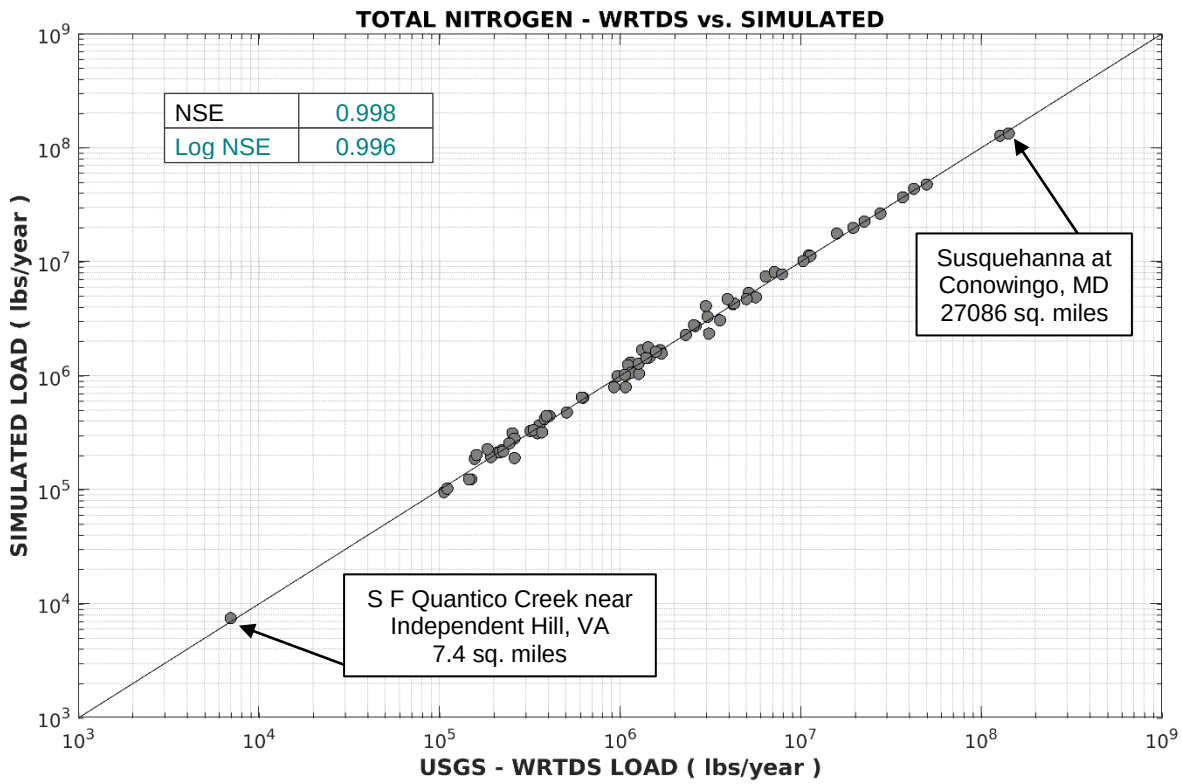

Figure 10-66. WRTDS and Watershed Model average annual nitrogen loads are shown for 77 monitoring sites. The figure shows a good agreement between the two estimates across different spatial scales.

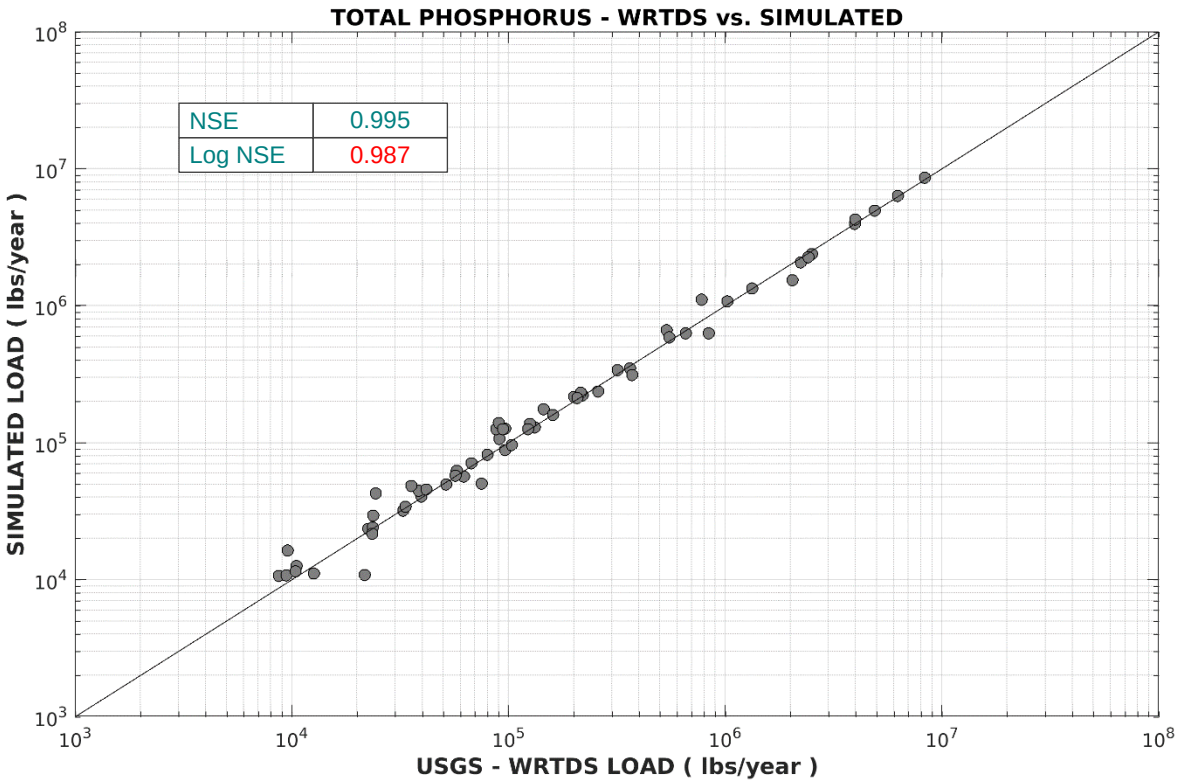

Figure 10-67. WRTDS and Watershed Model average annual phosphorus loads are shown for 61 monitoring sites. The figure shows a good agreement between the two estimates across different spatial scales.

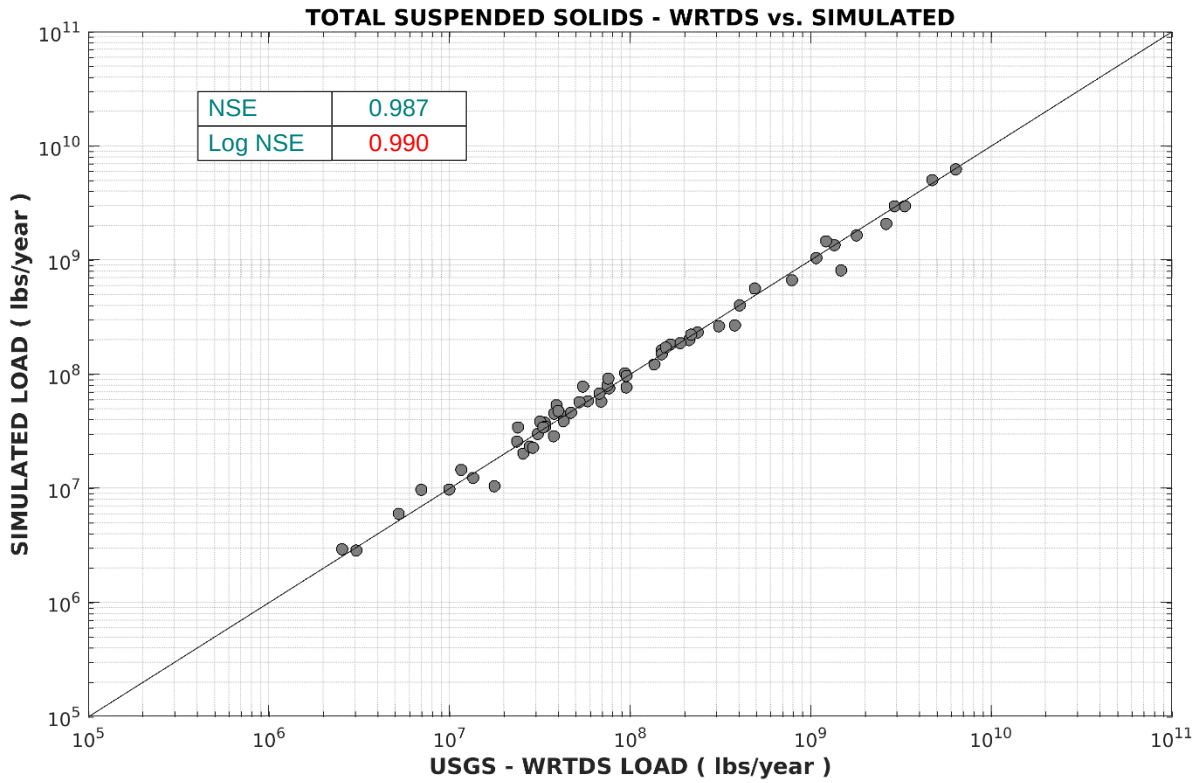

Figure 10-68. WRTDS and Watershed Model average annual sediment loads are shown for 60 monitoring sites. The figure shows a good agreement between the two estimates across different spatial scales.

Table 10-35: Average annual nitrogen loads from Watershed Model and WRTDS. Difference between the two has been tabulated as percent bias. Positive bias indicates an over simulation of loads as compared to WRTDS.

RIVER SEG	RIVER NAME	AREA (sq miles)	SIMULATED (lb/yr)	WRTDS (lb/yr)	BIAS (%)
EL0_4562_0003	NANTICOKE R	72	9.972E+05	9.679E+05	3%
EL2_4400_4590	MARSHYHOPE CREEK NEAR ADAMSVILLE, DE	47	3.710E+05	3.564E+05	4%
EM2_3980_0001	CHOPTANK RIVER NEAR GREENSBORO, MD	117	4.813E+05	5.048E+05	-5%
EU1_2650_0001	BIG ELK CREEK AT ELK MILLS, MD	53	6.463E+05	6.237E+05	4%
JA1_7600_7570	DEEP CREEK NEAR MANNBORO, VA	158	2.149E+05	2.093E+05	3%
JA2_7550_7280	APPOMATTOX RIVER AT FARMVILLE, VA	312	4.214E+05	3.796E+05	11%
JA5_7480_0001	APPOMATTOX RIVER AT MATOACA, VA	1340	1.453E+06	1.408E+06	3%
JB3_6820_7053	CHICKAHOMINY RIVER NEAR PROVIDENCE FORGE, VA	246	3.151E+05	3.468E+05	-9%
JL1_6560_6440	MECHUMS RIVER NEAR WHITE HALL, VA	95	1.884E+05	1.557E+05	21%
JL4_6520_6710	RIVANNA RIVER AT PALMYRA, VA	699	1.702E+06	1.318E+06	29%
JL7_6800_7070	JAMES RIVER AND KANAWHA CANAL NEAR RICHMOND, VA	6750	1.147E+07	1.108E+07	4%
JL7_7100_7030	JAMES RIVER AT CARTERSVILLE, VA	6251	1.129E+07	1.127E+07	0%
JU1_6300_6650	BULLPASTURE RIVER AT WILLIAMSVILLE, VA	110	1.949E+05	1.915E+05	2%

JU2_6410_6640	CALFPASTURE RIVER ABOVE MILL CREEK AT GOSHEN, VA	141	1.237E+05	1.489E+05	-17%
JU2_6600_6810	BACK CREEK NEAR MOUNTAIN GROVE, VA	134	1.249E+05	1.449E+05	-14%
PL0_4510_0001	NW BRANCH ANACOSTIA RIVER NEAR HYATTSVILLE, MD	52	1.945E+05	1.924E+05	1%
PL0_5010_5130	ACCOTINK CREEK NEAR ANNANDALE, VA	24	9.644E+04	1.063E+05	-9%
PL0_5540_5490	S F QUANTICO CREEK NEAR INDEPENDENT HILL, VA	7	7.535E+03	6.952E+03	8%
PM1_3510_4000	CATOCTIN CREEK NEAR MIDDLETOWN, MD	67	3.306E+05	3.171E+05	4%
PM1_4430_4200	CATOCTIN CREEK AT TAYLORSTOWN, VA	93	3.374E+05	3.307E+05	2%
PM2_2860_3040	MONOCACY RIVER AT BRIDGEPORT, MD	173	1.322E+06	1.144E+06	16%
PM7_4820_0001	POTOMAC RIVER NEAR WASH, DC	11569	4.821E+07	4.974E+07	-3%
PS2_6730_6660	SOUTH RIVER NEAR WAYNESBORO, VA	127	3.162E+05	2.522E+05	25%
PS3_5100_5080	N F SHENANDOAH RIVER NEAR STRASBURG, VA	772	2.751E+06	2.609E+06	5%
PS4_6360_5840	S F SHENANDOAH RIVER NEAR LYNNWOOD, VA	1076	4.271E+06	4.222E+06	1%
PS5_5240_5200	S F SHENANDOAH RIVER AT FRONT ROYAL, VA	1635	5.384E+06	5.135E+06	5%
PU0_3000_3090	ANTIETAM CR E BR	93	8.006E+05	9.236E+05	-13%
PU1_3030_3440	TONOLOWAY CR	114	4.471E+05	4.063E+05	10%
PU1_3100_3690	SIDELING HILL CREEK NEAR BELLEGROVE, MD	104	2.248E+05	2.213E+05	2%
PU1_3940_3970	GEORGES CR	75	1.909E+05	2.598E+05	-27%
PU2_3090_4050	ANTIETAM CREEK NEAR SHARPSBURG, MD	280	2.352E+06	3.097E+06	-24%
PU2_3370_4020	TOWN CR	157	2.837E+05	2.593E+05	9%
PU2_4220_3900	OPEQUON CREEK NEAR MARTINSBURG, WV	277	1.248E+06	1.097E+06	14%
PU2_4360_4160	PATTERSON CREEK NEAR HEADSVILLE, WV	218	3.201E+05	3.680E+05	-13%
PU3_3290_3390	CONOCOCHEAGUE CREEK AT FAIRVIEW, MD	502	4.930E+06	5.627E+06	-12%
PU3_3680_3890	WILLS CREEK NEAR CUMBERLAND, MD	253	1.027E+06	1.085E+06	-5%
PU3_3860_3610	CACAPON RIVER NEAR GREAT CACAPON, WV	681	1.067E+06	1.146E+06	-7%
PU4_4310_4210	SOUTH BRANCH POTOMAC RIVER NEAR SPRINGFIELD, WV	1462	2.785E+06	2.559E+06	9%
RU2_6090_6220	RAPIDAN RIVER NEAR RUCKERSVILLE, VA	115	2.294E+05	1.835E+05	25%
RU3_6170_6040	RAPIDAN RIVER NEAR CULPEPER, VA	467	1.460E+06	1.418E+06	3%
RU4_5640_0003	RAPPAHANNOCK RIVER AT REMINGTON, VA	606	1.051E+06	1.272E+06	-17%
RU5_6030_0001	RAPPAHANNOCK RIVER NEAR FREDERICKSBURG, VA	1596	4.321E+06	4.271E+06	1%
SJ4_2660_2360	RAYSTOWN BRANCH JUNIATA RIVER AT SAXTON, PA	750	3.084E+06	3.562E+06	-13%
SJ6_2130_0003	JUNIATA RIVER AT NEWPORT, PA	3351	1.775E+07	1.581E+07	12%
SL2_2410_2700	PEQUEA CR	155	3.295E+06	3.039E+06	8%
SL2_3060_0001	DEER CR	171	1.688E+06	1.660E+06	2%
SL3_1710_1740	PENNS CREEK AT PENNS CREEK, PA	306	1.460E+06	1.452E+06	1%
SL3_2290_2260	SHERMAN CREEK AT SHERMANS DALE, PA	207	1.288E+06	1.260E+06	2%
SL3_2400_2440	YELLOW BREECHES CREEK NEAR CAMP HILL, PA	215	1.649E+06	1.472E+06	12%
SL3_2420_2700	CONESTOGA RIVER AT CONESTOGA, PA	475	1.017E+07	1.032E+07	-1%
SL3_2460_2430	WEST CONEWAGO CREEK NEAR MANCHESTER, PA	516	4.764E+06	3.912E+06	22%
SL4_2140_2240	SWATARA CREEK NEAR HERSHEY, PA	482	7.495E+06	6.362E+06	18%
SL4_2370_2330	CONODOGUINET CREEK NEAR HOGESTOWN, PA	449	4.727E+06	5.000E+06	-5%
SL9_2490_2520	SUSQUEHANNA RIVER AT MARIETTA, PA	25863	1.282E+08	1.270E+08	1%

SL9_2720_0001	SUSQUEHANNA RIVER AT CONOWINGO, MD	27086	1.337E+08	1.407E+08	-5%
SU3_0370_0490	COHOCTON RIVER NEAR CAMPBELL NY	467	1.581E+06	1.685E+06	-6%
SU3_0710_0910	TUNKHANNOCK CREEK NEAR TUNKHANNOCK, PA	391	1.028E+06	1.055E+06	-3%
SU4_0300_0310	UNADILLA RIVER AT ROCKDALE NY	562	2.286E+06	2.299E+06	-1%
SU5_0610_0600	CHEMUNG RIVER AT CHEMUNG NY	2506	8.175E+06	7.140E+06	14%
SU6_0480_0520	SUSQUEHANNA RIVER AT CONKLIN NY	2234	7.851E+06	7.845E+06	0%
SU7_0720_0003	SUSQUEHANNA RIVER NEAR WAVERLY NY	4924	1.999E+07	1.949E+07	3%
SU7_0850_0730	SUSQUEHANNA RIVER AT TOWANDA, PA	7783	2.672E+07	2.752E+07	-3%
SU7_1120_1140	SUSQUEHANNA RIVER AT WILKES-BARRE, PA	9995	3.697E+07	3.667E+07	1%
SU8_1610_1530	SUSQUEHANNA RIVER AT DANVILLE, PA	11225	4.412E+07	4.228E+07	4%
SW5_1350_0003	PINE CREEK BL L PINE CREEK NEAR WATERVILLE, PA	938	1.790E+06	1.429E+06	25%
SW5_1540_0003	WB SUSQUEHANNA RIVER AT KARTHAUS, PA	1387	4.093E+06	2.975E+06	38%
SW7_1640_0003	WEST BRANCH SUSQUEHANNA RIVER AT LEWISBURG, PA	6823	2.261E+07	2.251E+07	0%
WM1_3660_3910	GWYNNS FALLS AT VILLA NOVA, MD	33	2.036E+05	1.599E+05	27%
WU2_3020_3320	GUNPOWDER FALLS AT GLENCOE, MD	159	7.990E+05	1.066E+06	-25%
XL1_4690_0001	WESTERN BRANCH AT UPPER MARLBORO MD	93	2.151E+05	2.150E+05	0%
XU0_4130_4070	PATUXENT RIVER NEAR UNITY, MD	35	2.193E+05	2.237E+05	-2%
XU3_4650_0001	PATUXENT RIVER NEAR BOWIE, MD	349	1.634E+06	1.569E+06	4%
YM2_6120_6430	MATTAPONI RIVER NEAR BOWLING GREEN, VA	256	2.579E+05	2.422E+05	6%
YM4_6620_0003	MATTAPONI R	593	6.525E+05	6.109E+05	7%
YP1_6570_6680	LITTLE RIVER NEAR DOSWELL, VA	107	1.034E+05	1.104E+05	-6%
YP3_6330_6700	NORTH ANNA RIVER AT HART CORNER NEAR DOSWELL, VA	463	4.457E+05	3.894E+05	14%
YP4_6720_6750	PAMUNKEY RIVER NEAR HANOVER, VA	1098	1.437E+06	1.394E+06	3%

Table 10-36: Average annual phosphorus loads from Watershed Model and USGS-WRTDS. Difference between the two has been tabulated as percent bias. Positive bias indicates an over simulation of loads as compared to WRTDS.

RIVER SEG	RIVER NAME	AREA (sq miles)	SIMULATED (lb/yr)	WRTDS (lb/yr)	Bias (%)
EL0_4562_0003	NANTICOKE R	72	2.947E+04	2.368E+04	24%
EL2_4400_4590	MARSHYHOPE CREEK NEAR ADAMSVILLE, DE	47	2.369E+04	2.249E+04	5%
EM2_3980_0001	CHOPTANK RIVER NEAR GREENSBORO, MD	117	3.201E+04	3.256E+04	-2%
EU1_2650_0001	BIG ELK CREEK AT ELK MILLS, MD	53	4.075E+04	3.945E+04	3%
JA5_7480_0001	APPOMATTOX RIVER AT MATOACA, VA	1340	1.299E+05	1.319E+05	-2%
JB3_6820_7053	CHICKAHOMINY RIVER NEAR PROVIDENCE FORGE, VA	246	4.485E+04	3.839E+04	17%
JL7_6800_7070	JAMES RIVER AND KANAWHA CANAL NEAR RICHMOND, VA	6750	1.551E+06	2.040E+06	-24%
JL7_7100_7030	JAMES RIVER AT CARTERSVILLE, VA	6251	2.397E+06	2.514E+06	-5%
PL0_4510_0001	NW BRANCH ANACOSTIA RIVER NEAR HYATTSVILLE, MD	52	2.417E+04	2.346E+04	3%
PM1_3510_4000	CATOCTIN CREEK NEAR MIDDLETOWN, MD	67	2.176E+04	2.338E+04	-7%
PM2_2860_3040	MONOCACY RIVER AT BRIDGEPORT, MD	173	1.268E+05	9.612E+04	32%
PM7_4820_0001	POTOMAC RIVER NEAR WASH, DC	11569	3.986E+06	3.946E+06	1%

PS3_5100_5080	N F SHENANDOAH RIVER NEAR STRASBURG, VA	772	2.380E+05	2.581E+05	-8%
PS5_5240_5200	S F SHENANDOAH RIVER AT FRONT ROYAL, VA	1635	6.678E+05	5.352E+05	25%
PU0_3000_3090	ANTIETAM CR E BR	93	4.859E+04	3.539E+04	37%
PU1_3030_3440	TONOLOWAY CR	114	1.640E+04	9.555E+03	72%
PU1_3100_3690	SIDELING HILL CREEK NEAR BELLEGROVE, MD	104	1.072E+04	8.697E+03	23%
PU1_3940_3970	GEORGES CR	75	1.105E+04	1.263E+04	-13%
PU2_3090_4050	ANTIETAM CREEK NEAR SHARPSBURG, MD	280	1.069E+05	9.054E+04	18%
PU2_3370_4020	TOWN CR	157	1.256E+04	1.050E+04	20%
PU2_4220_3900	OPEQUON CREEK NEAR MARTINSBURG, WV	277	1.259E+05	8.736E+04	44%
PU2_4360_4160	PATTERSON CREEK NEAR HEADSVILLE, WV	218	1.094E+04	2.156E+04	-49%
PU3_3290_3390	CONOCOCHEAGUE CREEK AT FAIRVIEW, MD	502	2.226E+05	2.191E+05	2%
PU3_3680_3890	WILLS CREEK NEAR CUMBERLAND, MD	253	4.596E+04	4.174E+04	10%
PU3_3860_3610	CACAPON RIVER NEAR GREAT CACAPON, WV	681	8.181E+04	7.945E+04	3%
PU4_4310_4210	SOUTH BRANCH POTOMAC RIVER NEAR SPRINGFIELD, WV	1462	2.181E+05	2.001E+05	9%
RU3_6170_6040	RAPIDAN RIVER NEAR CULPEPER, VA	467	3.514E+05	3.632E+05	-3%
RU5_6030_0001	RAPPAHANNOCK RIVER NEAR FREDERICKSBURG, VA	1596	6.314E+05	6.549E+05	-4%
SJ4_2660_2360	RAYSTOWN BRANCH JUNIATA RIVER AT SAXTON, PA	750	1.378E+05	1.254E+05	10%
SJ6_2130_0003	JUNIATA RIVER AT NEWPORT, PA	3351	1.107E+06	7.784E+05	42%
SL2_2410_2700	PEQUEA CR	155	2.329E+05	2.148E+05	8%
SL2_3060_0001	DEER CR	171	7.117E+04	6.723E+04	6%
SL3_1710_1740	PENNS CREEK AT PENNS CREEK, PA	306	5.069E+04	7.475E+04	-32%
SL3_2290_2260	SHERMAN CREEK AT SHERMANS DALE, PA	207	5.682E+04	6.223E+04	-9%
SL3_2400_2440	YELLOW BREECHES CREEK NEAR CAMP HILL, PA	215	6.304E+04	5.745E+04	10%
SL3_2420_2700	CONESTOGA RIVER AT CONESTOGA, PA	475	5.922E+05	5.517E+05	7%
SL3_2460_2430	WEST CONEWAGO CREEK NEAR MANCHESTER, PA	516	3.129E+05	3.707E+05	-16%
SL4_2140_2240	SWATARA CREEK NEAR HERSHEY, PA	482	3.399E+05	3.174E+05	7%
SL4_2370_2330	CONODOGUINET CREEK NEAR HOGESTOWN, PA	449	1.400E+05	8.990E+04	56%
SL9_2490_2520	SUSQUEHANNA RIVER AT MARIETTA, PA	25863	8.667E+06	8.315E+06	4%
SL9_2720_0001	SUSQUEHANNA RIVER AT CONOWINGO, MD	27086	6.349E+06	6.227E+06	2%
SU3_0370_0490	COHOCTON RIVER NEAR CAMPBELL NY	467	8.910E+04	9.601E+04	-7%
SU3_0710_0910	TUNKHANNOCK CREEK NEAR TUNKHANNOCK, PA	391	9.654E+04	1.033E+05	-7%
SU4_0300_0310	UNADILLA RIVER AT ROCKDALE NY	562	2.129E+05	2.072E+05	3%
SU5_0610_0600	CHEMUNG RIVER AT CHEMUNG NY	2506	6.340E+05	8.390E+05	-24%
SU6_0480_0520	SUSQUEHANNA RIVER AT CONKLIN NY	2234	1.079E+06	1.021E+06	6%
SU7_0720_0003	SUSQUEHANNA RIVER NEAR WAVERLY NY	4924	2.091E+06	2.226E+06	-6%
SU7_0850_0730	SUSQUEHANNA RIVER AT TOWANDA, PA	7783	2.283E+06	2.408E+06	-5%
SU7_1120_1140	SUSQUEHANNA RIVER AT WILKES-BARRE, PA	9995	4.987E+06	4.896E+06	2%
SU8_1610_1530	SUSQUEHANNA RIVER AT DANVILLE, PA	11225	4.284E+06	3.982E+06	8%
SW5_1350_0003	PINE CREEK BL L PINE CREEK NEAR WATERVILLE, PA	938	1.264E+05	9.388E+04	35%
SW5_1540_0003	WB SUSQUEHANNA RIVER AT KARTHAUS, PA	1387	1.774E+05	1.450E+05	22%
SW7_1640_0003	WEST BRANCH SUSQUEHANNA RIVER AT LEWISBURG, PA	6823	1.335E+06	1.331E+06	0%
WM1_3660_3910	GWYNNS FALLS AT VILLA NOVA, MD	33	1.083E+04	9.433E+03	15%

WU2_3020_3320	GUNPOWDER FALLS AT GLENCOE, MD	159	4.292E+04	2.435E+04	76%
XL1_4690_0001	WESTERN BRANCH AT UPPER MARLBORO MD	93	4.998E+04	5.137E+04	-3%
XU0_4130_4070	PATUXENT RIVER NEAR UNITY, MD	35	1.155E+04	1.043E+04	11%
XU3_4650_0001	PATUXENT RIVER NEAR BOWIE, MD	349	1.256E+05	1.225E+05	3%
YM4_6620_0003	MATTAPONI R	593	5.765E+04	5.676E+04	2%
YP3_6330_6700	NORTH ANNA RIVER AT HART CORNER NEAR DOSWELL, VA	463	3.420E+04	3.336E+04	3%
YP4_6720_6750	PAMUNKEY RIVER NEAR HANOVER, VA	1098	1.599E+05	1.599E+05	0%

10.6.4.4 Annual Loads at RIM and WRTDS Sites

The quality of agreement between the WRTDS and the simulated annual loads for the nine river input monitoring (RIM) stations as well as several monitoring stations with WRTDS data was evaluated in terms of correlation and Nash-Sutcliffe efficiency statistics. The correlation coefficient was used as an indicator of temporal consistency in annual loads between different models, where a value of 1 for the correlation coefficient indicates a perfect positive fit. Similarly, a value of 1 for NSE indicates perfect agreement between two datasets. *Figure **10-69***, *Figure **10-70***, and *Figure **10-71*** show correlation coefficients for the RIM stations for nitrogen, phosphorus and sediment. It is not surprising that the correlations are high given that the flow, which is a dominant driver of the transport processes, is well calibrated in the model as shown earlier in *Figure **10-58***, *Figure **10-59***, and *Figure **10-60***. Even though phosphorus and sediment are relatively difficult to calibrate due to considerable variability in annual loads as compared to nitrogen, the correlations are equally comparable to nitrogen indicating a good model performance for nitrogen, phosphorus and sediment.

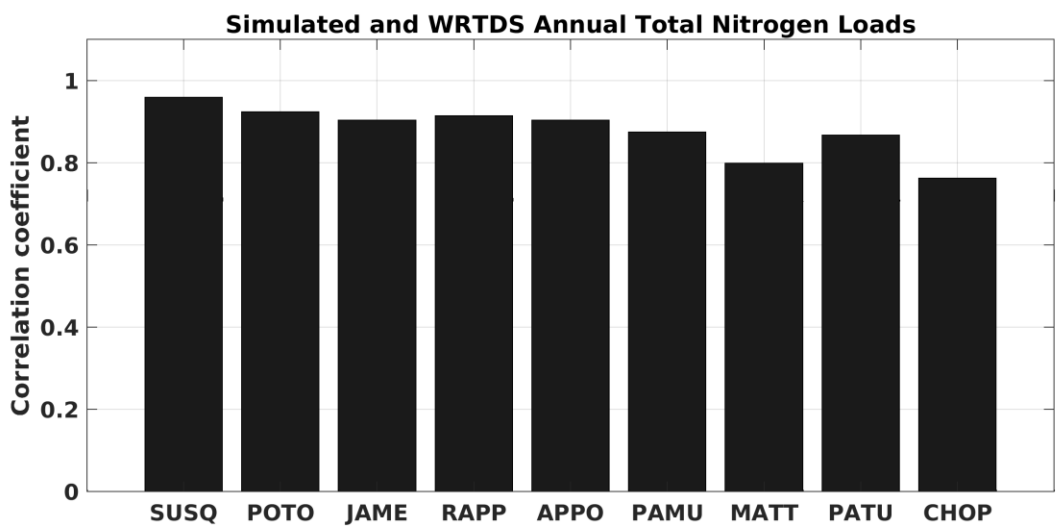

Figure 10-69. The correlation coefficients showing the degree of agreement between the simulated and WRTDS annual nitrogen loads for the 9 RIM sites. A correlation coefficient of 1 indicates a perfect match for every year.

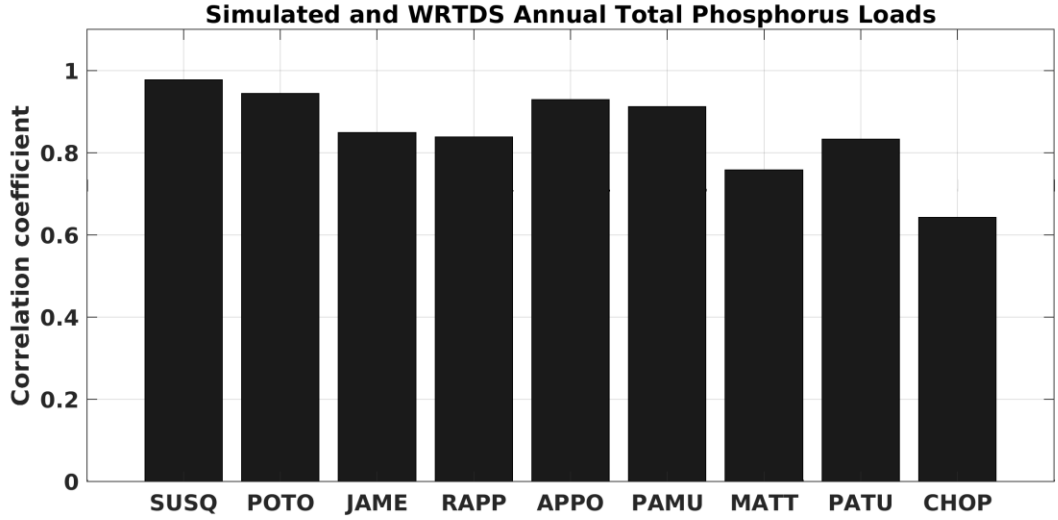

Figure 10-70. The correlation coefficients showing the degree of agreement between the simulated and WRTDS annual phosphorus loads for the 9 RIM sites. A correlation coefficient of 1 indicates a perfect match for every year.

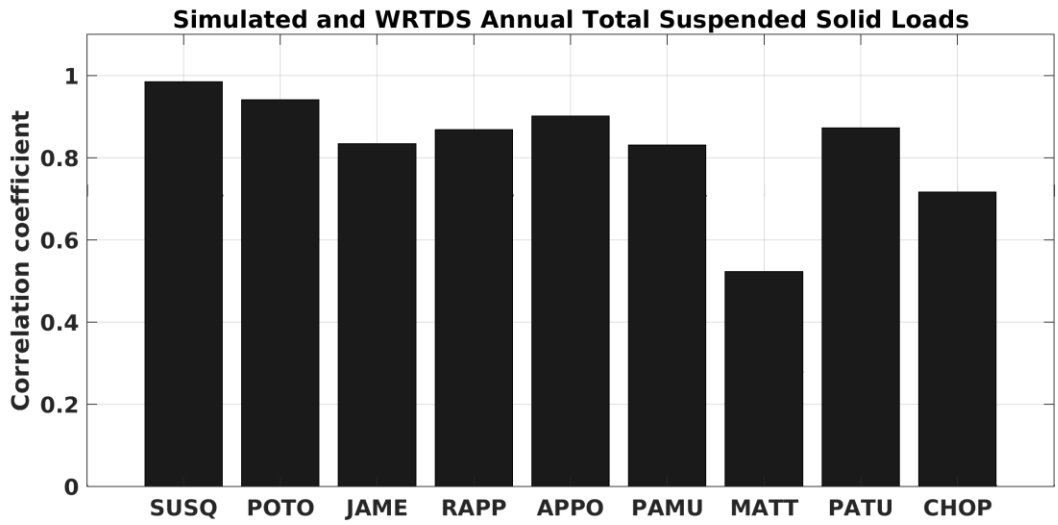

Figure 10-71. The correlation coefficients showing the degree of agreement between the simulated and WRTDS annual suspended solid loads for the 9 RIM sites. A correlation coefficient of 1 indicates a perfect match for every year.

Nash-Sutcliffe Efficiencies of the n*itrogen, phosphorus, and sediment annual loads are shown in* ***Figure 10-72****, Figure* ***10-73****, and Figure* ***10-74*** respectively. It is another metric for assessing the model performance for the annual delivery of nutrients for the RIM sites.

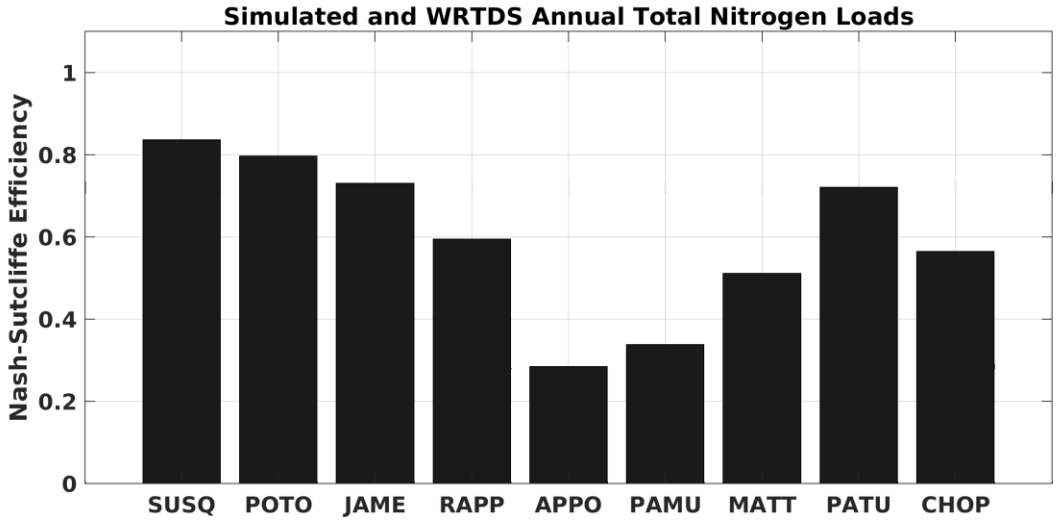

Figure 10-72: Nash-Sutcliffe Efficiencies (NSEs) for annual nitrogen loads. NSEs show the degree of agreement between simulated and USGS-WRTDS annual nitrogen loads for the nine long-term river input monitoring (RIM) sites.

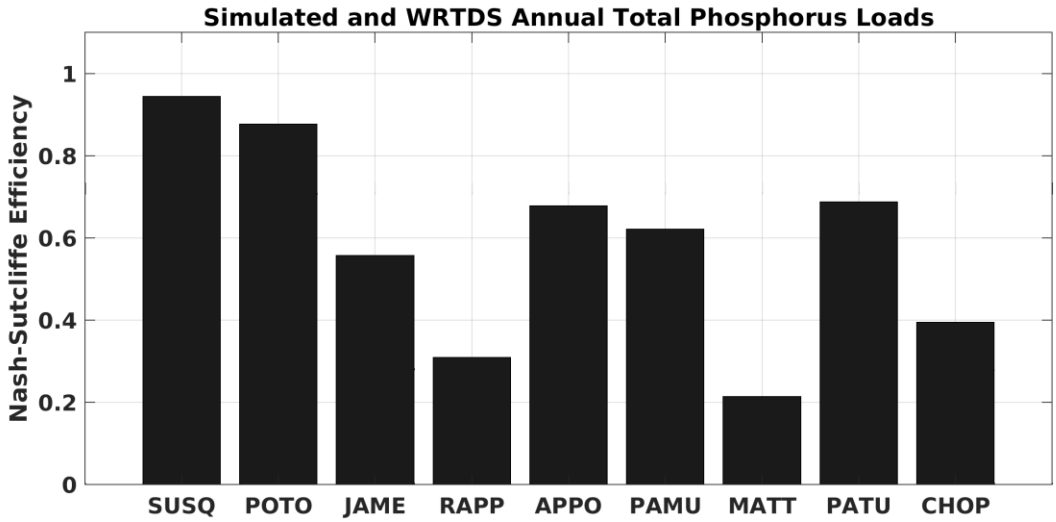

Figure 10-73: Nash-Sutcliffe Efficiencies (NSEs) for annual phosphorus loads. NSEs show the degree of agreement between simulated and USGS-WRTDS annual phosphorus loads for the 9 long-term river input monitoring (RIM) sites.

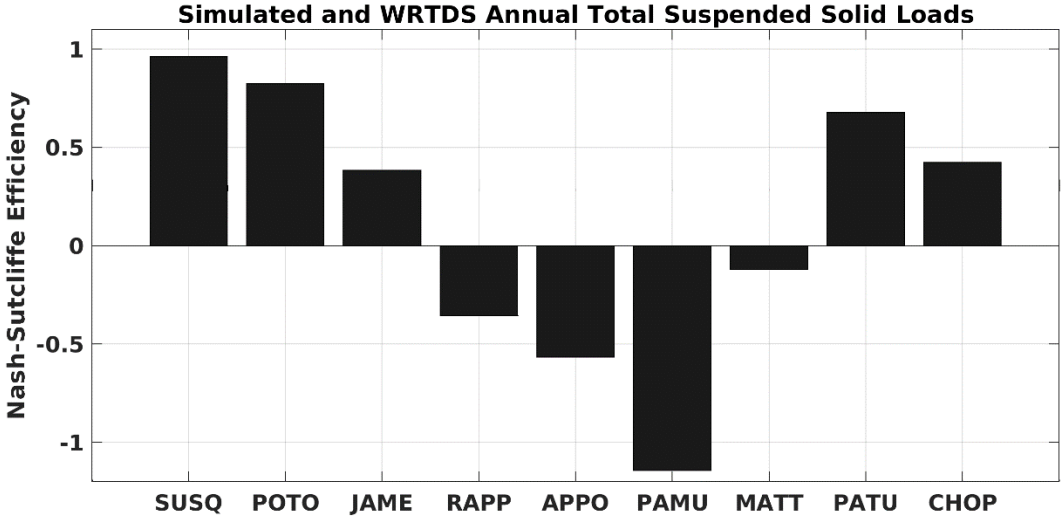

Figure 10-74: Nash-Sutcliffe Efficiencies (NSEs) for annual suspended solid loads. NSEs show the degree of agreement between simulated and USGS-WRTDS annual suspended loads for the 9 long-term river input monitoring (RIM) sites.

The agreement between simulated and WRTDS annual loads were assessed for all monitoring sites with WRTDS data across the watershed. The distribution of correlation coefficients and Nash-Sutcliffe efficiencies for nitrogen, phosphorus, and sediment have been shown in the Figure 10-75 and Figure 10-76.

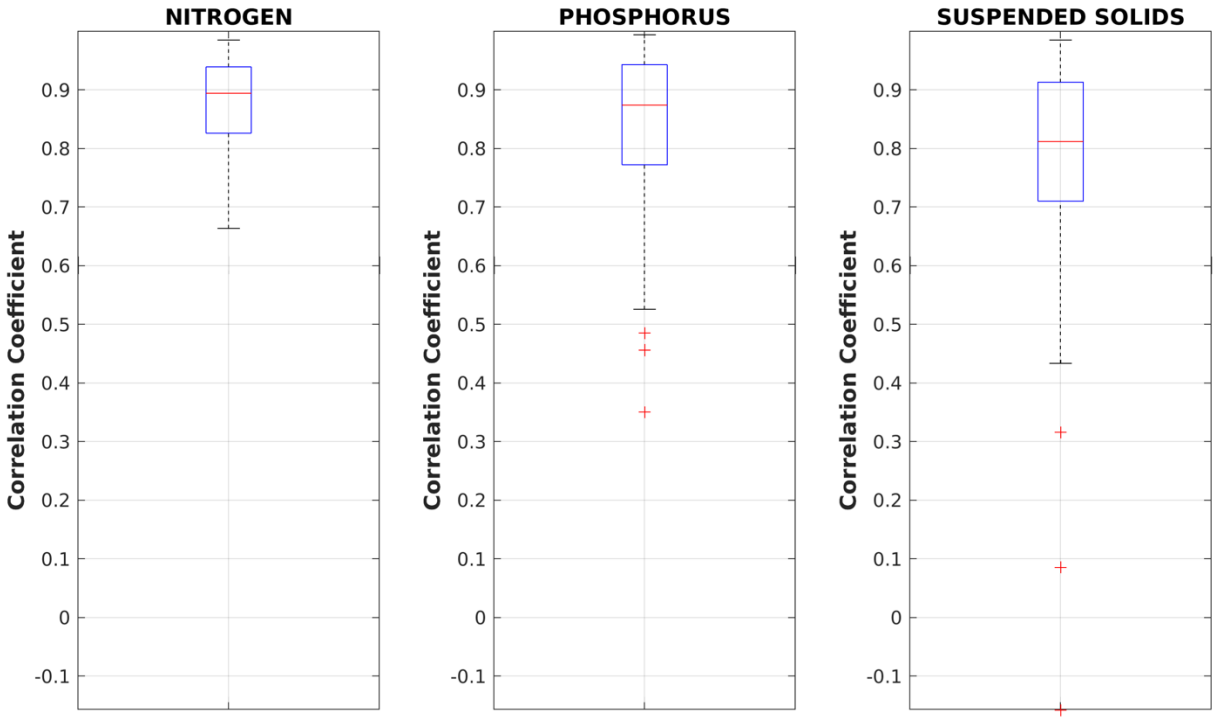

Figure 10-75: Agreement between the simulated and USGS-WRTDS annual nitrogen, phosphorus, and sediment loads. The distribution includes 72, 58 and 57 monitoring sites for nitrogen, phosphorus and sediment respectively. *A correlation coefficient of 1 for a monitoring site indicates a perfect match in loads for every year.*

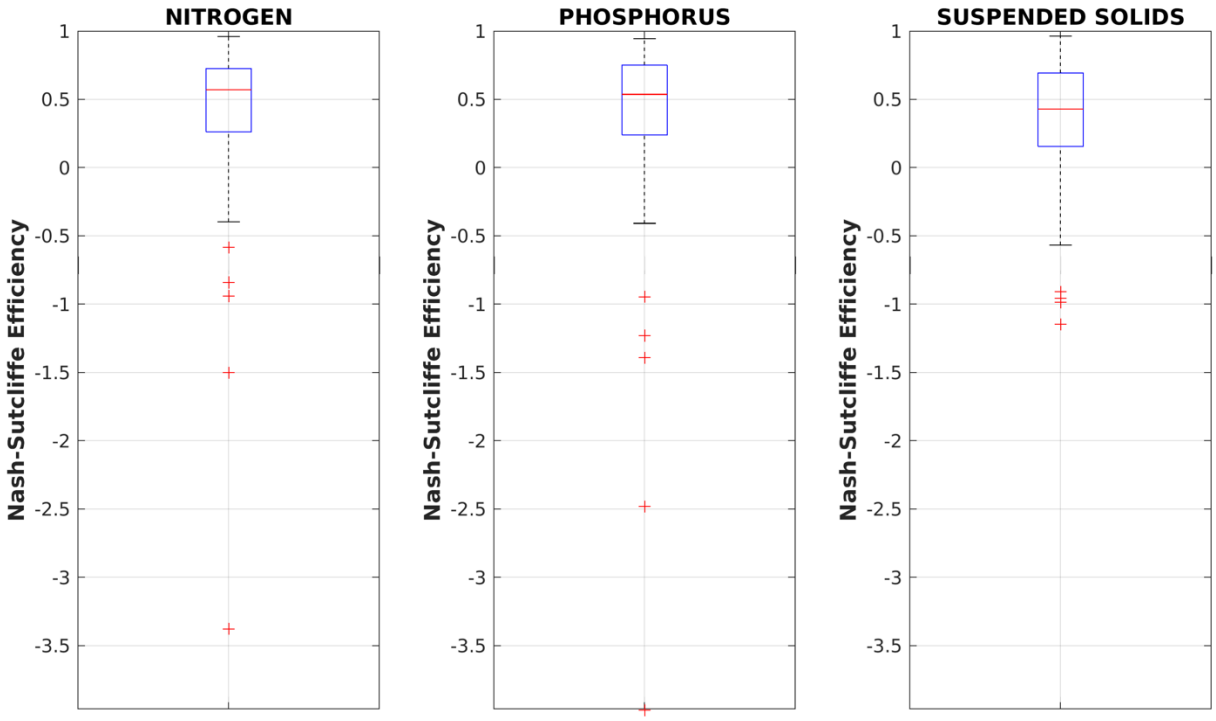

Figure 10-76: Nash-Sutcliffe Efficiencies (NSEs) showing the agreement between simulated and USGS-WRTDS annual nitrogen, phosphorus, and sediment loads. The distribution includes 72, 58 and 57 monitoring sites for nitrogen, phosphorus and sediment respectively. *NSE of 1 for a monitoring site indicates a perfect match in loads for every year.*

10.6.4.5 Monthly Loads at the RIM and WRTDS Sites

The comparison of simulated monthly and USGS-WRTDS loads to evaluate degree of agreement and model performance. The quality of agreement between the WRTDS and the simulated monthly loads for the nine river input monitoring (RIM) stations as well as several monitoring stations with WRTDS data was evaluated in terms of correlation and Nash-Sutcliffe efficiency statistics. The correlation coefficient was used as an indicator of temporal consistency in annual loads between different models, where a value of 1 for the correlation coefficient indicates a perfect positive fit. Similarly, a value of 1 for NSE indicates perfect agreement between two datasets. Figure **10-77**, Figure **10-78**, and Figure **10-79** show correlation coefficients for the RIM stations for nitrogen, phosphorus and sediment respectively.

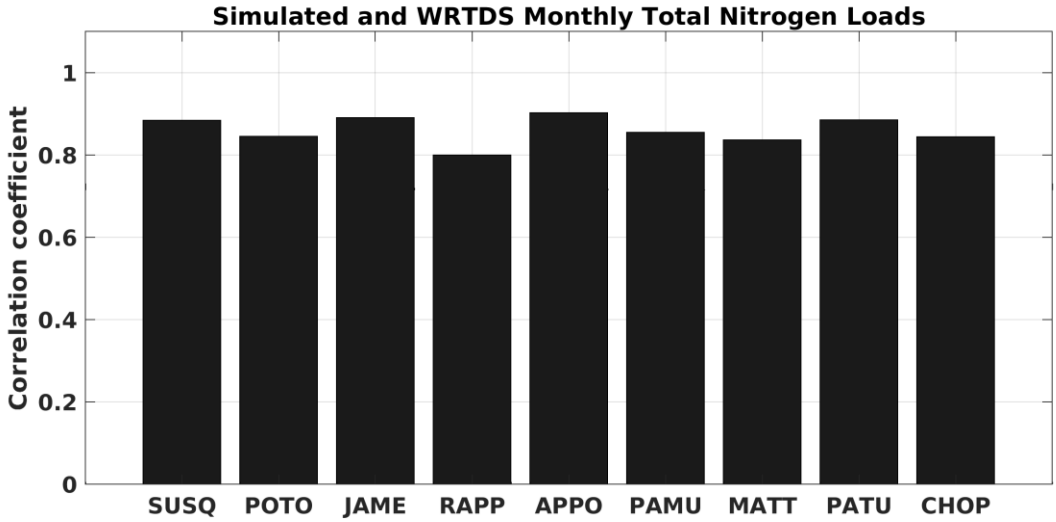

Figure 10-77: *The correlation coefficients showing the degree of agreement between the simulated and WRTDS monthly nitrogen loads for the 9 RIM sites. High correlation coefficients show good agreement in nitrogen loads for the RIM stations. A correlation coefficient of 1 indicates a perfect match for every year.*

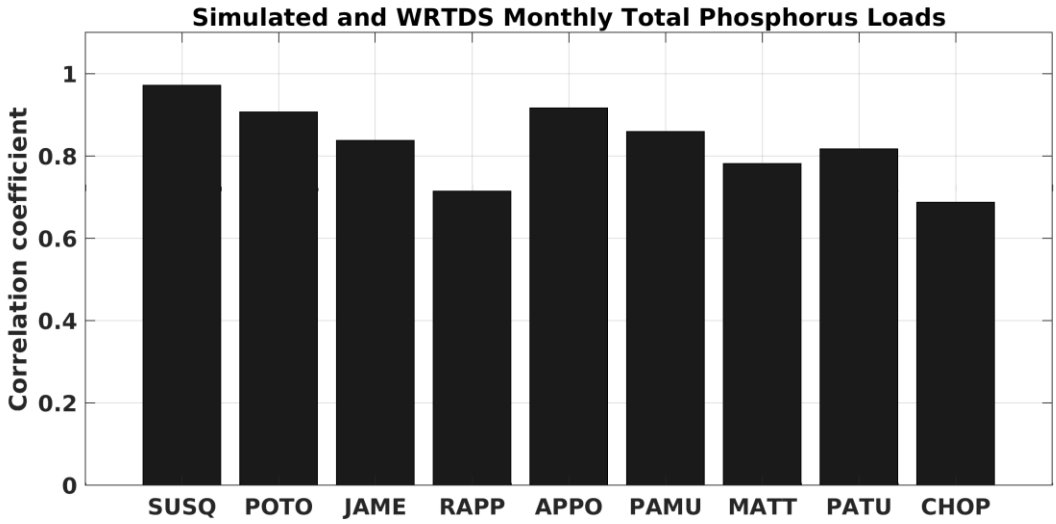

Figure 10-78: *The correlation coefficients showing the degree of agreement between the simulated and WRTDS monthly phosphorus loads for the 9 RIM sites. High correlation coefficients show good agreement in phosphorus loads for the RIM stations. A correlation coefficient of 1 indicates a perfect match for every year.*

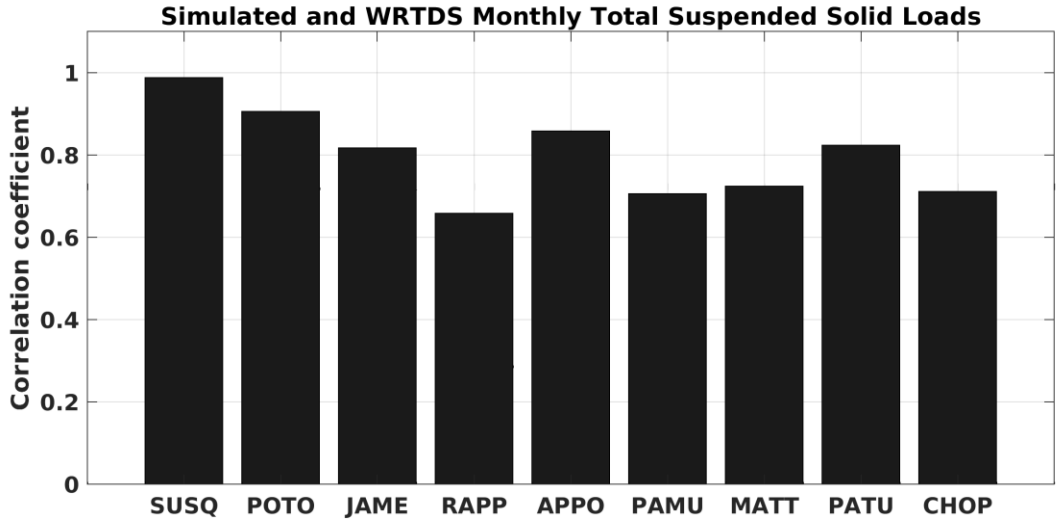

Figure 10-79: *The correlation coefficients showing the degree of agreement between the simulated and WRTDS monthly sediment loads for the 9 RIM sites. High correlation coefficients show good agreement in sediment loads for the RIM stations. A correlation coefficient of 1 indicates a perfect match for every year.*

Nash-Sutcliffe Efficiencies of the nitrogen, phosphorus, and sediment monthly loads are shown in Figure 10-80, Figure 10-81, Figure 10-82 respectively. It is another metric for assessing the model performance for the simulated monthly nutrients and sediment loads for the RIM sites.

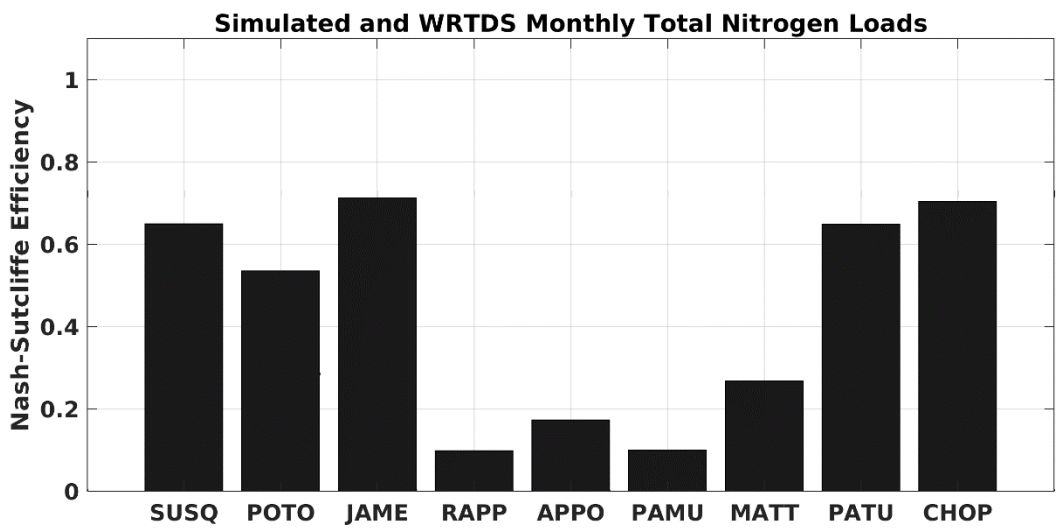

Figure 10-80: *Nash-Sutcliffe Efficiencies (NSEs) for monthly nitrogen loads. NSEs quantify the degree of agreement between simulated and USGS-WRTDS monthly nitrogen loads for the 9-long-term river input monitoring (RIM) sites.*

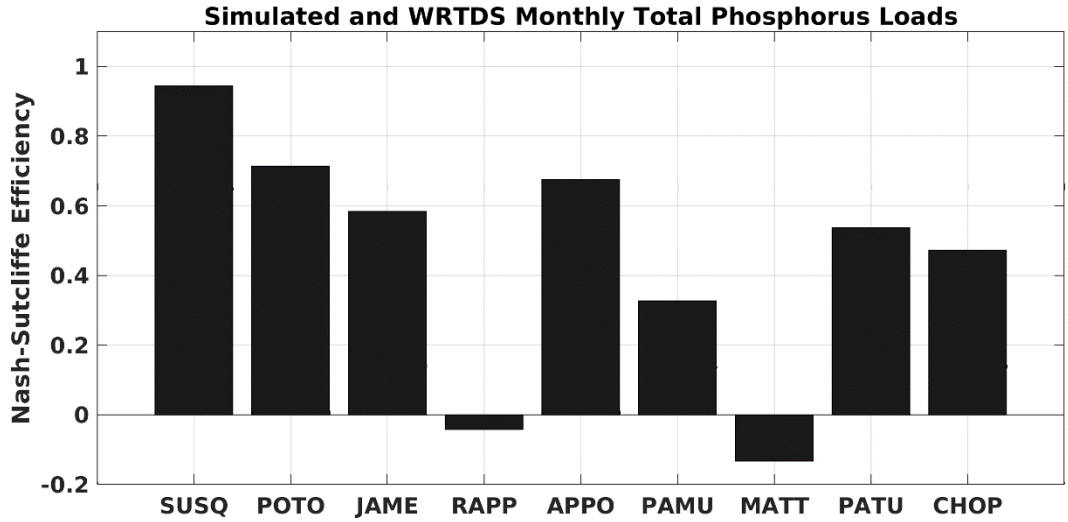

Figure 10-81: *Nash-Sutcliffe Efficiencies (NSEs) for monthly phosphorus loads. NSEs quantify the degree of agreement between simulated and USGS-WRTDS monthly phosphorus loads for the 9-long-term river input monitoring (RIM) sites.*

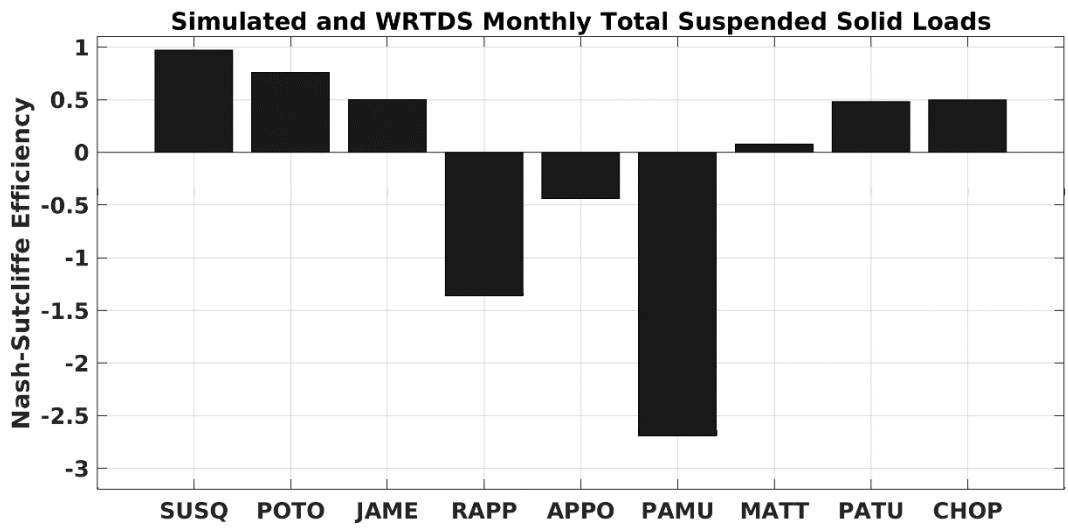

Figure 10-82: *Nash-Sutcliffe Efficiencies (NSEs) for monthly sediment loads. NSEs quantify the degree of agreement between simulated and USGS-WRTDS monthly sediment loads for the 9-long-term river input monitoring (RIM) sites.*

The agreement between simulated and WRTDS monthly loads were assessed for all monitoring sites across the watershed with WRTDS data. The distribution of correlation coefficients and Nash-Sutcliffe efficiencies for nitrogen, phosphorus, and sediment have been shown in the Figure 10-83 and Figure 10-84.

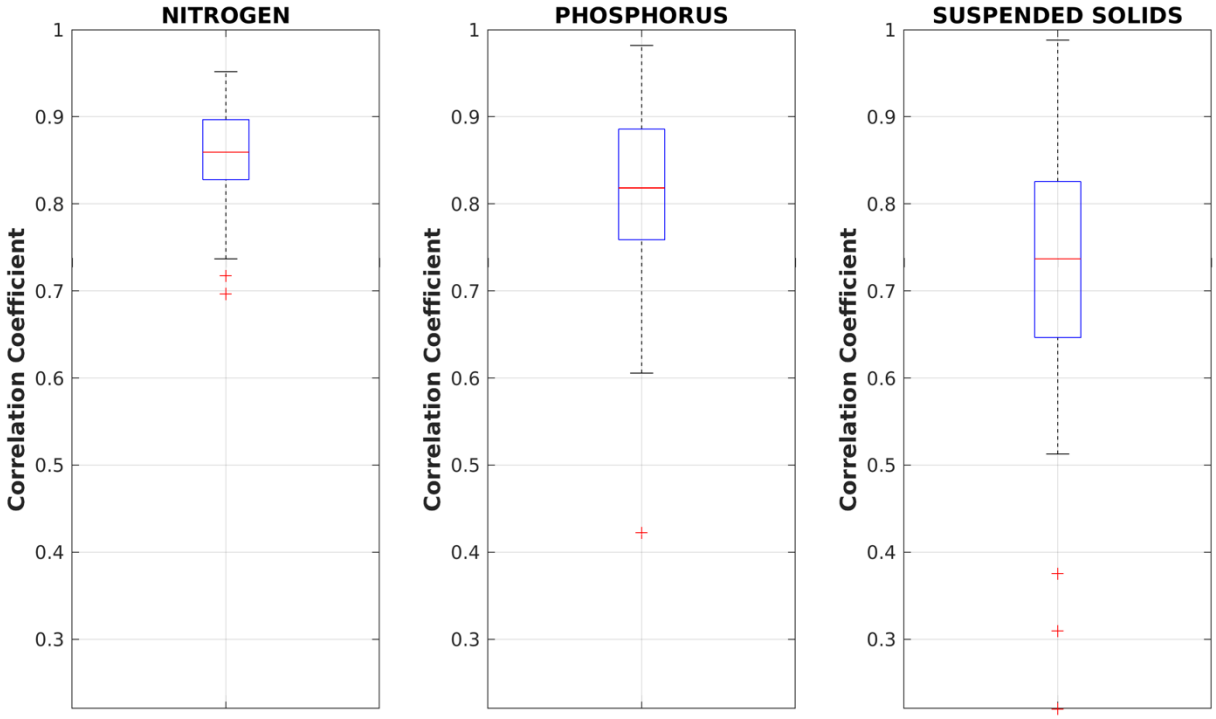

Figure 10-83: Agreement between the simulated and USGS-WRTDS monthly nitrogen, phosphorus, and sediment loads. The distribution includes 72, 58 and 57 monitoring sites for nitrogen, phosphorus and sediment respectively. *A correlation coefficient of 1 for a monitoring site indicates a perfect match in loads for every month.*

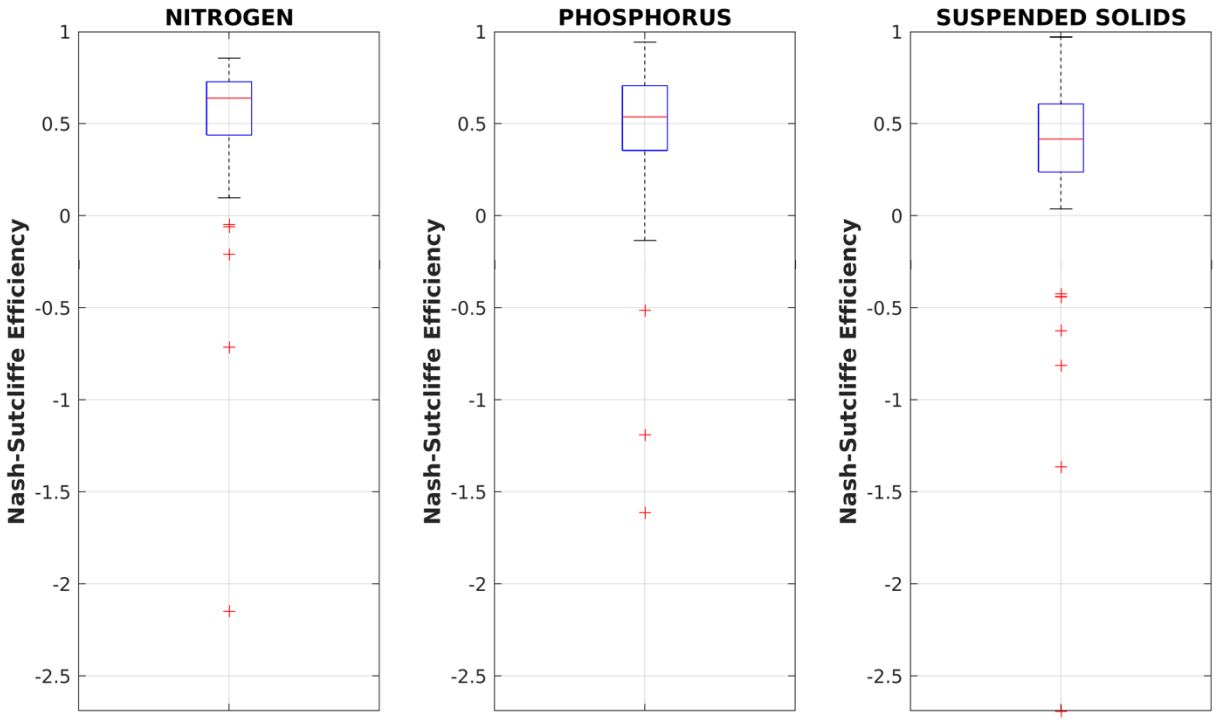

Figure 10-84: Nash-Sutcliffe Efficiencies (NSEs) showing the agreement between simulated and USGS-WRTDS monthly nitrogen, phosphorus, and sediment loads. The distribution includes 72, 58 and 57 monitoring sites for nitrogen, phosphorus and sediment respectively. *NSE of 1 for a monitoring site indicates a perfect match in loads for every month.*

10.6.4.6 Geographic Efficiencies

One of the purposes of the watershed model, in terms of its use in aiding the decision-making process and effective implementations of management practices, is to simulate the spatial or geographic variability in nutrient and sediment response. Therefore, an evaluation of model performance on that specific aspect is warranted. In the previous sub-sections, the model performance was evaluated in terms of agreement between the simulated and WRTDS nutrients and sediment loads. However, the loads are a function of the watershed size and it is likely to be higher for larger watersheds. So, the model performance can be evaluated in terms load per unit area (pounds per acres) for the watersheds, which would sufficiently describe the differences in nutrient and sediment responses.

Model performance was evaluated for its ability to simulate spatial or geographic differences in nutrients and sediment responses by comparing the per acre load. The comparison was made for all monitoring sites where WRTDS loads were available. The per acre load for a watershed was calculated as the ratio of average annual load and the drainage area of basin. The Nash-Sutcliffe Efficiency (NSE) was calculated to quantify the predictive capability of the model in simulating the spatial variability in the nutrient and sediment responses. Figure 10-85 shows the nitrate, nitrogen, phosphorus and sediment water quality responses comparing the simulated and WRTDS per acre loads (as pounds per acre). The NSEs for the water quality constituents are referred as geographic efficiencies, where higher (close to 1) values of NSEs indicate model was successful in reproducing geographic variability in the water quality response.

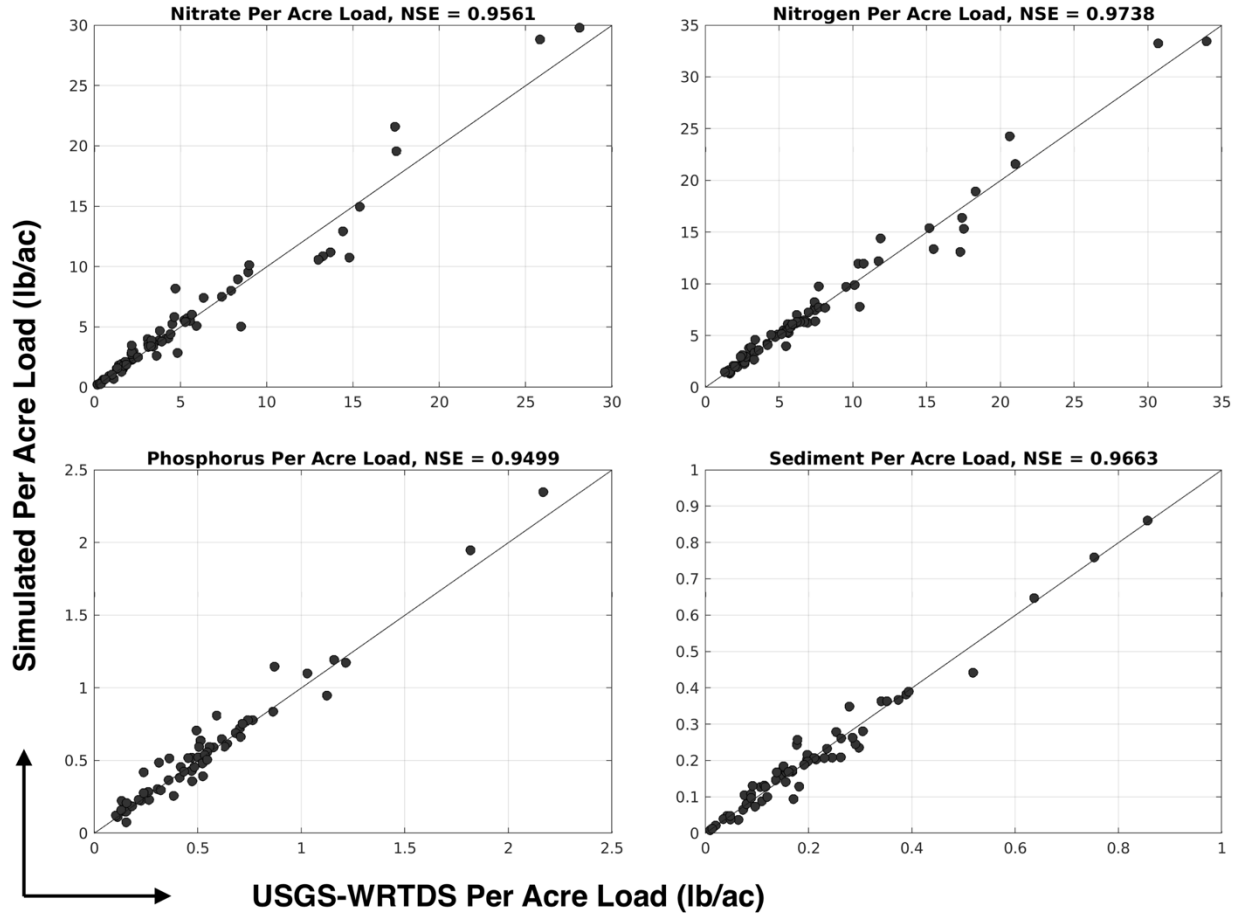

Figure 10-85: Geographic efficiencies for nitrate, nitrogen, phosphorus, and sediment. Geographic efficiencies

10.7 Simulation of the Lower Susquehanna Reservoirs

10.7.1 Introduction to the system

The Susquehanna River is the largest tributary to the Chesapeake Bay. Its 27,500-square mile watershed drainage area includes south-central New York, central and eastern Pennsylvania, and northeastern Maryland. The Susquehanna River contributes approximately 41 percent of the nitrogen, 25 percent of the phosphorus, and 27 percent of the suspended sediment (SS) to the tidal Bay (Linker et al. 2016b).

Three hydropower plants were built between 1910 and 1931 to take advantage of the river power of the lower 39 miles and have been in continuous operation since. The uppermost pool, Lake Clarke, ends at the Safe Harbor Dam. Lake Aldred ends at the Holtwood Dam. The most downstream impoundment, the Conowingo Pool, ends at the Conowingo Dam (*Figure **10-86***).

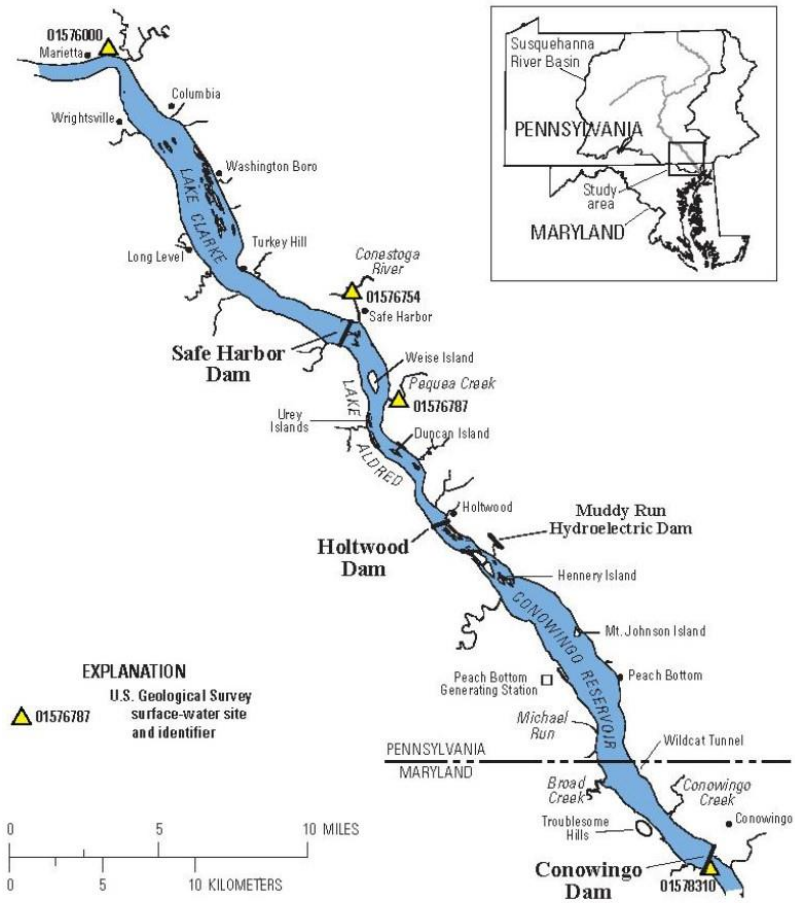

Figure 10-86: The Lower Susquehanna River Reservoir System (From Langland 2015)

Much recent work has focused on the Lower Susquehanna reservoir system and how, over time, sedimentation has filled in the three reservoirs, altering their behavior. Hirsch (2012) found that scouring of sediment may be increasing over time in the Conowingo based on an analysis of monitoring below the Conowingo. Langland (2015) used monitoring and bathymetric data to show that sedimentation had altered all three reservoirs. The upper two reservoir pools, Lake Clarke and Lake Aldred, reached capacity prior to the beginning of the Phase 6 simulation period (1985 to 2014) and are considered to be in dynamic steady-state, meaning that the long-term mass of sediment into and out of the reservoirs is in balance, but would not be in balance over shorter time periods. Recent research has indicated that the most downstream reservoir, the Conowingo, is at or approaching a dynamic steady-state as well. In May 2015, the US Army Corps of Engineers and Maryland Department of the Environment published the Lower Susquehanna River Watershed Assessment LSRWA (USACOE and MDE, 2015). The LSRWA found through modeling and monitoring analysis that the reservoir system had changed its trapping behavior in recent decades but did not fully quantify the change. The Chesapeake Bay Program's Scientific and Technical Advisory Committee (STAC) held a workshop on the Conowingo reservoir January 13th and 14th, 2016 (Linker et al. 2016a). Generally speaking, the Conowingo had been trapping about half the phosphorus and 10 percent of the nitrogen during the mid-1990s but is now (mid-2010s) essentially not trapping additional materials over the long-term (Zhang et al., 2013; 2016a; and 2016b; and Zhang, 2016).

Gross and others (1978) compared concentrations and flows at Harrisburg and Conowingo monitoring sites and generally found that the reservoir system was trapping a little more than half of the sediment in most years, however tropical storms Agnes (June 1972) and Eloise (September 1975) were scour events that produced much more sediment from scour in the reservoirs than was received by the reservoirs. The estimated peak concentration of suspended sediment for Agnes was 10,000 mg/l and for Eloise was 2,800 mg/l. Including Eloise as a 30-year event, but leaving out the 200-year event Agnes, it can be calculated from Table 1 in Gross and others (1978) that the reservoir inputs and outputs were roughly equal during the decade of 1966-1976.

10.7.2 Information Needed to Simulate the Lower Susquehanna System

In order to effectively calibrate the Phase 6 Watershed Model and to prepare the model to answer management questions four questions were identified as described in the subsections below. On February 14th, 2017, the Modeling Workgroup reached consensus on the first three questions and the final one on April 4th, 2017.

10.7.2.1 Question 1: What Is the Current State of the Conowingo and the Two Upper Reservoirs With Regard To Long-Term Mass Balance?

Based on an abundance of evidence, all three reservoirs in the Lower Susquehanna reservoir system are currently in dynamic equilibrium (Hainly et al., 1995; Hirsch, 2012; Langland 2009, 2015; Zhang et al., 2013, 2015, 2016). The concept of dynamic equilibrium is that there is no long-term trapping of sediment or nutrient occurring within the reservoir. In other words, inputs are roughly equal to outputs over a sufficiently long period of years although in any given year, the reservoir pools can act as a source or a sink with periods of scour and deposition. This conclusion is supported by multiple analyses using statistical analysis of monitoring data, process-based models, and bathymetric studies. There is general agreement among all of these analyses that the reservoirs have reached capacity, however, consistent with the concept of dynamic equilibrium, there is disagreement about precisely when it occurred.

Hainly and others (1995) estimate that the upper two reservoirs have been in dynamic equilibrium for more than half a century. Langland (2009 and 2015) shows through bathymetric surveys that the storage capacity of the Conowingo has been decreasing since its construction. Langland (2015) estimated that less than 10 percent of the capacity remained as of 2011.

Hirsch (2012) calculated dramatic increases in sediment and phosphorus loads using analyses of monitoring data, particularly in high flows indicating increased scour and lower deposition. Zhang has published extensively using similar methods applied to upstream and downstream stations (Zhang et al., 2013; 2015; 2016a; 2016b; 2016; and Zhang, 2016) to show that the lower Susquehanna Reservoir system reached dynamic equilibrium within the past decade.

The Lower Susquehanna River Watershed Assessment (U.S. Army Corps of Engineers and MDE, 2015), found that the Conowingo was in dynamic equilibrium at the time of publication through a consideration of literature and through modeling undertaken for the effort.

HDR modeling presented at the CBP modeling workgroup suggests that the Conowingo has been in equilibrium since the mid-1990s.

10.7.2.2 Question 2: What Information Can Be Used to Estimate the Change In Scour and Deposition Over Time for the Purposes Of Calibration?

Multiple studies have shown that the relationship between flow and concentration is changing over time downstream of the Conowingo reservoir. This has been attributed to changes in scour and deposition related to changes in the bathymetric state of the reservoirs. Linker and others (2016b), Zhang and others (2016a and 2016b) are examples in the literature. *Figure **10-87*** shows the ability of WRTDS to track the changes in the flow-concentration relationship that are observed over time. Based on this analysis, the Modeling Workgroup found that loads generated by WRTDS were appropriate to use to calibrate scour and deposition parameters and their change over time in the Phase 6 simulation of the Conowingo.

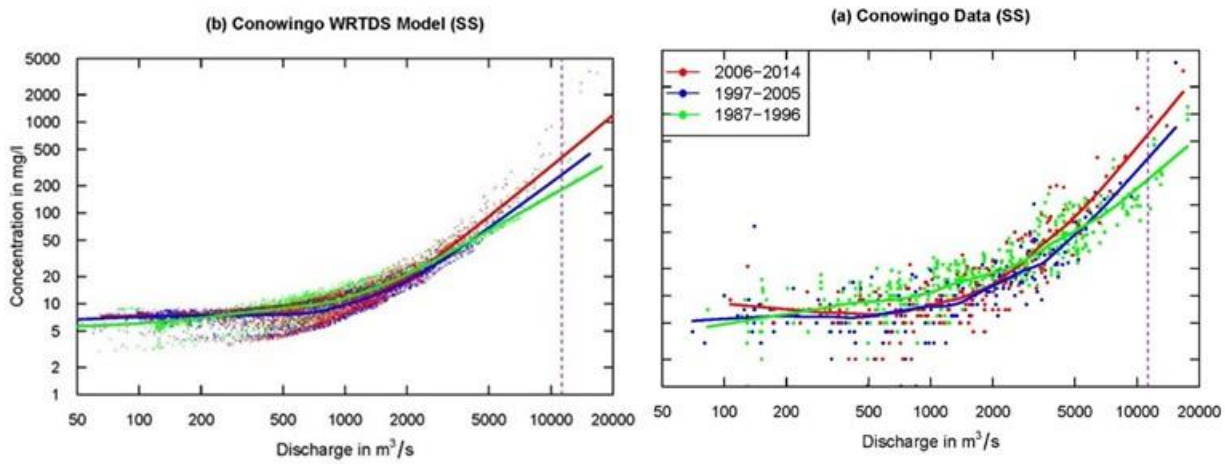

Figure 10-87: relationship between TSS concentration and flow at Conowingo monitoring station

10.7.2.3 Question 3: Does the Trapping Efficiency Change with Different Levels of Nutrient Inputs?

Early CBP watershed models allowed the biogeochemical simulation of HSPF to determine the change in trapping efficiency as nutrient loading changed for all river reaches, including the reservoirs in the lower Susquehanna system. During the Phase II Watershed Implementation Plan (WIP) development process, the partnership decided that the trapping efficiency should remain constant across nutrient reduction scenarios for planning purposes. This was implemented in 2011 for the Phase 5.3.2 Watershed Model. The structure of Phase 6 continues this assumption unless a change is explicitly modeled.

HDR modeling found that this assumption of a constant delivery factor is valid in their model through a wide range of nutrient and sediment reduction scenarios. *Figure **10-88*** shows the output to input ratio for nutrient reduction and increase scenarios. Note that ratios above one are not sustainable in the long run. These are likely due to a short spin-up period in the model. Based on this work and the current assumption of the CBP partnership , the Modeling Workgroup determined that the assumptions of constant delivery factors stand.

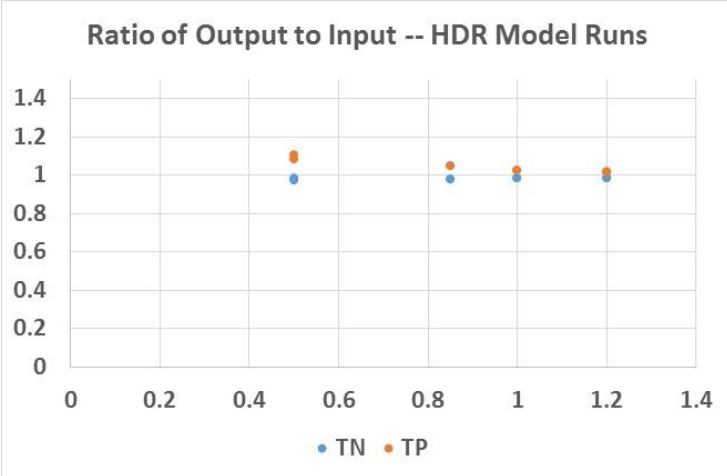

Figure 10-88:Output to Input ratios in the Conowingo Pool Model

10.7.2.4 Question 4: How Does the Availability of Organics Change with Respect to Flow?

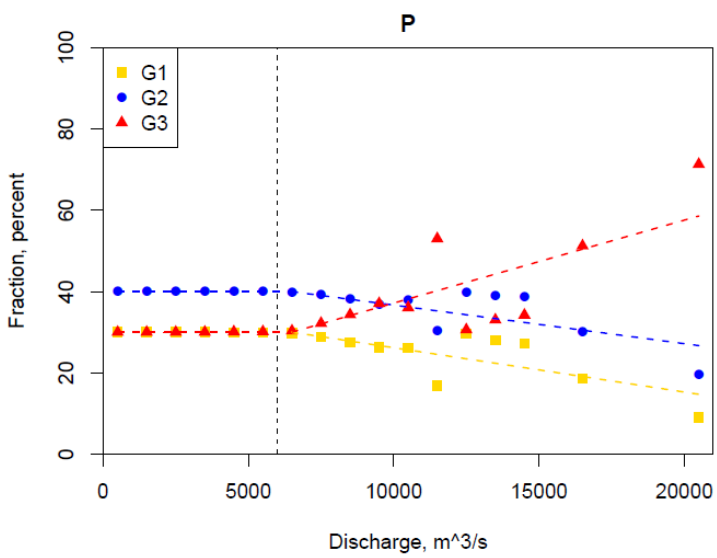

Figure 10-89: Conowingo Pool Model estimates of the bioavailability of particulate organic phosphorus under different flows. A separate analysis was done for particulate organic nitrogen and particulate organic carbon.

The Conowingo Pool Model (CPM) used sediment cores collected for the purpose of parameterizing model particulate organics in the Conowingo Reservoir sediment bed. Using the core data, the CPM explicitly modeled the burial and diagenetic transformation of particulate organics in the sediment. Biogeochemical processes decrease the bioavailability of organics as they decay in the sediments over time. Larger scour events tended to mobilize sediment and particulate organics with a longer sediment bed retention time and therefore less bioavailable particulate organics are available during high flow events at mass wasting flows greater than about 230,000 cfs at Conowingo. The results of the modeling are shown in *Figure 10-90*. The G1, G2, and G3 particulate organic phosphorus in *Figure 10-90* are in descending values of their decay rates to inorganic nutrients, i.e., their bio-availability. The G1 fraction is the most labile with half-life reaction rates of days, G2 has a half-life of weeks, and G3 has a half-life of decades.

Equations are derived from the plots and are shown in *Table **10-37***.

Table 10-37: Equations for G1/G2/G3 particulate organics from Conowingo scour for phosphorus and nitrogen.

Percent G Fraction for P & N	For Q <= 6500 m^3/s	For Q > 6500 m^3/s
G1P, percent	30.0	-0.0010913*(Q-6500) + 30
G2P, percent	40.0	-0.0009493*(Q-6500) + 40
G3P, percent	30.0	+0.0020422*(Q-6500) + 30
G1N, percent	15.0	-0.000749*(Q-6500) + 15
G2N, percent	45.0	-0.001638*(Q-6500) + 45
G3N, percent	40.0	+0.0023878*(Q-6500) + 40

10.7.3 Simulation of Conowingo Infill in the Phase 6 Model Structure

A number of model refinements were made to the Phase 6 Model in order to better simulate the Conowingo Reservoir's infill condition. One improvement was the incorporation of enhanced one-dimensional HEC-RAS2 models developed by WEST Inc. of Lake Clarke and Lake Aldred to better estimate sediment inflows to the Conowingo Reservoir. The refinement allowed sediment estimates for the first time at the two major reservoirs above the Conowingo allowing an improved overall sediment input-output mass balance over all flow conditions.

In addition, guided by WRTDS estimates (Zhang et al. 2016) decreased deposition rates of sediment and particulate nutrients in the Conowingo reservoir were applied annually over the entire 1985 to 2013 Phase 6 simulation period for better consistency with observed sediment and phosphorus data. Also, guided by the observational record and WRTDS estimates, increased erosion rates during mass wasting events in the Conowingo reservoir were applied as appropriate. Finally, changes in particulate organic scour bioreactivity as discussed in Section 10.7.2.4 were applied in the Phase 6 Model.

A four-step calibration process was followed to simulate changes in Conowingo response with infill:

> Step 1: Estimate the model parameters for the Conowingo response at late-1980s and early-1990s infill state. In this step, the setting velocity and deposition critical shear stress parameters were calibrated while the least possible scour was assumed with scour critical shear stress corresponding to 350,000 ft^3/s daily flow, and erodibility. The settling velocities for phytoplankton and refractory organic are also calibrated. The sediment and nutrient parameters provide opportunities for achieving better agreement for both sediment and phosphorus responses with observations.

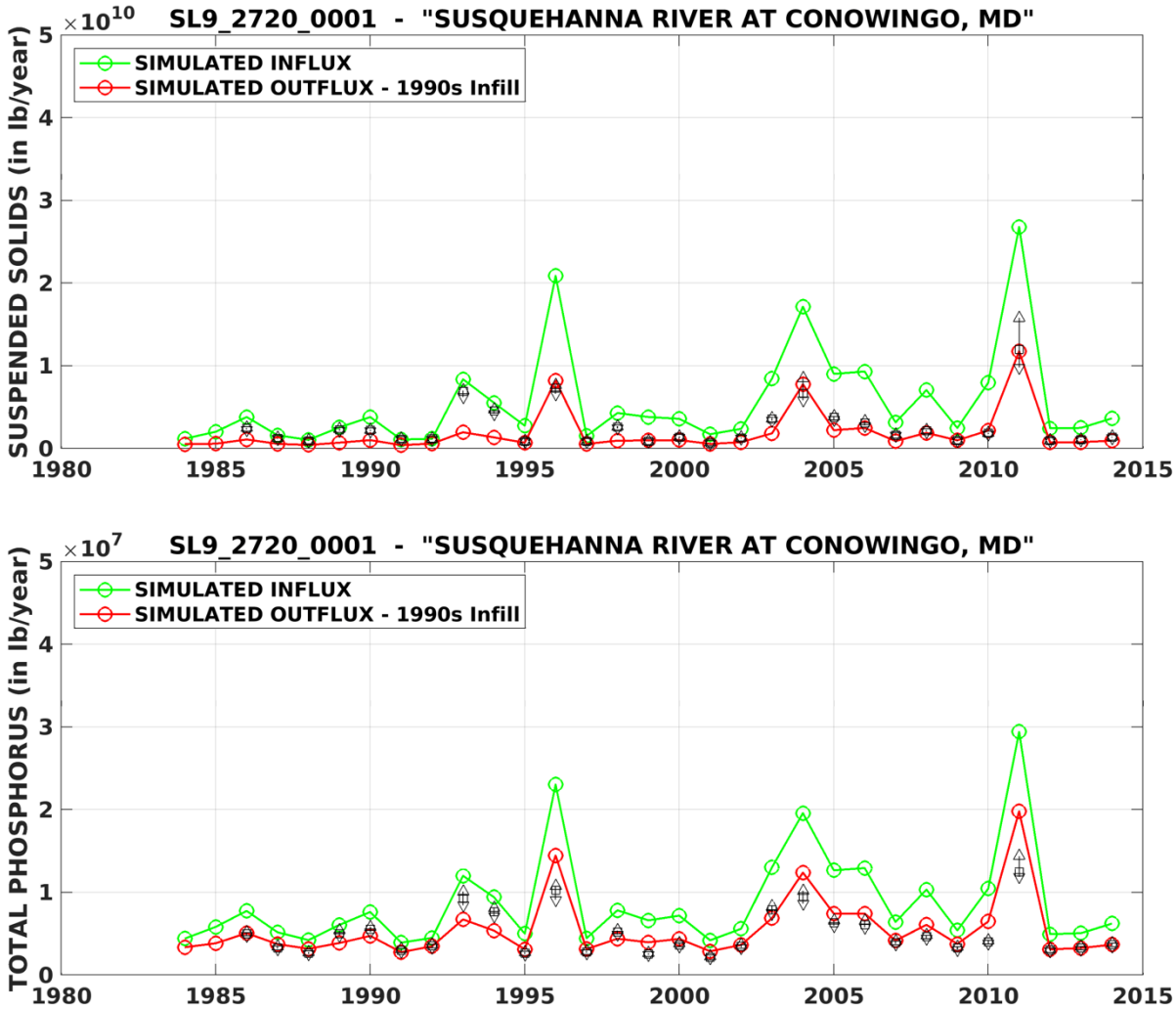

Figure 10-90: Step 1 of 4 of the Conowingo Infill calibration where model parameters were calibrated to simulate late 1980s and early 1990s infill state following the estimates obtained from the WRTDS analysis and observations for that period. Black circles and arrows show the estimate from the early 1990s Stationary WRTDS model and uncertainty quantified using bootstrap method. The early 1990s Stationary WRTDS model provides estimated loads for the early 1990s states of both watershed and Conowingo infill.

Step 2: Estimate changes in deposition behavior with the early 2010s infill state. In this step, settling velocities for silt, clay, refractory organics and phytoplankton are calibrated with the guidance of WRTDS based estimate for changes in deposition as well as the estimates for the uncertainty bounds. Monitoring data was used to guide the estimation of settling velocities changes needed under different flow regimes.

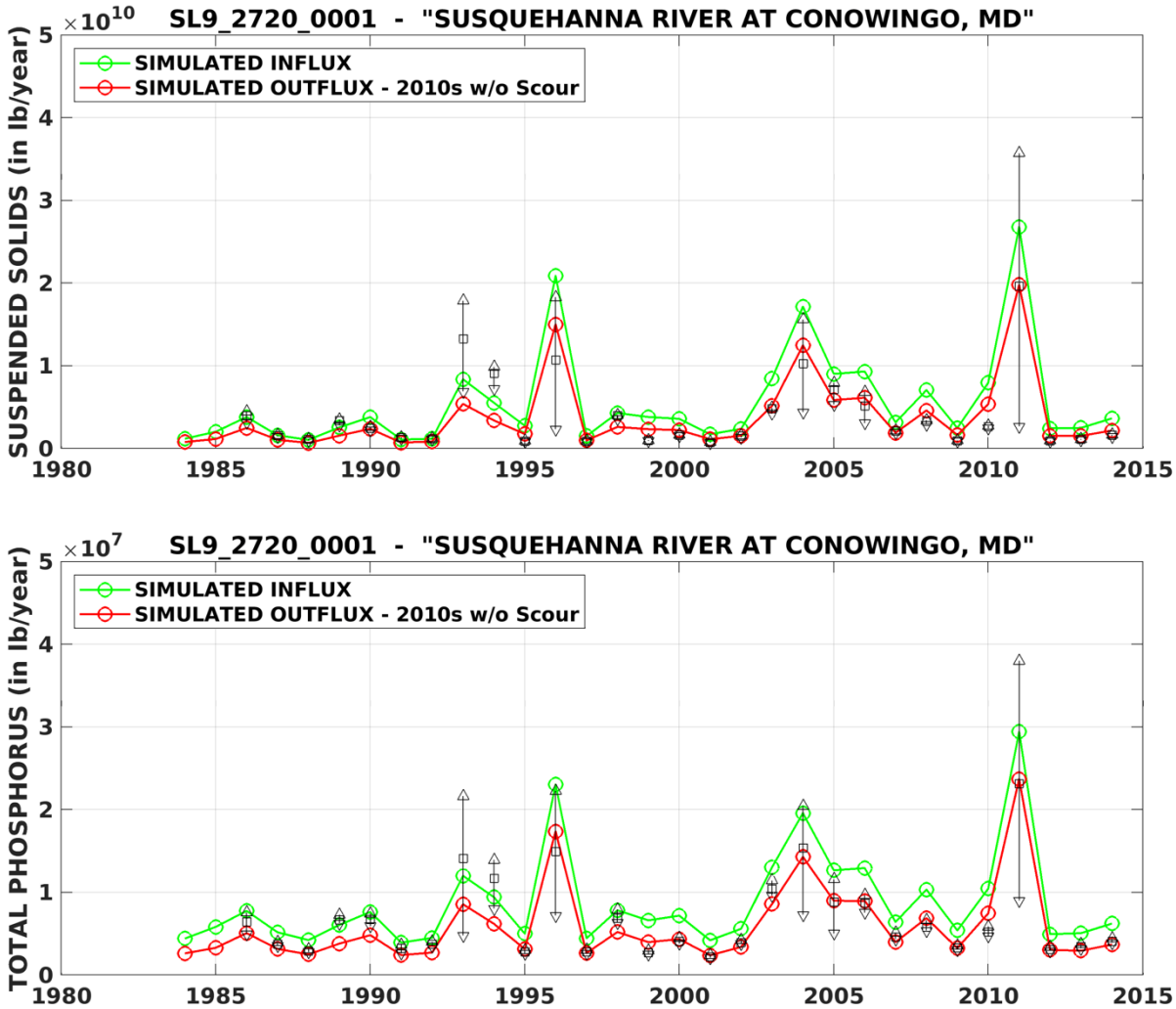

Figure 10-91: Step 2 of 4 of the Conowingo Infill calibration where model parameters were calibrated to match estimated changes in deposition response with the early 2010s infill state obtained from the WRTDS analysis. Black circles and arrows show the estimate from the early 2010s Stationary WRTDS model after subtracting out the changes in scour and uncertainty quantified using bootstrap method. The early 2010s Stationary WRTDS model provides estimated loads for the early 2010s states of both watershed and Conowingo infill.

Step 3: Estimate changes in the scour behavior with the early 2010s infill state. In this step, erodibility is calibrated with the guidance of WRTDS based estimate for changes in scour as well as estimates for the uncertainty bounds.

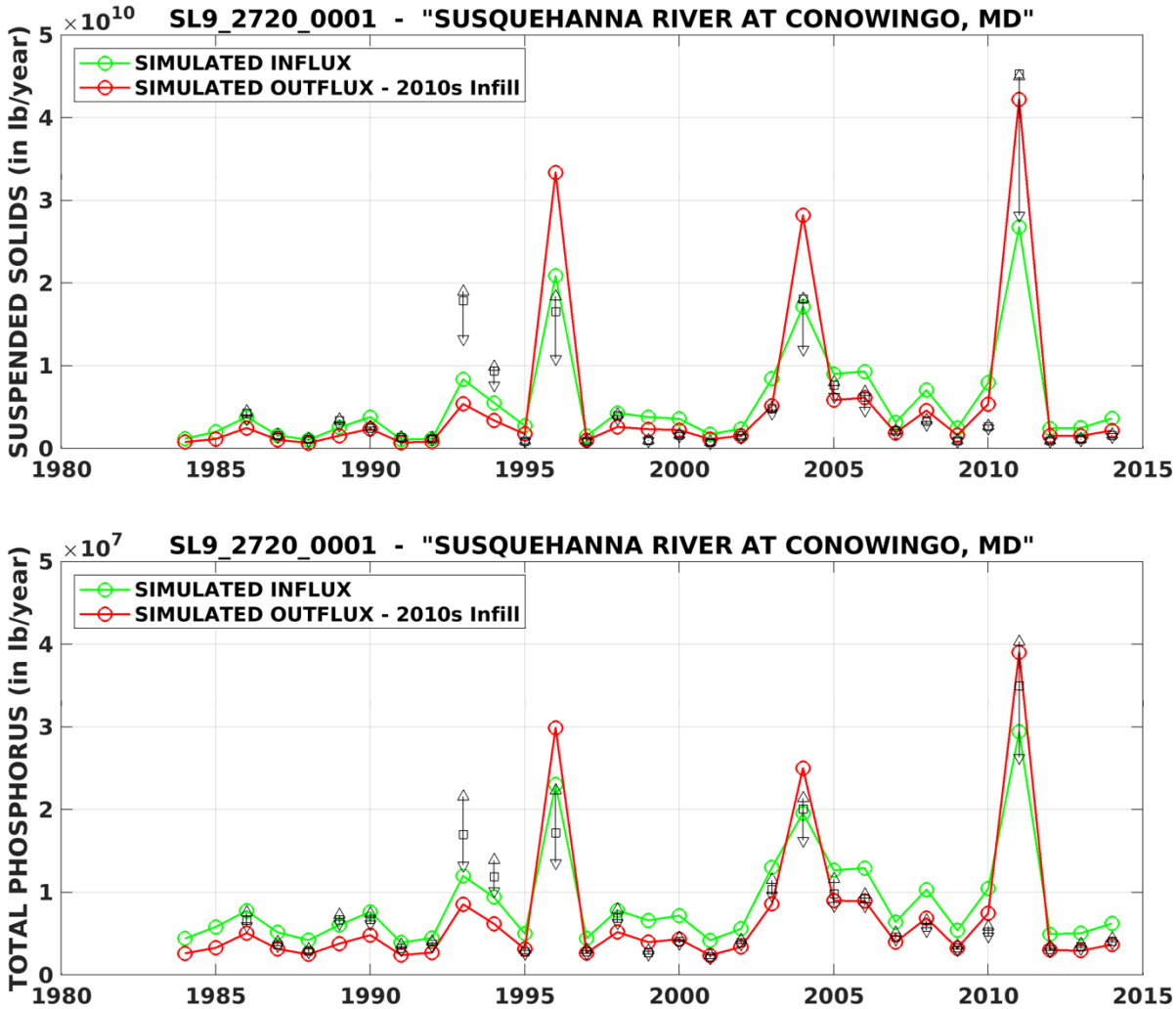

Figure 10-92: Step 3 of 4 of the Conowingo Infill calibration where model parameters were calibrated to match estimated changes in scour response with the early 2010s infill state obtained from the WRTDS analysis. Black circles and arrows show the estimate from the early 2010s Stationary WRTDS model and uncertainty quantified using bootstrap method. The early 2010s Stationary WRTDS model provides estimated response for the early 2010s states of both watershed and Conowingo infill.

Step 4: Estimate the temporal variability in the deposition and scour. In this step, parameters estimated in the previous steps for the early 1990s and early 2010s infill state are varied over time in the simulation. The parameters were varied with considerations to (a) mass balance for silt, clay, and phosphorus, (b) achieving best possible agreement with the monitoring data for nitrate, nitrogen, dissolved orthophosphate, phosphorus and sediment during the simulation period, (c) agreement with USGS-WRTDS nitrate, nitrogen, dissolved orthophosphate, phosphorus, and sediment loads.

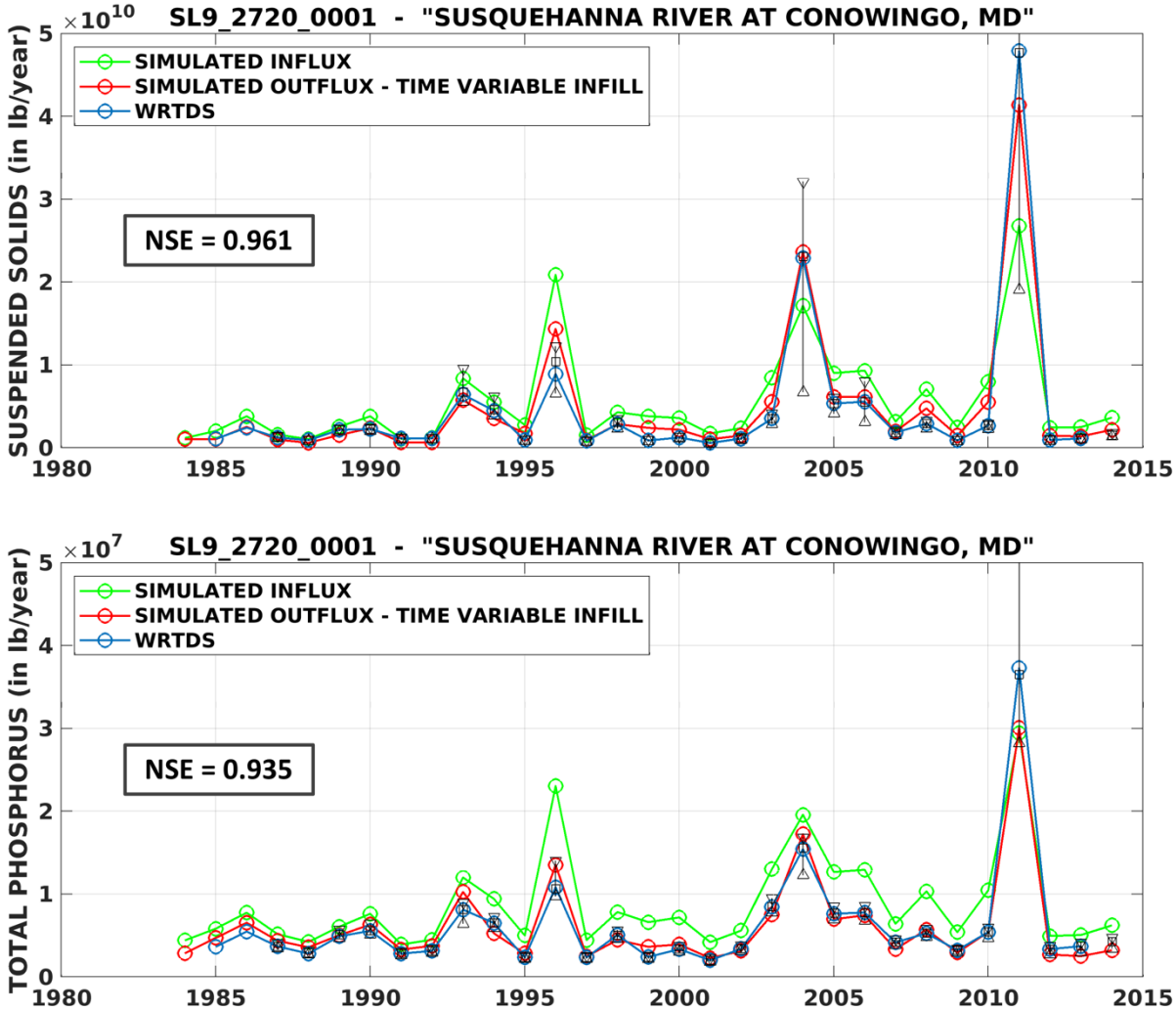

Figure 10-93: : Step 4 of 4 of the Conowingo Infill calibration where the model parameters estimated in the steps 1 through 3 for early 1990s and early 2010s were temporally varied in the simulation to achieve agreement with monitoring data and standard USGS-WRTDS loads. The temporal variability in model parameters represent the changes in the behavior, i.e. the decrease in net trapping capacity, of the reservoir with the increase in infill. Nash-Sutcliffe efficiencies (NSE) show good agreement between the simulated and WRTDS loads.

Figure 10-93 and ***Figure 10-94*** show the quality of time variable infill response for the Conowingo reservoir is show in terms of agreement in annual and monthly loads. The monthly input and output time series show that for most of the months during the 1985-2014 simulation period, the reservoir is trapping nitrogen, phosphorus, and sediment loads as input is higher than output. Three storm events where flow greater than 400,000 ft^3/s was recorded have been highlighted in the ***Figure 10-94*** – (a) 1996 Ice Jam and Big Melt event, (b) Tropical storm Ivan, and (c) Tropical storm Lee. The simulated input and output response in the figures show that among these storms the 1996 Ice Jam event was a net depositional event, which matches with the finding of Langland (2015) based on an analysis of bathymetric surveys. However, the figures show that there was net erosion during 2004 and 2011 events. It shows that calibrated time variable infill response matches with the findings and

understanding of prior studies for the Conowingo infill and its impact on nutrient and sediment transport.

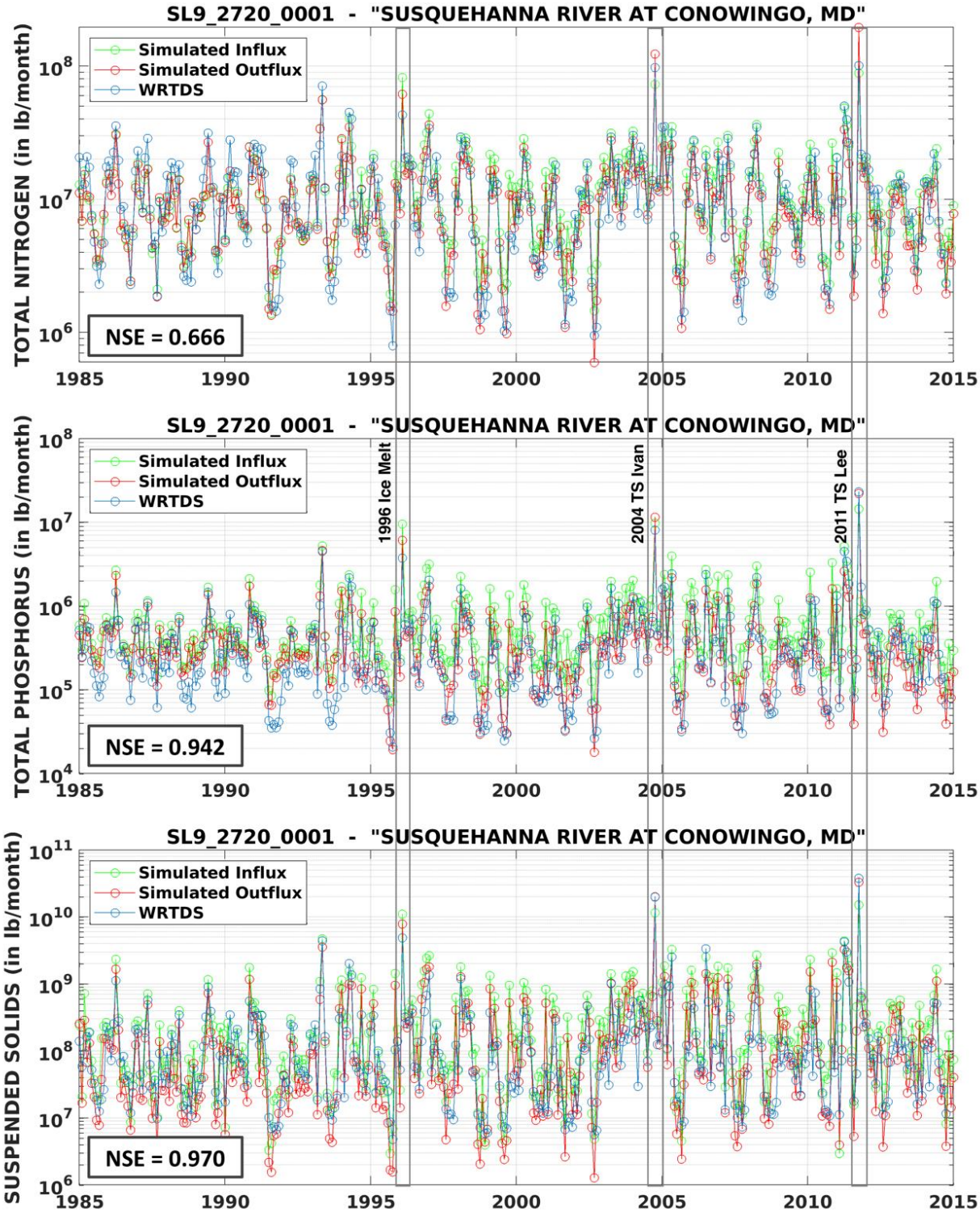

Figure 10-94: Monthly influx, outflux and WRTDS nitrogen, phosphorus, and sediment loads. High Nash-Sutcliffe efficiencies (NSE) show good agreement in simulated and WRTDS loads. Influx and Outflux timeseries show periods of net deposition and scour. Three key events during the simulation period are shown where the stormflow was greater than 400,000 ft^3/s but 1996 was a net deposition period but there was net erosion in 2004 and 2011 events.

10.7.4 STAC Workshop Recommendations on Conowingo Infill and the Phase 6 Model Response

The three major recommendations from the STAC Conowingo workshop (Linker et al. 2016a) described in the August 18, 2016 STAC letter to the Management Board are as follows

- Efforts to model the effects of Conowingo on net accumulation or release of nutrients and sediment from the reservoir should be evaluated based on its ability to "hindcast" data from water quality observations and statistical analyses.
- In order to quantify the influence Conowingo infill has on Chesapeake water quality, three primary issues should be considered for modeling:

  - Address biogeochemical processes related to sediment scour and nutrient cycling that may influence bioavailability in reservoir sediments, under variable flow ranges in the Conowingo Reservoir.

  - Ensure representation of effects of Conowingo inputs to Chesapeake Bay for the full range of flow conditions including 'extreme' high-flow events.

  - Improve representation of reactivity of particulate organic matter in Conowingo outflow.

- Moving forward, an effort should be made to link the sediment transport and biogeochemical models in the 2010 Water Quality and Sediment Transport Model (WQSTM) to enhance modeling of the transport and fate of organic nutrients in the tidal Bay.

The STAC recommendations are addressed in the Phase 6 simulation as follows.

Workshop Recommendation 1: Efforts to model the effects of Conowingo on net accumulation or release of nutrients and sediment from the reservoir should be evaluated based on its ability to "hindcast" data from water quality observations and statistical analyses.

Explicit simulation of the changes over time in the net transport of nutrients and sediment in the Conowingo Reservoir due to reservoir infill is a major advance of the Phase 6 simulation which has been supported by extensive Conowingo infill monitoring, research, and modeling since 2010. The improved understanding of the infill process and its consequences for increased nutrient transport to the tidal Bay has provided a dynamic Phase 6 simulation of the Conowingo Reservoir that changes with infill conditions and is calibrated to long-term river monitoring stations above and below the Conowingo and with guidance from the latest research findings.

In Phase 5 the Conowingo simulation was only a general representation of its long-term average behavior, and the simulation lacked the dynamic changes observed in the reservoir over the past several decades. In the Phase 6 simulation of Conowingo infill, the reservoir simulation is responsive to increased infill with a reduction of particulate deposition and increase of the potential for sediment scour (reduced critical shear stress) over the entire 1985 to 2013 Phase 6 simulation period. The Phase

6 calibrated Conowingo simulation is fully capable to "hindcast" data from water quality observations and statistical analyses consistent with a reservoir in dynamic equilibrium.

Workshop Recommendation 2: In order to quantify the influence Conowingo infill has on Chesapeake water quality, three primary issues should be considered for modeling:

2a: Address biogeochemical processes related to sediment scour and nutrient cycling that may influence bioavailability in reservoir sediments, under variable flow ranges in the Conowingo Reservoir.

The HydroQual-HDR simulation of the Conowingo Pool and the UMCES assessment of particulate organics in Conowingo sediment examined mass, shear stress, and the degree of reactivity of 1) labile - highly reactive organic material with oxidation time scales of several weeks (G1), 2) refractory, less reactive material with time scales of several months (G2), and 3) effectively inert, largely non-reactive material (G3). The UMCES research and HydroQual HDR simulation of the G1, G2, and inert G3 particulate organics in Conowingo Reservoir sediment provided essential information to address the mobilization and relative reactivity of particulate organic nutrients from Conowingo.

Specifically, the quantification of the sediment components of G1, G2, and G3 organics in Conowingo sediment were used to drive the simulation of organic scour and transport from the Conowingo Reservoir by the HydroQual-HDR Conowingo Pond Mass Balance Model (CPMBM). The CPMBM simulated fraction of G1, G2, and G3 in total organic phosphorus transported from the Conowingo are represented in the figure and table below and the associated regressions of the percent of G1, G2, and G3 in phosphorus organics with riverine flow are incorporated into the Phase 6 Model. Similar quantifications are made for organic nitrogen and carbon. Using these approaches the simulated dissolved and organic nutrients transported from the Conowingo are well represented and reflect the observed conditions of Conowingo infill in dynamic equilibrium.

Augmenting the improved simulation of particulate nutrients under conditions of dynamic equilibrium in the Conowingo, the native HSPF simulation provided sufficient representation of dissolved phosphate (PO_4^-) and ammonia (NH_4^+) flux from Conowingo sediment with high flow driven sediment scour by using a model-user set flux based on observations.

2b: Ensure representation of effects of Conowingo inputs to Chesapeake Bay for the full range of flow conditions including 'extreme' high-flow events.

The representation of effects of Conowingo inputs to Chesapeake Bay for the full range of flow conditions including 'extreme' high-flow events was done using WRTDS guidance over the full range of flows, which were augmented with observations during the extreme high flow events to further guide the Phase 6 simulation of the Conowingo reservoir. Decreased deposition over time with increasing infill was consistent with WRTDS and other observations (Zhang et al. 2016; Langland 2015). In addition, scour was calibrated with the critical shear stress of bottom scour from the Conowingo Reservoir increasing over time with increased infill. The approaches of decreased particle deposition and increased bottom critical shear stress with infill demonstrably improved the simulation's agreement with observation and was entirely consistent with reservoir infill theory and the recommendations of the STAC Conowingo workshop. In addition to the calibration for Conowingo, an enhanced one-dimensional HEC-RAS2 model of Lake Clarke and Lake Aldred was applied to estimate sediment inflows

to the Conowingo Reservoir and improving the overall input output mass balance over all flow conditions.

2c: Improve representation of reactivity of particulate organic matter in Conowingo outflow.

The simulation approach in the Phase 6 Watershed Model described above in 2a and 2b was used to represent the additional transport of particulate nutrients form the Conowingo under dynamic equilibrium infill conditions. To further address the fate of the particulate organic phosphorus and nitrogen and particulate inorganic phosphorous scoured from the Conowingo and transported to tidal water core studies were conducted by UMCES. The tidal water sediment core studies provided insight as to what changes in nutrient flux would be expected from sediment cores that were capped by an influx of Conowingo sediment, similar to what would occur during scour from Conowingo during extreme high flows. A collection of cores from different regions of the upper Bay confirmed the simulated flux behavior of the WQSTM in the upper Bay downstream of Conowingo discharge.

In addition to the work on the reactivity of organic particulate nutrients, particulate inorganic phosphorus (PIP) in iron bound and other forms was also considered in the monitoring, research, and Conowingo Pool Modeling work that was used to guide the CBP Phase 6 Watershed and WQSTM models. The tidal water core studies conducted by UMCES confirmed the WQSTM approach of PIP non-reactivity in the water column until the potential for dissolved phosphate (PO_4^-) release form PIP when the PIP is incorporated into anoxic sediment.

Workshop Recommendation 3: Moving forward, an effort should be made to link the sediment transport and biogeochemical models in the 2010 Water Quality and Sediment Transport Model (WQSTM) to enhance modeling of the transport and fate of organic nutrients in the tidal Bay.

The Modeling Workgroup fully agrees that the next generation of tidal water quality and sediment transport model should have fully linked and integrated sediment transport and biogeochemical models. This is an active area of simulation research, and examples of the linkage of simulated sediment transport and sediment/water column biogeochemical processes are now operational, such as in the CPMBM used in the current Conowingo study. The linkage could be particularly important in regions of high estuarine deposition of sediment and particular nutrients with subsequent nutrient outflux determined by the presence and extent of bottom water hypoxia. Opportunities for examining the potential for this linkage will be in the January 2018 STAC workshop *Chesapeake Bay Program Modeling Beyond 2018: A Proactive Visioning Workshop.*

10.7.5 Phase 6 estimates of changes in loads in dynamic equilibrium

All three reservoirs in the Lower Susquehanna reservoir system are currently in approximate equilibrium or long-term equilibrium or dynamic equilibrium (Hainly et al., 1995; Hirsch, 2012; Langland 2009, 2015; Zhang et al., 2013, 2015, 2016). Three reservoirs now under dynamic equilibrium have periods of trapping and scour but there is no long-term trapping of sediment or nutrient occurring within the reservoir. To that effect, model parameters for the three reservoirs were estimated representing current state of dynamic equilibrium such that there was no net trapping or scour for each reservoir over the 30-year simulation period. Specifically, the dynamic equilibrium ensured that inputs for silt, clay, total nitrogen and total phosphorus were equal to outputs.

The calibrated model was used to quantify changes in loads under different infill states. Figure **10-95** shows simulated responses for sediment, phosphorus and nitrogen under infill states for early 1990s, time-variable 1985-2014 infill, early 2010s, and dynamic equilibrium. It is noted that in the simulation of these infill states the inputs to the reservoir system did not change but changes in the reservoir response are simulated by the model and the corresponding changes in transport is estimated for nutrients and sediment for these infill states. Figure **10-95** shows the incremental increase in sediment and nutrients transport between early-1990s, time-variable infill during 1985-2014 calibration period, early 2010s, and dynamic equilibrium. It shows that the changes in transport due infill also occur during the years when flow is lower than scour threshold throughout the year, and that the changes in reservoir response is not limited scour years. The figure also shows that under different infill states, but in particular in the dynamic equilibrium state, where the inputs to the reservoir system over the 30-year simulation period is equal to outputs, there are periods and years of deposition that apparent for the year with the magnitude of simulated transport less than input.

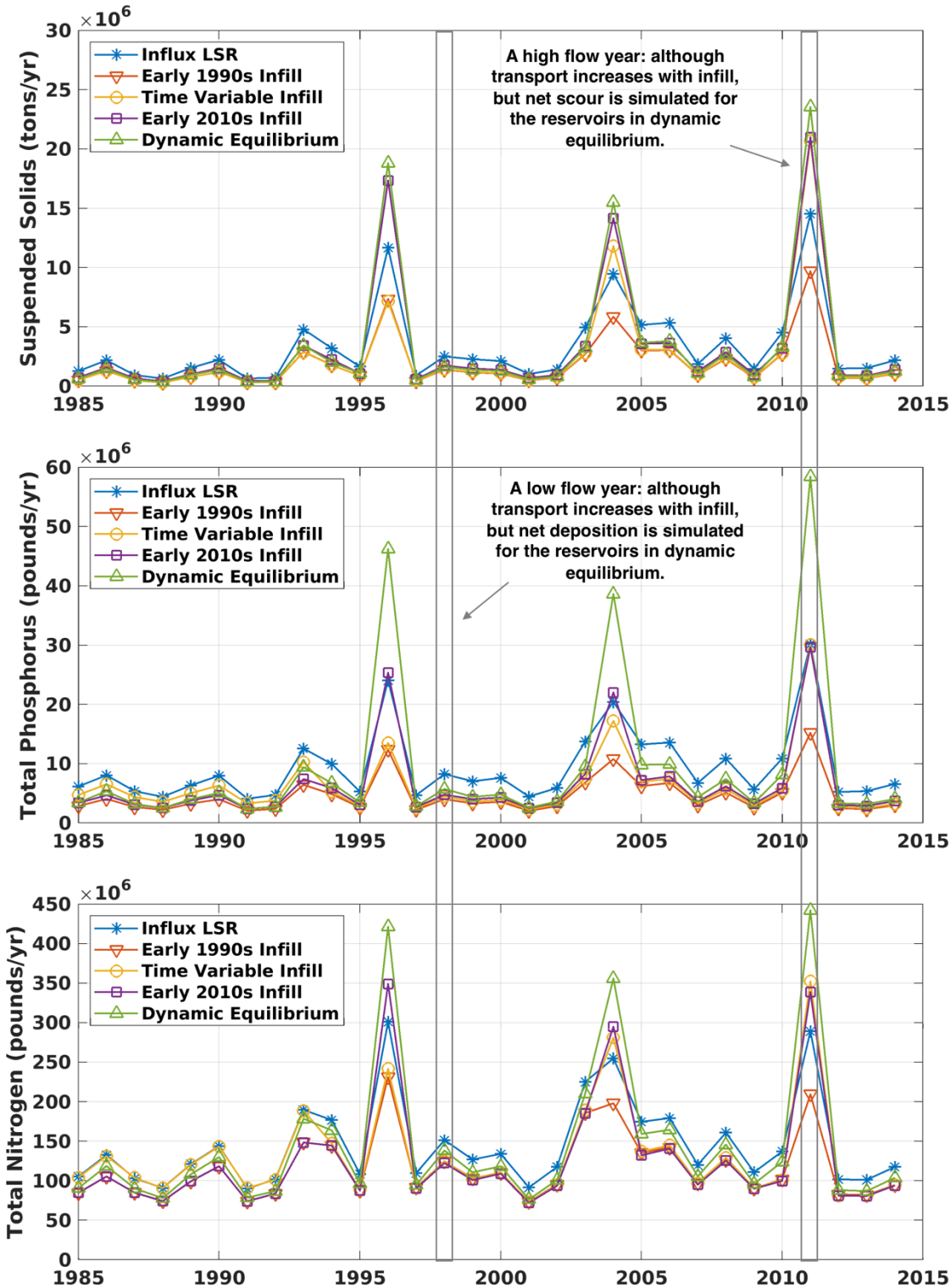

Figure 10-95: Simulated changes in annual sediment and nutrients transport with infill.

The changes in 1991-2000 average annual nutrients and sediment loads were estimated between the estimated time variable infill for the calibration (1990s infill state) and the reservoirs in dynamic

equilibrium (Figure **10**-**96**). These two key infill states represent the differences in reservoir states that was assumed in 2010 TMDL Assessment and the current dynamic equilibrium state. The differences in the transport of nutrient species were also calculated, which shows almost all of the change in nitrogen delivery due to infill is in the form of organic nitrogen, and the change in phosphorus delivery is divided between particular inorganic phosphorus and particulate organic phosphorus. Specifically, nitrogen delivery increased by around 20 Mlbs-N/year, of which little less 98% was due to changes in organic nitrogen response; the phosphorus delivery increased by 3.5 Mlbs-P/year, of which about 48% was particulate inorganic and 51% organic phosphorus.

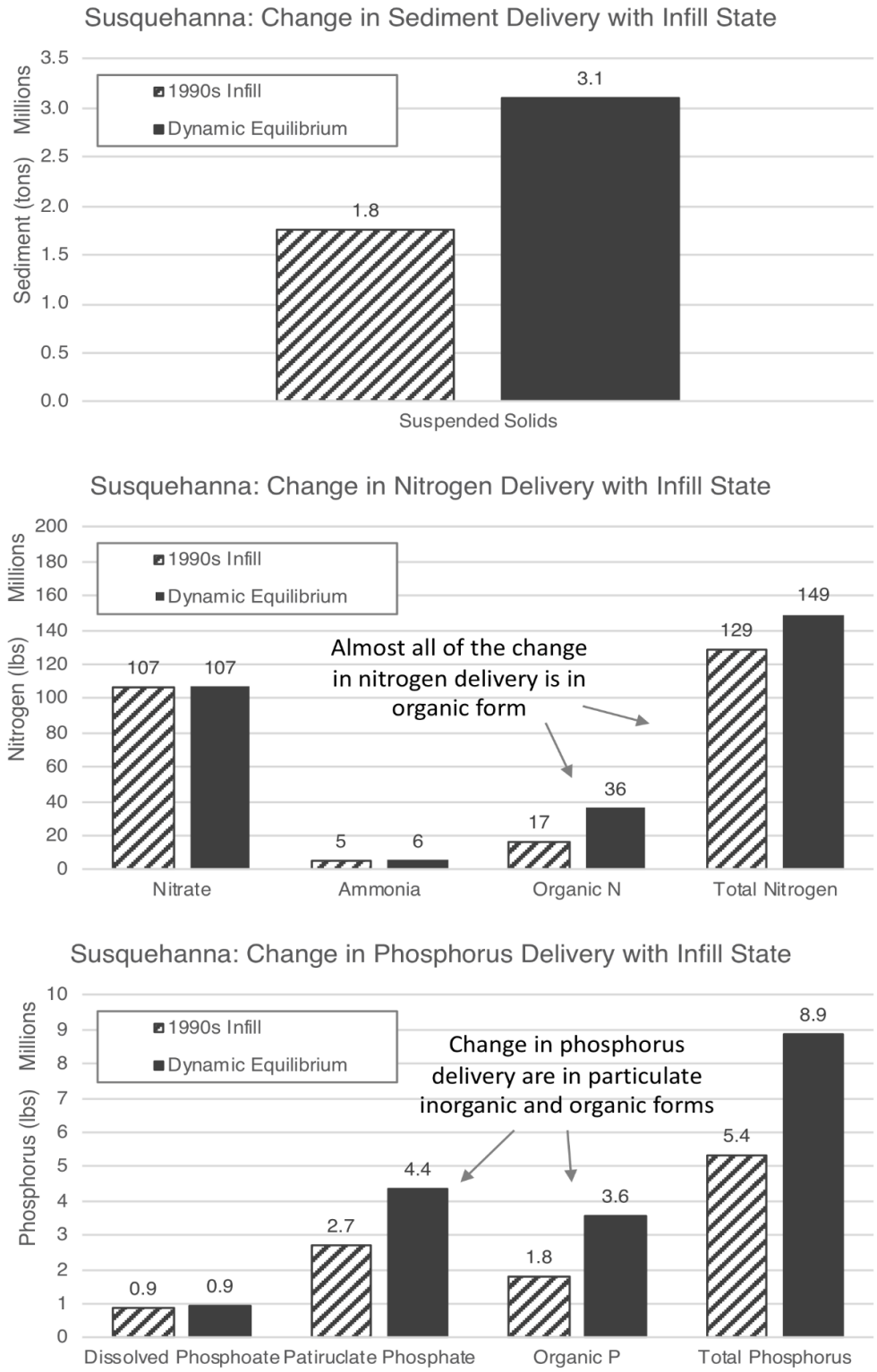

Figure 10-96: Average annual change in sediment, phosphorus, and nitrogen delivery between the calibrated time-variable infill for 1991-2000 (1990s infill state) and dynamic equilibrium.

The model was applied to a management scenario with Phase 2 WIP level of effort on 2010 land use (WIP2 Scenario) to estimate responses for different reservoir infill states. Figure 10-97 shows simulated annual responses for sediment, phosphorus and nitrogen with reservoirs under infill states of early 1990s, time-variable 1985-2014 infill, early 2010s, and dynamic equilibrium. Although for the amount of nutrients and sediment arriving to the reservoirs decreased with the management practices of WIP2 Scenario, but they did not change between these four infill state scenarios. Therefore, the simulated changes in the reservoir response and the corresponding changes in transport of nutrients and sediment are entirely due to corresponding infill states. Model results show incremental increase in sediment and nutrients transport between early-1990s, time-variable infill estimated for 1985-2014 model calibration, early 2010s, and dynamic equilibrium. In that respect, the behavior of reservoir response for different infill states for the WIP2 Scenario was similar to that for the watershed under 1991-2000 management, and where the changes in reservoir response was not limited scour years but the changes in transport due infill also occurred during the years when flow was lower than scour threshold throughout the year. The figure also shows that under different infill states, but in particular in the dynamic equilibrium infill state, where the inputs to the reservoir system over the 30-year simulation period is equal to outputs, there are periods and years of deposition that is reflected for the years with the magnitude of simulated transport being less than input.

The changes in average annual nutrients and sediment loads for the scenario during average hydrology period of 1991-2000 were estimated between the time variable infill state (1990s infill state) and the reservoirs in dynamic equilibrium (Figure 10-98). These two key infill states represent the differences in reservoir states that was assumed in 2010 TMDL Assessment and the current infill state of approximate equilibrium or long-term equilibrium or dynamic equilibrium (Langland 2009; Hirsch 2012). The differences in the transport of nutrient species were also calculated, which shows almost all of the change in nitrogen delivery due to infill is in the form of organic nitrogen, and the change in phosphorus delivery is divided between particular inorganic phosphorus and particulate organic phosphorus. Specifically, nitrogen delivery increased by around 13.4 Mlbs-N/year, of which more than 98% was due to changes in organic nitrogen response; the phosphorus delivery increased by 1.75 Mlbs-P/year, of which about 43% was particulate inorganic and 56% organic phosphorus.

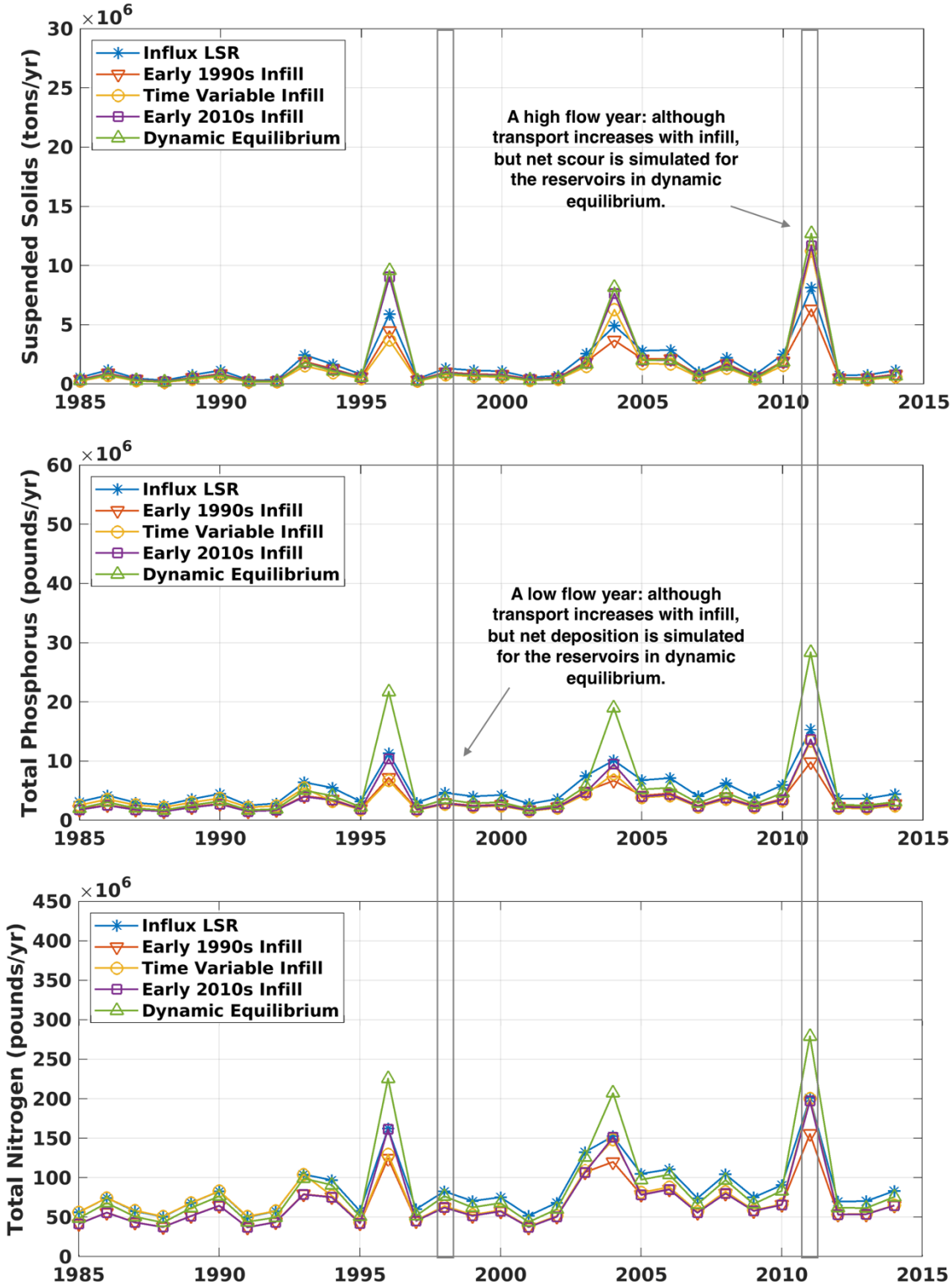

Figure 10-97: Simulated changes in annual sediment and nutrients transport with infill for the scenario with WIP Phase 2 level of effort on 2010 land use.

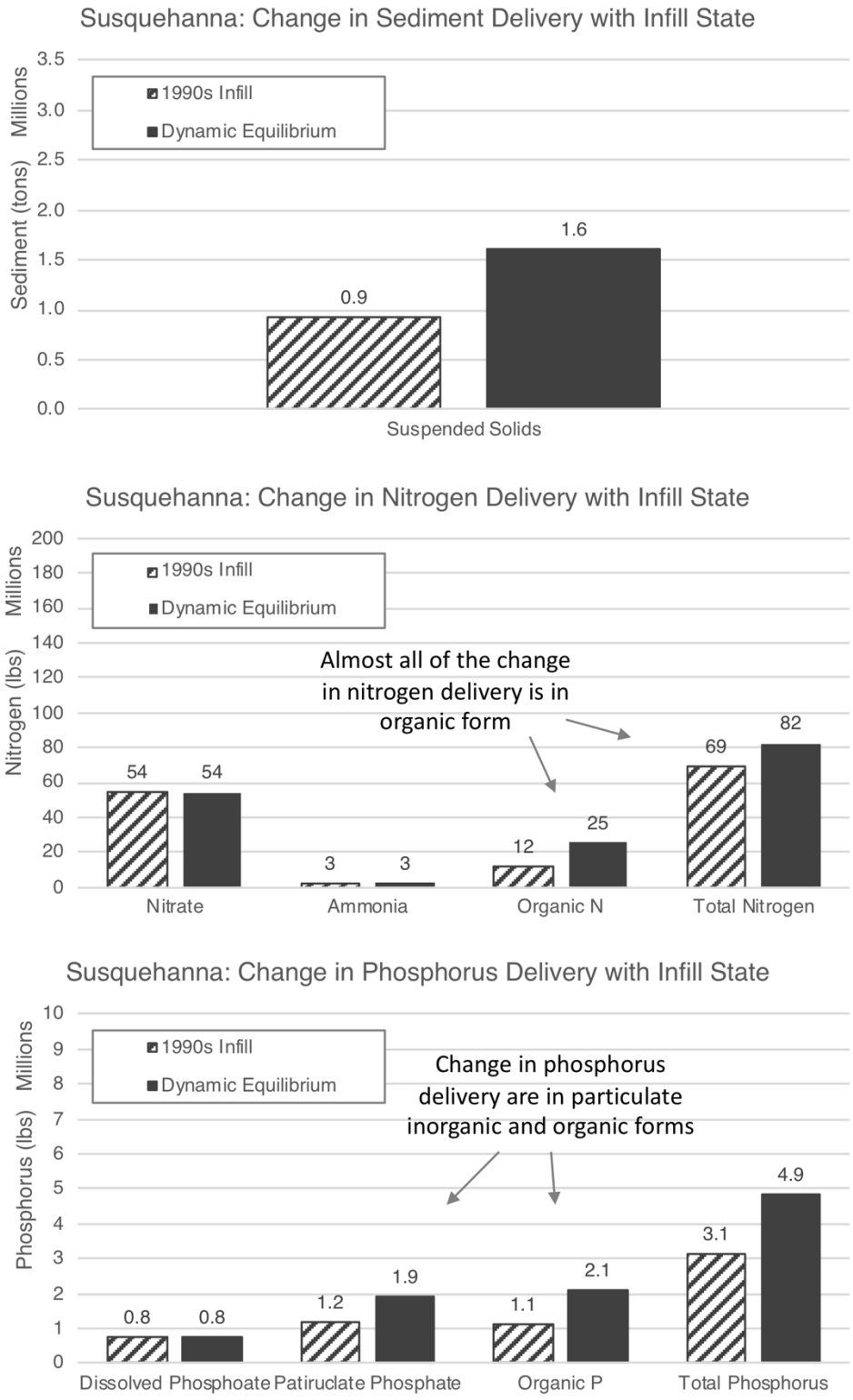

Figure 10-98: Average annual change in sediment, phosphorus, and nitrogen delivery between the calibrated time-variable infill for 1991-2000 (1990s infill state) and dynamic equilibrium for the scenario with WIP Phase 2 level of effort on 2010 land use.

10.8 River-to-Bay Delivery Factors

River-to-bay delivery factors are defined as the fraction of nutrients and sediment that are transported from any given watershed segment to the tidal waters. These factors are based on estimates from the HSPF simulations of riverine nutrients and sediment transport that are calibrated to the observations at hundreds of monitoring stations.

River-to-bay delivery factors are calculated on the basis of total nitrogen and total phosphorus rather than the species of these nutrients. Since nitrogen species 'spiral' as they travel down streams (Ensign and Doyle, 2006), changing from dissolved inorganic nitrogen (DIN) to particulate nitrogen (PN) and back again multiple times before reaching the estuary, we can't calculate a separate delivery factor for the individual species. An example is illustrative. Consider the case if there were nothing but Ammonia (NH_3) sources in a watershed. The downstream load would still arrive as Nitrate (NO_3), Ammonia (NH_3), and Organic Nitrogen (ORGN), but the river-to-bay factors calculated on the individual nitrogen species (i.e. ratio of delivered and edge-of-stream loads) would be very small for NH_3 and infinite for NO_3 and ORGN.

The transport factors for the river segments are calculated as the ratio of average annual output to input loads for the 1991-2000 average hydrology period. *Figure **10-99*** shows the distribution of transport factors for the calibrated river segments in the watershed. The transport factor value of less than 1 indicates output was less than input load during the specified period. The River-to-bay delivery factor for a river segment is the multiplication of transport factors of the river segment and all downstream segments. *Figure **10-100*** shows the distribution of River-to-bay delivery factors for nitrogen, phosphorus, and suspended sediment for the watershed river segments. *Figure **10-101***, *Figure **10-102***, and *Figure **10-103*** show a comparison of River-to-bay delivery factors of Phase 5.3.2 and Phase 6 Models for nitrogen, phosphorus, and sediment respectively. There are three land-river segments in the Chesapeake Bay Watershed (CBWS) with EOT delivery factors of zero: N51095JBO_7051_0001, N24005WM0_3881_3880, N24013WM0_3881_3880. The two in MD (beginning with N24) represent Liberty Reservoir, which is used for water supply and does not have an outflow. The one in Virginia (beginning with N51) is the location of the Little Creek Reservoir, which also does not spill.

River-to-bay delivery factors would change as stream chemistry changes in different management scenarios. However, as a decision of the WQGIT in 2010, these factors are held constant for management scenarios to aid in the development of Watershed Implementation Plans. In the calibration, delivery and transport factors vary. In scenarios, constant delivery factors are used because variation in the factors between scenarios would mask independent assessment of the impact of BMPs and land use changes. The variation in river delivery and transport factors in the calibration is often due to nutrient limitation, as BMPs may control one nutrient more than another. In the riverine simulation, just as in actual rivers, this tends to drive simulated concentrations toward nutrient limitation. Once nutrient concentrations fall below the Michaelis-Menten constants for algal growth, which are specified in the user-supplied HSPF constants (Bicknell et al. 2001), then algal growth and nutrient uptake decreases, allowing more of the nonlimited nutrient to be transported through the river segment.

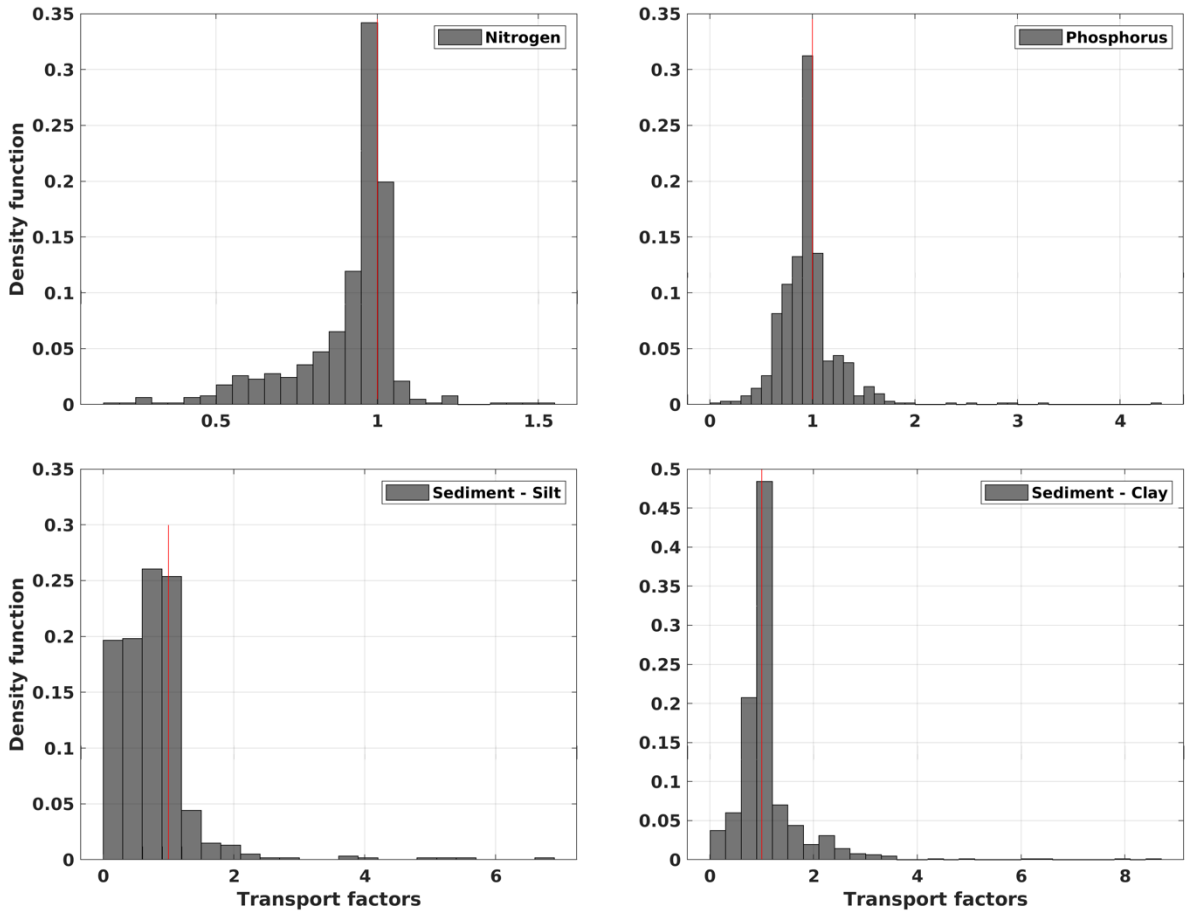

Figure 10-99: The distribution of transport factors (i.e. the ratio of average annual output to input) for the simulated river segments.

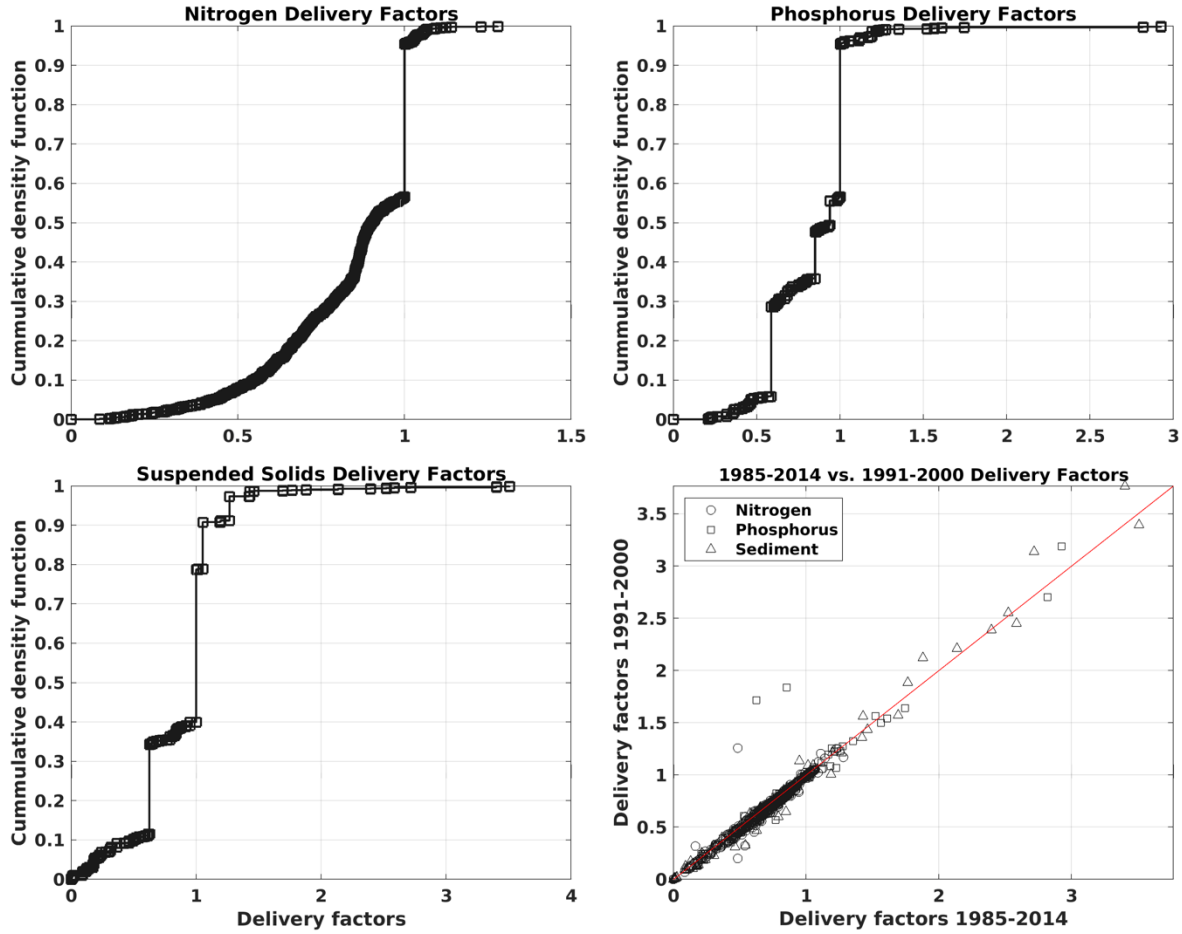

Figure 10-100: The distribution of the river-to-bay delivery factors for the watershed.

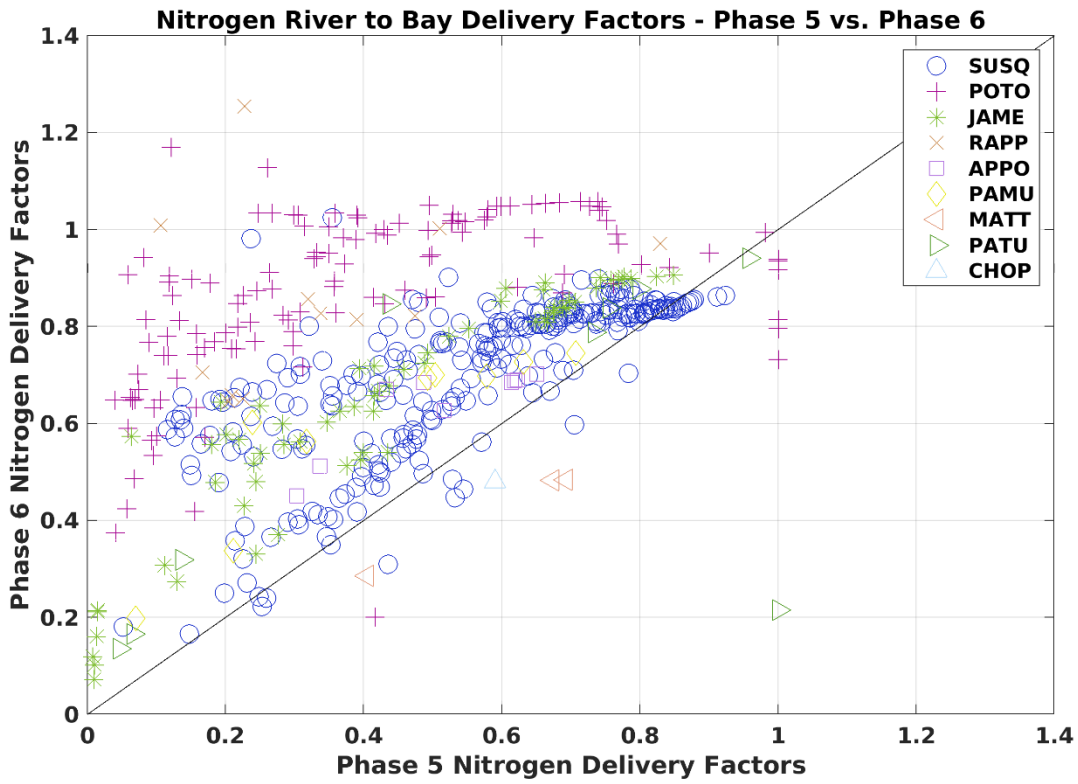

Figure 10-101: River-to-bay nitrogen delivery factors for the river segments in Phase 5 and Phase 6.

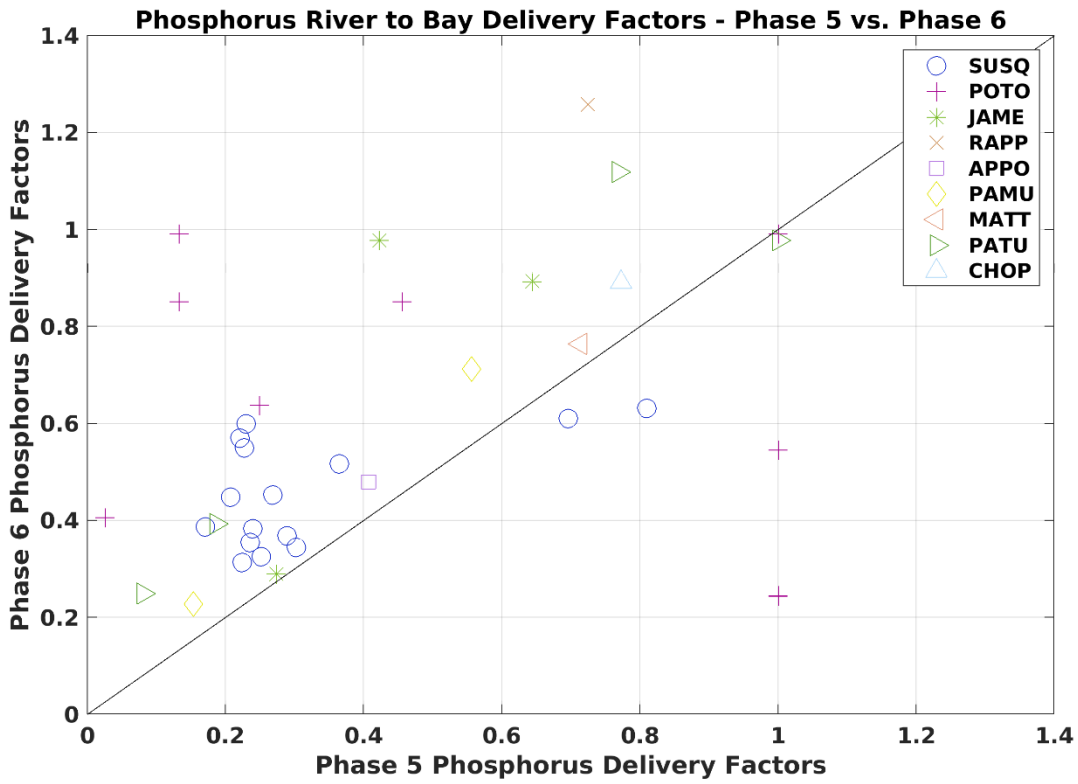

Figure 10-102: River-to-bay phosphorus delivery factors for the river segments in Phase 5 and Phase 6.

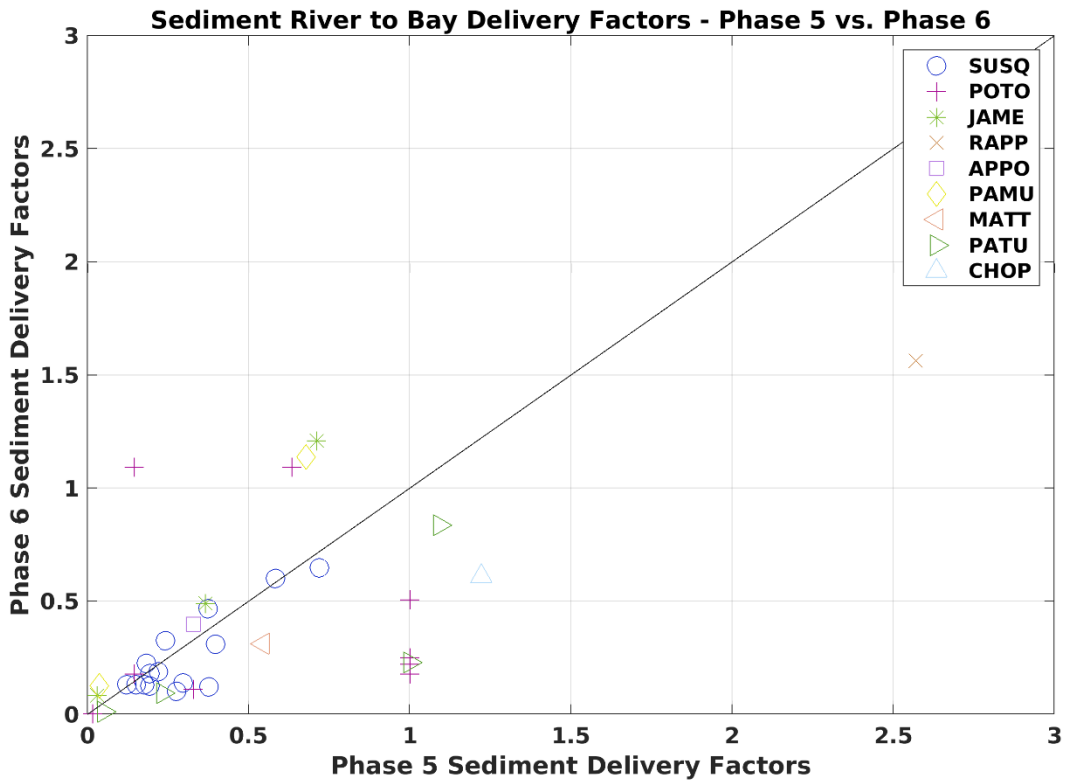

Figure 10-103: River-to-bay sediment delivery factors for the river segments in Phase 5 and Phase 6.

The differences in the river-to-bay delivery reflects the new science on the quantification of riverine transport and they are more consistent with literature and more recent statistical models, specifically USGS-SPARROW (Ator et al., 2011) that heavily relies on the observations for the estimation of the loads. Issues involving these aspects are discussed in more detail in Section 2.2.1.3. On average about 70 million pounds of nitrogen is lost annually in the river system, of which denitrification and phytoplankton settling are the major processes regulating about 70% of the total nitrogen processing (Figure **10-104**). Similarly on average about 6 million pounds of phosphorus is lost annually into the rivers, of which settling of phytoplankton and particulate inorganic phosphorus regulate about 65% of the total phosphorus processes (Figure **10-104**). The average River-to-bay delivery factors for the watershed were estimated as 0.80, 0.77, and 0.80 for nitrogen, phosphorus, and sediment respectively during the average hydrology period of 1991 to 2000 (Figure **10-105**). The River-to-bay delivery factors for the nine River Input Monitoring Basins vary with slightly more processing of nutrients and sediment in smaller river basins. However, the delivery factors did not vary much for the 1991-2000 average hydrology and 1985-2014 calibration periods. *Figure **10-106*** shows the spatial variability of River-to-bay delivery factors for nitrogen and phosphorus in the Chesapeake Bay Watershed.

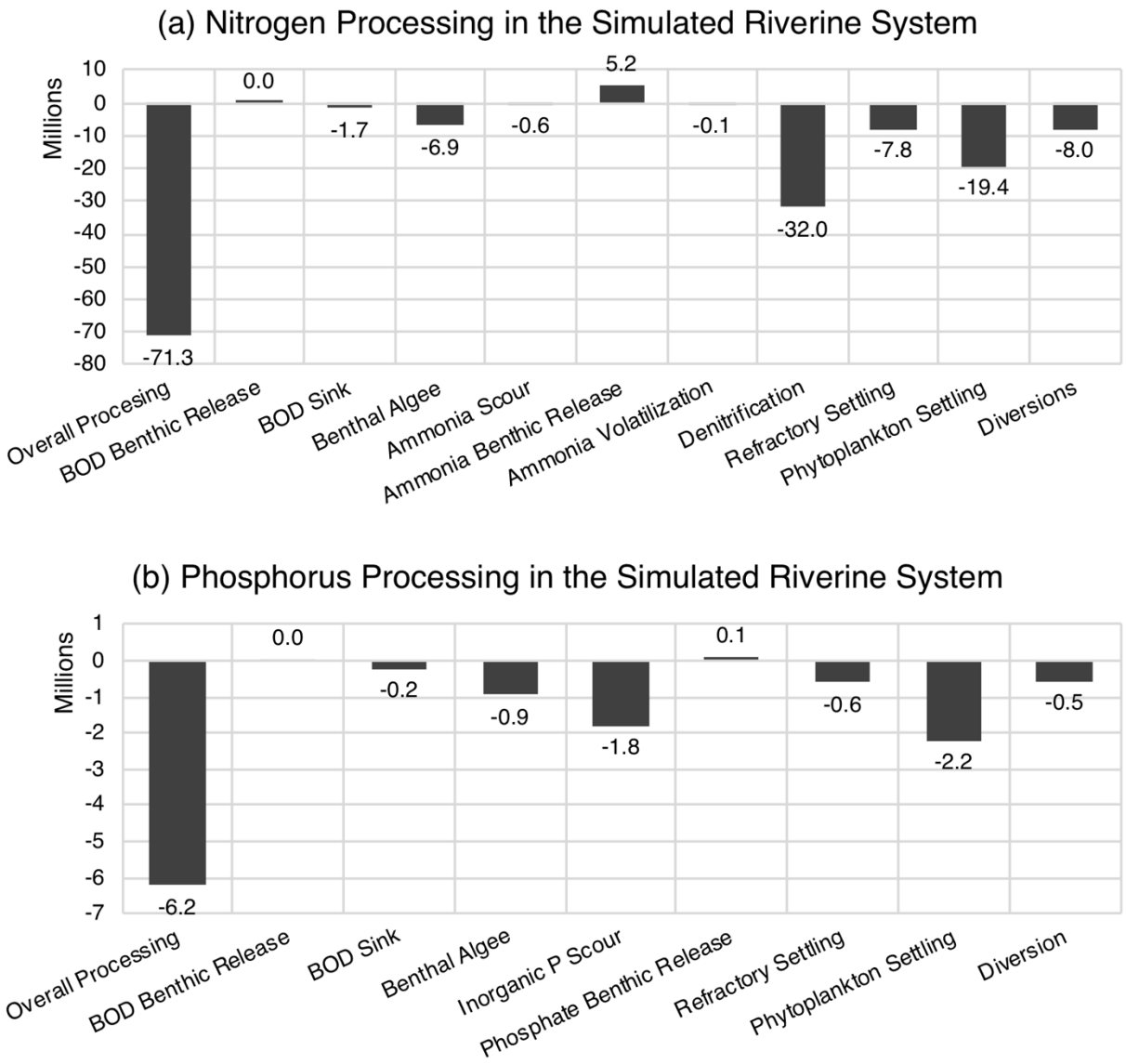

Figure 10-104: Calibrated processing of nitrogen and phosphorus in the simulated riverine system. Denitrification and phytoplankton settling processes were major driver of nitrogen processing, whereas for phosphorus the settling phytoplankton and particulate inorganic orthophosphate were important.

(a) Nitrogen - River to Bay Delivery Factors for Major Basins

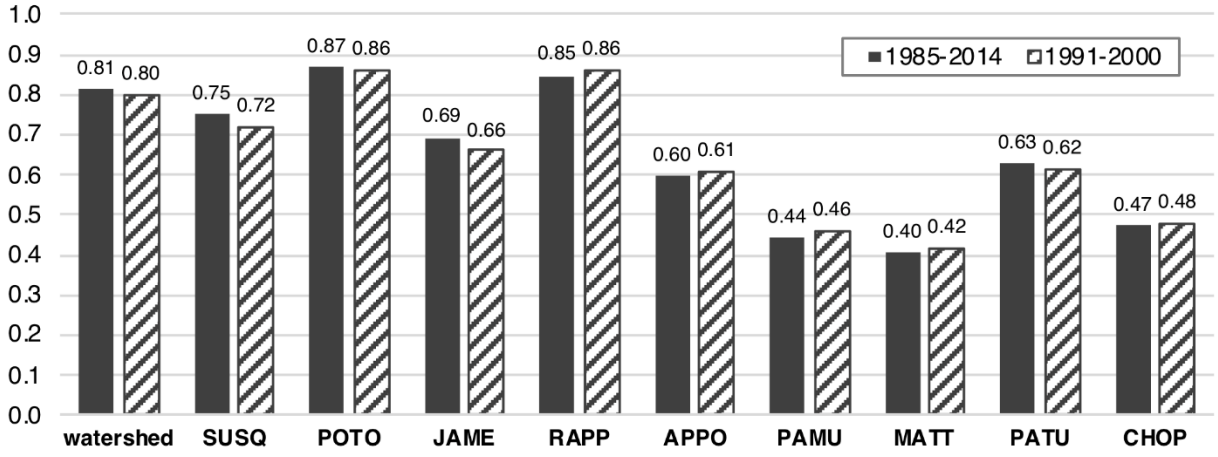

(b) Phosphorus - River to Bay Delivery Factors for Major Basins

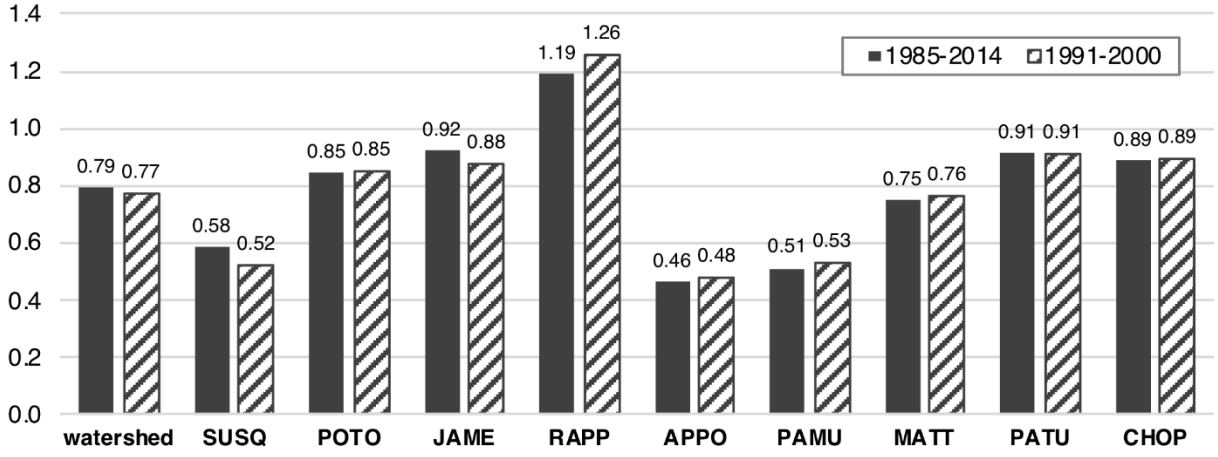

(c) Sediment - River to Bay Delivery Factors for Major Basins

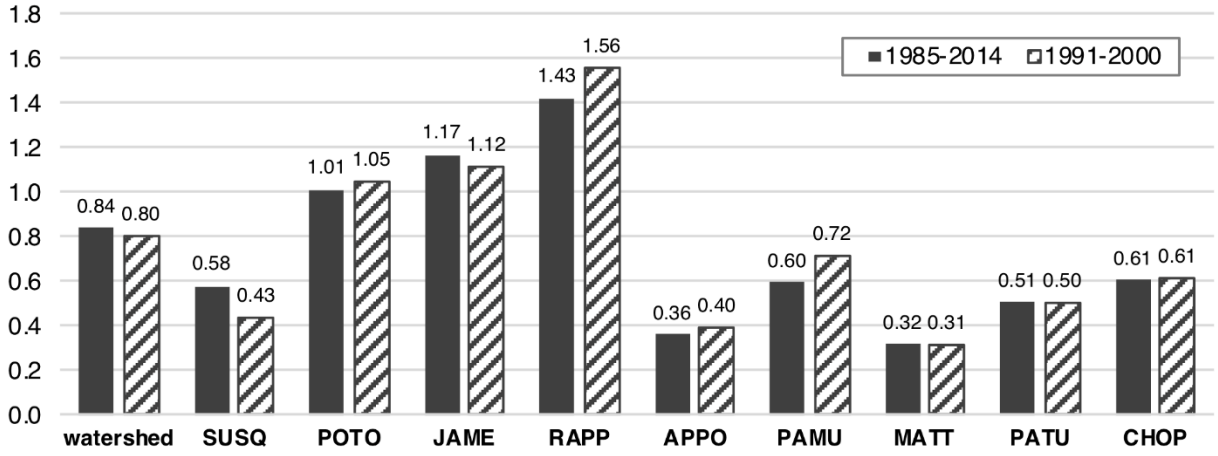

Figure 10-105: River-to-bay nitrogen, phosphorus, and sediment delivery factors for the Chesapeake Bay watershed and its major river basins.

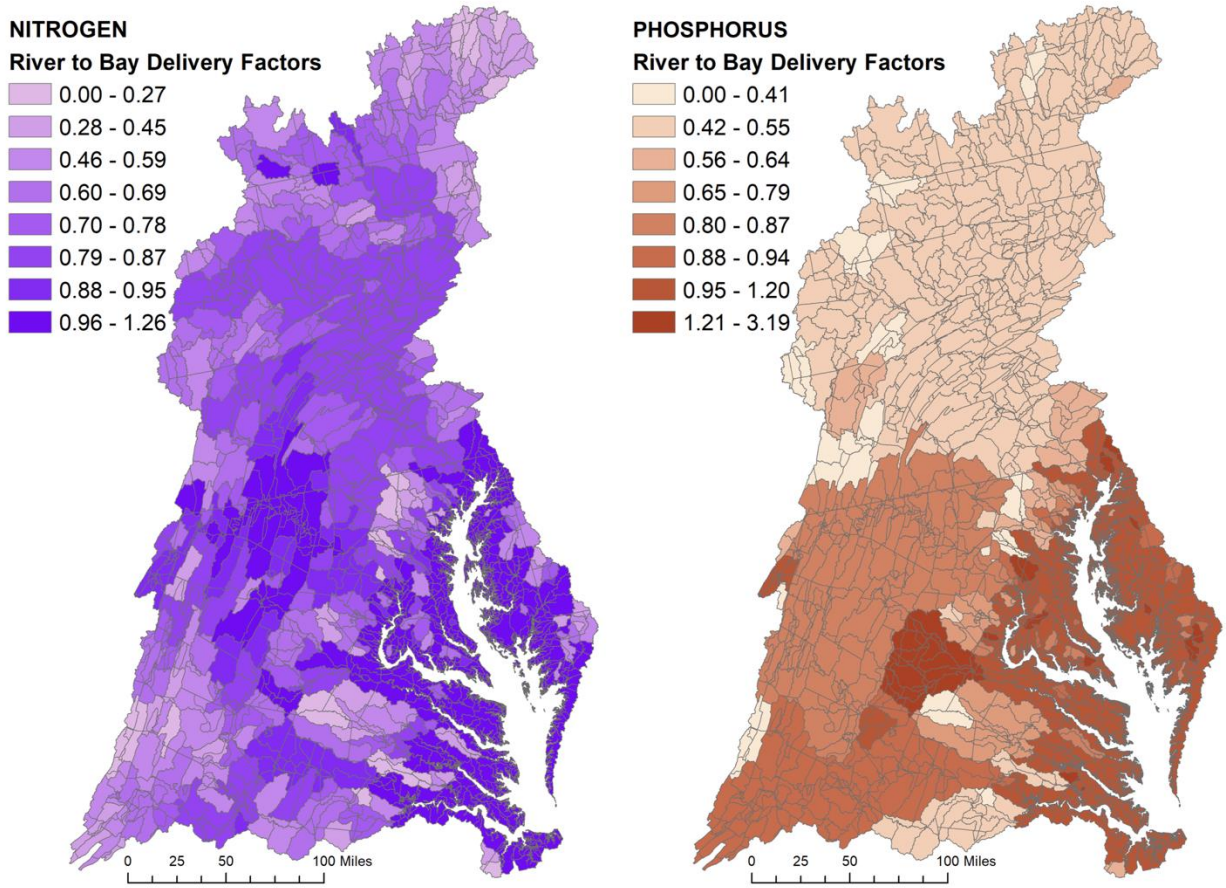

Figure 10-106: Spatial variability in river-to-bay delivery factors. (a) river-to-bay delivery factors for nitrogen. (b) river-to-bay delivery factors for phosphorus.

10.9 Outputs of the Dynamic simulation Watershed Model

CAST, or the time-averaged Phase 6 model, produces output to be used by the CBP partnership as the official estimate of loading for a given scenario. The dynamic simulation of the Phase 6 model is constrained to equal the output of CAST, prior to the application of river-to-bay factors, for any given land-river segment and load source. As discussed in Section 10.8 the dynamic simulation provides the river-to-bay factors to CAST from the calibration. In management scenarios the dynamic simulation will calculate delivery in simulated rivers which may differ from the results of CAST due to changes in input nutrients and sediment. The dynamic model is used to load the estuarine model and also can produce output on spatial and temporal scales not available to the public through CAST.

10.9.1 Output Files That Are Available Outside of CAST

Figure 10-1, repeated at right for convenience shows the calculations for a land use in a land-river segment. The factors are described in sections of the Phase 6 Watershed Model documentation corresponding to factor name. The output from CAST is available to the public at the edge-of-stream (EOS) or edge-of-tide (EOT) scale. EOS is prior to the application of stream and river delivery factors. EOT are loads that the Bay and tidal tributaries receive.

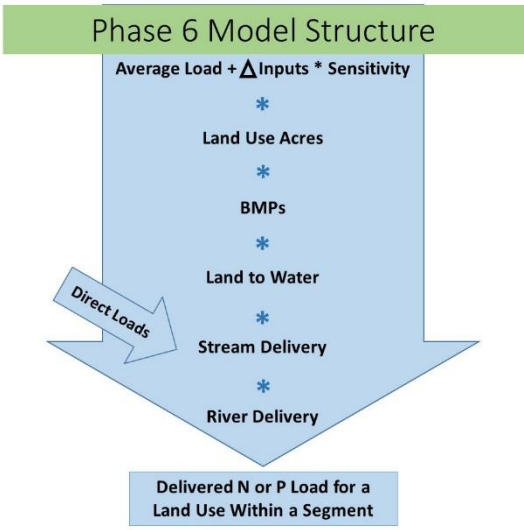

Additional scales, used in the calculation of EOS or EOT loads, are available upon request from CAST or the dynamic model. Table 10-38 describes the available scales and provides a crosswalk between naming conventions in the two parts of the Phase 6 model. Note that the scale names may not directly correspond to a physical scale. The edge-of-field scale is not what might be expected as runoff from a field.

Table 10-38: Comparison of available scales in the Phase 6 CAST and dynamic model

Scale name in dynamic model	Scale name in CAST	Description
Edge of Plot (EOP)	N/A	Average Load + ∑(Δinputs * sensitivity)
Edge of Field (EOF)	Scenario Average Load (SAL)	EOP * land-to-water factors
Edge of Stream (EOS)	Edge of Stream (EOS)	EOF with BMP effects other than tidal BMPs
Edge of River (EOR)	Edge of River (EOR)	EOS * stream-to-river factors
Delivered (DEL)	N/A	EOR * river-to-bay factors
BAY	Edge of Tide (EOT)	DEL + tidal BMPs

Simulated fluxes for the load sources from land simulation and riverine fluxes for flow and water quality parameters can be output at hourly, daily, monthly, annual and average annual time steps.

10.9.2 Linkage with the Estuarine Model (WQSTM)

The Chesapeake Bay Program partnership uses a suite of models that include a land use change model and models of the airshed, watershed, and estuary. The output of the Phase 6 dynamic watershed model is supplied to the estuarine model, known as the CBP's Water Quality and Sediment Transport Model (WQSTM) to estimate the effects of different loading scenarios on Chesapeake Bay water quality.

From time to time, the output of the dynamic model is also used as input to other estuarine models developed and operated by academic institutions, state governments, or contractors. The linkage between the dynamic model and an estuarine model can be achieved with the development of a geospatial linkage and an ontological linkage.

The geospatial linkage is a crosswalk of estuarine model segments and watershed model segments. Recall that most river segments have simulated rivers, but that some that drain directly to tidal water do not. The simulated rivers that are pour points for river networks must each be matched with an

estuarine model cell. The land-river segments that do not have simulated rivers must be matched with the collection of cells receiving output from them. Additionally, each point source facility must be mapped to an estuarine model cell.

The variables and units used in the watershed model are likely not the variables and units used for the estuarine model and so an ontological linkage establish a crosswalk between the model variables. Appendix 10E describes this process in detail.